PHOTOPOLARIMETRY OF SCATTERING SURFACES AND THEIR INTERPRETATION BY COMPUTER MODEL

FINAL REPORT

NASA CONTRACT NASW-3201

PRINCIPAL INVESTIGATOR: MILO WOLFF

(NASA-CR-162514) PHOTOPOLARIMETRY OF SCATTERING SURFACES AND THEIR INTERPRETATION BY COMPUTER MODEL Final Report (International Technology Associates, Inc.) 123 p HC A06/MF A01 CSCL 03B G3/91

N80-14002

Unclas 15437

SUBMITTED BY

INTERNATIONAL TECHNOLOGY ASSOCIATES, INC.

7303 NORTH MARINA PACIFICA DRIVE

LONG BEACH, CALIFORNIA 90803

NOVEMBER 1979

PHOTOPOLARIMETRY OF SCATTERING SURFACES AND THEIR INTERPRETATION BY COMPUTER MODEL

Final Report

TABLE OF CONTENTS

International Technology Associates, Inc.

7303 N. MARINA PACIFICA DRIVE • LONG BEACH, CALIFORNIA 90803

PHOTOPOLARIMETRY OF SCATTERING SURFACES AND
THEIR INTERPRETATION BY COMPUTER MODEL

SUMMARY

The computer model of Wolff (1975) of a rough planetary surface is simplified and revised. Close adherence to the actual geometry of a pitted surface and the inclusion of a new function for diffuse light has resulted in a quantitative model comparable to observations by plenetary satellites and asteroids.

A new function is derived to describe diffuse light emitted from a particulate surface. The function is in terms of the indices of refraction of the surface material, particle size, and viewing angles.

Computer-generated plots are made that describe the observable and theoretical light components for the Moon, Mercury, Mars and a spectrum of asteroids. Other plots describe the effects of changing surface material properties.

Mathematical results are generated to relate the parameters of the negative polarization branch to the properties of surface pitting.

The range of validity and accuracy of the various Albedo-polarization rules is discussed in terms of the computer surface model, and the CSM taxonomy is matched with the predictions of the Model.

An explanation is offered for the polarization of the rings of Saturn, and the average diameter of ring objects is found to be 30 to 40 centimeters.

light, 2) doubly-reflected light, 3) diffusely reflected light, 4) effects of shadow that creates the opposition effect, and 5) effects of snade on double-reflections that create the negative branch.

Despite the model's success in dealing with polarization, it suffered in demanding long computer routines to examine even minor parameter changes, and was not subject to mathematical analysis to provide further insights.

In this article, an improved model is created in which the detailed mechanisms of reflection in a surface are examined so as to provide the model with a closer relationship to the physical structure of the surface. Also, the long computer routines are replaced by a simpler model of the double-reflection process using four representative light paths to represent the doubles processes in each of four quadrants. The result is a simpler, more tractable model which can be calculated easily and which provides additional insight to the reflection processes taking place in a rough surface. The model provides both polarimetric and photometric equations as a function of the phase angle and physical surface properties.

The Model

It is assumed that the solar-system environment contains a meteroid flux which more or less uniformly impacts the surface of airless planets. The resulting surfaces are not assumed identical but the impaction process produces similar pits and jagged particles ranging from micron-sized dust to larger particles which are in turn covered with pits and particles. All variations of this type of surface are sufficiently similar to justify a model of light reflection in which the dominant processes are:

1) single reflection
2) double reflection in pits and between particles

3) diffuse, non-polarizing reflection, and,

4) the production of shade and shadow

The identification of variations from the model in measurements of solar system bodies is an objective of the analysis.

Diffuse reflection is defined as the sum of all processes except single and double reflection, and includes refraction, higher-order reflection, and particle scattering. It is assumed that the diffuse light is unpolarized because processes requiring three or more events in a random jagged surface will almost certainly produce randomized light.

<u>The Unique Properties of Pits</u>

Despite the apparent disorder of a rough particulate surface, it turns out that there exist mathematically describeable properties of such surfaces, which are important to the photopolarimetric measurements of the reflected light. Unfortunately, perhaps because scientists are disciplined orderly thinkers, we have acquired an antipathy to the apparent disorder of a dirt surface. Reflecting this attitude, it has been commonplace to substitute for a surface, an array of spheres or a cloud of random particles which can be attacked by neat, known mathematical methods. It is argued here that this has led to some erroneous conclusions, and, if one wants to have a reliable model and a descriptive mathematical formalism, then it is necessary to directly examine the geometric properties of the real surface itself.

The random pits, holes and interstices of an impacted surface have the geometric property of partically trapping light rays in a manner that suppresses the probability of single-reflection while enhancing the probability of double-reflection. Consider the fate of a ray which enters a pit but has not yet headed outwards. The probability of getting out with only a single reflection decreases the farther in the ray goes. The probability of a single-reflected ray getting out is equal to the solid angle occupied by "clear sky" (as the ray sees things from down in the hole) divided by 4π. That is

$$\text{Singles probability} = P_1 = (\text{angular apeture})/4\pi$$

Note that we are not talking about the probability of optical reflection which is given by the Fresnel equations and must also be a factor, but about the geometric probability of "getting out" or happening as a single reflection, as if the rays were billard balls. In that follows this will always be called the <u>geometric probability</u> (of the surface structure). Note that if P_1 = singles geometric probability and P_2 is for doubles, etc. then

$$P_1 + P_2 + P_3 .. = 1$$

We can approximate the singles geometric probability by assuming that the diameter of pits is about equal to the depth of pits. Then, we have that $P_1 = \pi d^2/4\pi d^2 \cdot 4 = 1/16$ which is very much smaller than that obtained from cloud models.

It is the character of a pit to return a ray back into its source hemisphere with two or more reflections. Accordingly, the geometric probability of double reflection and higher order reflections are enhanced over cloud models or flat surfaces. Although pits come in all shapes, the concept is illustrated at opposition in Figure 1 using hemispherical pits. Two reflections will always occur in Figure 1A if a ray enters inside of the center circle, so the geometric probability is proportional to the circle area. If a ray enters the annulus outside, three or more reflections will occur with a probability proportional to the annulus area.

The relative probabilities are approximated knowing that the circle

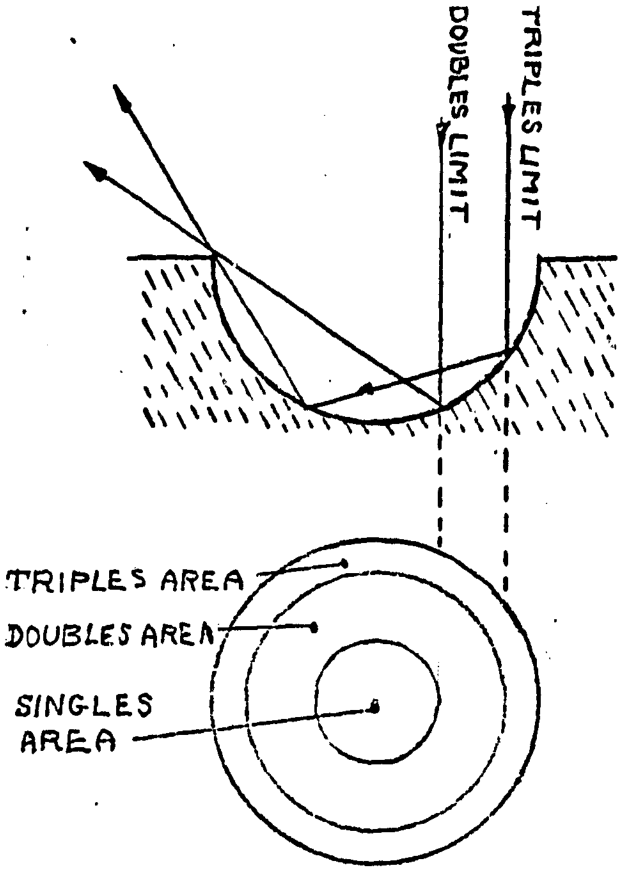

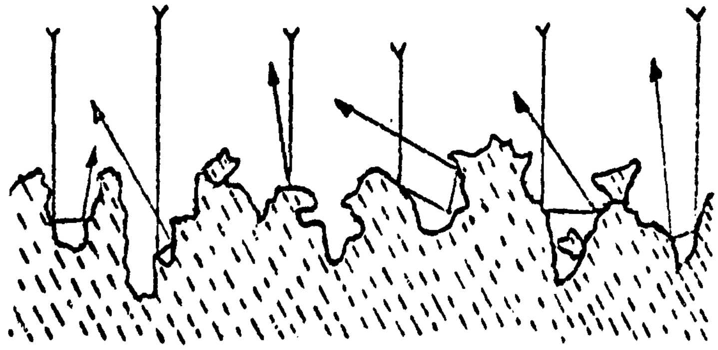

FIGURE 1. This illustrates an optical property of pits. At opposition a hemispherical pit creates about four times as many double reflections as singles. All higher multiples are about equal to the amount of doubles.

A more realistic surface behaves similarly to the hemispherical surface, but depends on the extent of the surface ruggedness.

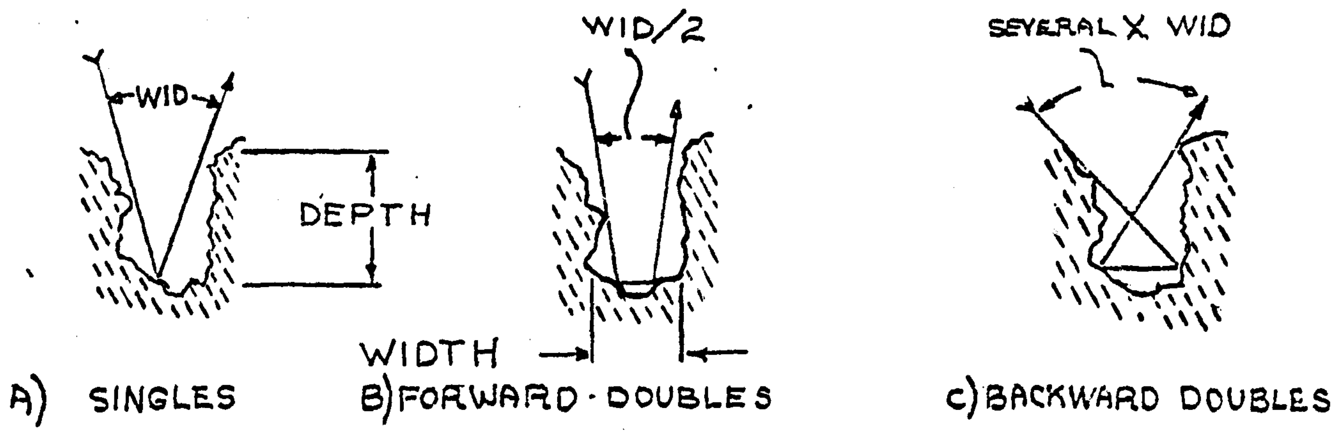

FIGURE 2. The angular distribution of the reflected light depends on the average width to depth ratio of the surface pits. The angular distribution also depends on the type and direction of the reflection. Forward-going double reflections are most constricted in entrance and exit from a pit. Backward-going doubles are least constricted, with sideways doubles and singles being intermediate. WID is a computer parameter proportional to the width to depth ratio.

radii are the sides of a $45^\circ - 90^\circ$ triangle. So, using the fact that the sum of all probabilities equal unity, we obtain

$$P_1 \simeq 1/8$$
$$P_2 \simeq 4/8$$
$$P_3 + P_4 \ldots \simeq 3/8$$

we have arrived at the important result that the geometric probability of double reflection is about 4 times larger than single reflection. This is quite opposite to the impression gained from using random cloud models that ignore the special character of a pitted surface. Of course, we have not yet counted the single reflections that strike the external surface without entering a pit. If such external areas were assumed equal to the space between touching round pits, then the P_1 geometric probability becomes about 1/4 instead of 1/8. P_2, P_3 etc. are decreased proportionately.

Relatively simple observations of the rough airless planets allows one to deduce that the proportion of singly-reflected rays is very small in the light emitted from them. Indeed, a convincing experiment can be done with two sheets of paper - one of them glossy and one of them rough. Look at the reflection of an electric lamp from the glossy paper, at all possible phase angles. One can easily see the large increase of reflectivity predicted by Fresnel's equations at phase angles of 160-180 degrees. Note that this phenomenon identifies single reflection. Now, repeat the experiment using the rough paper; there is no increase seen at large phase angles. It is concluded that single-reflections from the rough paper, and the rough planets, are highly attenuated - contrary to conclusions based on random cloud models.

On the Effects of Fine Dust

Electron microscope photographs of lunar surface particles by Bowell, Dollfus, and Geake (1972) showed the particles to be heavily coated with tiny particles of wavelength-sized dimensions (1 micron). This dust has a major effect on the optical properties of the surface.

Because of the small size of the dust particles and this top-layer location, the dust is able to reflect much more light than its proportion of mass in the total surface layer would indicate, especially at opposition. The opposition effect is a phenomenon due primarily to shadowing by the large particles on a surface (particles which are opaque to the light being observed). When not in shadow, the dust particles adhering to the bottoms of pits enhance the reflectivity. If the dust particles are not opaque, which is to be expected if they are small, then a large fraction of the light refracted into them is reversed by internal reflections and emitted to the observer. The bottoms of pits and other areas are then much brighter than if the dust were not there.

The presence of fine dust might be detected by measurement of the amplitude of the opposition peak. Knowledge of fine dust presence may be a useful clue to the history and composition of the body observed.

Calculations of the computer model for the Moon and comparison with measured properties of lunar rocks lead to the deduction that the Moon must have considerable fine dust. Otherwise, the reported average size (about 20 microns) of particles is incompatible with the lack of specular reflection from the Moon.

Because dust, if present, is the <u>first reflecting layer</u>, it is of prime interest. Especially so since the attention of research activities has tended to overlook the tiny volume of dust in favor of the more interesting large particles and rocks. It has become very easy to assume that the optical surface consists of the particles and rocks rather than the inconspicuous dust.

The computer surface model can accommodate one surface layer which can be particles of any size (an average size is assumed). In the model, the uppermost layer gives rise to the diffuse component of light which is a function of particle size, indices of refraction, wavelength, and the angles of observation. If there is no dust, the diffuse component is due to a layer of large particles and a comparison of observations with the model will yield relatively small values of absorptivity (because the particles are large). If dust exists, the comparison will yield large values of absorptivity (because the particles are small). The product of absorptivity and particle size can be closely estimated from measurements of the amount of diffuse light. Accordingly, computations of absorptivity and size using measured data is one means of identifying dust presence. Another means may be in matching the shapes of photometric and polarimetric curves.

It is interesting that the Moon possesses a two component (in size) optical surface. The reasons why this has occurred are not at all clear. It would probably be a mistake to assume that two-size optical layers have occurred elsewhere, since all size combinations appear possible. In the case of small asteroids, there is reason to believe that dust created by meteoritic impact might not be retained by the low gravity.

Calculating Fine Dust Effects

The presence of fine dust particles adhering to large particles not only has interesting consequences concerned with the capture of light rays. It also brings to mind a concept put forth in a poem by Johnathan Swift

(1865), later paraphrased by Fielder (1920).

> "Big fleas have little fleas to
> Plague, perplex and bite 'um,
> Little fleas have lesser fleas
> and so on.... ad infinitum."

The application of this concept to airless planets greatly reduces the area available for specular reflection. For, if one takes the area of outjutting particles as $\sim$ 25%, and this area in turn is covered with smaller particles, and so on, then the net area of specular reflection is .25 x .25 x .25 . . . ad infinitum. In the model here, the effect is to increase diffuse light at the expense of singles, while double reflections remain about the same.

It is probable that the lunar surface reflects relatively small amounts of singles. This would be reflected in polarimetric data as a decrease of P (Max) and increase in P (Min.). Bowell, Dollfus and Geake (1972) have compared the optical properties of lunar samples with adherent dust against the polarization found for laboratory materials and noted the decrease of amplitude of maximum polarization P(max) accompanied by an increase of P(min) amplitude in the lunar samples, as would be expected from this concept.

In this model, fine dust is accounted for by a factor DUS which has a value 1.0 for total dust coverage, and 0 for none. Note that FORTRAN-style notation, such as "DUS" will be used for some mathematical variables in this article, especially those that actually appear as such in the FORTRAN program given in the appendix.

The Single Reflections of the Model

Assume that the incident sunlight is unpolarized. After each reflection from a surface, Fresnel's laws state there will be a component of light, $E_{\perp}$, polarized perpendicular to the plane of incidence, and a component, $E_{//}$, polarized parallel to the plane of incidence. The reflection coefficients for the two components are taken as

$$X = 2\left|E_{\perp}\right|^2/I_s = \left|a-b\right|^2/\left|a+b\right|^2 \quad \text{and} \tag{1}$$

$$Y = 2\left|E_{//}\right|^2/I_s = \left|c-b\right|^2/\left|c+b\right|^2 \tag{2}$$

where $a = \cos i$

$$b = (m^2 - \sin^2 i)^{1/2} \tag{3}$$

$$c = m^2 \cos i = m^2 a \tag{4}$$

and i is the angle of incidence, equal to half the phase angle G, and m is the complex index of refraction defined by $m = n(1-i\chi)$, and I_S is the intensity of incident sunlight.

The polarization fraction P is given by

$$P = (X-Y)/(X+Y) \tag{5}$$

The singles intensity function is composed of two terms. An opposition term depending upon reflections from pits and affected by shadows, and a term due to reflections, external to pits, unaffected by shadows. Both terms can be diminished by the effects of fine adhering dust.

For the opposition term, it will be assumed there exists an average width/depth ratio, WID, which characterizes the pits of the surface, as in Figure 2. At phase angles G< WID, most of the surface is in shadow and the value of the term falls to near zero. Using an exponential to represent the function, the term is,

$$\text{opposition intensity} \propto \frac{WID}{8}(1 - DUS)\exp(-G/WID)^2 \qquad (6)$$

The opposition term becomes zero for singles if the insides of the pits are covered with dust that absorbs or converts all the incident light into diffuse light.

The externally reflected term requires choosing that fraction of the surface which is exposed and available for specular reflection. This fraction, EXT, is expected, as discussed, to be in the range $0.1 < EXT < 0.3$ for meteorite-impacted surfaces, but conceivably could be different for exotic surface materials.

Summarizing, the singly-reflected light intensity is given by

$$I_1 = I_s\left\{EXT\ (1\text{-}DUS)SHAD + WID\ (1 - DUS)(\exp(G/WID)^2\right\}\left\{\frac{X + Y}{2}\right\} \qquad (7)$$

A Comment on Reflection of Singles

The absence of intense reflection of light from the Moon and Mercury, at near grazing angles of observation is Prima Facia evidence that single reflection is small because Fresnel's equations predict reflectivity (for singles) of 40% to 100% at phase angles of 160° to 180°. This strongly suggests that the factor EXT (external specular area) must be small in the computer model, or that DUS (fraction of fine dust coating) is large or a combination of both.

On the other hand, Mars, the Asteroids, and other outer planets and moons have never been observed at large phase angles, so the possibility of significant specular reflection of singles exists. The asteroids, especially, may be strong candidates to show some specular reflection, since some of them may be still young since formation by molecular condensation, and their small gravity may not retain fine dust created by meteroritic impact. The variation of the factor EXT and DUS in the computer model can show predictions of photopolarimetric curves for comparison with observations, and so it may be possible to detect such bodies even though observation at large phase angles is prohibited.

A second conclusion is that models and theories of light reflection from rough surfaces which are based upon an assumed domination by single reflection, are fundamentally unsound. The results of such models should be used with great caution.

The Doubly-reflected Light Function

The computer model of Wolff (1975) which made a many-rayed simulation of double reflections at all possible angles was convincing and yielded much information on the processes of light reflection, but the extreme complication of the computer routine made it cumbersome and not amenable to analysis. Using the experience of that model, a simpler analytic expression has been devised in which four rays, one in each of four quadrants, are used to calculate the properties of doubly-reflected light.

The new expression must still preserve the important properties of double reflection which are:

1) the net reflectivity depends on the product of two reflection coeffients;
2) intermediate light paths into left-right quadrants are calculated separately from paths going into forward or backward quadrants;
3) shadow attenuation can be applied to the forward quadrant paths, in accordance with the shadow geometry of a rough surface;
4) the net polarization calculates to zero at opposition; and,
5) the dependence on phase angle is closely preserved.

The four representative intermediate-path rays can be chosen in many ways, but one apparent choice is that ray which points directly through the center of each quadrant; i.e. exactly forward, exactly backward, left and right. These have the required properties, but the net reflectivity is about 20% less than the whole quadrant integration, so an adjustment factor of about 1.20 is in order.

In the left and right quandrants, the average intermediate path is always at right angles to the incoming and outgoing rays, so there is very little change of the average angles of incidence which are about 45°. It is therefore sufficient to use a fixed representative ray path to calculate reflectivity.

Although the angles of incidence can be fixed at 45°, the change of phase angle causes rotation and requires the use of the matrix calculation of Wolff (1975):

$$\begin{pmatrix} X_{2L} \\ Y_{2L} \end{pmatrix} = \left| M_{20} \right| \cdot \begin{pmatrix} X(45^\circ) \\ Y(45^\circ) \end{pmatrix} \cdot \left| M_{12} \right| \cdot \begin{pmatrix} X(45^\circ) \\ Y(45^\circ) \end{pmatrix} \cdot \begin{pmatrix} I_1 \\ I_2 \end{pmatrix}$$

These are greatly simplified because of the constant angle 45°, so

$$\left| M_{20} \right| = \left| M_{12} \right| = \begin{vmatrix} \mathrm{Cos}^2 (G/2) & \mathrm{Sin}^2 (G/2) \\ \mathrm{Sin}^2 (G/2) & \mathrm{Cos}^2 (G/2) \end{vmatrix}$$

where X(45°) and Y(45°) are reflection coefficients at 45°, I_1 and I_2 are the initial light components (we have chosen unity), and X_{2L} and Y_{2L} are the final double-reflected light components in the lateral (left and right) directions.

Only one such calculation is needed for each phase angle instead of hundreds as before.

The matrices containing sines and cosines of G/2 account for the interchange of Fresnel components as the phase angle changes from 0° to 180°.

In the forward and backward quadrants, the angles of incidence of the average rays at the two surfaces change in direct proportion to the phase angle, so the representative reflectivities become,

$$\text{Forward quadrant:}\quad \left\{\begin{array}{l} X_{2F} = 1.2\left\{X(45^\circ + G/4,\ MR,\ MI)\right\}^2 \\ Y_{2Y} = 1.2\left\{Y(45^\circ + G/4,\ MR,\ MI)\right\}^2 \end{array}\right. \qquad (9)$$

$$\text{Backward quadrant:}\quad \left\{\begin{array}{l} X_{2B} = 1.2\left\{X(45^\circ - G/4,\ MR,\ MI)\right\}^2 \\ Y_{2B} = 1.2\left\{X(45^\circ - G/4,\ MR,\ MI)\right\}^2 \end{array}\right. \qquad (10)$$

Probability Functions for Doubles

In addition to computing the reflectivity of the two surfaces, it is necessary to compute the geometric probability that two reflections will occur in the surface. An assumption is used here that the probability not used by refraction or by singles reflection, will be evenly divided between doubles and higher order reflections - as was found for the case of hemispherical pits. Maximum doubles probability occurs at opposition.

There are two terms of the maximum doubles probability; one term is due to reflections from inside of the pits, and a second term is due to dust-covered area outside of the pits. If there were no dust, the outside area results totally in singles. These two terms are:

$$GP2 = \underset{\text{geometric probability}}{\text{maximum doubles}} = 1/2(1 - EXT) + (EXT)(DUS) \qquad (11)$$

Equal number of incident light rays must go into each quadrant at opposition because of symmetry. It will be assumed that this is approximately true at all phase angles. To support this, one observes that polarization of the Moon and Mars are almost independent of the angle of incidence. Note that phase angle independence is not assumed - quite the contrary.

The probability of doubles escape from a pit depends on the phase angle in different ways for the different quadrants. This is because of the different angular paths taken by the rays as illustrated in Figure 2A, B, C. The forward rays are cramped for space to make two reflections and therefore a narrow exponential function with half the angular pit width is used as in Figure 2B. The backward, left and right quadrant rays are not constricted as the singles,so the exponential expression to express the phase angle dependence has four times the width.

Summing up, we can now write the intensity of the doubly-reflected light as the product of the reflectivity and the geometric probability, as follows:

$$\text{Left/right: } I_{2L} = I_{2R} = I_s(GP2)\exp(-G/4WID)\,(X_{2L}+Y_{2L})/2 \qquad (12)$$

$$\text{Foward: } I_{2F} = I_s(GP2)\exp(-2G/WID)\,(X_{2F}+Y_{2F})/2 \qquad (13)$$

$$\text{Backward: } I_{2B} = I_s(GP2)\exp(-G/4WID)\,(X_{2B}+Y_{2B})/2 \qquad (14)$$

where the left and right quadrant contributions are identical.

The total contribution of doubles is

$$I_2 = I_{2L} + I_{2R} + I_{2B} + I_{2F} \qquad (15)$$

II. A NEW FUNCTION TO COMPUTE DIFFUSE LIGHT

We seek a particular mathematical description of a well-known property of light diffusely reflected from particles. It is commonly observed that colored crystals appear white if they are finely ground. This is because light paths through the crystals are shorter when finely ground, and the total surface area is larger. Accordingly, the reflection opportunities, which appear white, are increased and the absorption opportunities, which produce color, are decreased. This phenomenon is an example of the calculation sought. Specifically, we want to find an expression for the emitted diffuse light as a function of particle size and the optical indices of the particles.

The advantage to be gained from this approach is that by using the measured albedo and an estimation of the real index, a calculation can be made of the product:

(particle size) x imaginery index)

Then, two measurements at different wavelengths, displaying different absorption, will yield an unambiguous particle size. Further measurements confirm the result.

This approach consists of four steps. First, the amount of light which enters the particulate surface is calculated. Second, the distances travelled inside the particles are calculated. Third, the amount of light emitted into the source semisphere is obtained, and finally, a normalized angular distribution function must be added to provide isotropic (assumed random) angular emission.

Step 1: Light Entering the Surface.

The amount of light refracted into the surface particles can be computed by assuming that all angles of incidence are equally likely, which is reasonable for a random jagged surface.

The weighted average coefficient of refraction, designated REF, is the integral overall angles of incidence, a:

$$REF = 1 - \frac{2}{\pi} \int_{0}^{\pi/2} \frac{1}{2} \left\{ X(a, MI, MR) + Y(A, MI, mr) \right\} da \qquad (16)$$

which can be numercially integrated easily in a computer program. For purposes of analysis, a simple approximation can be used,

$$REF \simeq 1 - 1/2 \left\{ X(45^{\circ}, MI, MR) + (Y(45^{\circ}, MR, MI) \right\} \qquad (17)$$

where the integral has been approximated by the value of the integral at the center (45°) of the integration range. This is perhaps no more than 5-15% in error.

Step 2 and 3: Light Paths Inside and Escape from the Particles.

After a photon enters a particle, it will bounce around inside by internal reflection, until it either escapes by striking a wall at an incident angle which is less than the critical angle, or, it will be absorbed. It follows that the length of the path traveled inside depends on the real index of refraction through the critical angle, on the size of the particle, and on the imaginary index which governs absorption.

The probability of escape depends on the size of the "Cone of escape" whose apex angle is the critical angle and which is formed around a perpendicular to the wall. If all angels of striking the wall are equally probable, then the escape probability is the ratio of the escape-cone solid-angle to the solid-angle of a hemisphere (2π radians). However, since an escaping ray can be emitted into either the outside hemisphere (really escapes), or into the planetside hemisphere (gets trapped again), the true probability of escape is 1/2 of that ratio. The escape cone solid angle will be dnoted CONE(n). For an index n=1.6, CONE/$4\pi \simeq 12\%$.

The emitted ray intensity at the Nth reflection is

$$\Delta I_N = - I_N \, \mathrm{CONE}/4\pi \, \Delta N \tag{18}$$

By regarding N as a functional variable, with little error, the above expression integrates immediately to

$$I_N = I_{N-1} \exp(-N \, \mathrm{CONE}/4\pi) \tag{19}$$

If the substance of the particle is absorbing, then the ray will also be diminished between reflections by absorption while travelling the paths of length N x D, where D is the average distance between reflections - about the same size as the particle diameter. This can be written

$$I_{N-1} = I_o \exp(-KDN) \tag{20}$$

where I_o is the intensity of a ray when it first enters the particle and K is the absorption coefficient; $K = 4\pi(MI)/\lambda$

Combining Eqns (18, 19, 20) yields the light emitted at each reflection

$$\Delta I_N = I_o \exp(-N(KD + \mathrm{CONE}/4\pi)) \times (\mathrm{CONE}/4\pi)\Delta N$$

The total emitted light is obtained by summing this expression over all reflections from 0 to ∞ . Again, to avoid a cumbersome procedure and result, an integral can replace the sum with little error.

$$\sum_{0}^{\infty} \Delta I_N \cong -\int_{0}^{\infty} I_o \exp(-N(KD + CONE/4\pi)) \times (CONE/4\pi)dN \qquad (21)$$

Integrating and replacing I_o with $I_s REF$, yields

$$I_3 = \text{Diffuse emitted light} = I_s REF/(1 + 4\pi KD/CONE)$$
$$= I_s REF/\left[1 + (4\pi)^2 D_\lambda MI/CONE\right] \qquad (22)$$

where I_s is the illuminance of the sun at the surface of the planet, D_λ is particle diameter in wavelengths, and REF is Eqn. (16 or 17), already obtained.

Equation (22) is the expression sought. It provides the intensity of diffuse emitted light as a function of the particle size D, and the indices of refraction, MR and MI which are contained in CONE, REF, and K. This result is somewhat surprising. One might expect an exponential attenuation of light to yield a sharp darkening as absorption is increased rather than the simple inverse relation obtained. But the summing of many paths results in a less severe attenuation.

Step 4: Angular Distribution of Diffuse Light from a Planet.

It is evident that diffuse light from a planet travels the least distance through the planet's surface in reaching an observer, when it comes from the sub-earth point and is at zero phase angle. At larger phase angles, the path through the surface assumes greater and greater values. The derivation of a function which describes the attenuation due absorption along the path is given by Wolff (1975, p. 1402). The result is classical and termed the Lommel=Seeliger function (L-S). In terms of the phase angle, G, and the longitude, L, it is:

$$\text{ATTENUATION} = 2\cos(G-L)/(\cos(G-L) + \cos L) \qquad (23)$$

In order to approximate the opposition effect, one can arbitrarily divide the light of Eqn. (24) into halves, one half of which is subject to opposition shadowing, thus Eqn. (24) is multiplied by

$$\text{Opposition factor} = \tfrac{1}{2} + \tfrac{1}{2}\exp\,(G/WID)$$

We can now reach our final conclusion by combining the above with the new result shown in Eqn. (22), and thus obtain a complete expression for diffuse light from a rough, particulate planetary surface:

$$\text{PLANET"S DIFFUSE LIGHT} = \frac{I_s\ 2\ REF\ \cos\,(G-L)\ (\tfrac{1}{2} + \tfrac{1}{2}\exp(G/WID))}{(1 + 4\pi KD/CONE)\ (\cos(G-L) + \cos L)} \qquad (24)$$

The physical interpretation of Eqn. (24) is that light enters a particulate surface and along its path successively enters various particles, bouncing around inside of them, exits, enters, etc. and eventually a part of the light reaches the surface and goes to the observer. Two photon capture probabilities are involved, one is capture by a particle and this probability increases with phase angle, G, and depends on L; the second is capture by the crystalline lattice inside the crystal and this depends on particle size, its length, and the indices of refraction.

Eqn. (24) is a new result. Its ultimate usefulness and accuracy in describing the emission of diffuse light remains to be tested by observation.

Case of An Entire Planet

If the entire planet is in the field of view of the measuring instrument, as must be the case when observing small objects, such as the unresolvable asteroids, the total signal is the integral over the visible, illuminated portion of the planet. A spherical body will be assumed.

The differential element of area in the integral must be a projection of the planet's surface onto a plane perpendicular to the line to the observer. Reference to Figure 3 provides an element dA = (R cosL cosl dL) (R dl(1 - cosL(1-cosl))). R is the planet radius, L is the longitude and l is the latitude. The illuminated part of the planet lies between longitude $-\pi/2$ and longitude $\pi/2$-G.

The integrand must sum over the three components of light I_1, I_2 and I_3:

$$I(\text{planet}) = E(\text{sun} \int_{-\frac{\pi}{2}}^{\frac{\pi}{2}} \int_{-\pi/2}^{\pi/2 - G} \left[I_1 + I_2 + I_3\right] dA$$

where the three components are given by Eqns, (7), (15) and (24).

The integration over latitude l is straight-forward and results

$$I(\text{planet}) = R^2 \int_{-\frac{\pi}{2}}^{\pi/2 - G} dL \left[2(\cos L)+\cos^2 L(\pi/2 - 2)\right] \left[I_1 + I_2 + I_3\right] \quad (25)$$

There appears to be no ready integral for Eqn. (25). If I = f(L), so in the computer model, this integration is carried out numerically.

Terminator of the Planet

At the location of the terminator, a function of G and L, the intensity of I_1, I_2 and I_3 must go to zero. Eqn. (23) accomplishes this for I_3. For I_1 and I_3, an approximation for the visible, illuminated area of a particle is useful:

$$SHAD = 1 + \frac{G}{L - \pi/2}$$

This is used as a multiplier of I_1 and I_2.

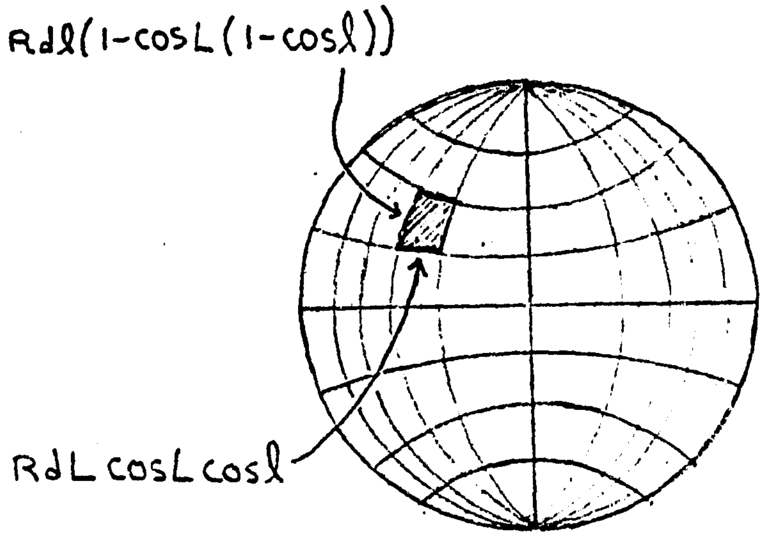

FIGURE 3. Integration over the visible illuminated surface of a planet uses an area element projected onto a surface perpendicular to the observer.
Diffusely-emitted light has a different angular dependence than singles or doubles and has a greater dependence upon longitude.

III. COMPUTER PLOTS OF THE NEW MODEL

The following sets of figures use the new surface model to plot quantities which are observable, as well as the separate components of polarization and light intensity which are not observable but of interest.

At first, the main goal of the plotting program was to produce a model which matched the Moon, since we know most about that surface. This was done by choosing suitable values of the parameters DUS, EXT, real index (MR), imaginary index (MI), pit width/depth (WID) and longitude. After those values were once determined, they were not altered during the production of this entire group of figure sets, except for the variation, one-by-one, to illustrate the effects of each parameter, shown in the figure sets.

The unusual discovery was made that by changing only MI, it was possible to reproduce the characteristics of much of the CSM taxonomy of asteroids. This is discussed at length in what follows. The quantitative matching of computer results with observations over a broad range of parameters and measurements is quite remarkable in view of the diverse properties concerned and the complex nature of the functions involved. It is concluded that the model can be regarded as quantitative for many purposes.

REAL REFRACTIVE INDEX (MR) VARIED
Figure 4A to Figure 4K

These curves illustrate a range of real refractive indices for common minerals found in the solar system. In view of the wide range, especially for metals, that could occur in small objects such as asteroids, caution must be used in asuming that this range describes all posibilities.

The real index affects the diffuse light component through the critical angle "escape cone" for light trapped inside the surface particles. A larger index results in a smaller escape cone so that a ray travels farther inside before escape. The longer travel path results in greater attenuation of the ray.

The index affects singly and doubly-reflected light by changing the Fresnel reflectivity. A larger index will produce more reflected light a situation just opposite to diffuse light.

The effects of changing the real index are very different for the two measureables : polarization and reflectivity. In the case of polarization, a small change of index results in a dramatically large change of both negative and positive polarization. This is because the opposite changes in the diffuse and reflected light components operate inversely in the polarization equations to produce a net large change.

On the other hand, for reflectivity, the two oppositely changing light components continue to oppose in the sum. Thus reflectivity can be almost constant, especially for index values about 1.7 to 1.8 . It is important to note that such changes will produce a general violation of all the Albedo-polarization Rules.

Reddening, like polarization, also shows dramatic changes when MR is changed. This might be used to detect violation of albedo determining rules.

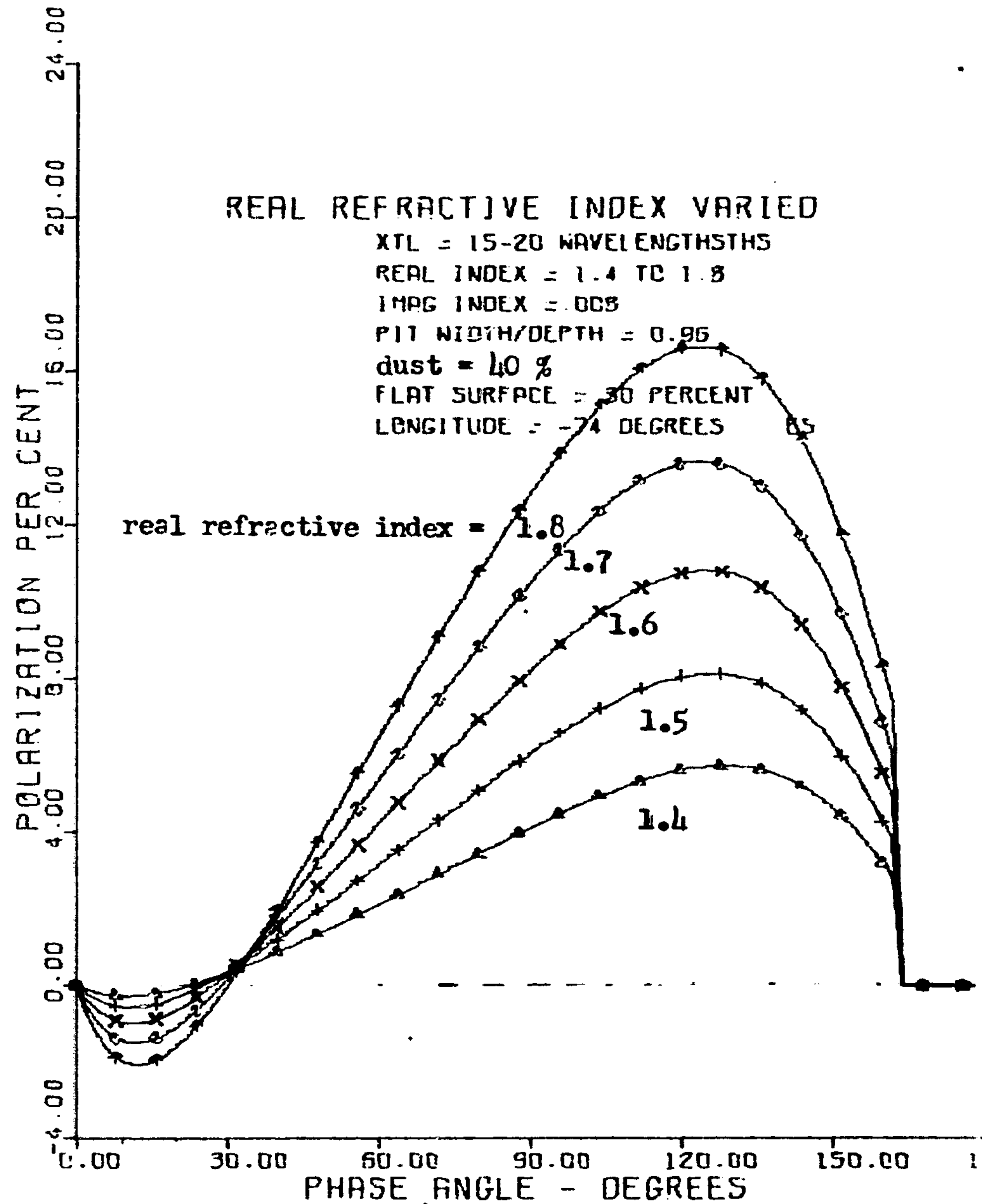

Figure 4 A. Polarization at a point on a planet.

The curves which best fit the Moon use a real index of 1.6 ± 0.5 . This agrees well with averages of Lunar samples;

Note that the ranges of indices for real minerals implies a significant range of polarization amplitudes.

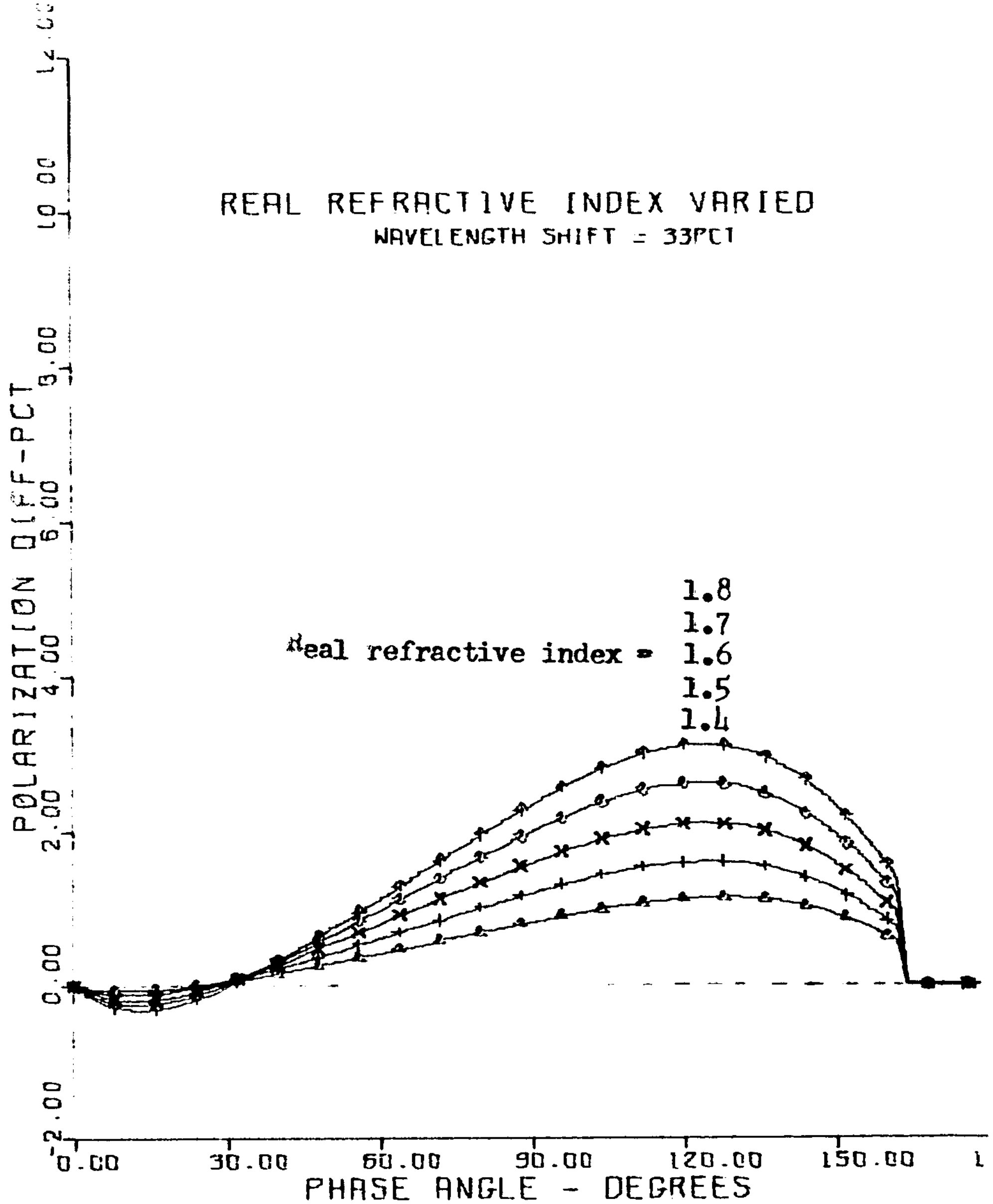

Figure 4-B. Polarization shift for a wavelength shift of 33 percent.

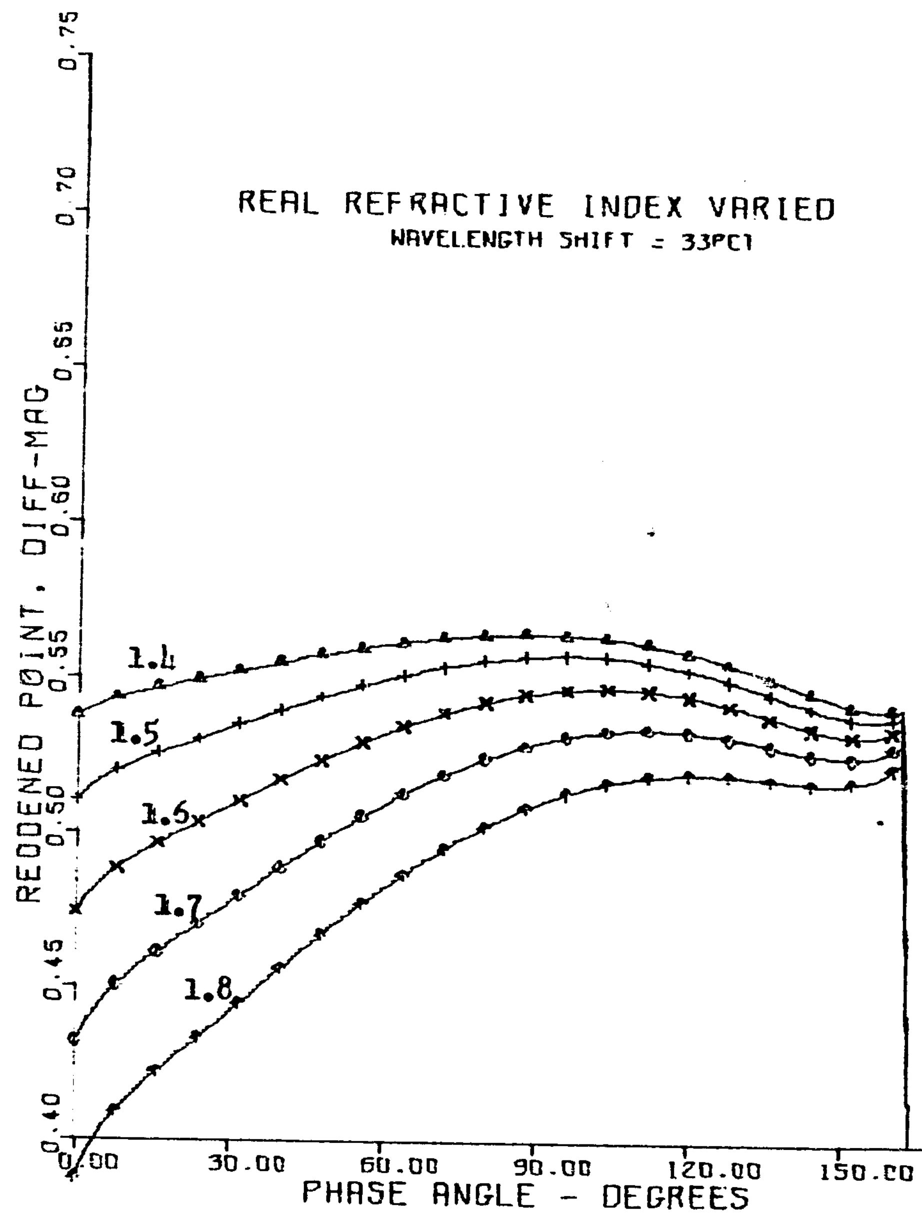

Figure 4-C. The reflectivity shift, in magnitudes, of a point on the planet, for a wavelength shift of 33 percent.

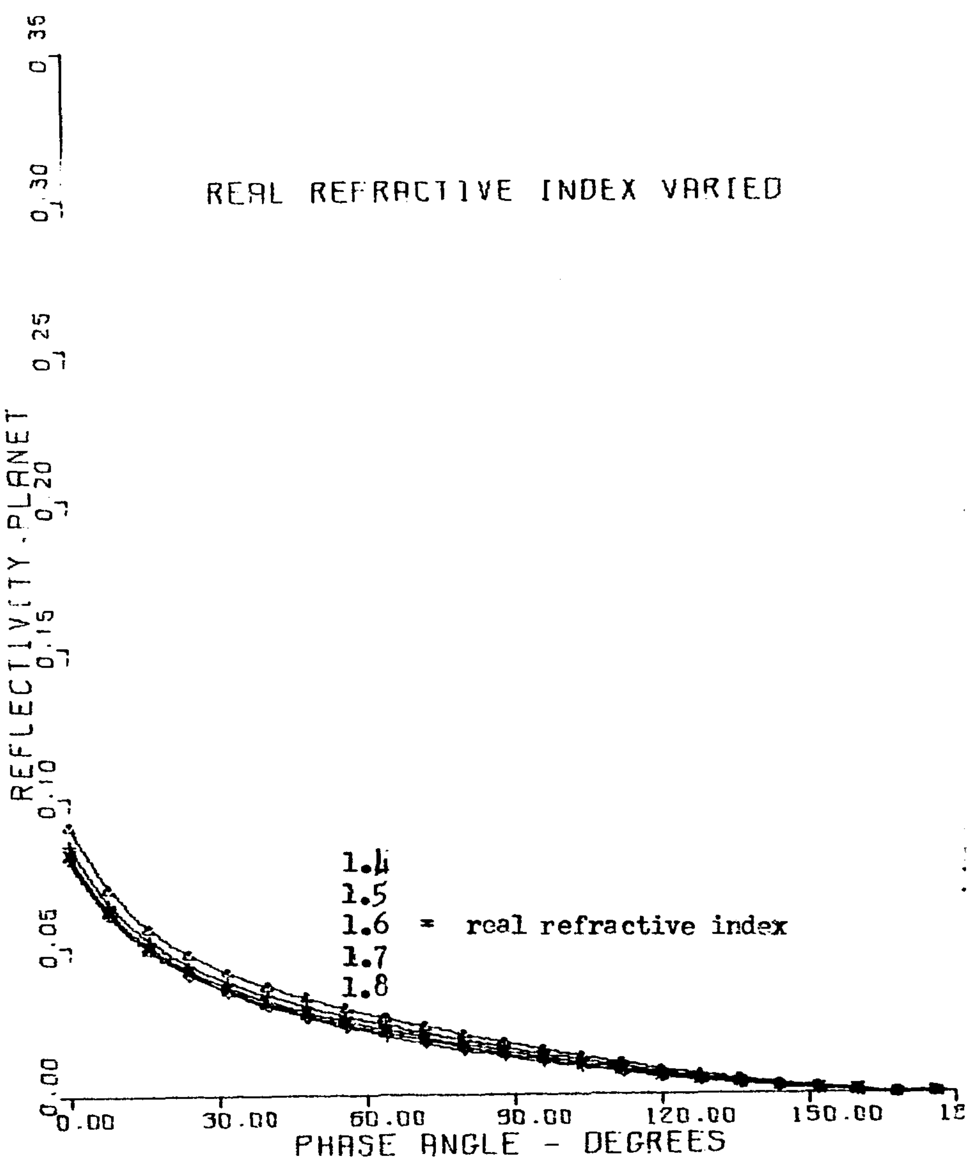

Figure 4 E. The integrated reflectivity of the entire planet.

The observed reflectivity of the Moon, .085, agrees with the real index of 1.6, if the parameters listed on Fig A of this set are assumed (or thus deduced).

Note that, despite wide variation of intensity of light components, the total is relatively constant, because the changes are opposite and offset each other.

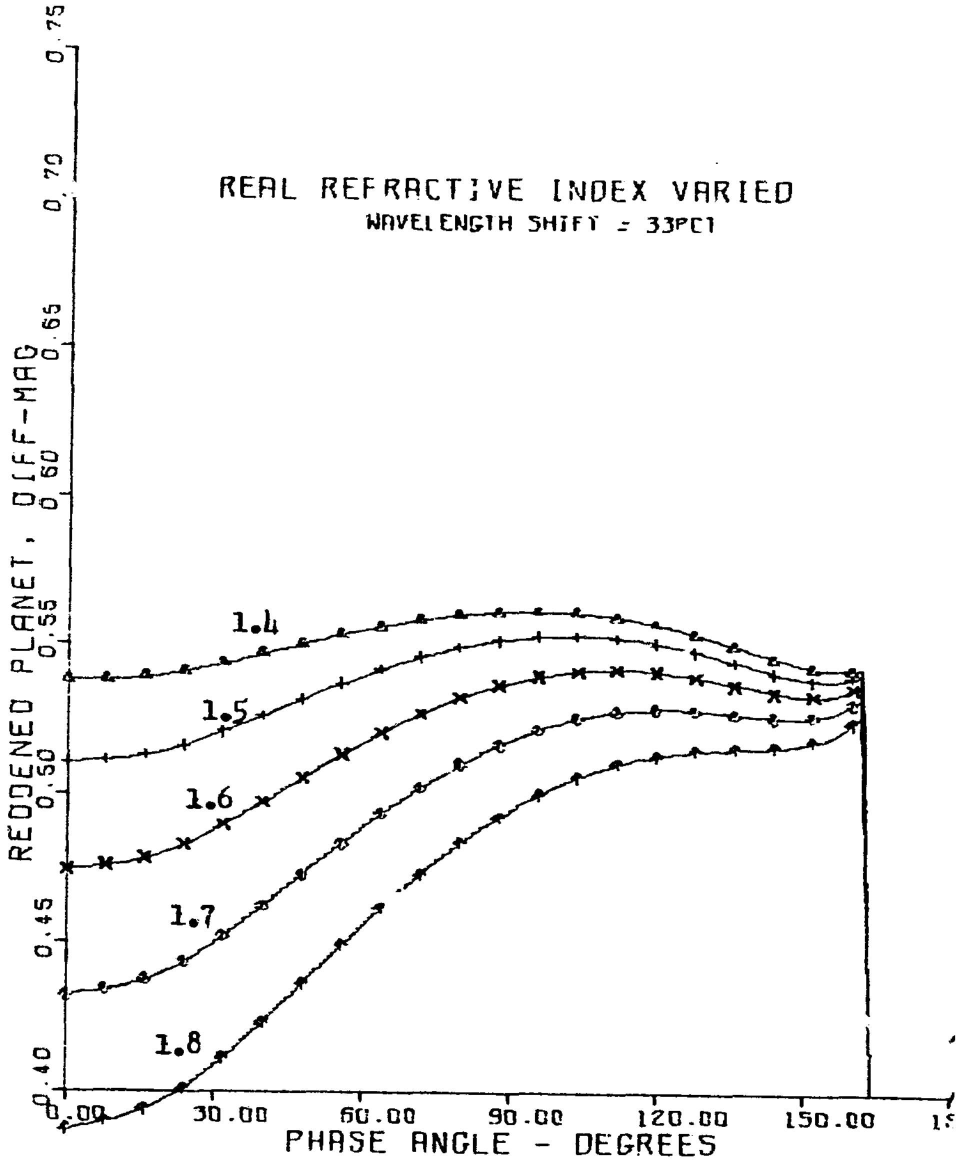

Figure 4 D. The reflectivity shift, in magnitudes, of the integrated planet, for a wavelength shift of 33 percent.

Note that the "reddening" (slope of curves) calculated here agrees with the observed rule, that darker bodies show greater reddening.

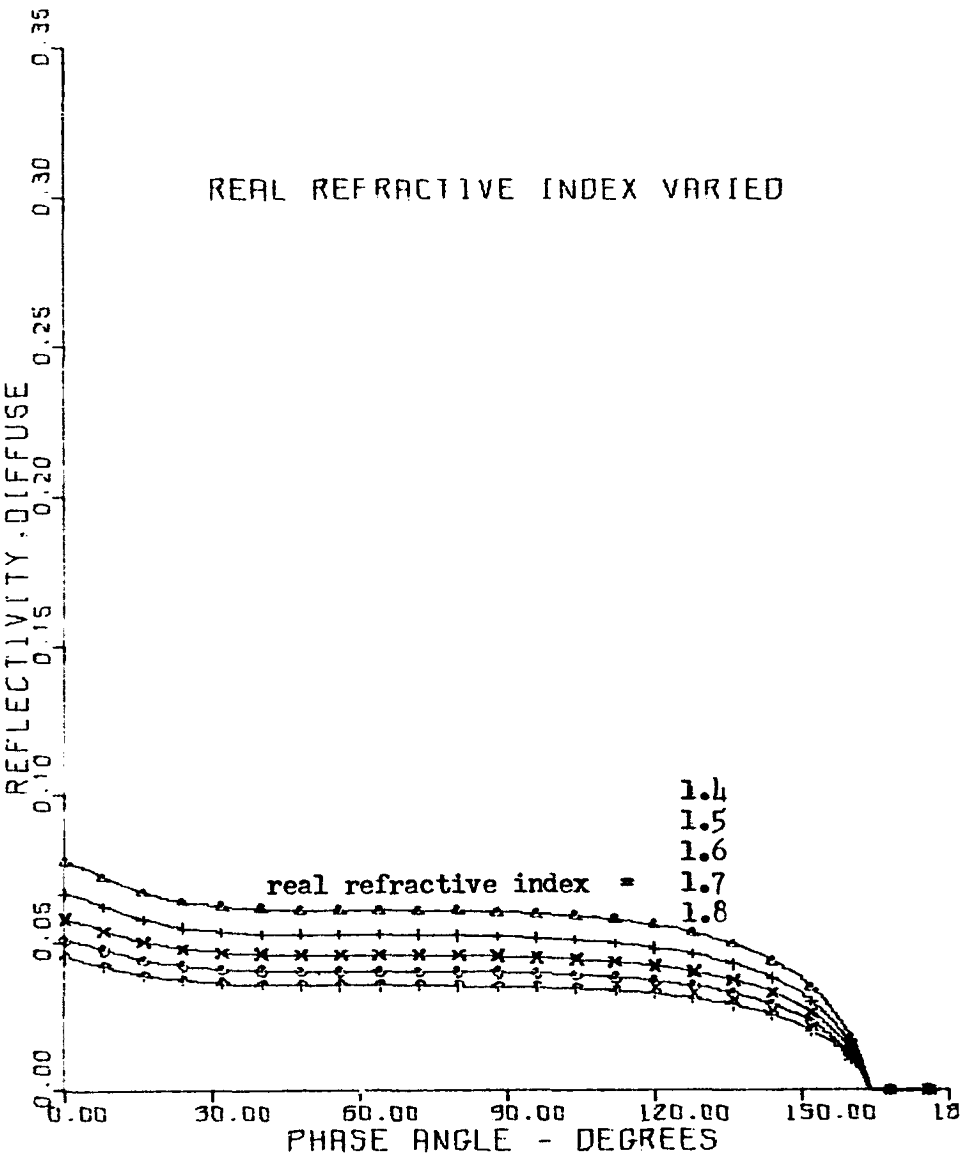

Figure 4-F. The diffuse component of light at a point on the planet. Diffuse light emerges from particles after inward refraction and multiple internal reflections.

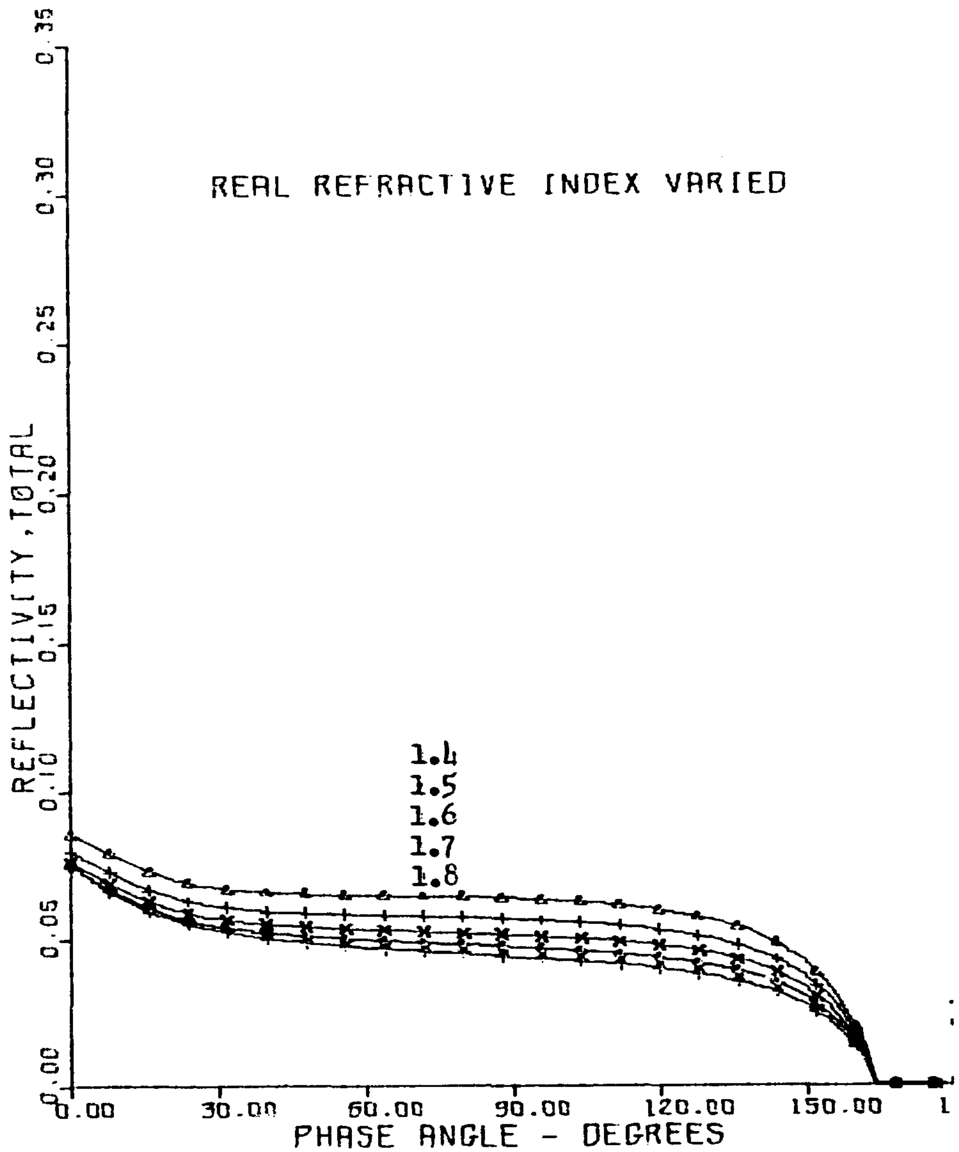

Figure 4 G. The total of all light components (singles + doubles + diffuse) at a point on a planet.

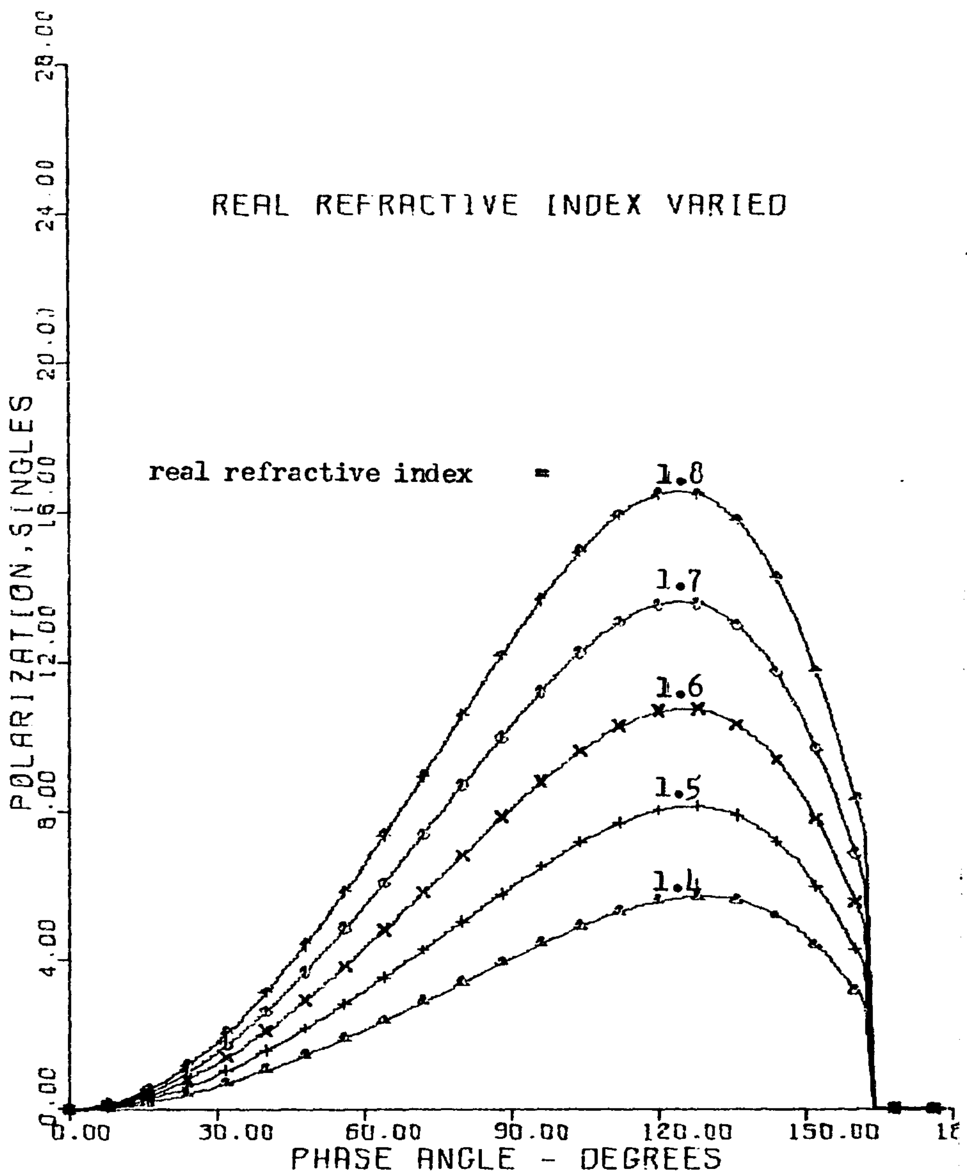

Figure 4 H. Polarization due to the singly-reflected component of light, alone.

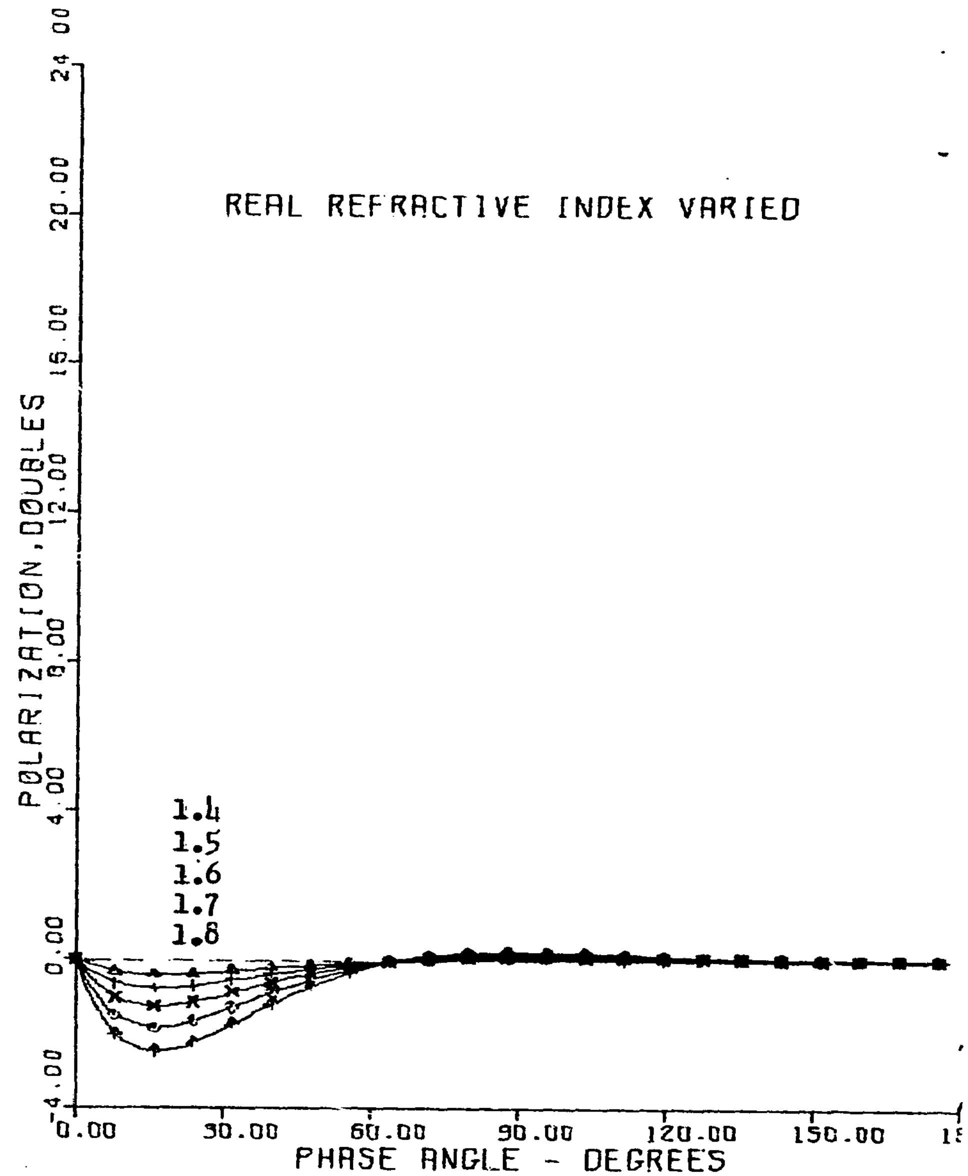

Figure 4 I. Polarization due to the doubly-reflected component of light, alone.

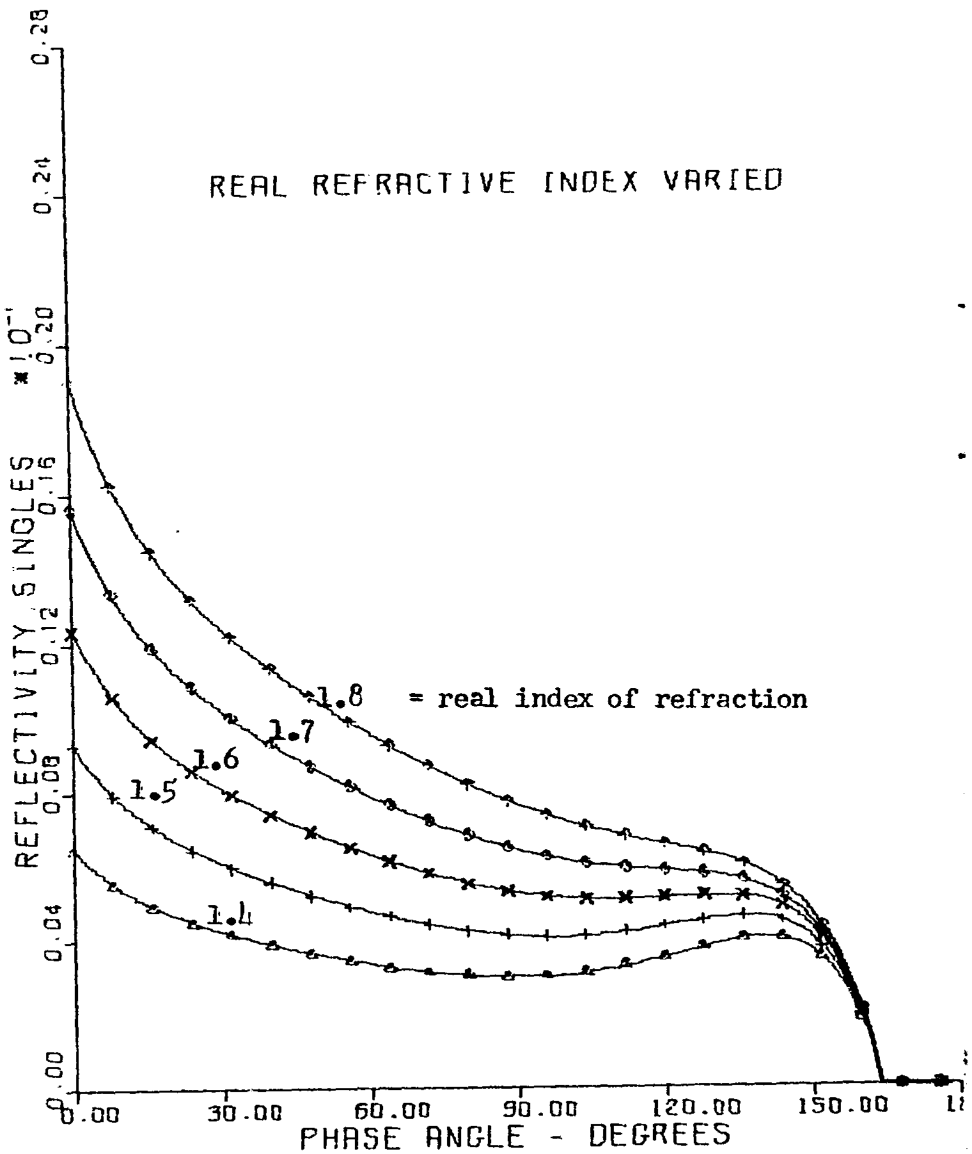

Figure 4 J. The intensity of the singly-reflected component of light.

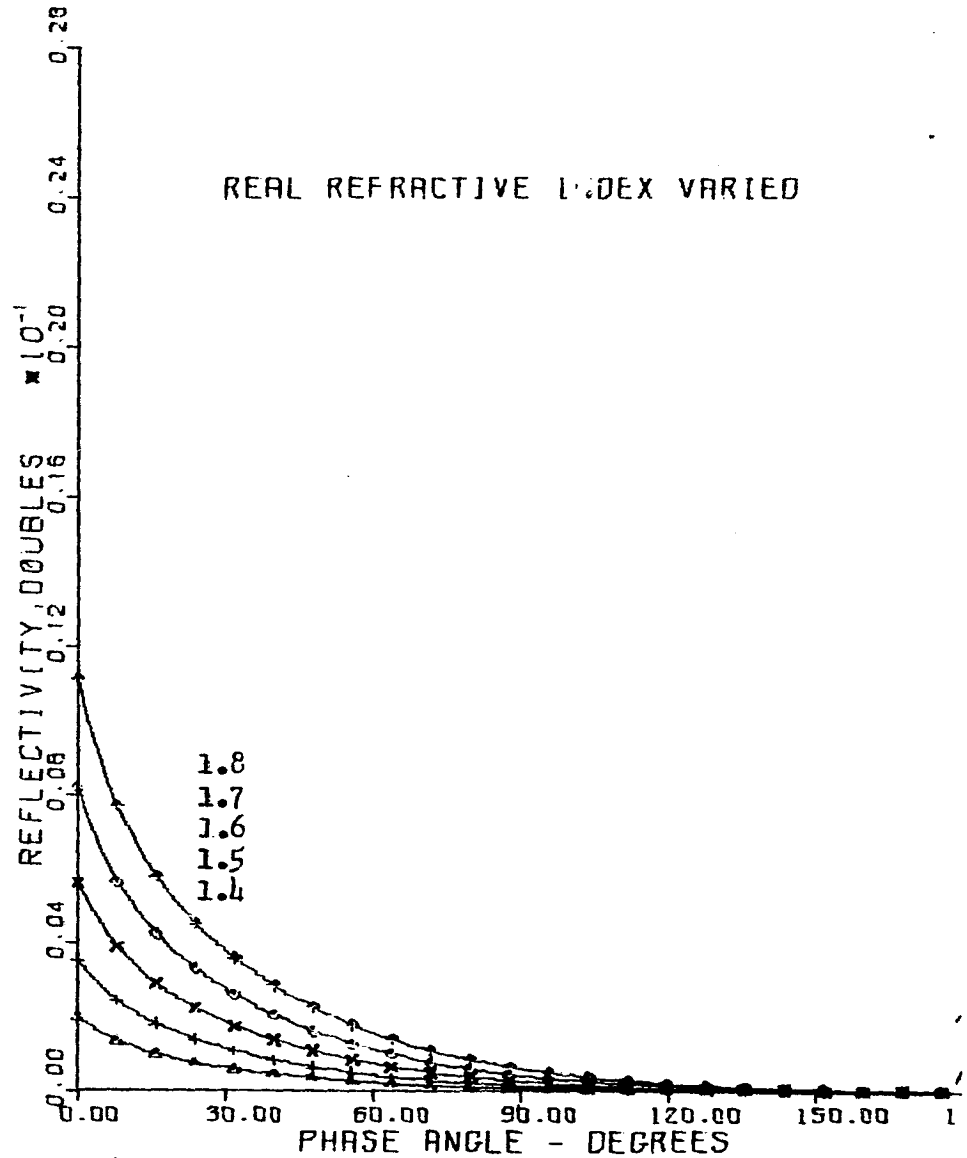

Figure 4 K. The intensity of the doubly-reflected component of light.

S - RANGE

IMAGINARY INDEX OF REFRACTION (MI) VARIED

Figures 5A to Figure 5K

These figures show the results of changing the imaginary (absorbtion factor) index in the range where it significantly affects only the diffuse c omponent of light. The range, .002 to .006, is thought to describe the S type asteroids because the resulting polarization and reflectivity correspond to observations of that group. Furthermore the resulting diffuse component of light dominates over the reflected components so that absorbtion spectra of the surface material should be seen, which again corresponds to the observations. Also, the resulting R/B color index corresponds to about half of the S asteroids and the remainder could be matched by the reasonable, and expected, assumption of some color change with wavelength.

The correspondence of this MI range with the S type becomes part of a logical orderly matching of the entire CSMR taxonomy by the same orderly increase of the MI index. The total of evidence for matching with the asteroid taxonomy seems pervasive.

If the above matching is accepted, then it is an immediate conclusion, that the S asteroids have a dusty, pitted, particulate surface comprised of semi-transparent grains of sizes 1 to 20 microns with the quantitative description shown in the upper right of this page.

As MI increases, passing through the range of S asteroids into the range of C asteroids, there seems to be no natural boundary between the groups, except that the surfaces of the Moon, Mars, and Mercury fall between. I can think of no logical reason why this happens.

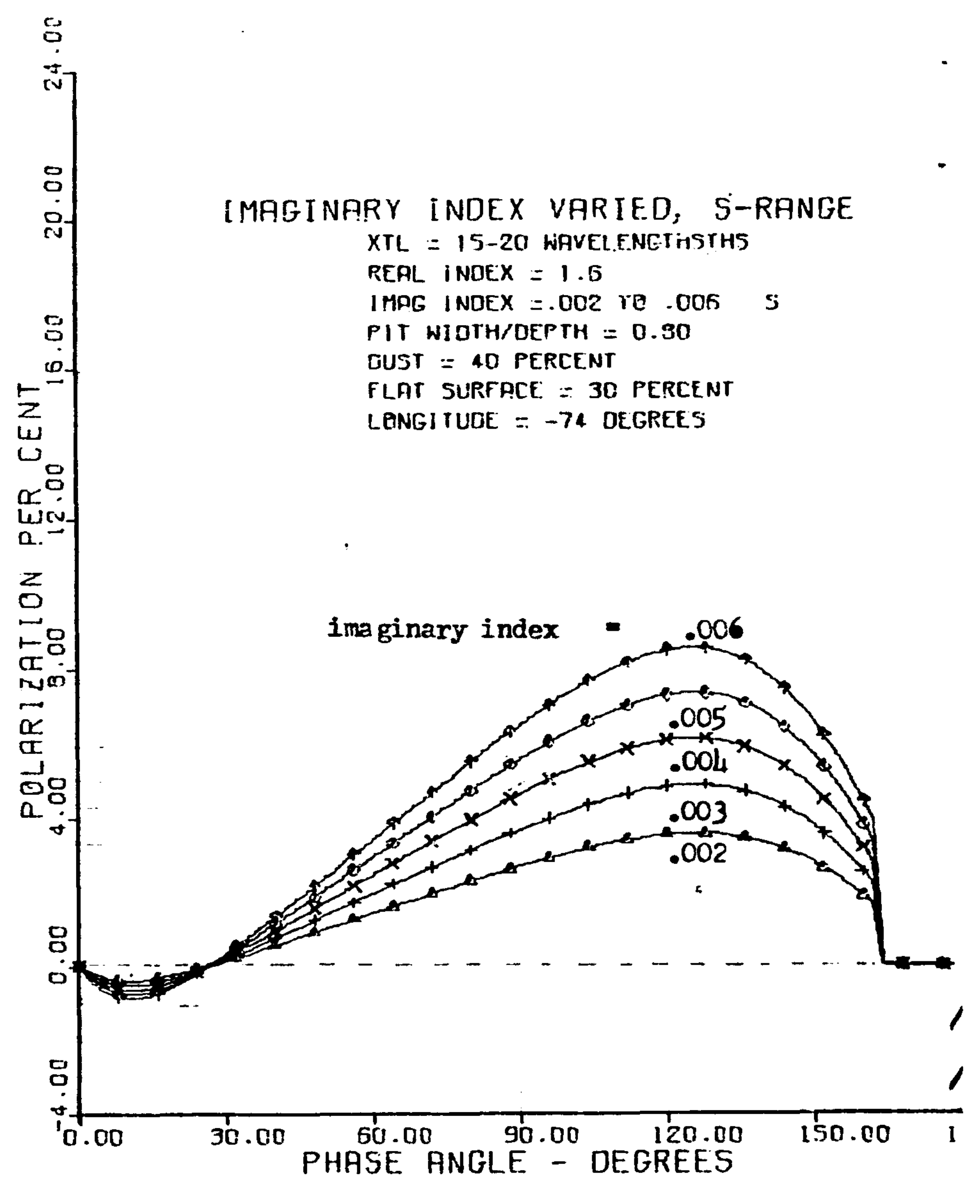

Figure 5A. Polarization at a point on a planet.

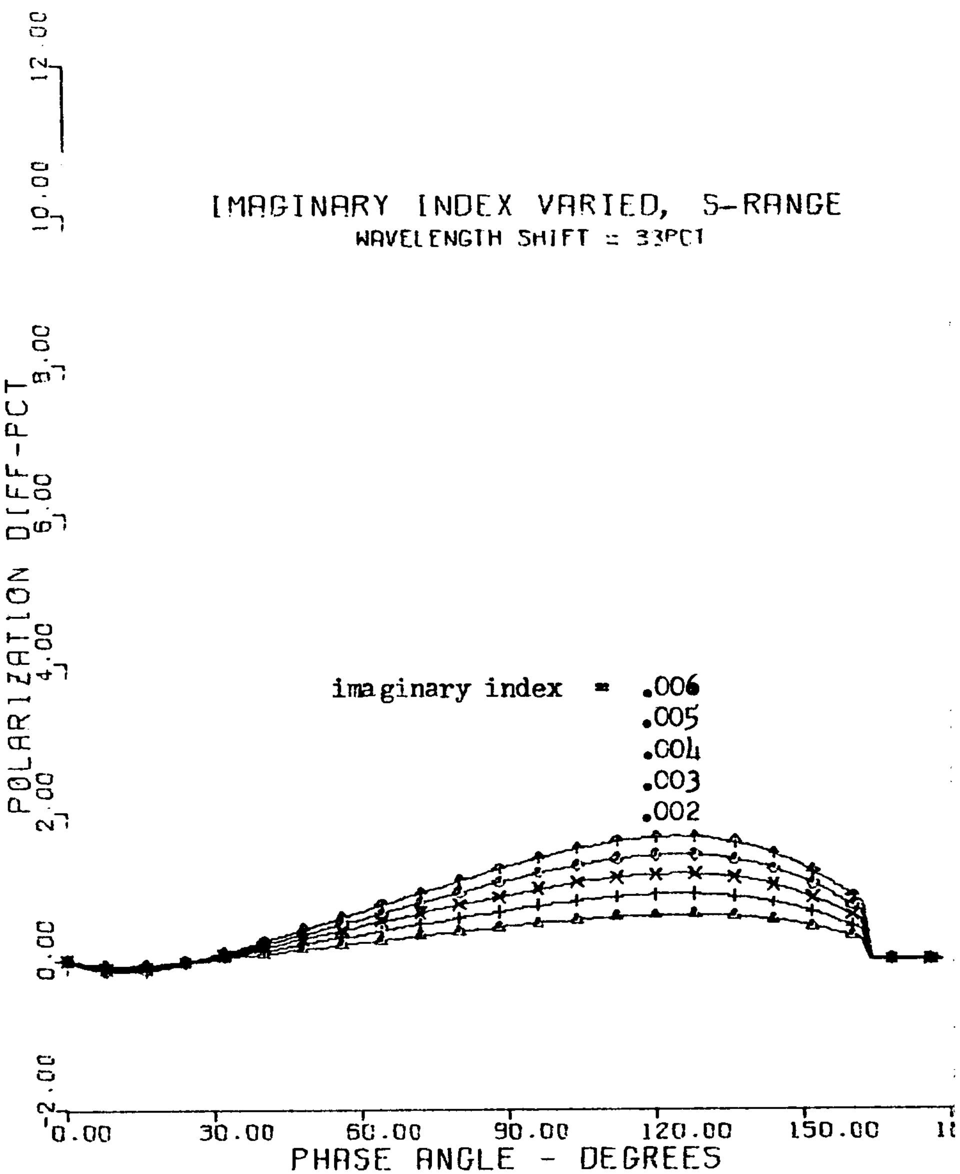

Figure 5 B. Polarization shift for a wavelength shift of 33 percent.

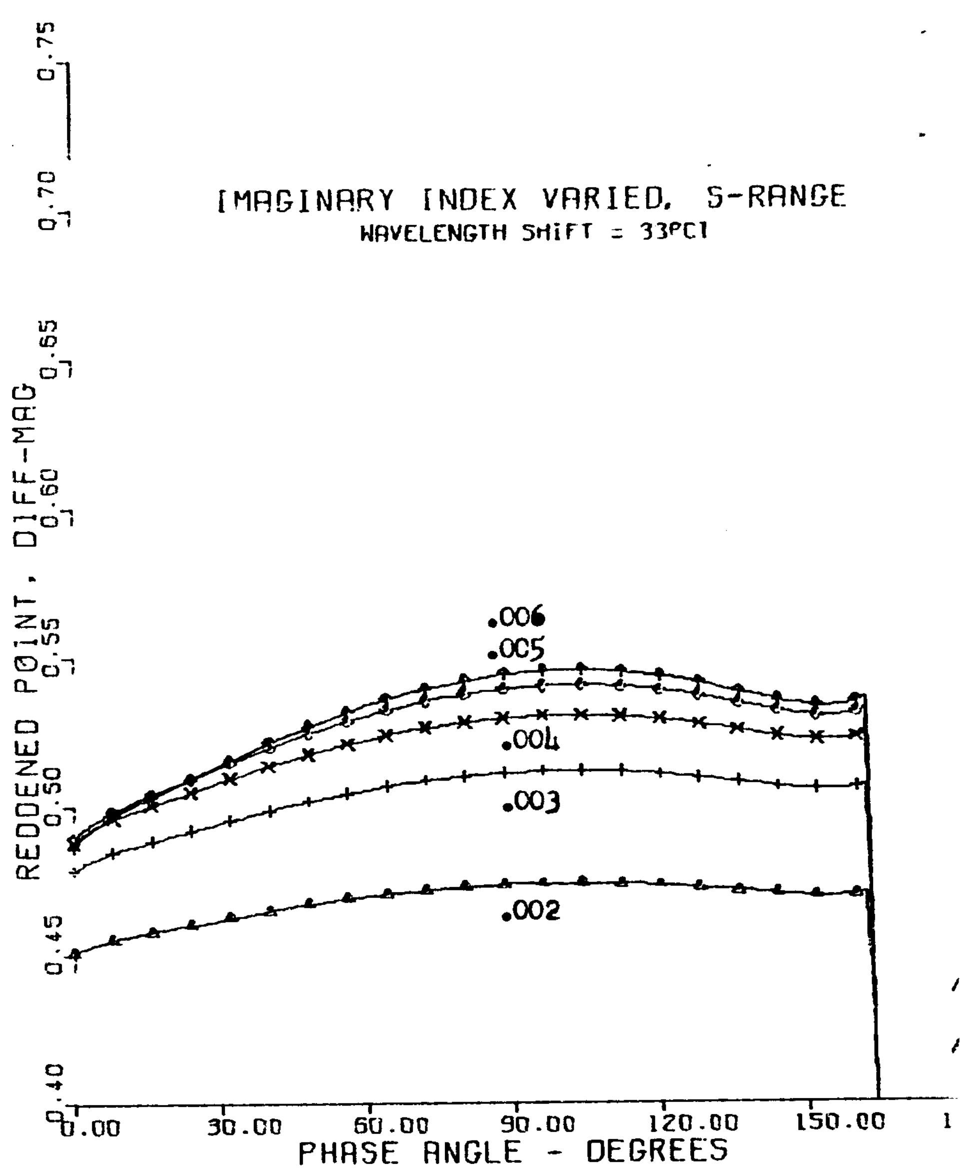

Figure 5 C. The reflectivity shift, in magnitudes, of a point on the planet, for a wavelength shift of 33 percent.

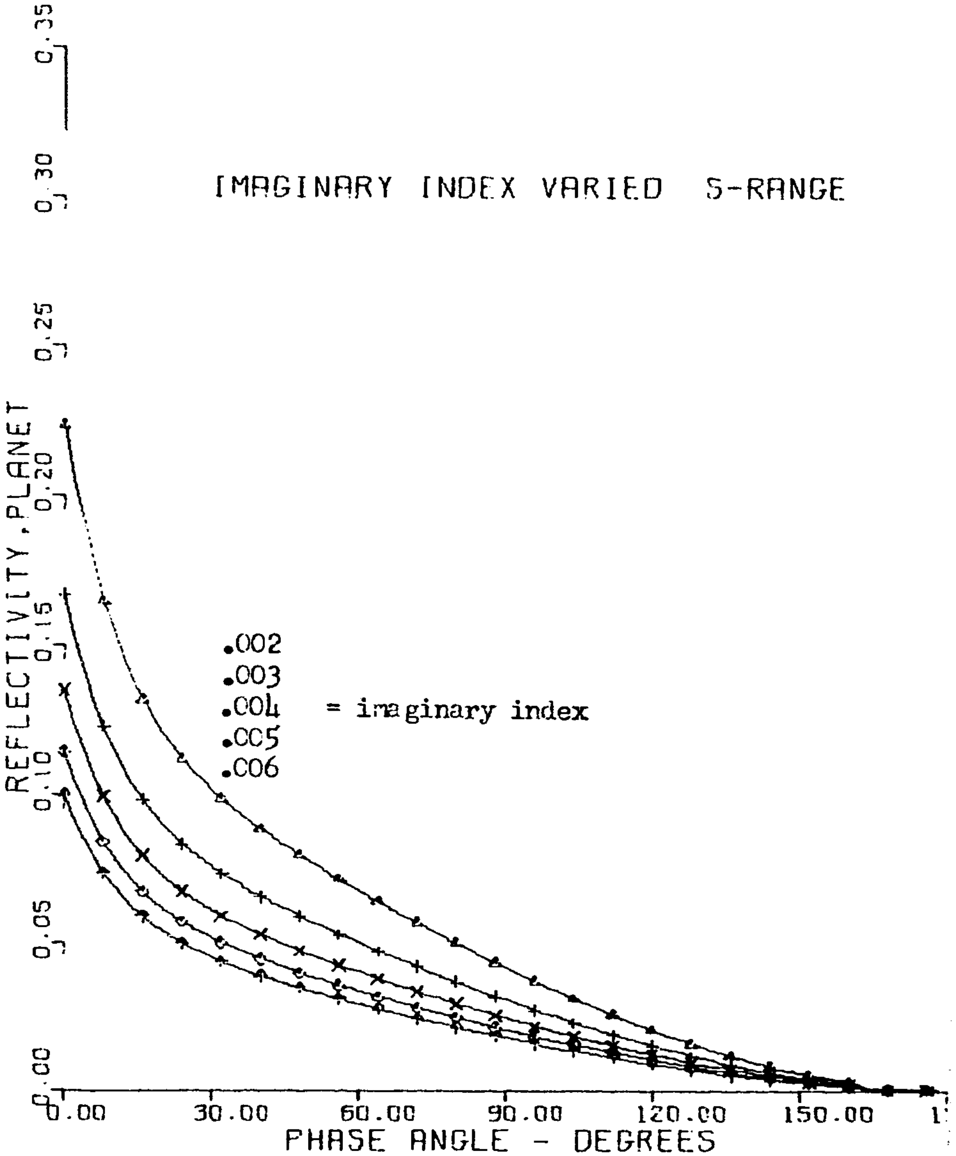

Figure 5 E. The integrated reflectivity of the entire planet.

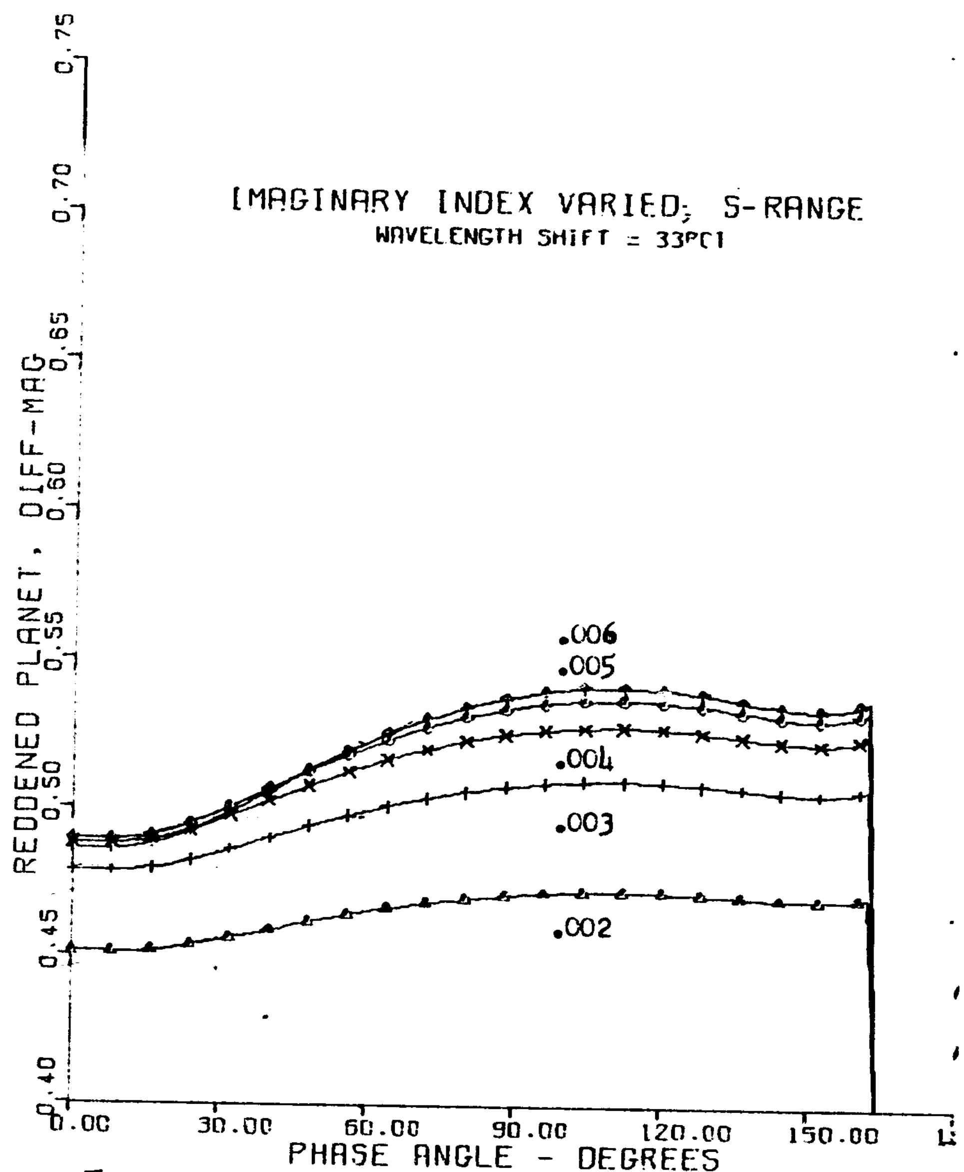

Figure 5 D. The reflectivity shift, in magnitudes, of the integrated planet, for a wavelength shift of 33 percent.

Note that the observed rule that darker bodies show greatest reddening, is reproduced by this calculation.

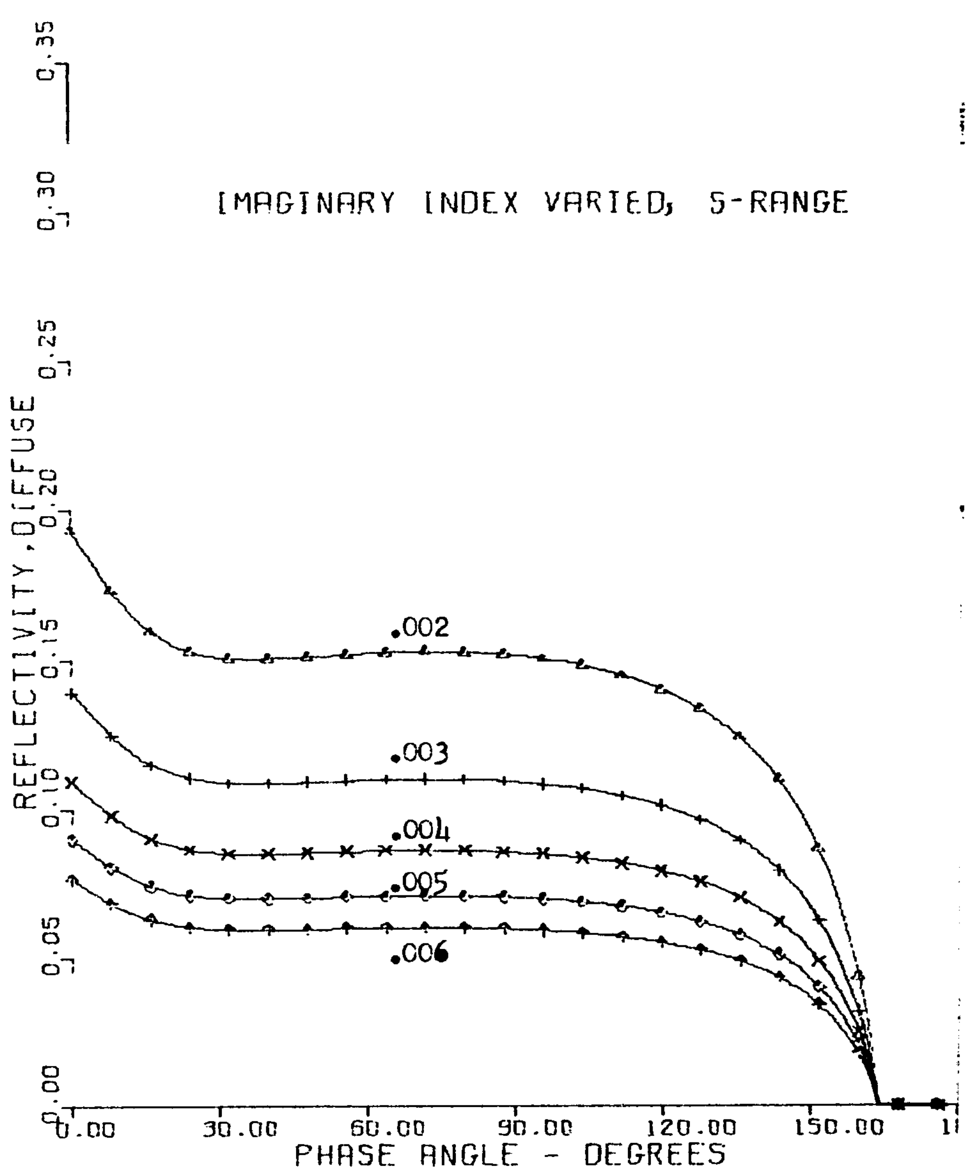

Figure 5 F. The diffuse component of light at a point on the planet. Diffuse light emerges from particles after inward refraction and multiple internal reflections.

Absorbtion of light inside the particles is increased as the imaginary index is increased.

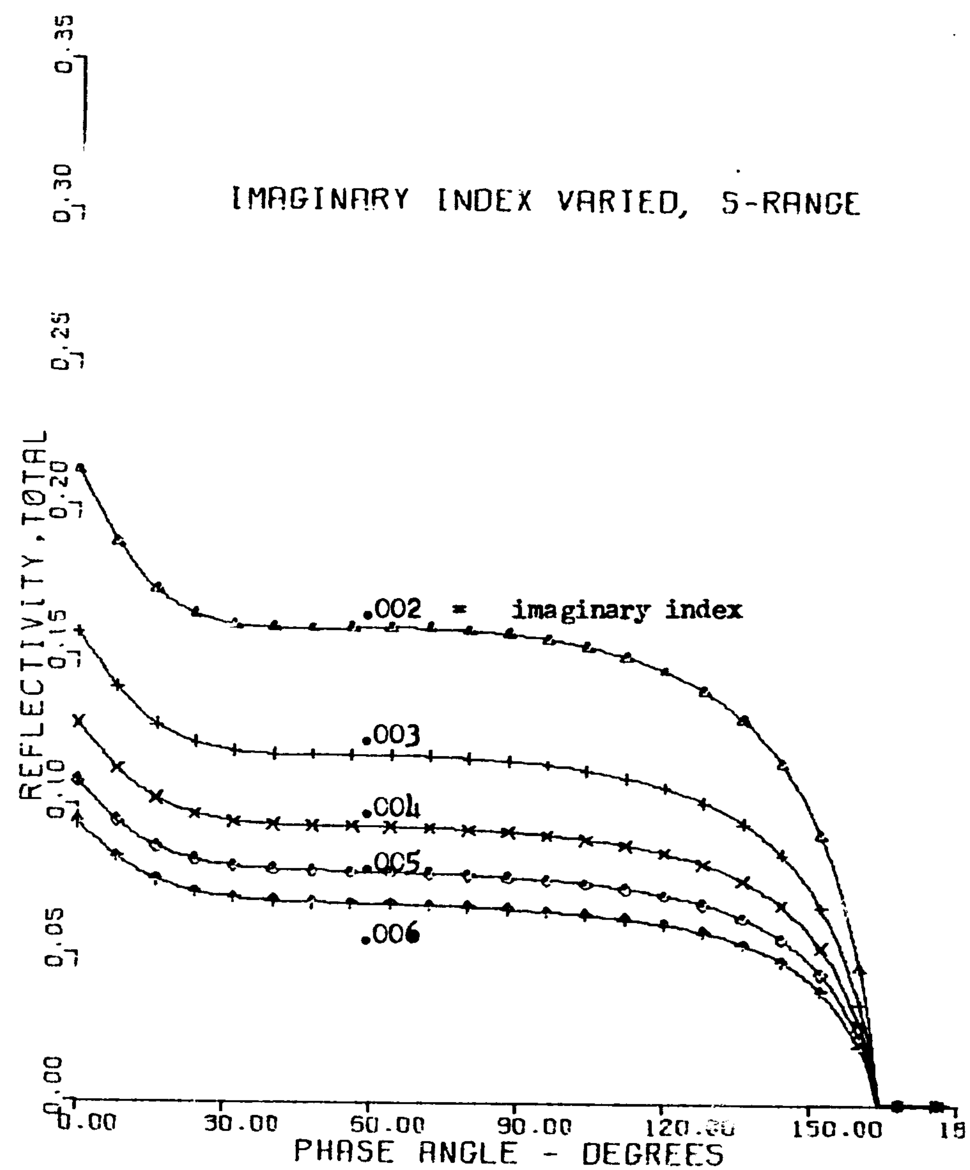

Figure 5 G. The total of all light components (singles + doubles + diffuse) at a point on the planet.

The total light is dominated by the diffuse component.

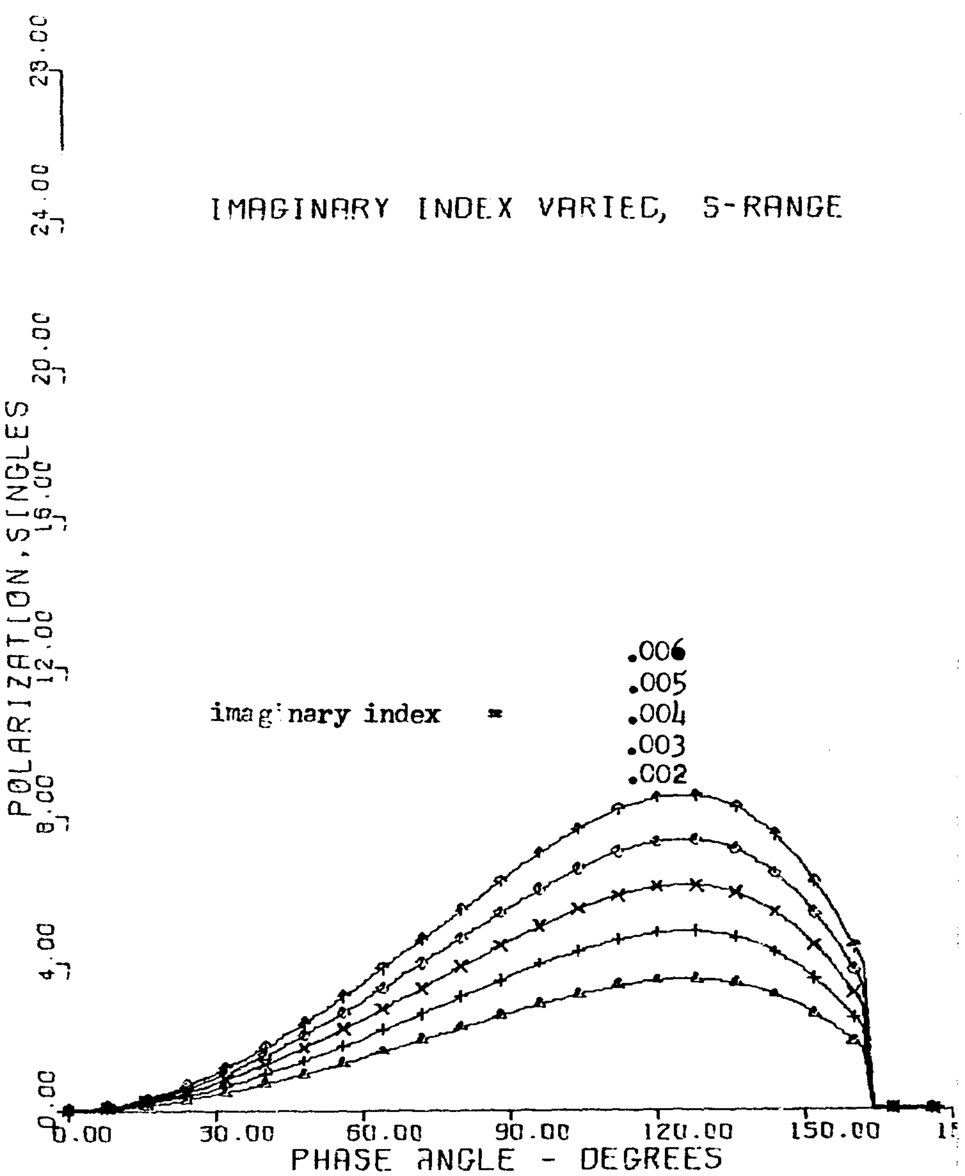

Figure 5 H. The polarization due to the singly-reflected component of light, alone.

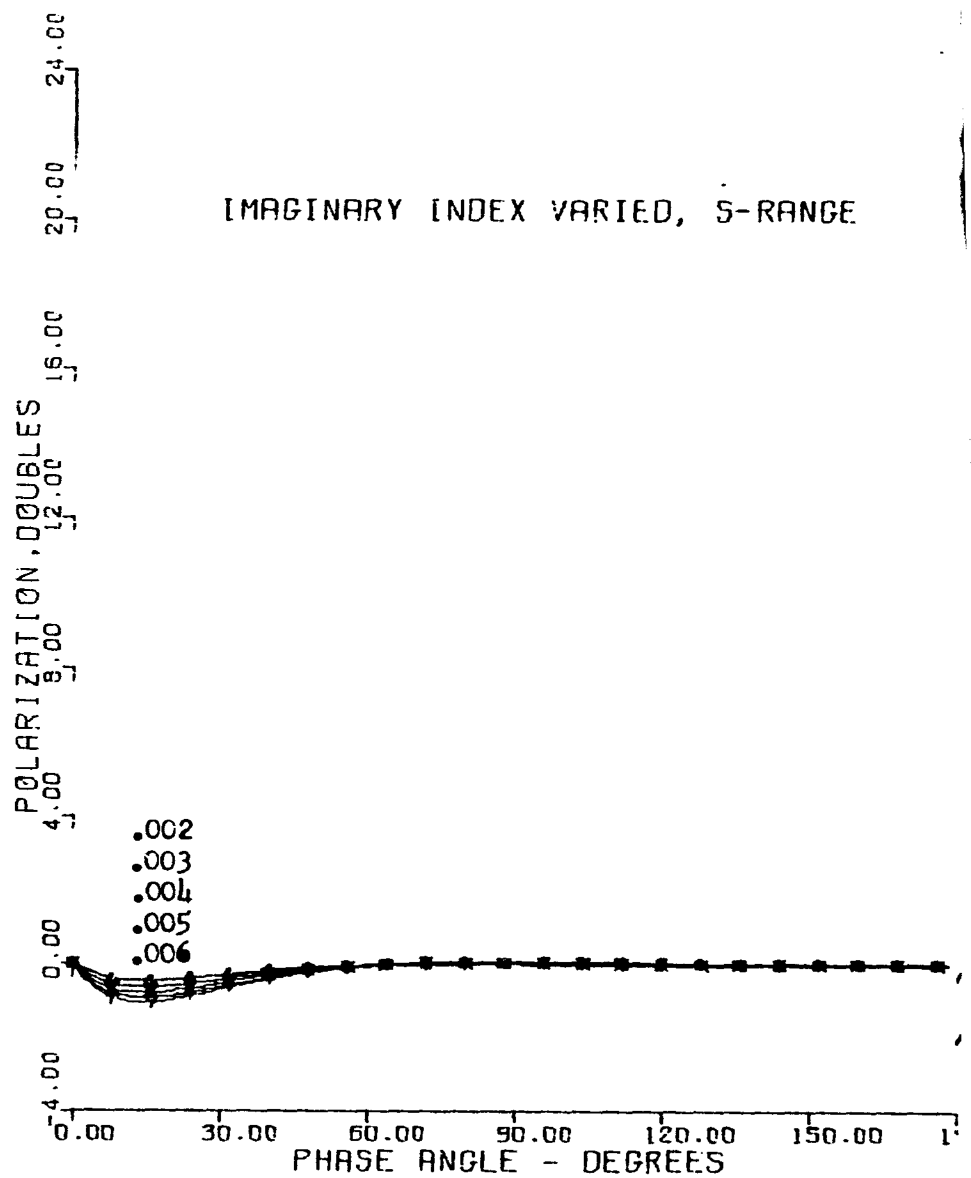

Figure 5 I. The polarization due to the doubly-reflected component of light, alone.

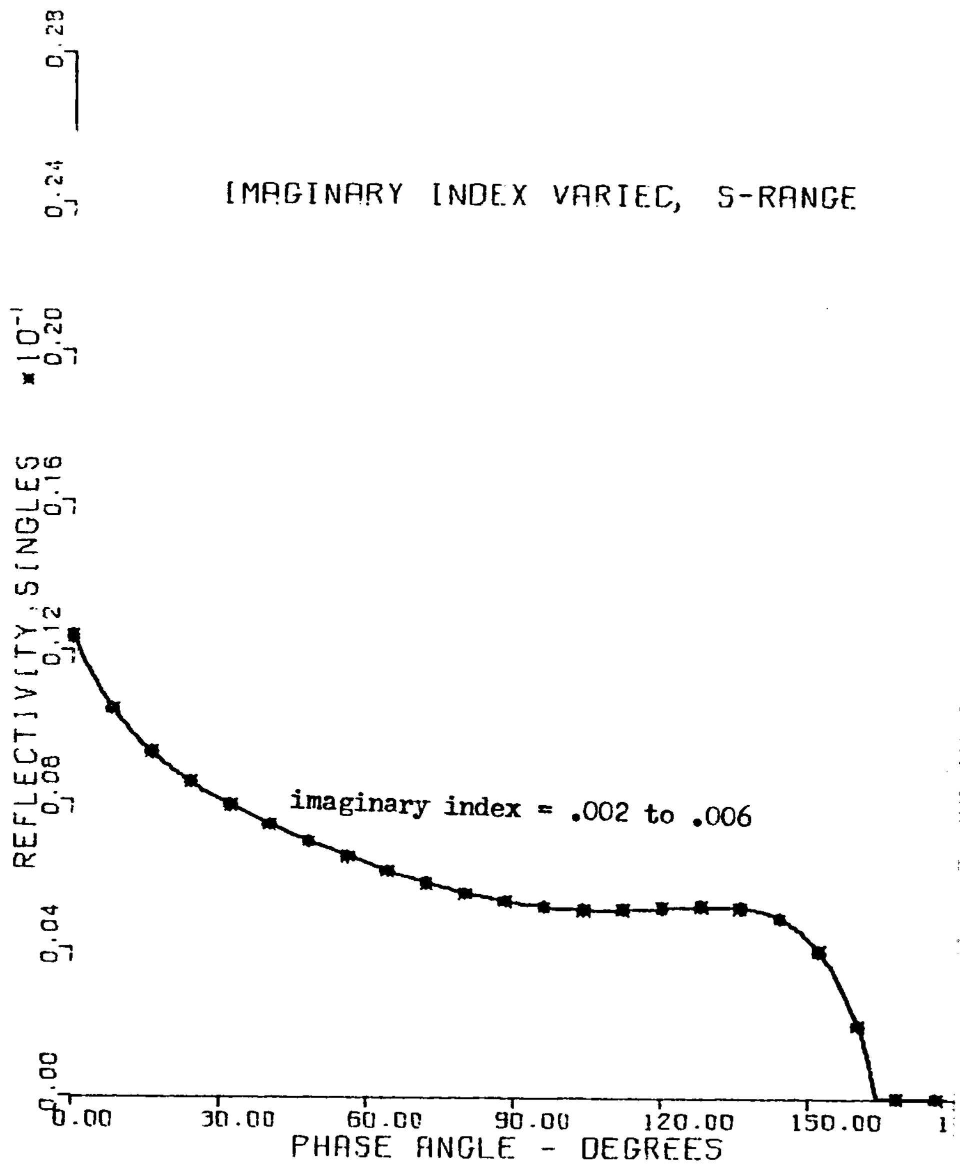

Figure 5 J. The intensity of the singly-reflected component of light.

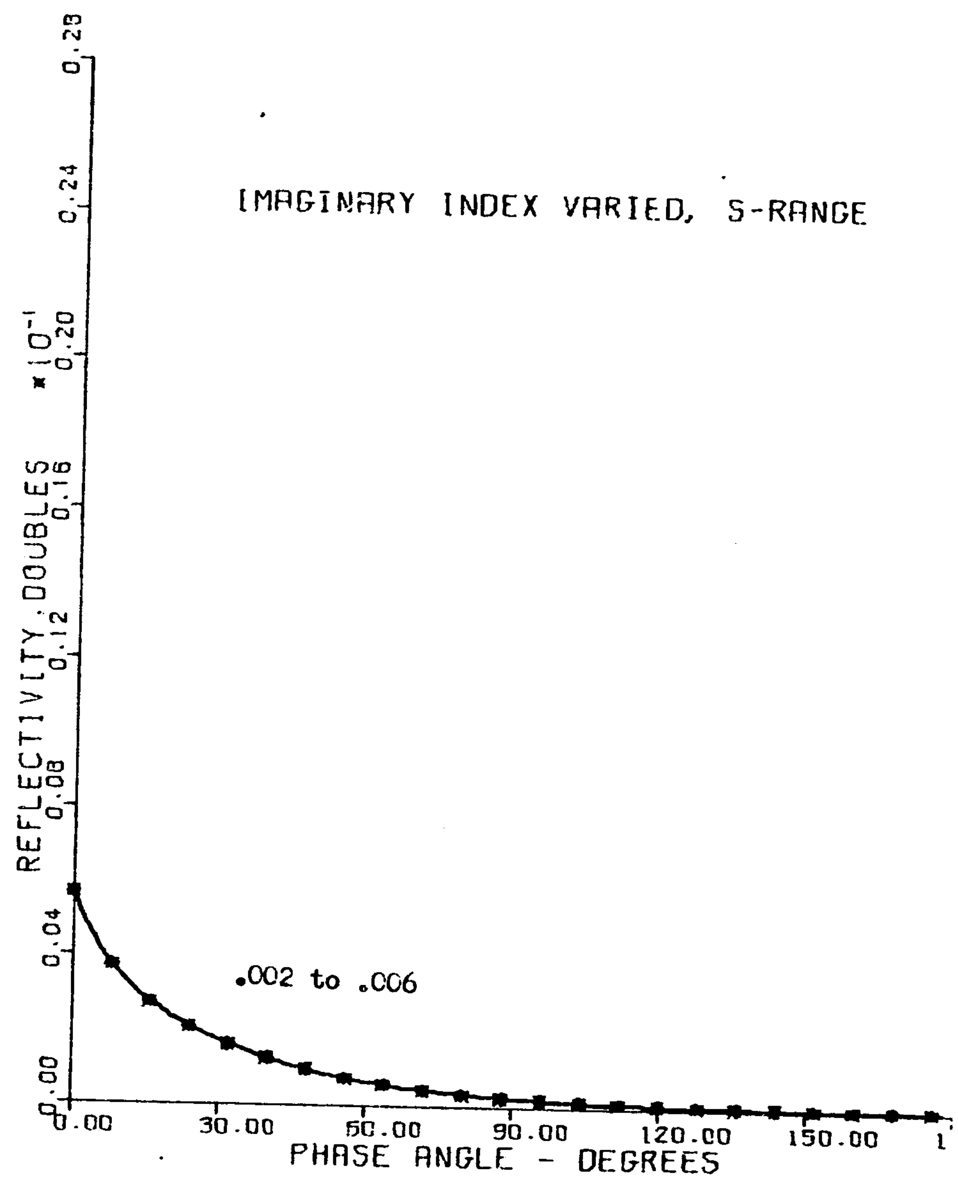

Figure 5 K. The intensity of the doubly-reflected component of light.

In these two figures, the reflected intensities are practically unchanged because the Fresnel reflectivity of the surface is hardly affected by the imaginary index which is very small compared to the real index of refraction.

IMAGINARY INDEX VARIED, C-RANGE

Figure 6 A to Figure 6 K

These figures show a range of the imaginary index which describes dark objects which may correspond to the C type asteroids of the CSM taxonomy. Features of the C asteroids - negative polarization, albedo, R/B index, and diminished absorbtion spectra - are all reproduced closely by this range of the imaginary index.

The lower reflectivity of the C objects compared to the S type arises from less diffuse light emerging from within the particles. Accordingly the expected intensity of absorbtion spectra is less.

In this range, MI affects mainly only the diffuse component of light. Just as for the S-range, MI is too small compared to the real index to appreciably affect the Fresnel reflectivity and the reflected light components.

Although scatter diagrams of the S and C asteroids show a marked discontinuity between the groups, as a function of absorbtion-dependent properties, this theoretical surface model does not. If a theoretical basis cannot be found, then an explanation must be sought in either origin or material of the two asteroid groups.

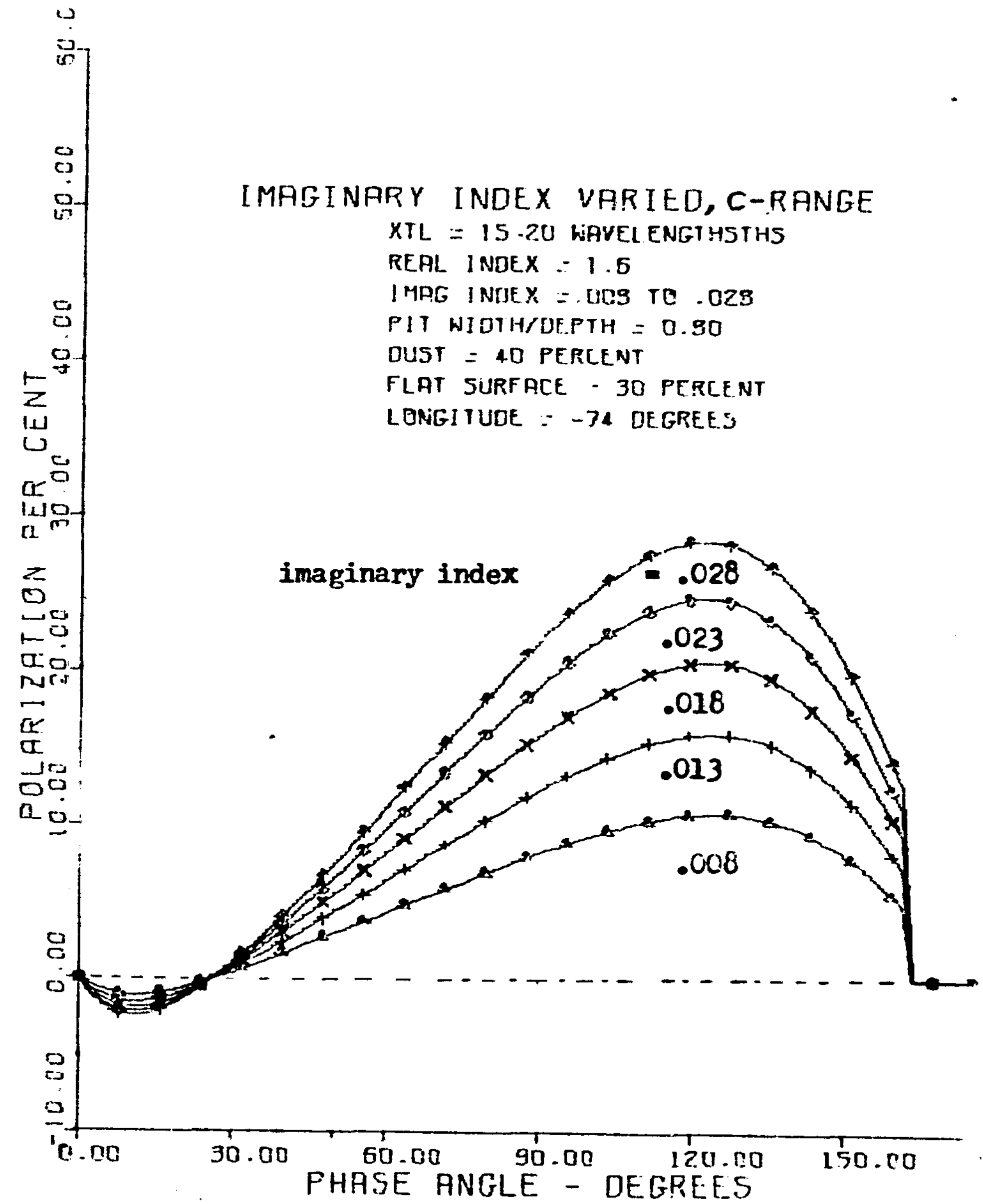

Fig 6 A. Polarization at a point on a planet.

The values of P-min and the inversion point match those of the C asteroids.

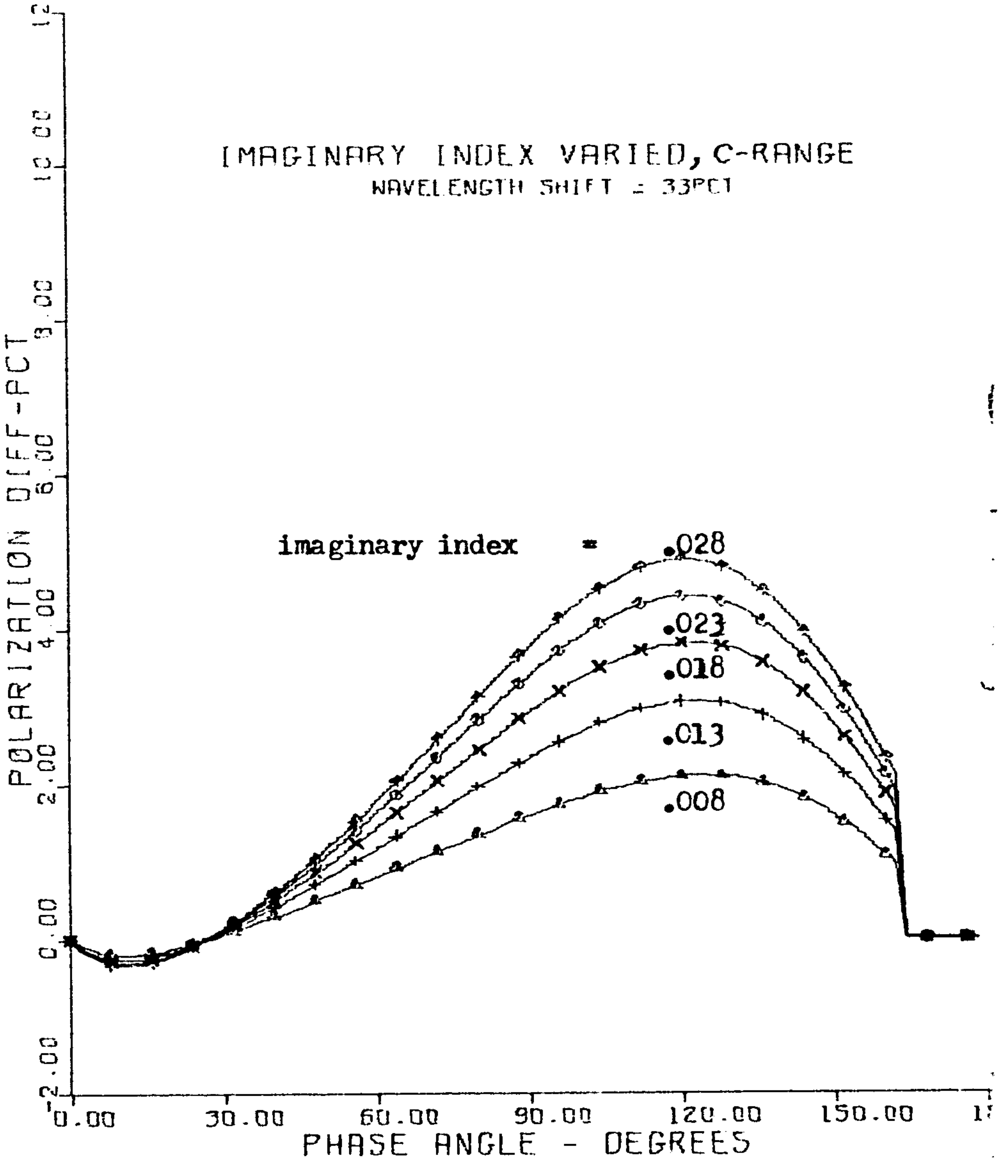

Figure 6 B. Polarization shift for a wavelength shift of 33 percent.

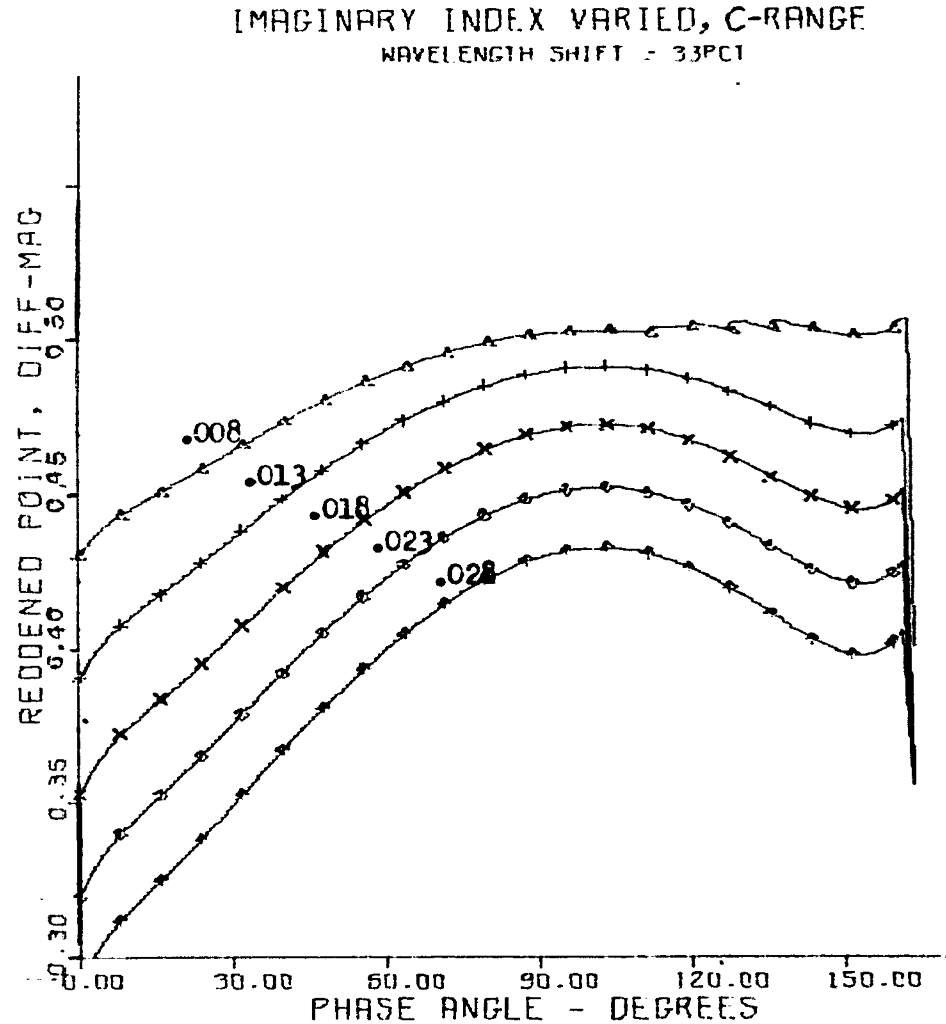

Figure 6 C. The reflectivity shift, in magnitudes, of a point on the planet, for a wavelength shift of 33 percent.

Note that the reddening (slope of reflectivity) increases when the imaginary index increases. This accords with the rule : darker bodies show greater reddening.

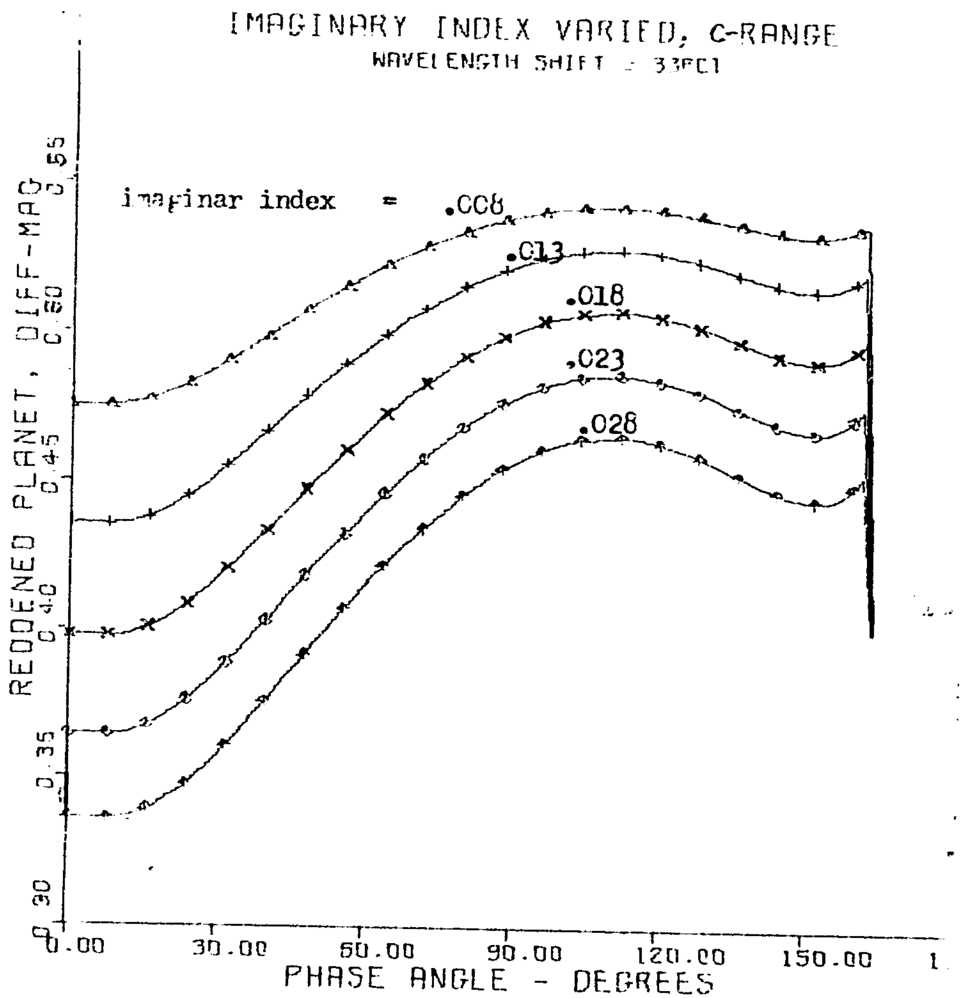

Figure 6 D. The reflectivity shift, in magnitudes, for a wavelength shift of 33 percent, of the integrated planet.

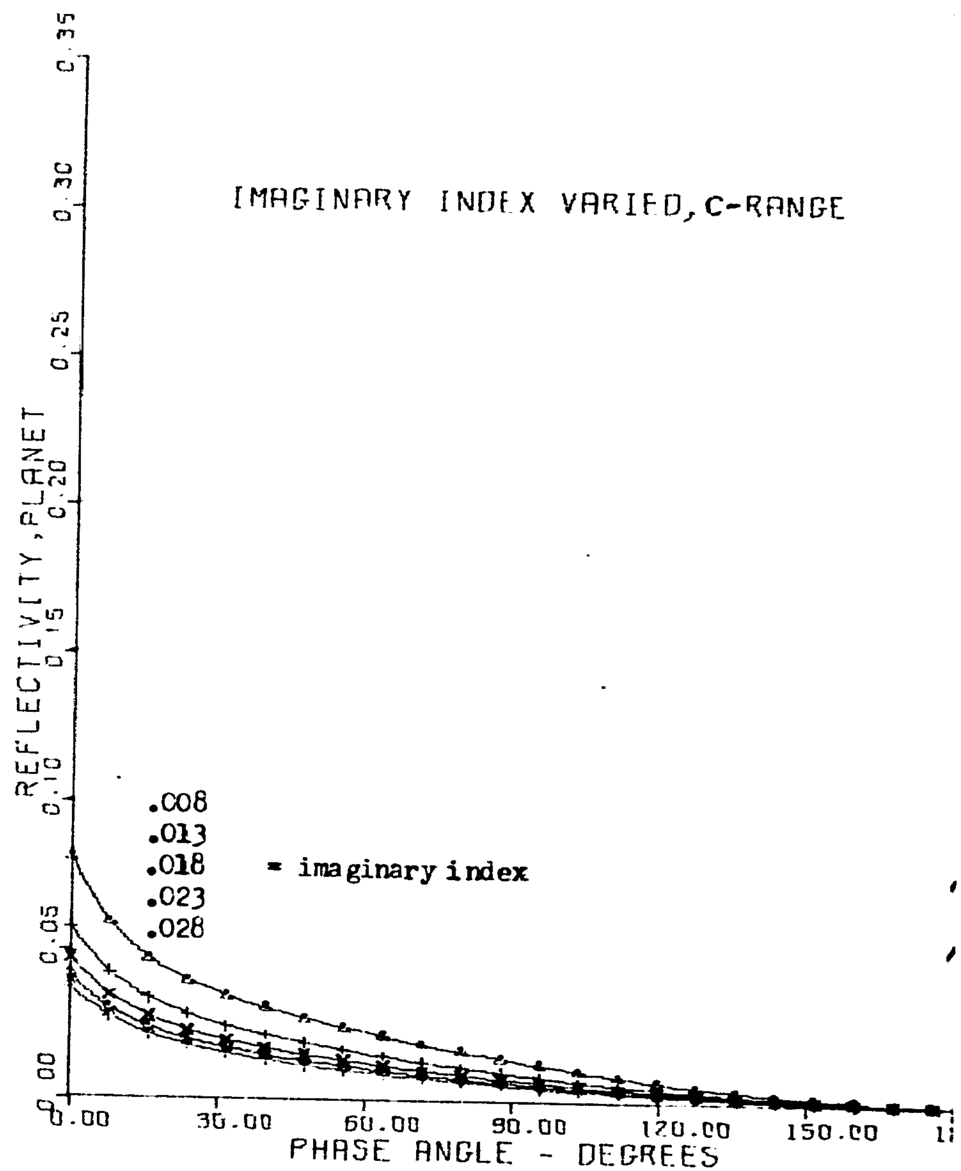

Figure 6 E. The integrated reflectivity of the entire planet.

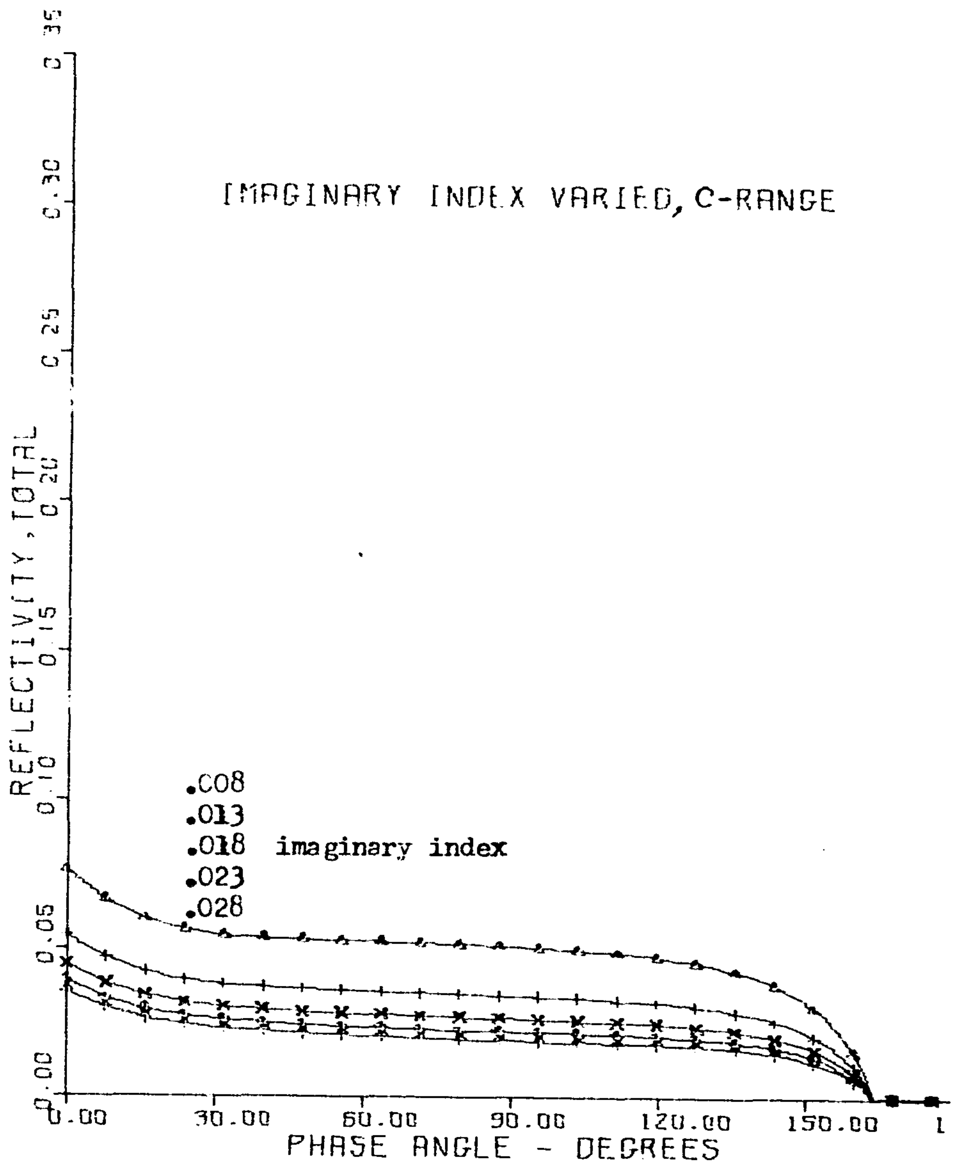

Figure 6G. The total of all light components (singles + doubles + diffuse) at a point on the planet.

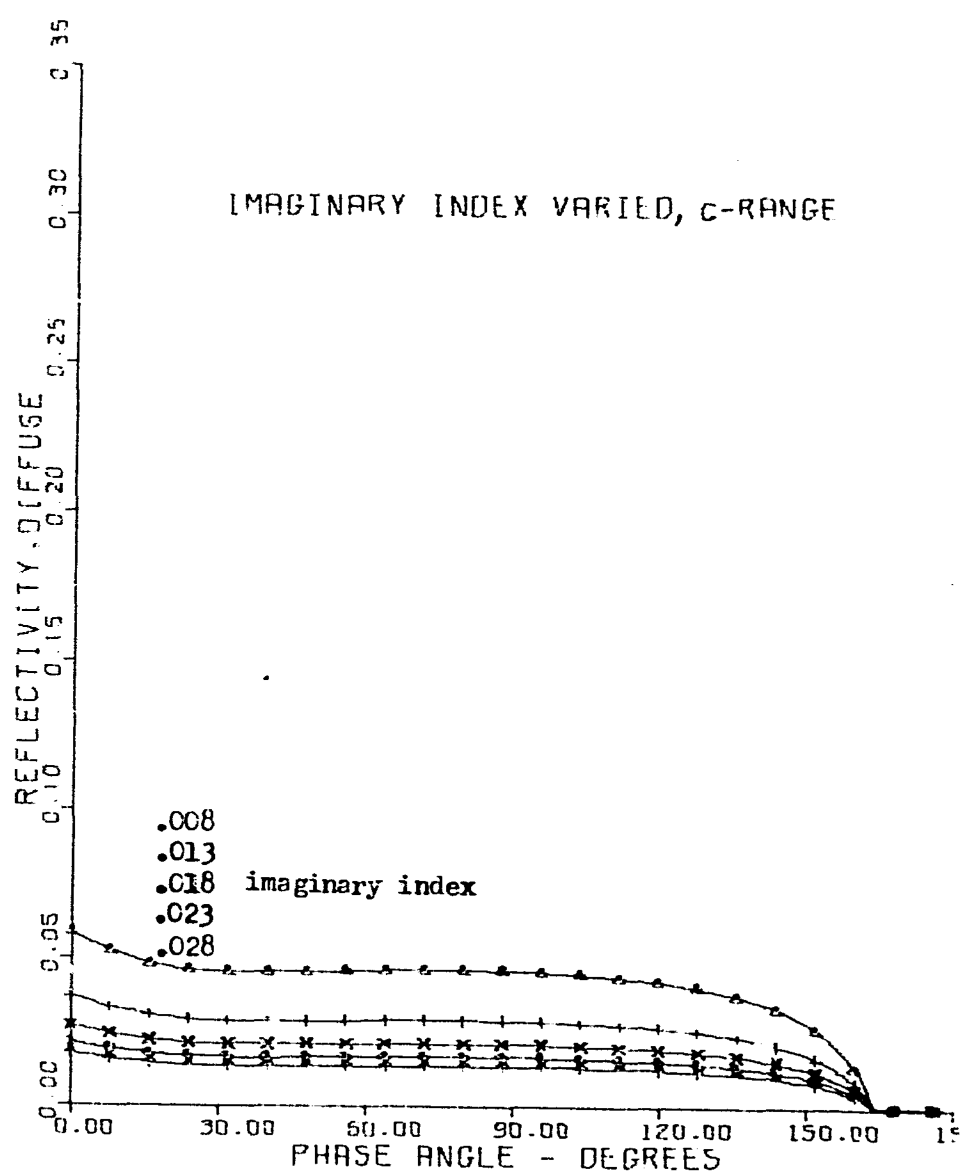

Figure 6F. The diffuse component of light at a point on the planet.

The imaginary index causes the absorbtion of light while it is traveling inside of the particles, so the diffuse light component is reduced. The reflected components are not affected however, because the index is still too small.

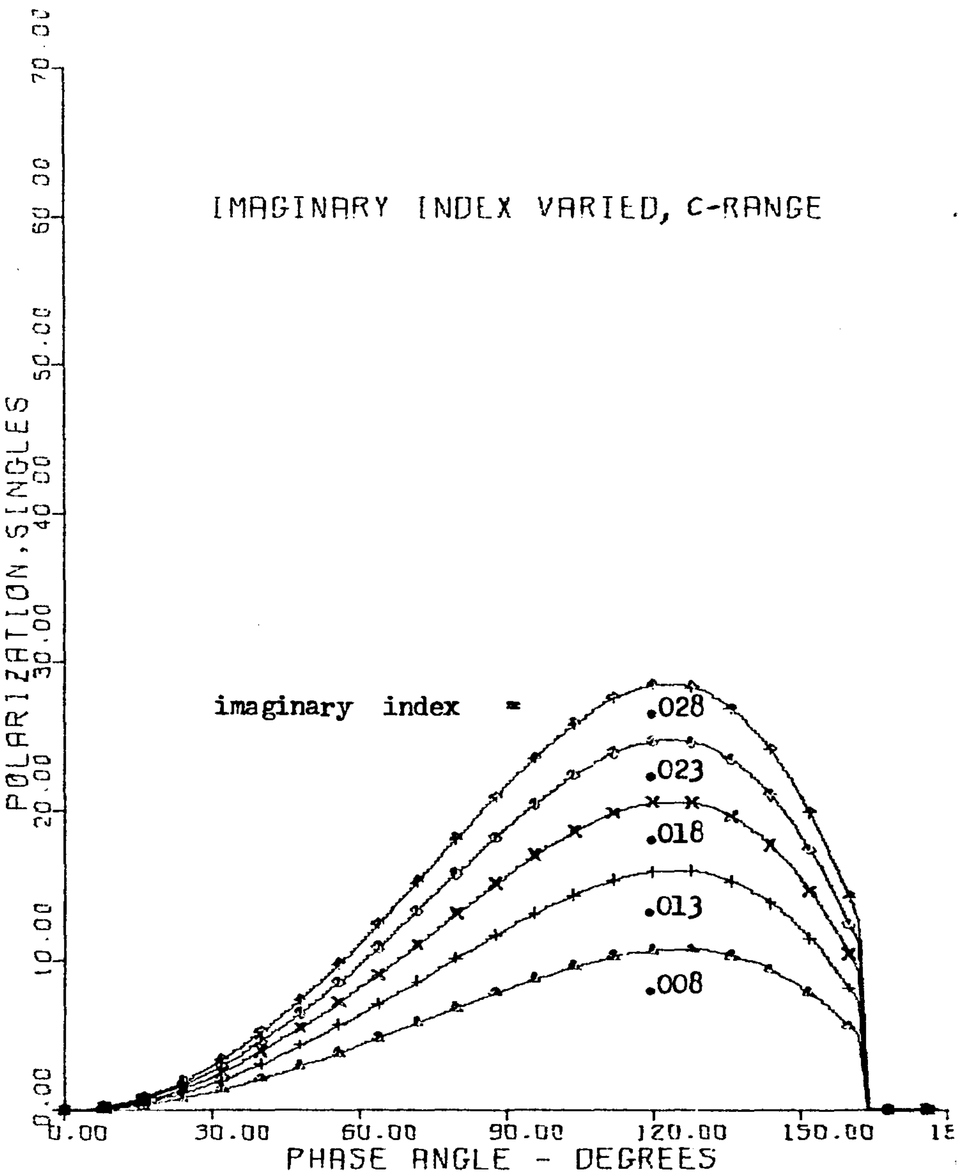

Figure 6 H. The polarization due to the singly-reflected component of light, alone.

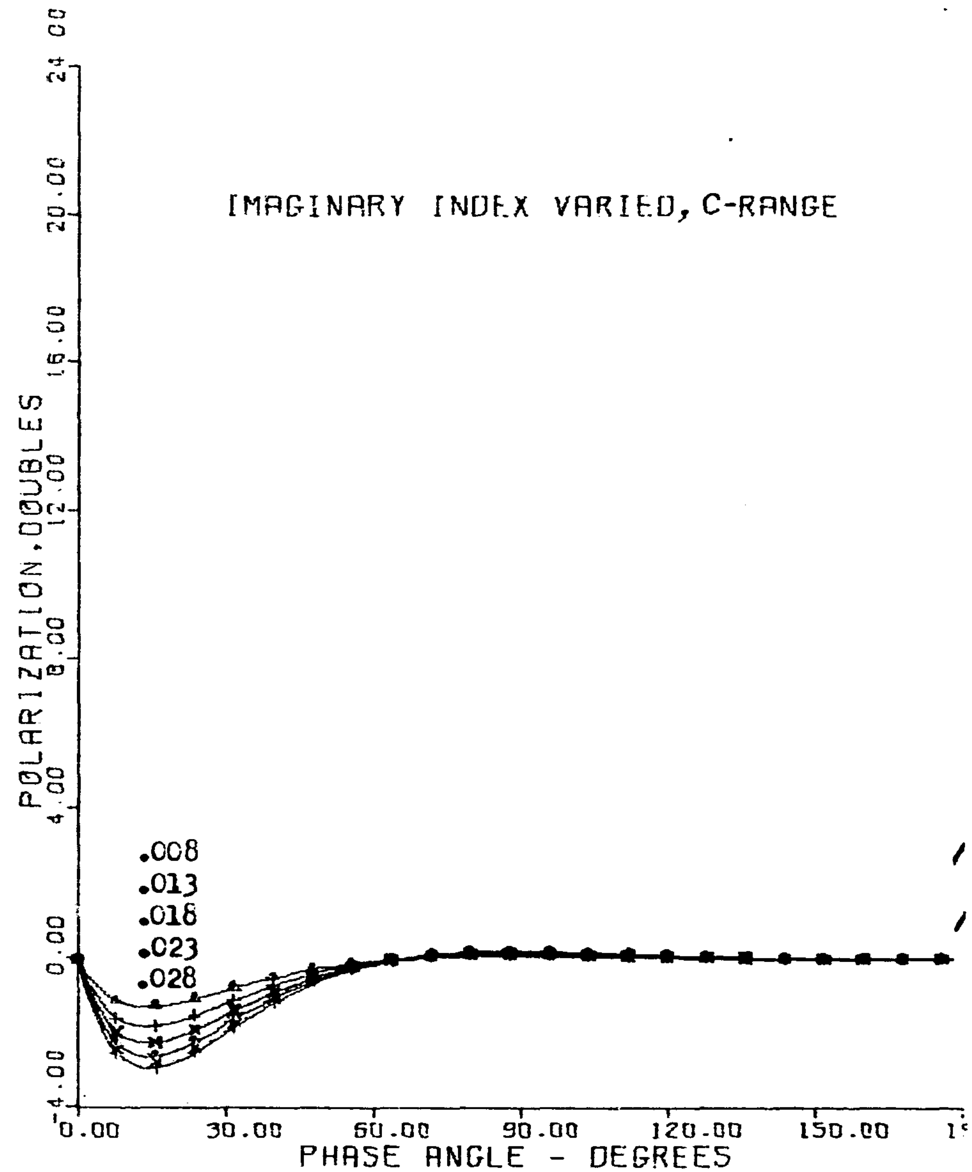

Figure 6 I. The polarization due to the doubly-reflected component of light, alone.

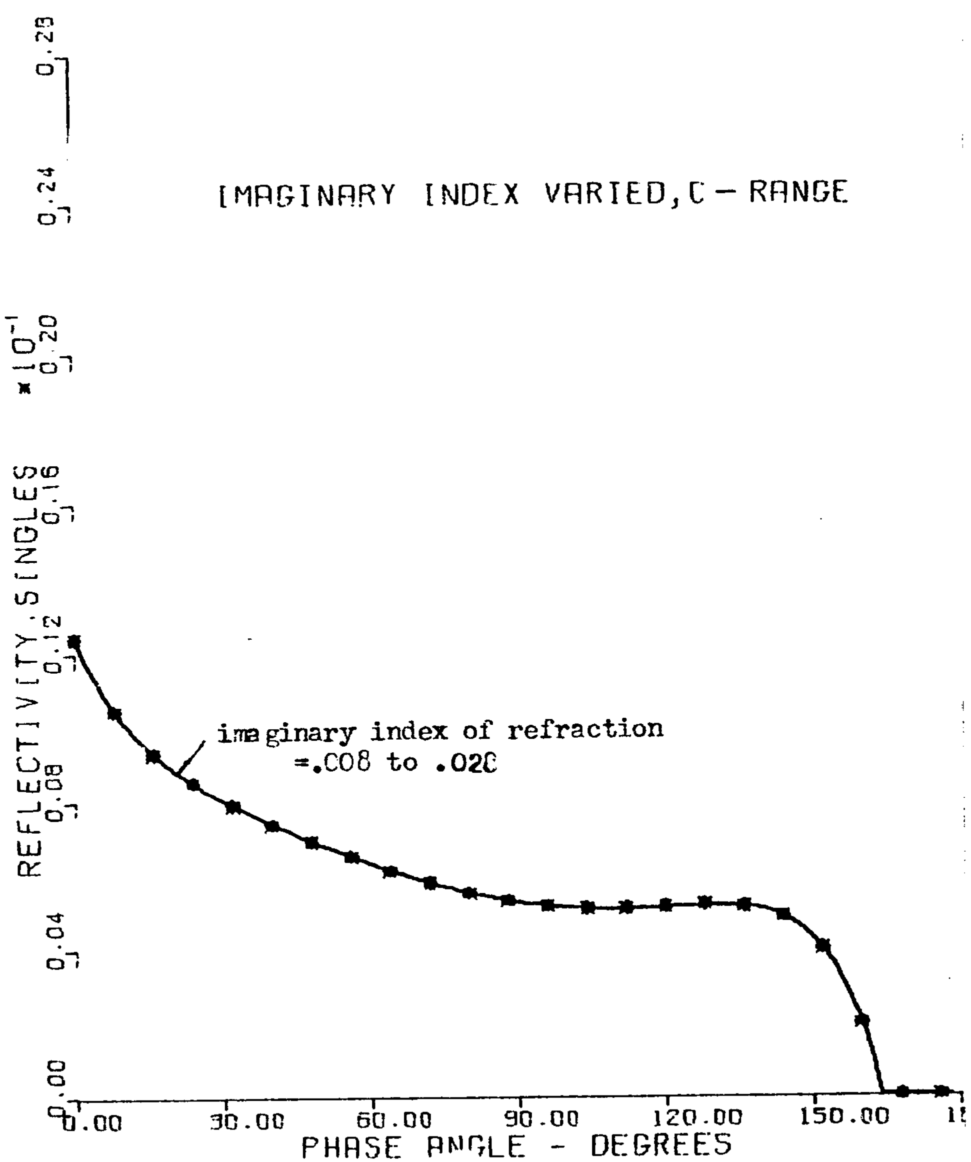

Figure 6 J. The intensity of the singly-reflected component of light.

There is no change of the Fresnel reflectivity in this range because the index is too small compared to the real index of refraction.

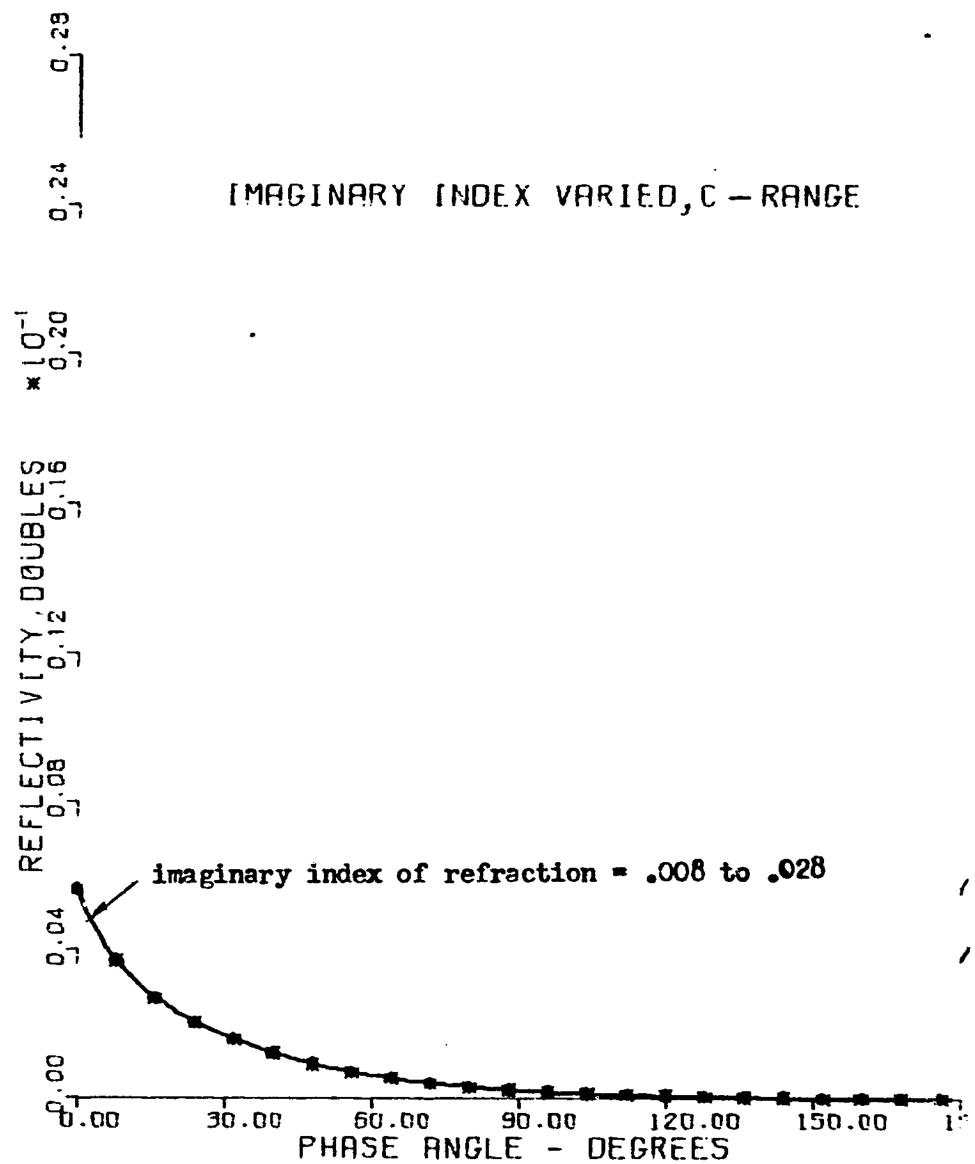

Figure 6 K. The intensity of the doubly-reflected component of light.

IMAGINARY INDEX (MI) VARIED, CM RANGE
Figure 7A to Figure 7K

These figures describe a group of very dark objects with a wide range of MI, .02 to 0.32. This range deliberately crosses from the C-range into the M-range in order to illustrate the unusual reflectivity minimum which occurs at MI equal to about 0.1 and accompanied by an inversion of several other measureables. This might be regarded as a natural boundary between the C and M groups, however there appears to be no reason to expect a discontinuity in the occurence of objects on scatter diagrams. Indeed, no such discontinuity is observed.

Near the value of 0.1, the imaginary index affects the diffuse light and the Fresnel reflectivity about equally; at this point the former is increasing and the latter is decreasing. This point will be termed the "CM boundary index" , as it marks the change from very dark mineral to metallic substances.

At the CM boundary, dominance of reflectivity passes from diffuse light, which will drop to zero as index is increased, to reflected light which will increase towards 100%, as a pure metallic condition is approached.

In a wholly pitted surface of a metallic body, double reflection probability greatly exceeds the probability for singles, and, as the reflectivity approaches one, the handicap of double attenuation at each surface is less severe. Therefore, one could expect a very large negative branch - as large as the positive - if any asteroids were wholly metallic. Such large negative branches have not been observed. It must be concluded that they do not exist, or if they do, their surfaces are not heavily pitted.

Obviously, near the CM Boundary Index, the Slope-albedo Rule (and also P-min or P-max Rules) totally fail. Further more, when MI is on the large side of 0.1, these rules have an entirely different proportion.

The mistaken use of the Albedo-polarization Rules near and higher than the CM Boundary Index would result in mistkenly placing M and E objects into the C group. It might be that reddening measurements could identify these cases, if theyexist.

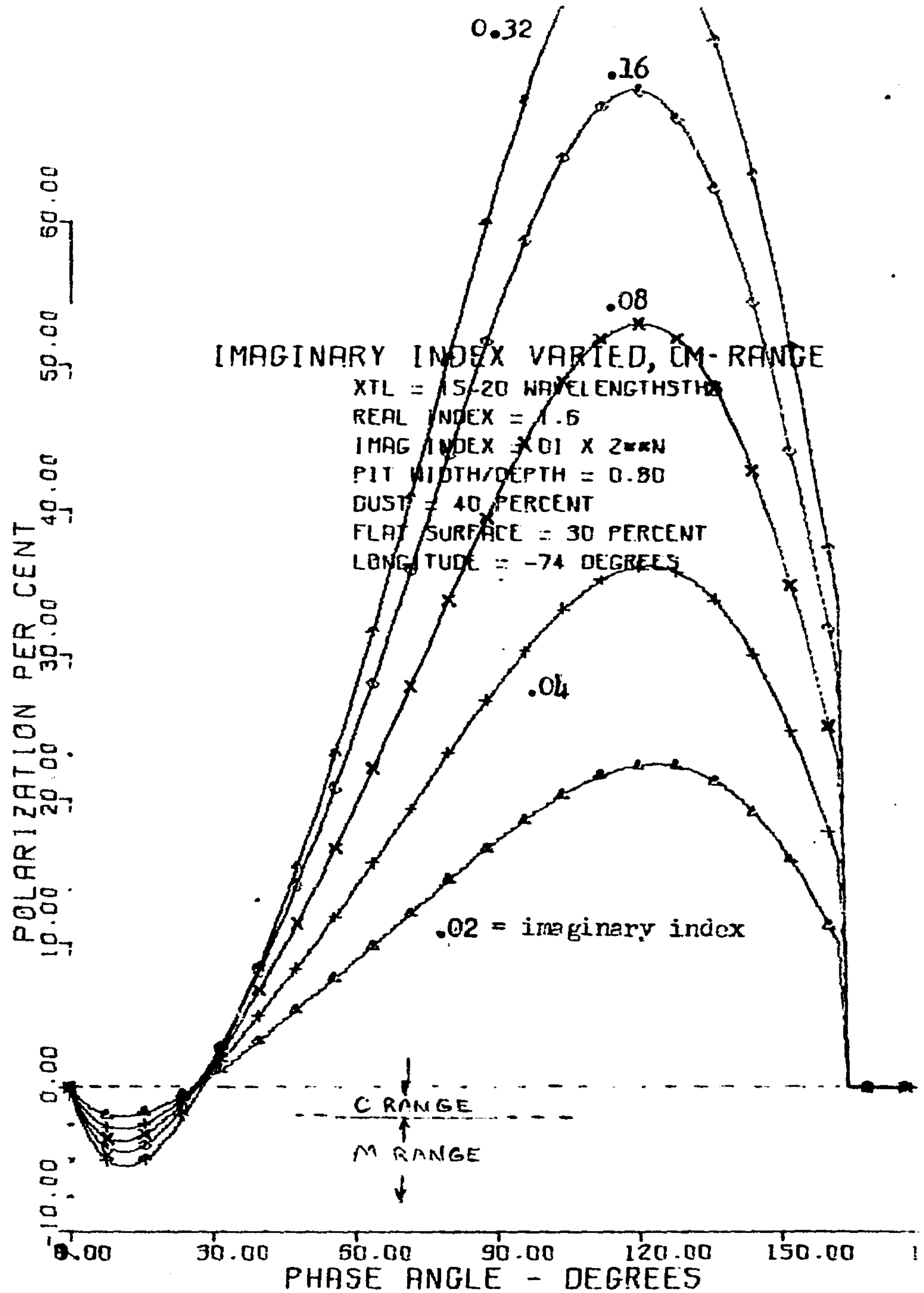

Figure 7 A. Polarization of a point on a planet.

NOTE THAT THE POLARIZATION SCALE IS MUCH LARGER ON THIS FIGURE THAN THE OTHERS.

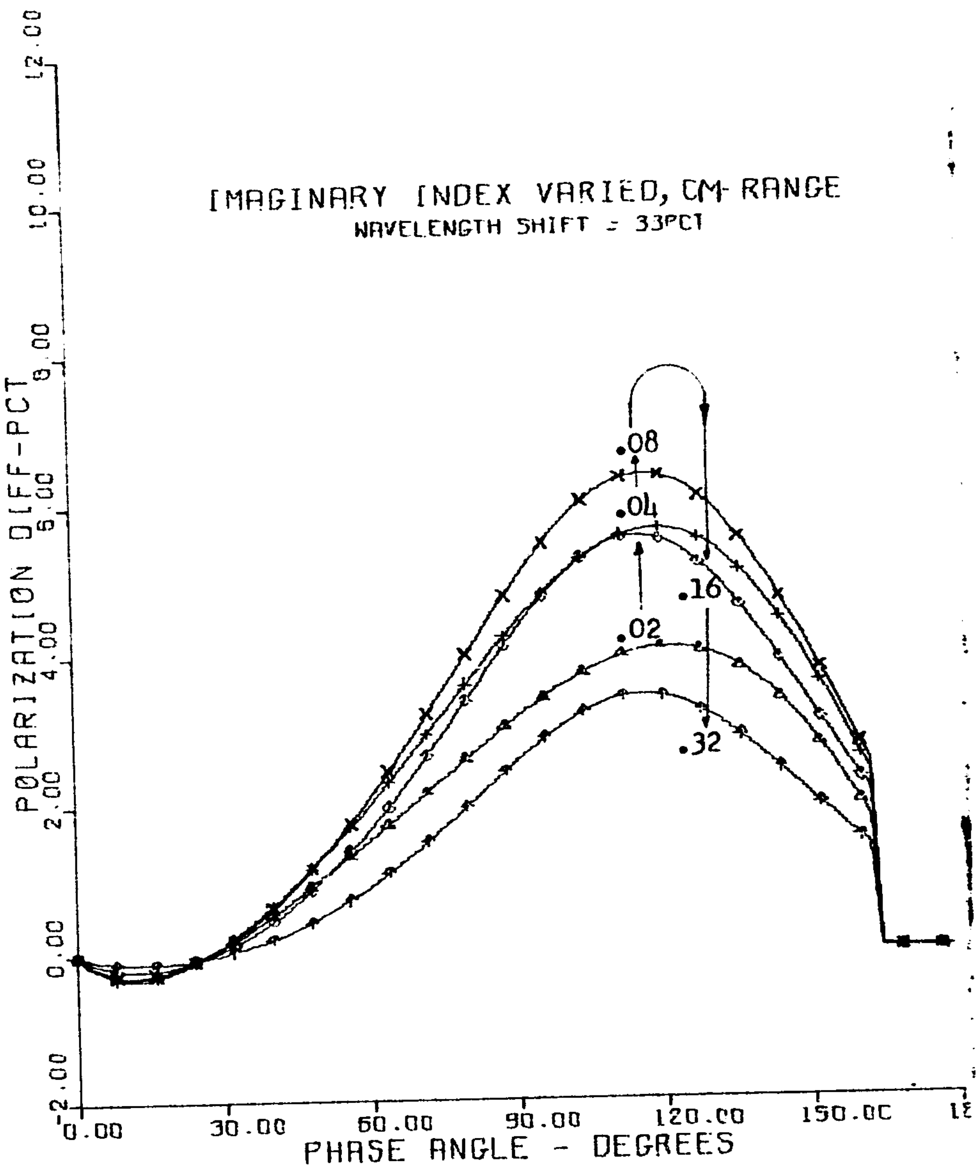

Figure 7 B. Polarization shift for a wavelength shift of 33 percent.

The inversion at the CM Boundary Index (.10) is clearly seen in this figure.

The reflectivity shift, in magnitudes, of a point on the planet, for a wavelength shift of 33 percent. The inversion here is in the slope.

FIGURE 7 C.

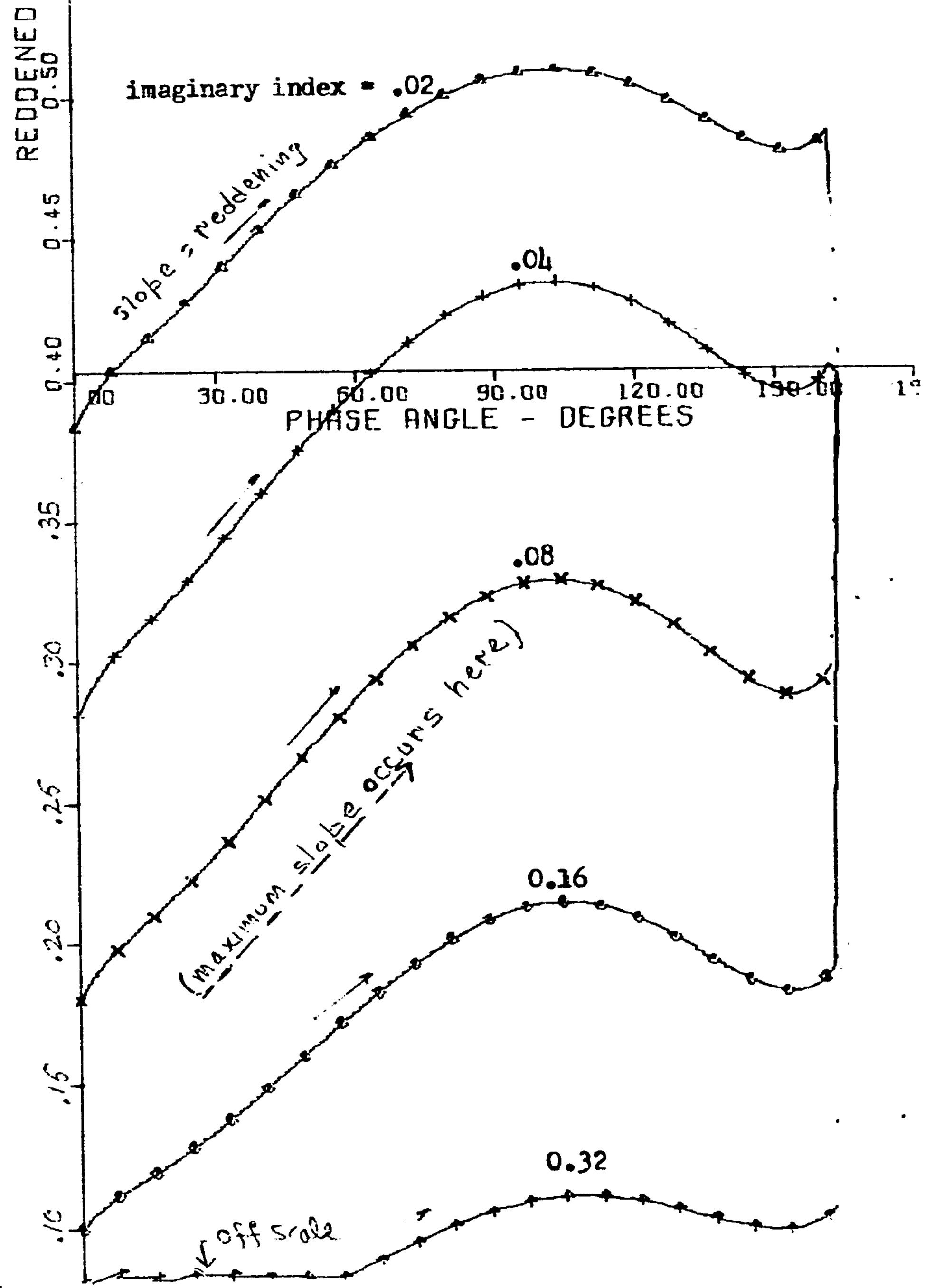

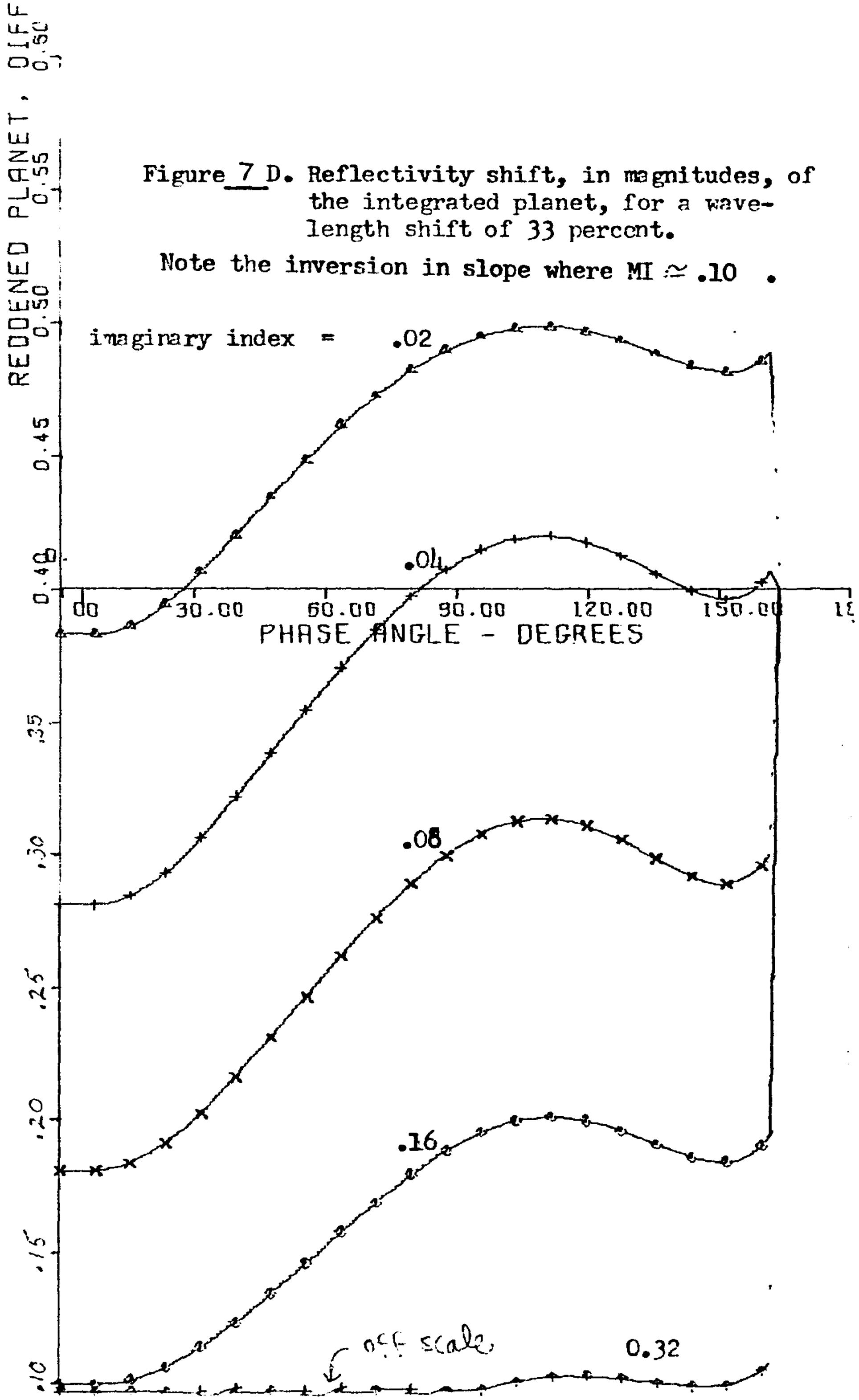

Figure 7 D. Reflectivity shift, in magnitudes, of the integrated planet, for a wave-length shift of 33 percent.

Note the inversion in slope where MI $\simeq$ .10 .

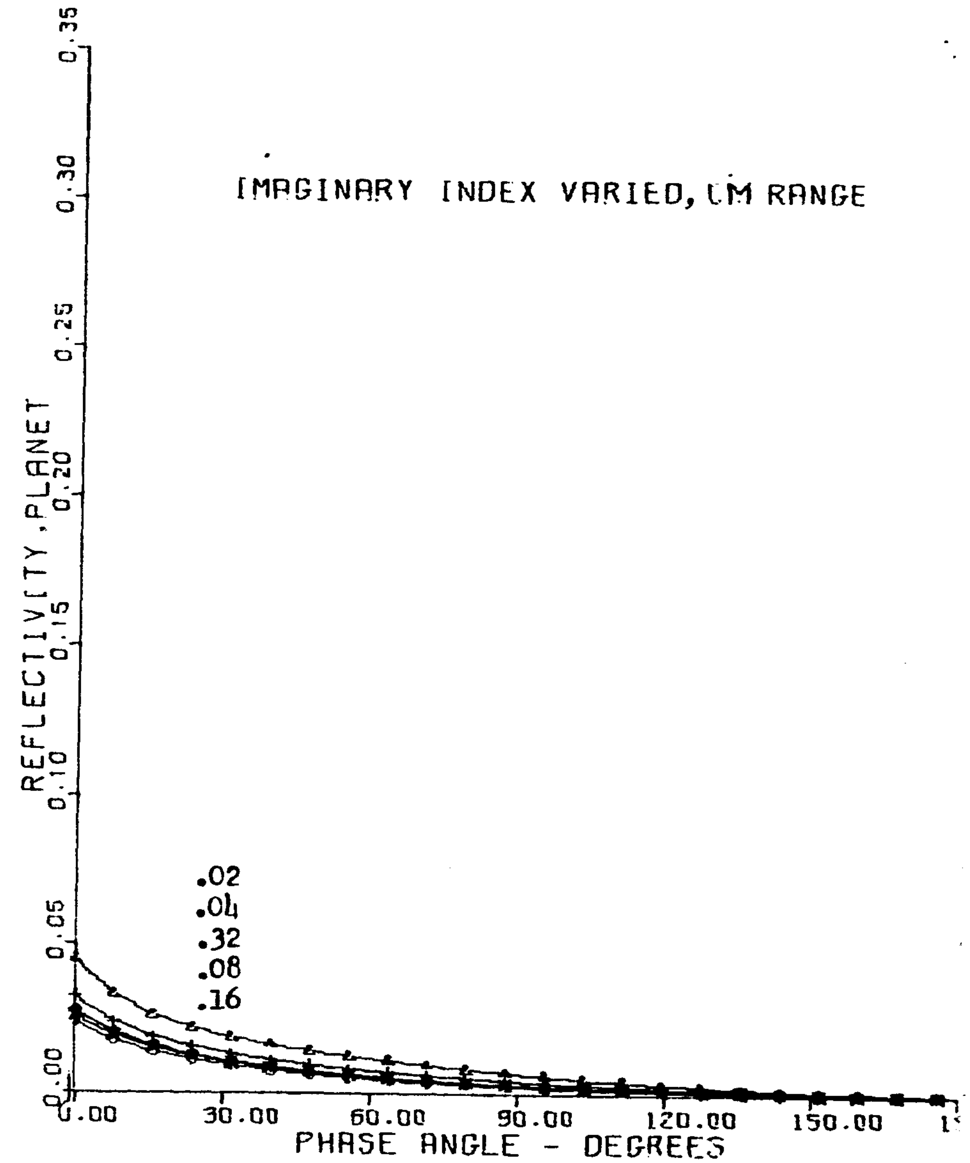

Figure 7 E. The integrated reflectivity of the entire planet.

Note that there is a reversal for MI larger than .016 ; the added reflectivity due to increased specular reflection has become larger than the loss of diffuse light.

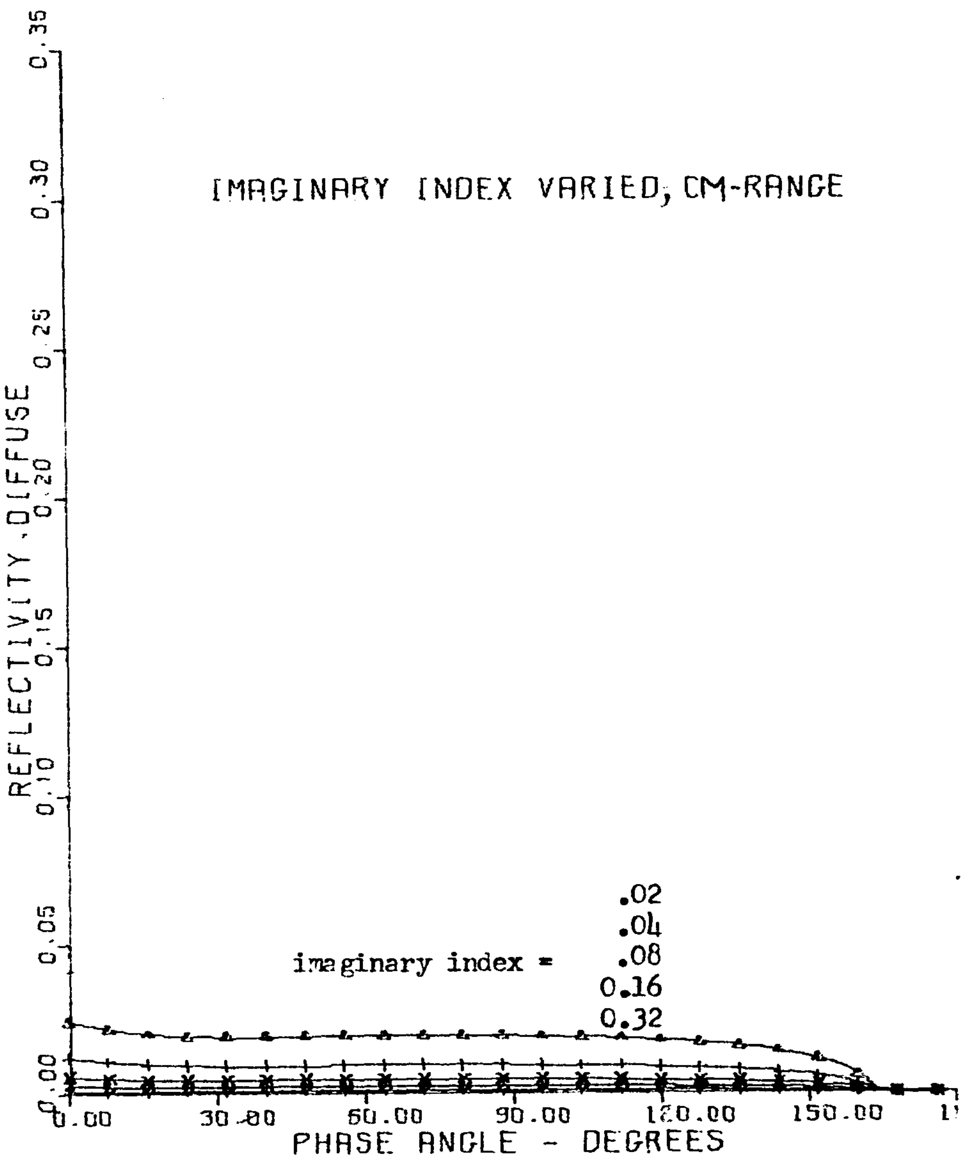

Figure 7 F. The diffuse component of light at a point on the planet.

The absorbtion becomes so large inside the particles for large MI (imaginary index) that the diffuse light is practically zero.

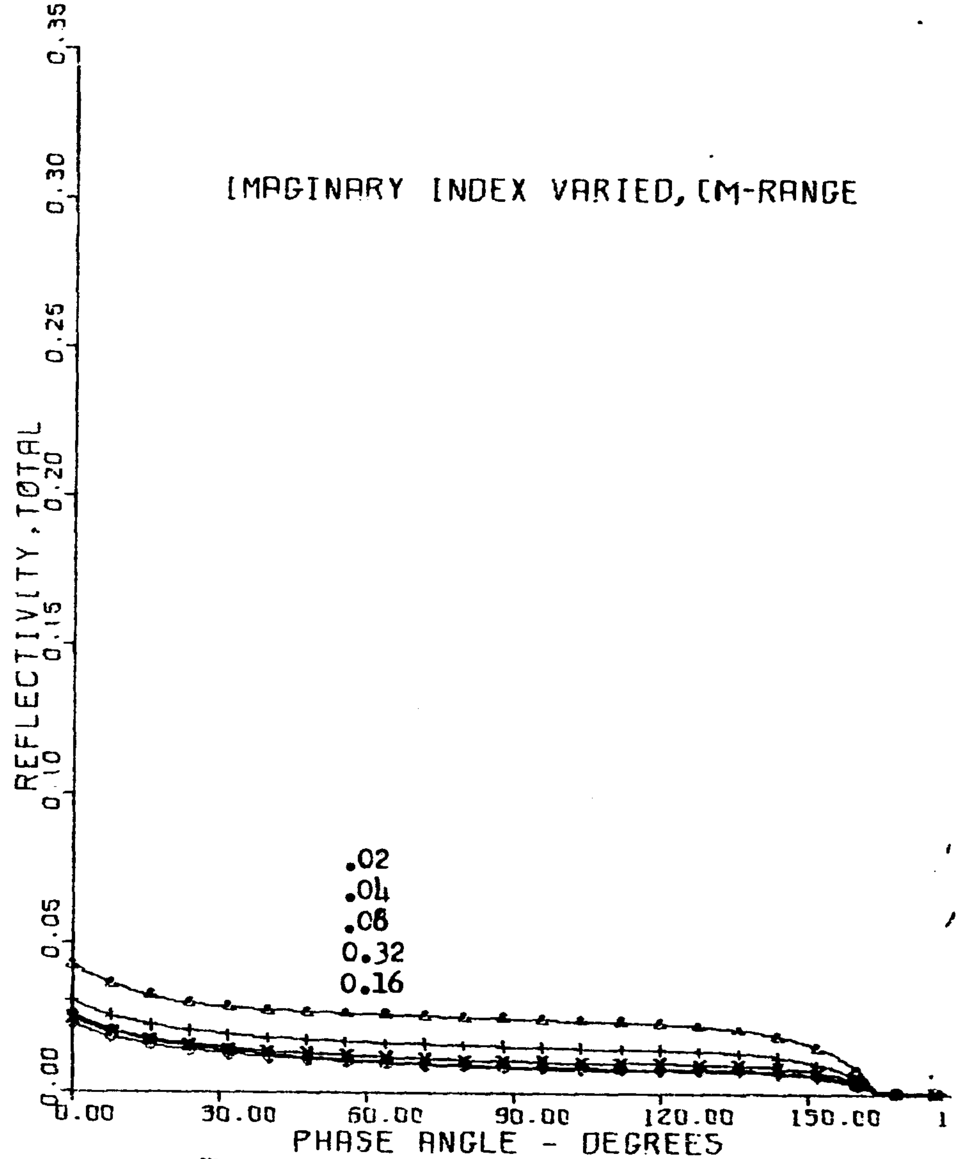

Figure 7 G. The total of all light components (singles + doubles + diffuse) at a point on the planet.

Note the inversion of order when MI becomes larger than 0.10 ; single and double reflected light has exceeded the diffuse light.

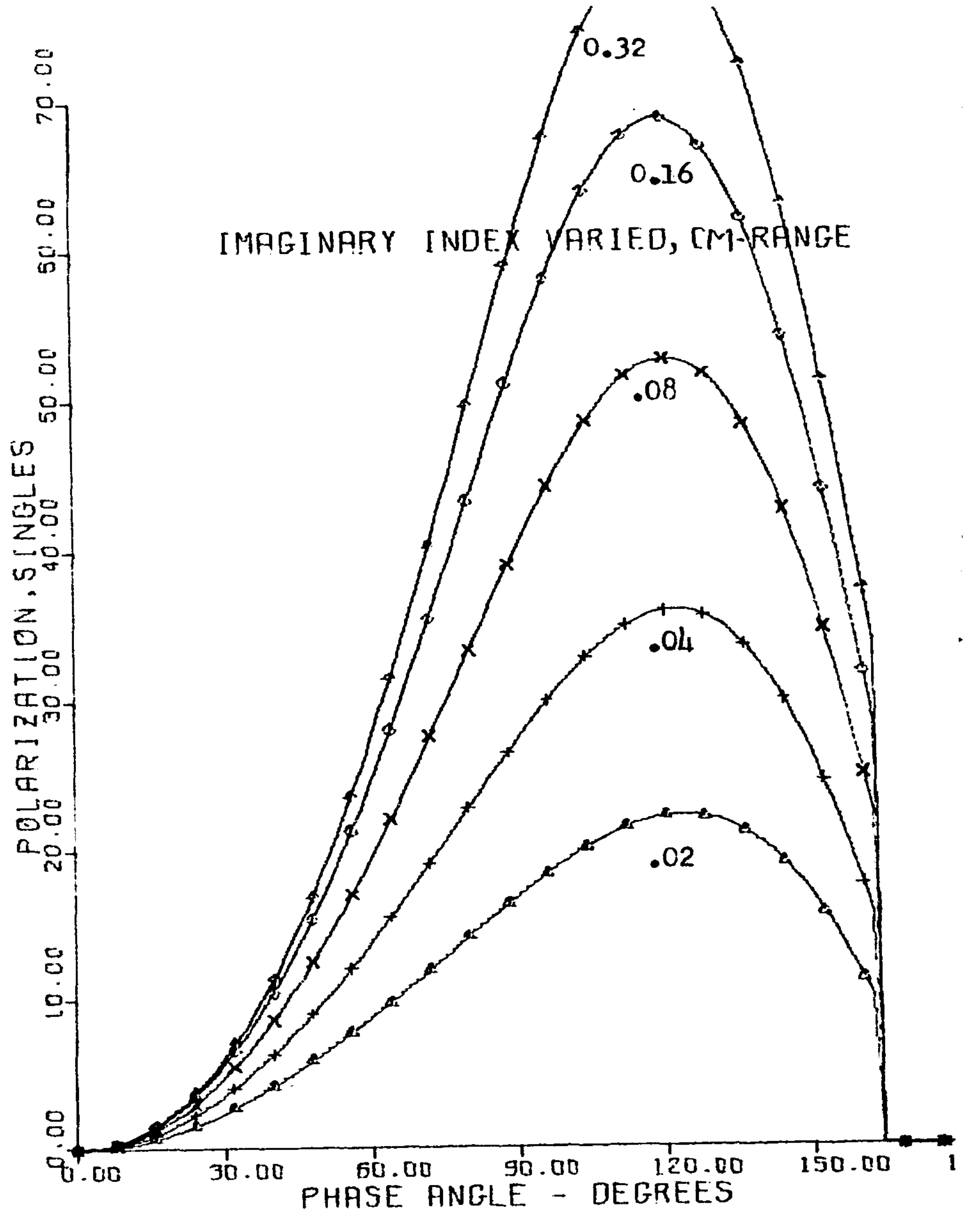

Figure 7 H. The polarization due to the singly-reflected component of light, alone.

Polarization is very large because the diffuse light is almost zero.

A LARGE POLARIZATION SCALE IS USED HERE.

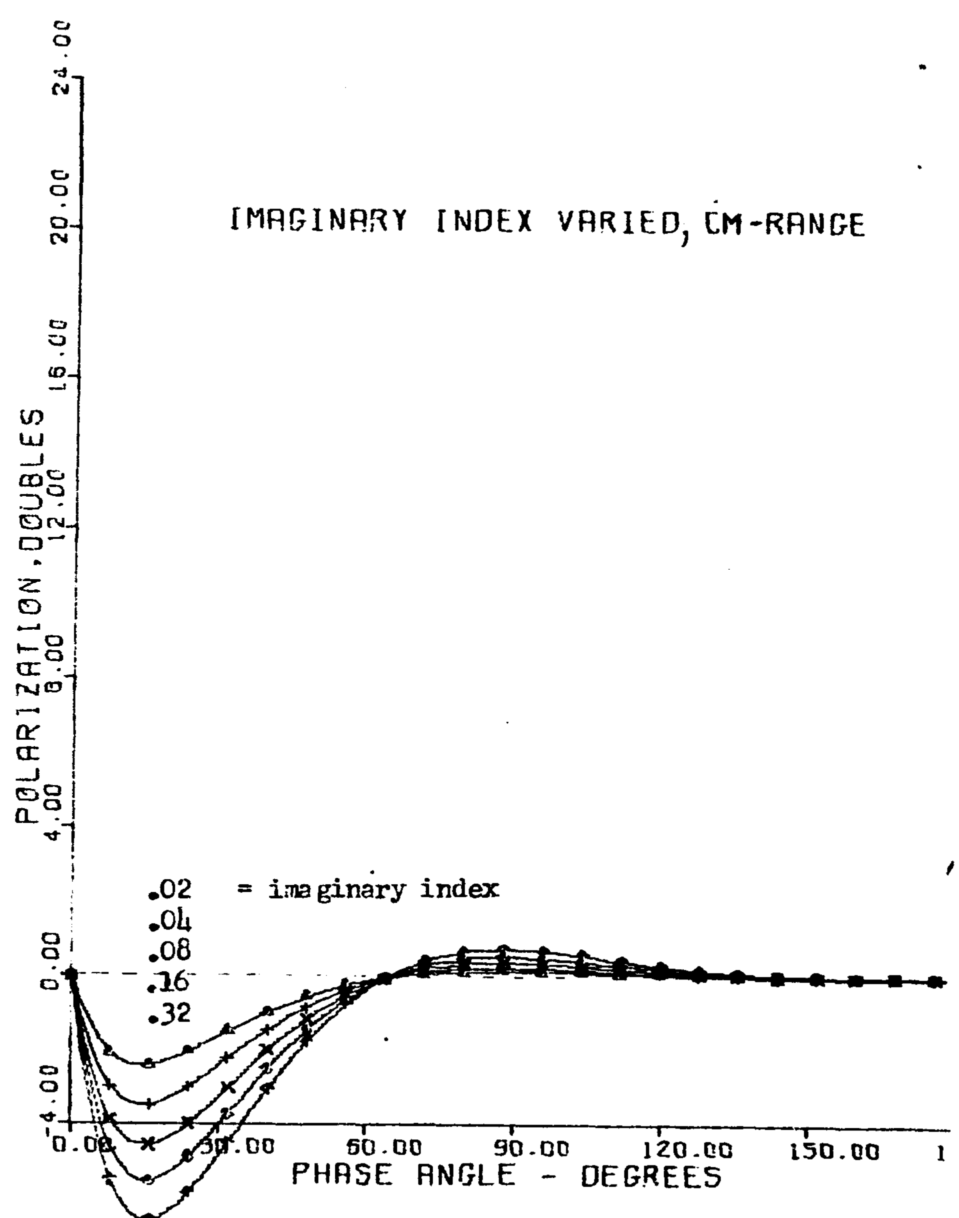

Figure 7 I. The polarization due to the doubly-reflected component of light, alone.

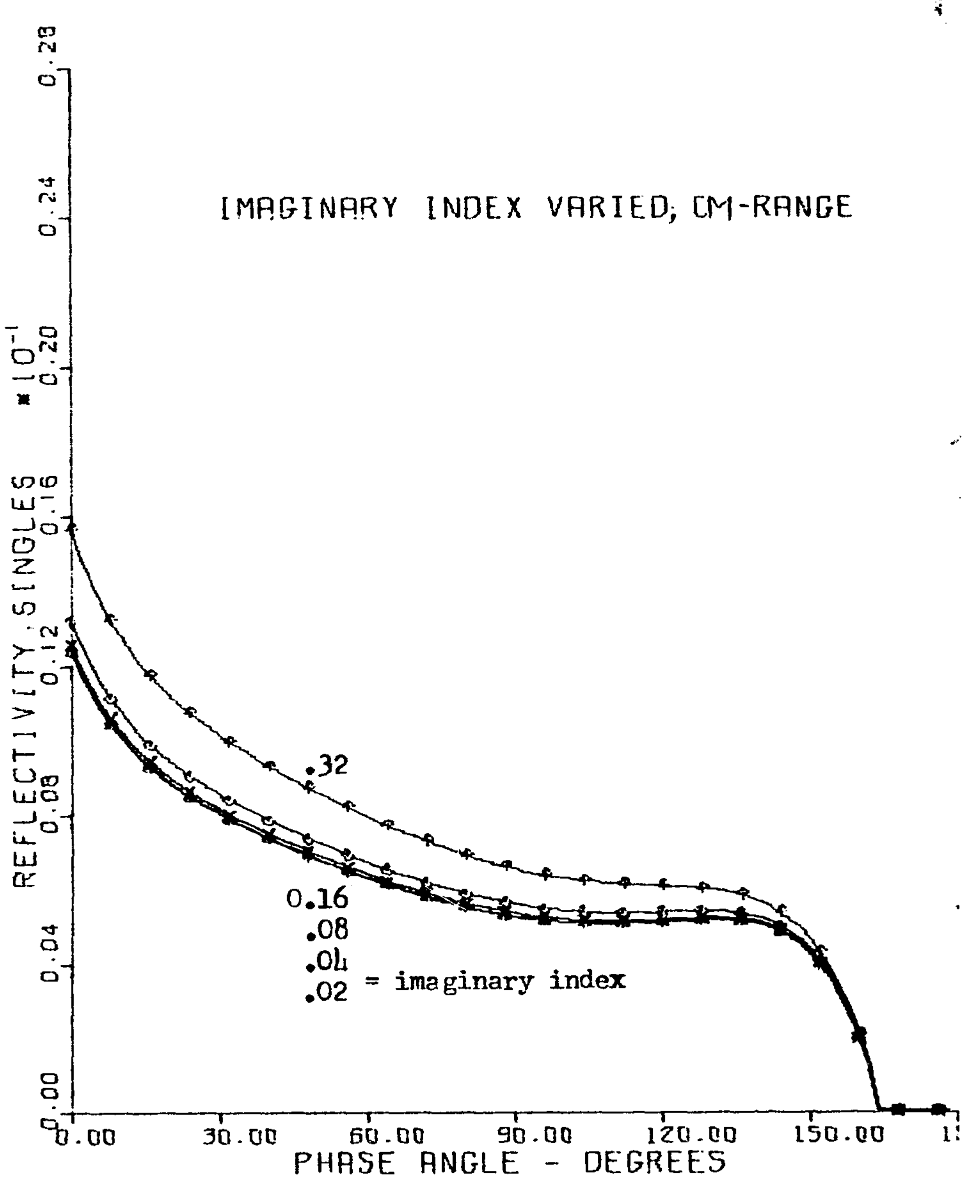

Figure 7 J. The intensity of the singly-reflected component of light.

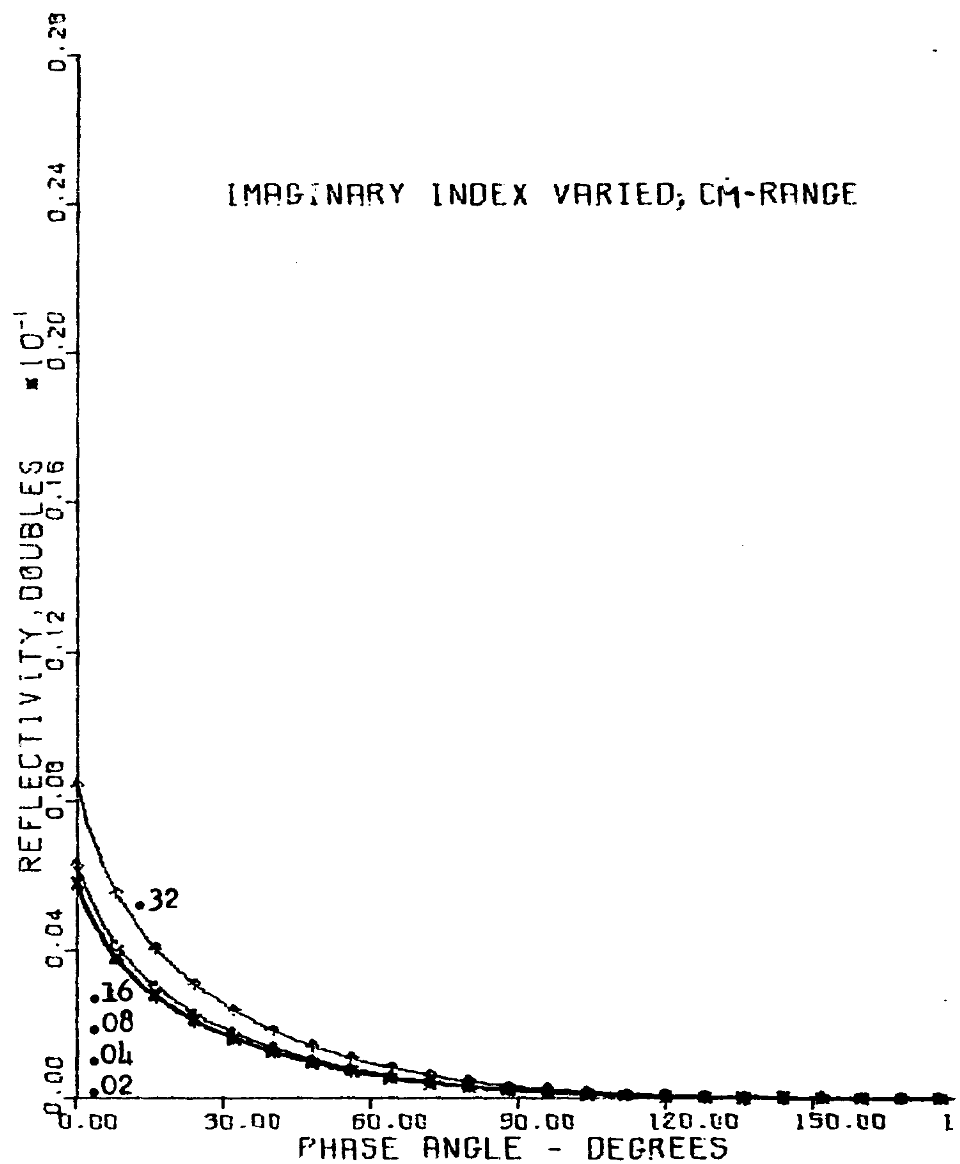

Figure 7 K. The intensity of the doubly-reflected component of light.

In these two figures, it is evident that the imaginary index has little effect on the fresnel reflectivity until it reaches a critical value of about 0.1 . This value appears to mark the boundary between the C and M domains of surfaces. It will be termed the "CM boundary index" . Also, apparently by coincidence, lunar-sized dusts become essentially opaque at this value of index.

IMAGINARY INDEX (MI) VARIED, M/E RANGE
Figure 8A to Figure 8K

These figures produce a description of objects which may correpond to the M and E objects of the CSM taxonomy. The range of MI, 0.2 to 0.6, represents approaching metallic condition of the material.

A good match is seen between these calculations and the M or E asteroids, for the parameters of reflectivity (high) and the R/B color index (low), as well as the absence of absorbtion spectra.

The calculated values of P-min are much too large compared to the observed M and E asteroids. One can conclude that the correspndence is incorrect, or, that the asteroids are mixtures, or, that the surfaces of metallic asteroids are not as heavily pitted and dusty as this computer model which closely matches the Moon in this respect.

The third choice above is attractive because it is well known that minerals become more malleable and less liable to fracture as they approach the metallic condition. Therefore, if the M and E asteroids are metallic, one expects them to have less pitted and dusty surfaces.

In order to reduce the negative branch by a factor of 3 for the M asteroids, and a factor of 3 for the E asteroids, a similar decrease of dust and pits is required, in the computer model.

Another uncertainty is the possible variation of the real refractive index, which has a very large effect on the polarization properties of a surface (see the figure set varying real index). For metals, the extremes of the real index are much wider than for crystalline minerals.

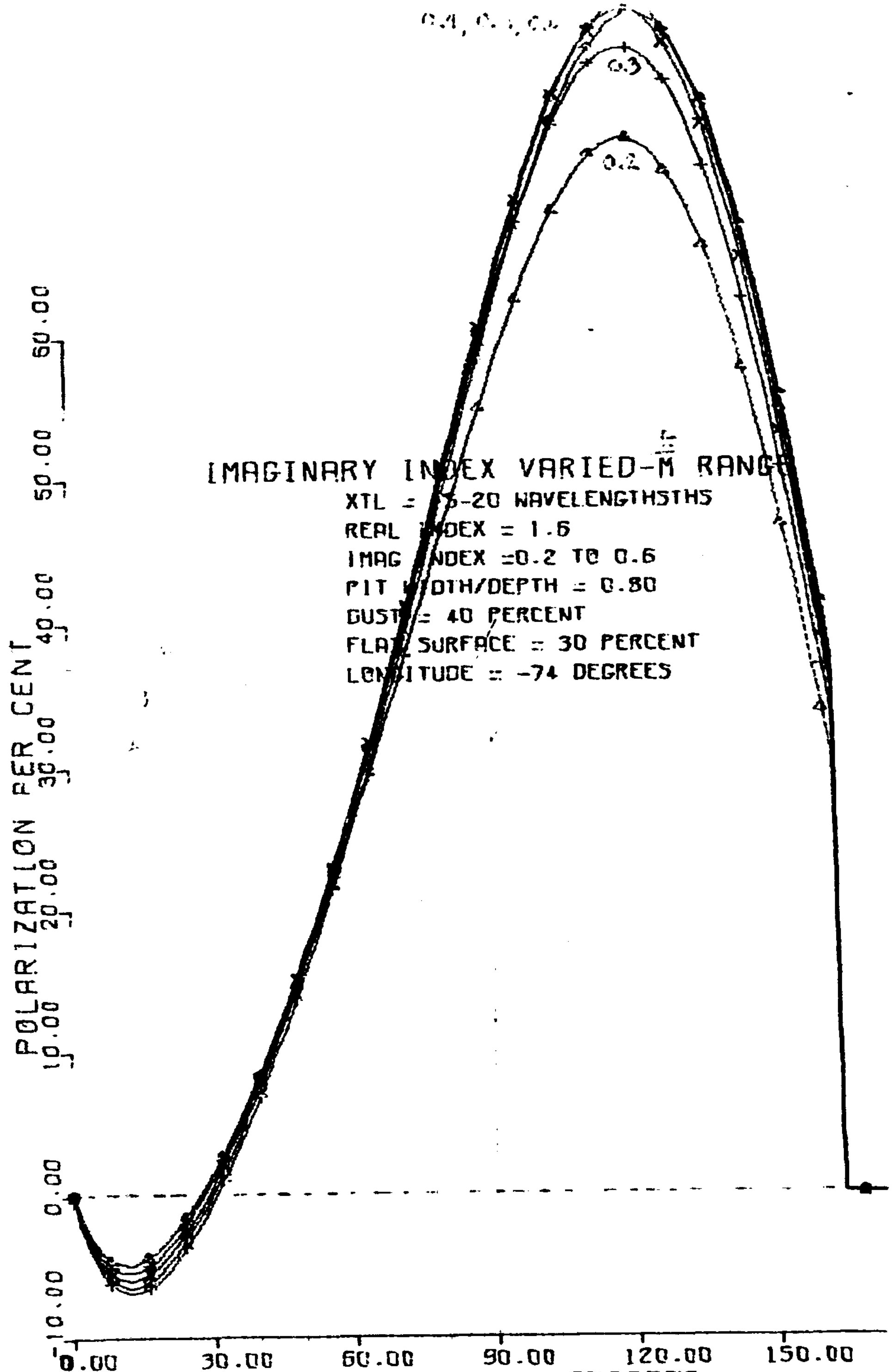

Figure 8 A. Polarization at a point on the planet.
Note the constant slope between 30° and 70°.

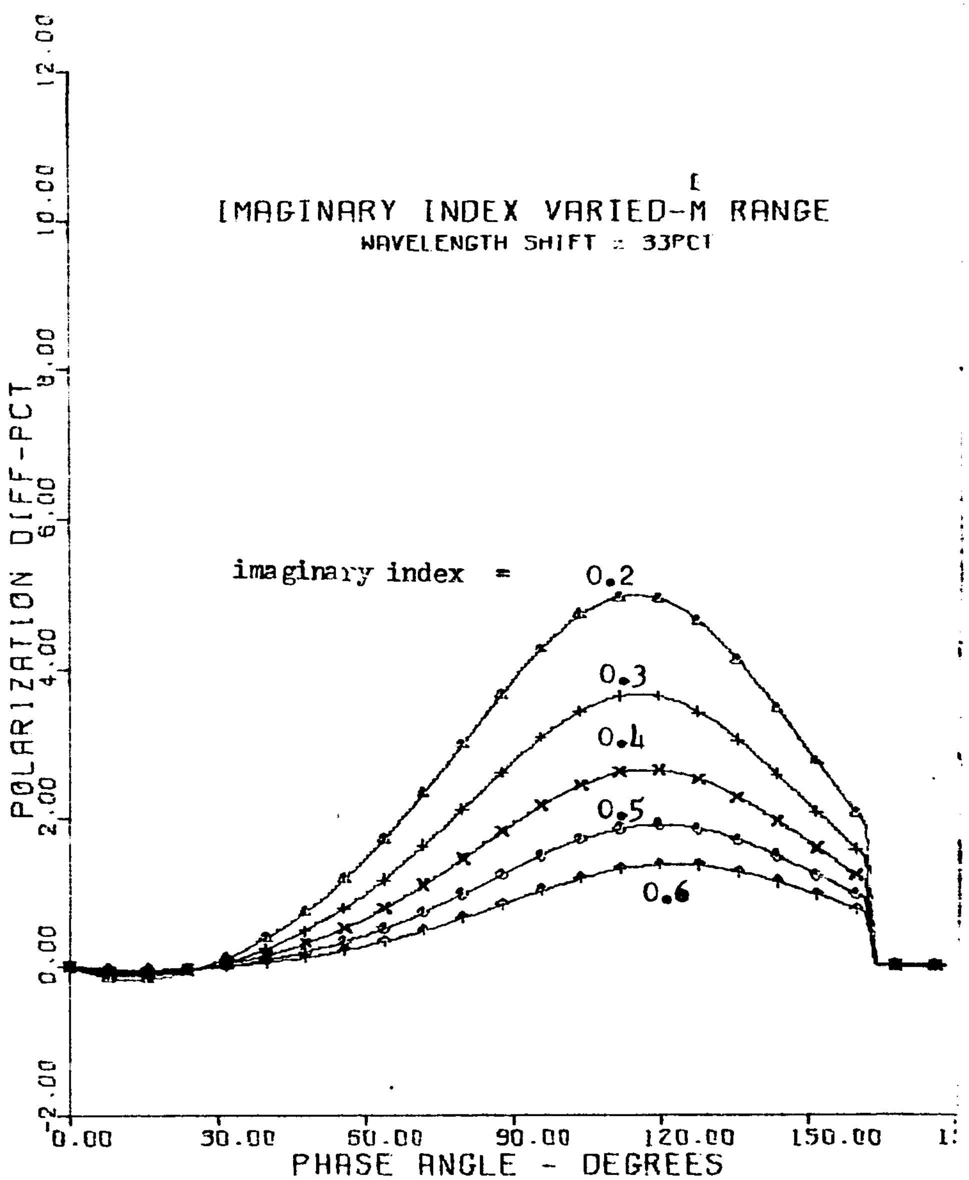

Figure 8B. Polarization difference (shift) for a wavelength shift of 33 percent.

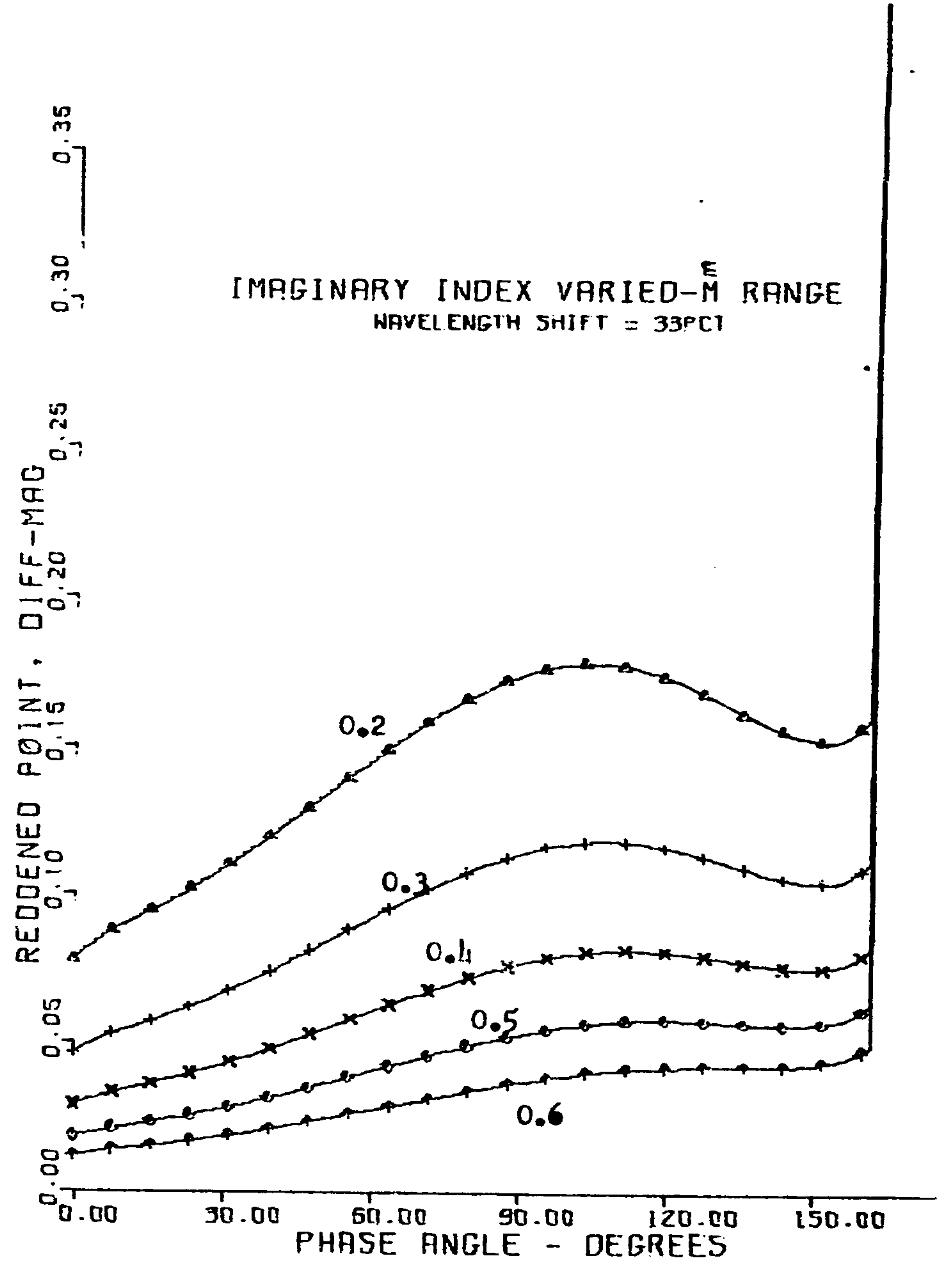

Figure 8 C. The reflectivity shift, in magnitudes, of a point on the planet, for a wavelength shift of 33 percent.

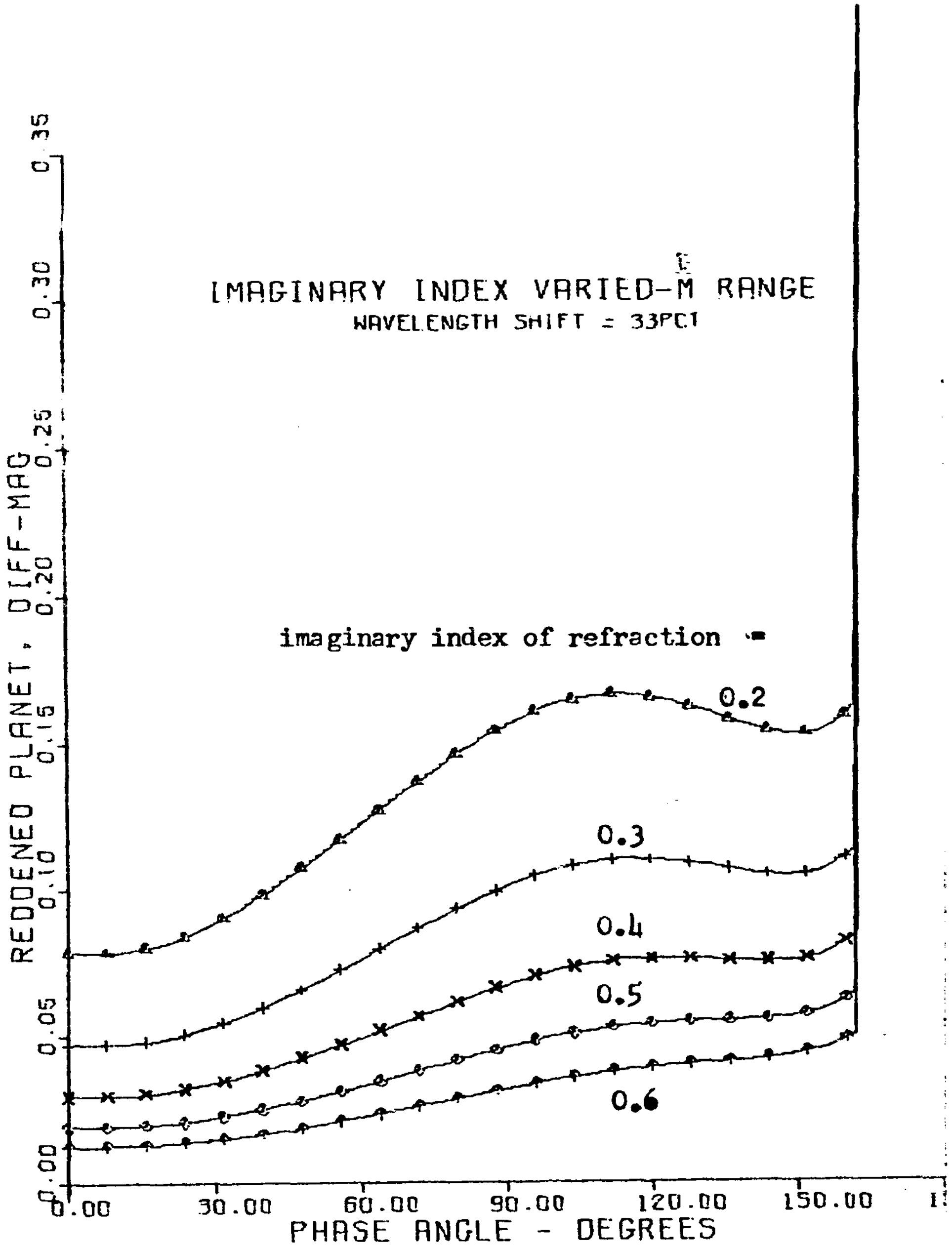

Figure 8 D. The reflectivity shift, in magnitudes, of the integrated planet, for a wavelength shift of 33 percent.

Note that, despite the reversal in Fig E (right), "reddening is still following the rule that the darkest bodies show the greatest reddening.

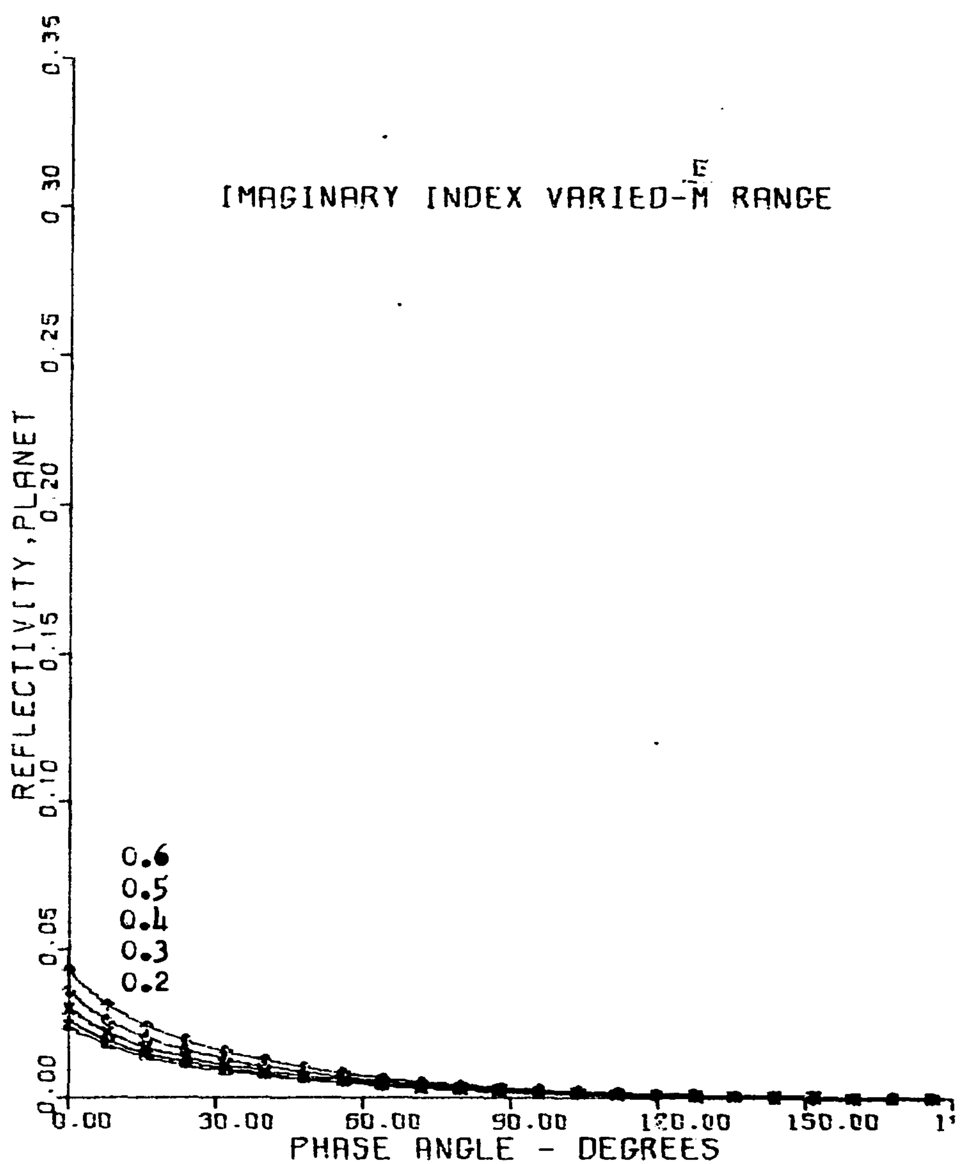

Figure 8 E. The integrated reflectivity of the entire planet.

Note that although the absorbtion (imaginary index) is increasing, the reflectivity is also increasing; just opposite to the case for low values of absorbtion.

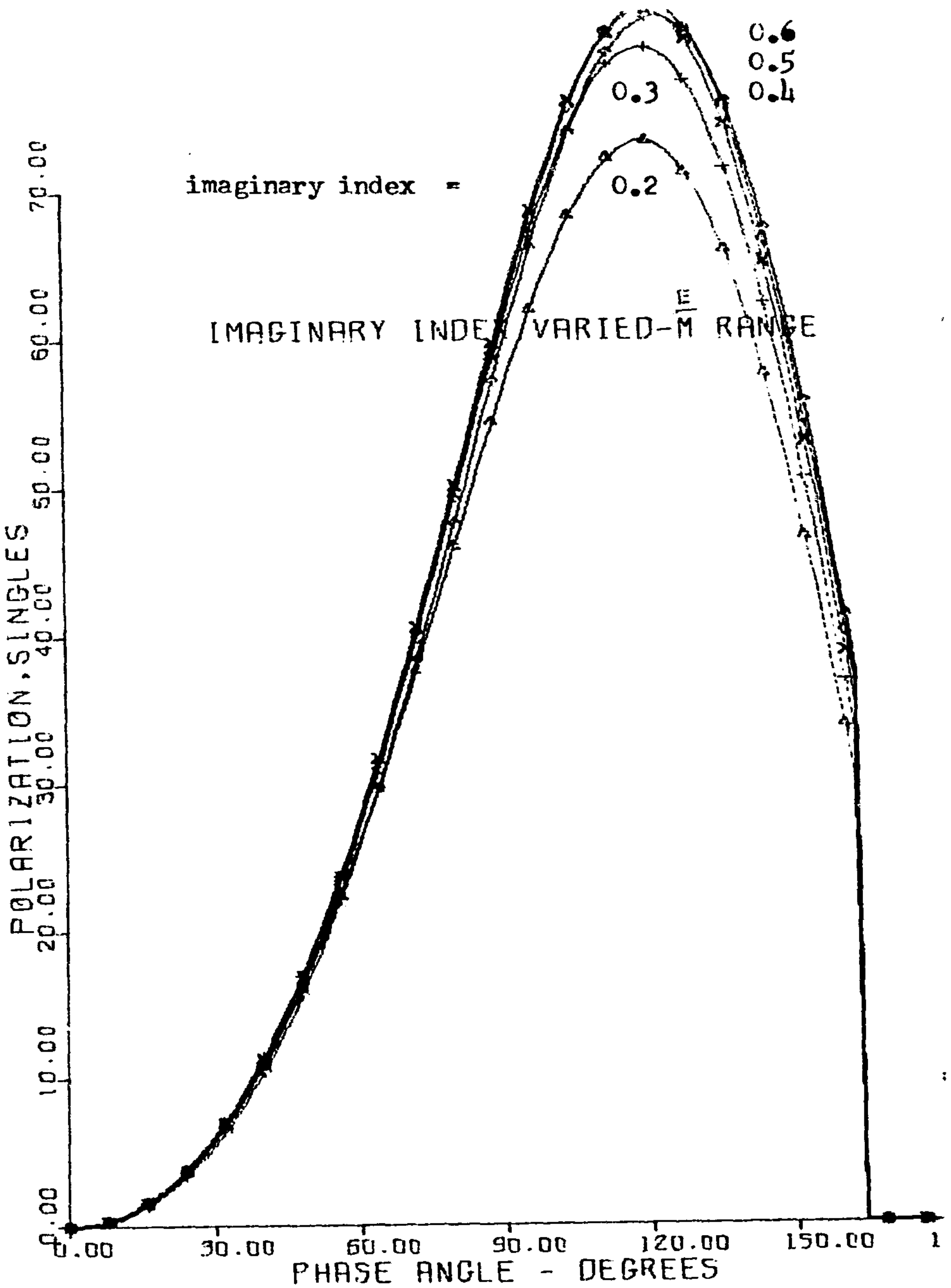

Figure 8H. The polarization due to the single-reflected component of light, alone.

The constancy of the slope, 30^{o} to 70^{o}, is due to the absence of a diffuse component of light.

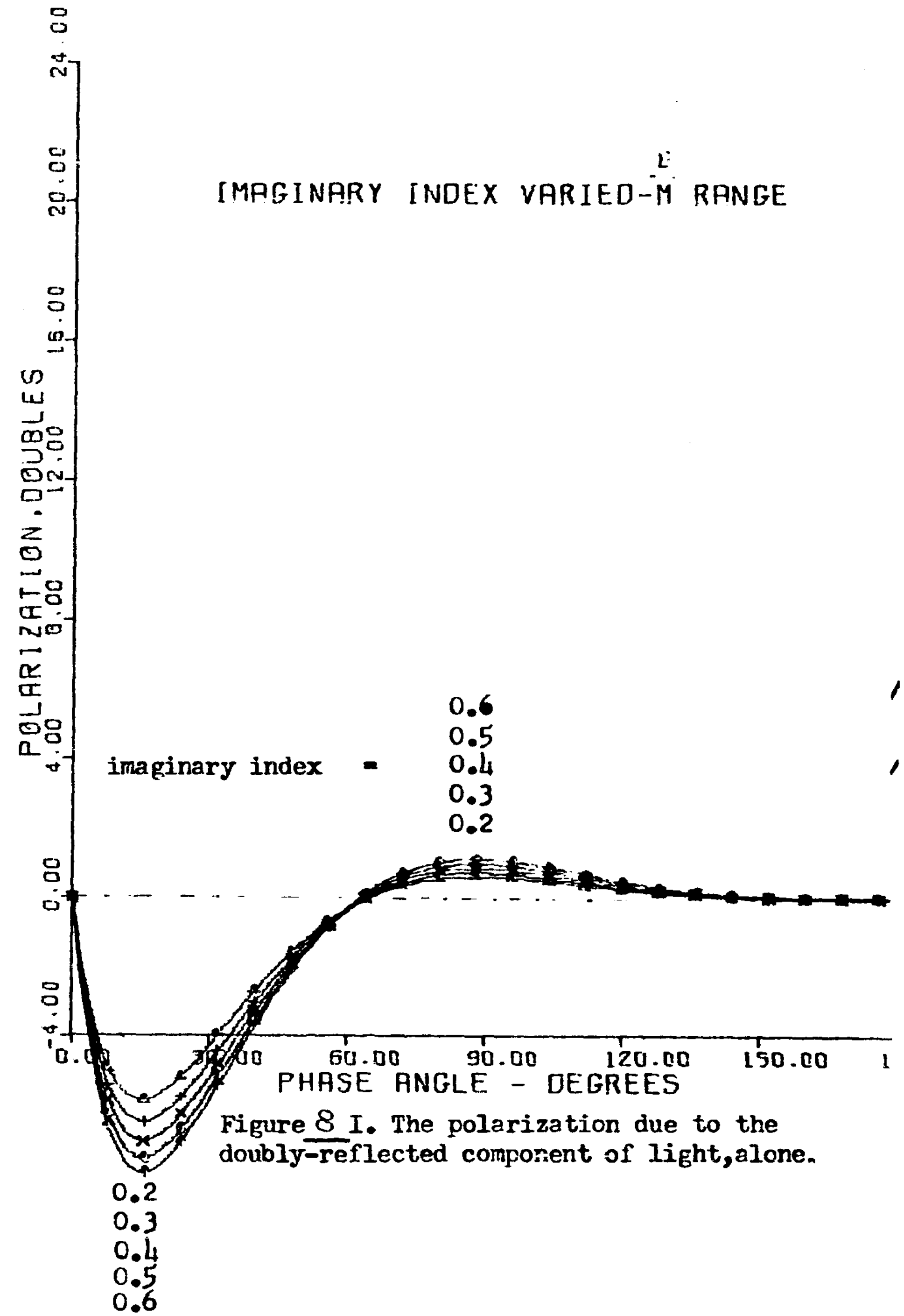

Figure 8 I. The polarization due to the doubly-reflected component of light,alone.

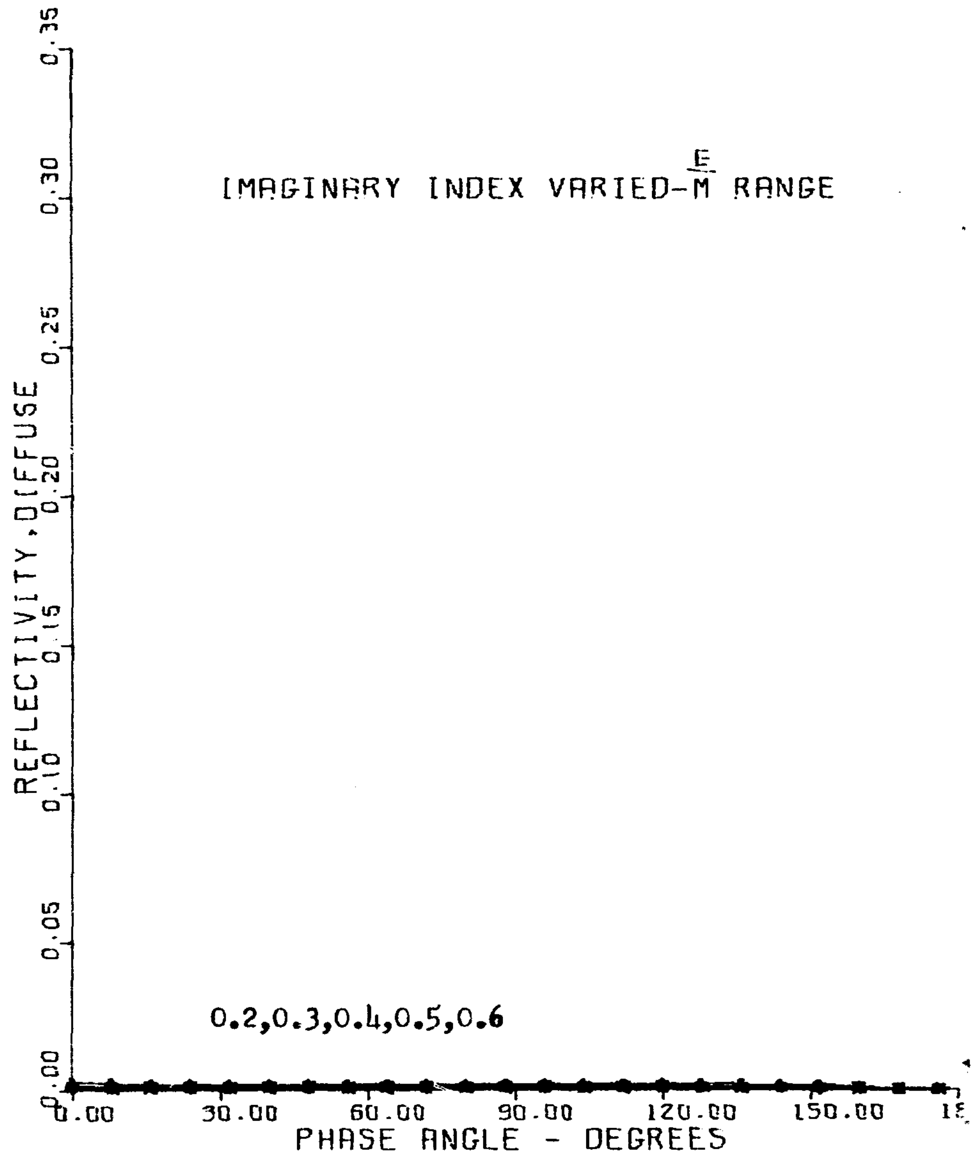

Figure 8F. The diffuse component of light.

The absorbtion is so large that the particles are black and diffuse light from within them is about nil.

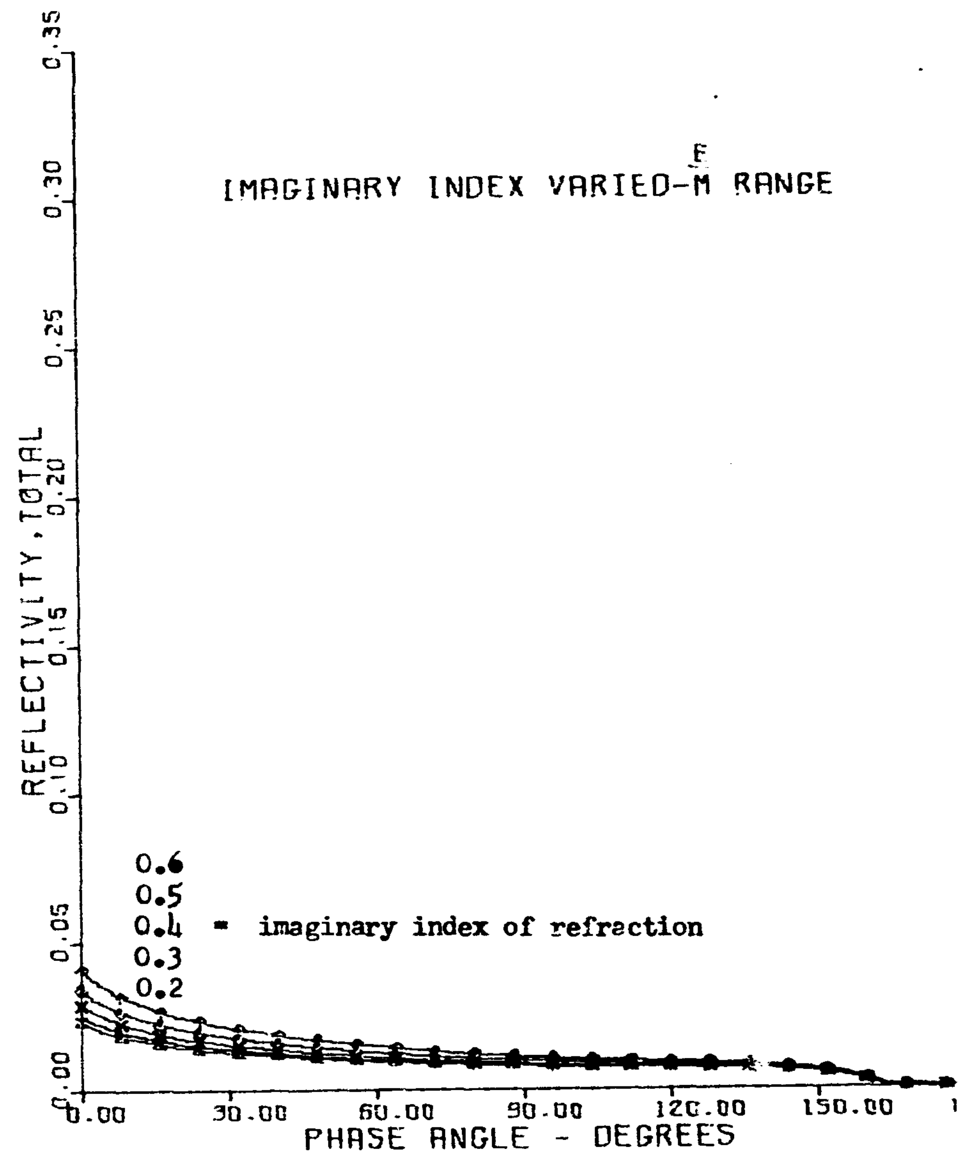

Figure 8G. The total of all light components (singles + doubles + diffuse).

Because the diffuse light is almost zero, the light is almost entirely due to singles and doubles.

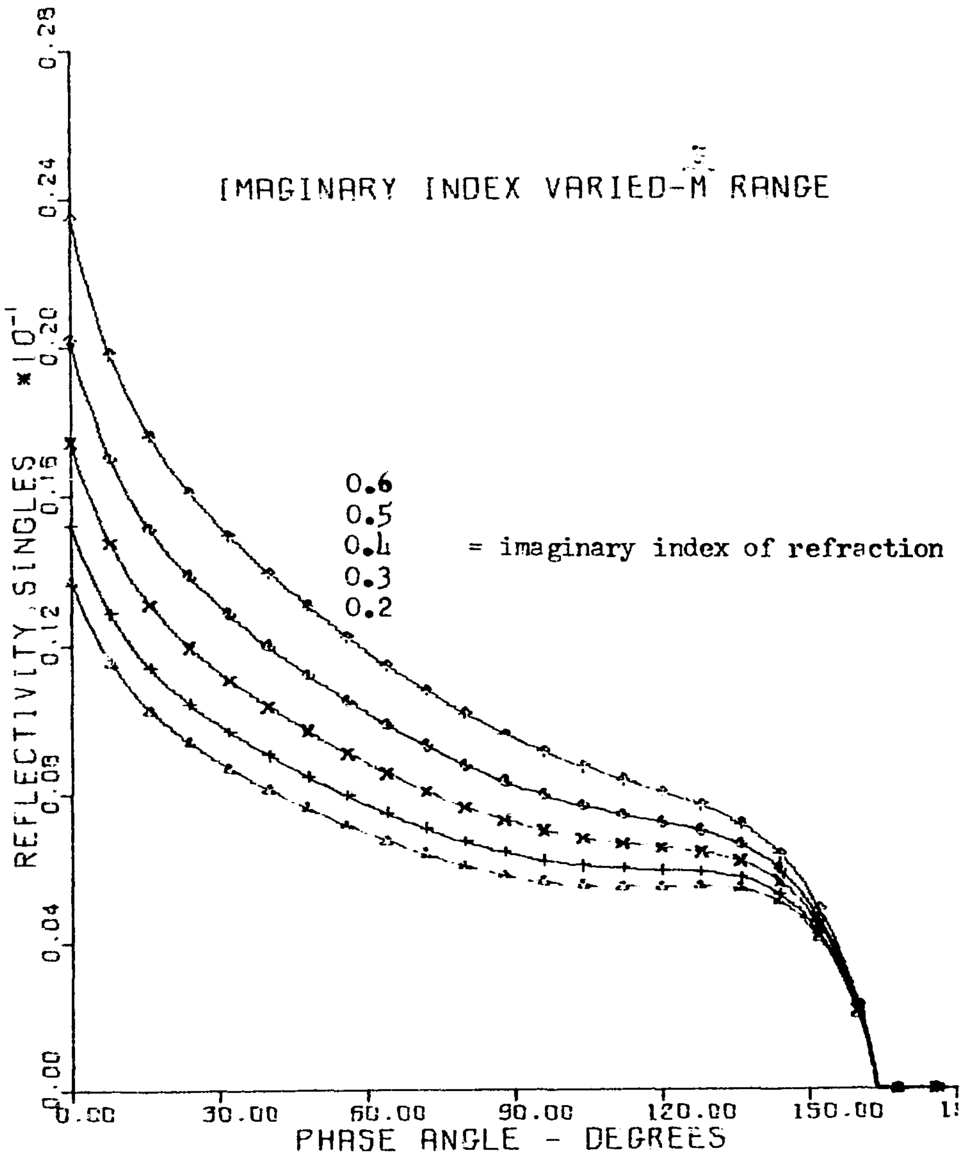

Figure 8J. The intensity of the singly-reflected component of light.

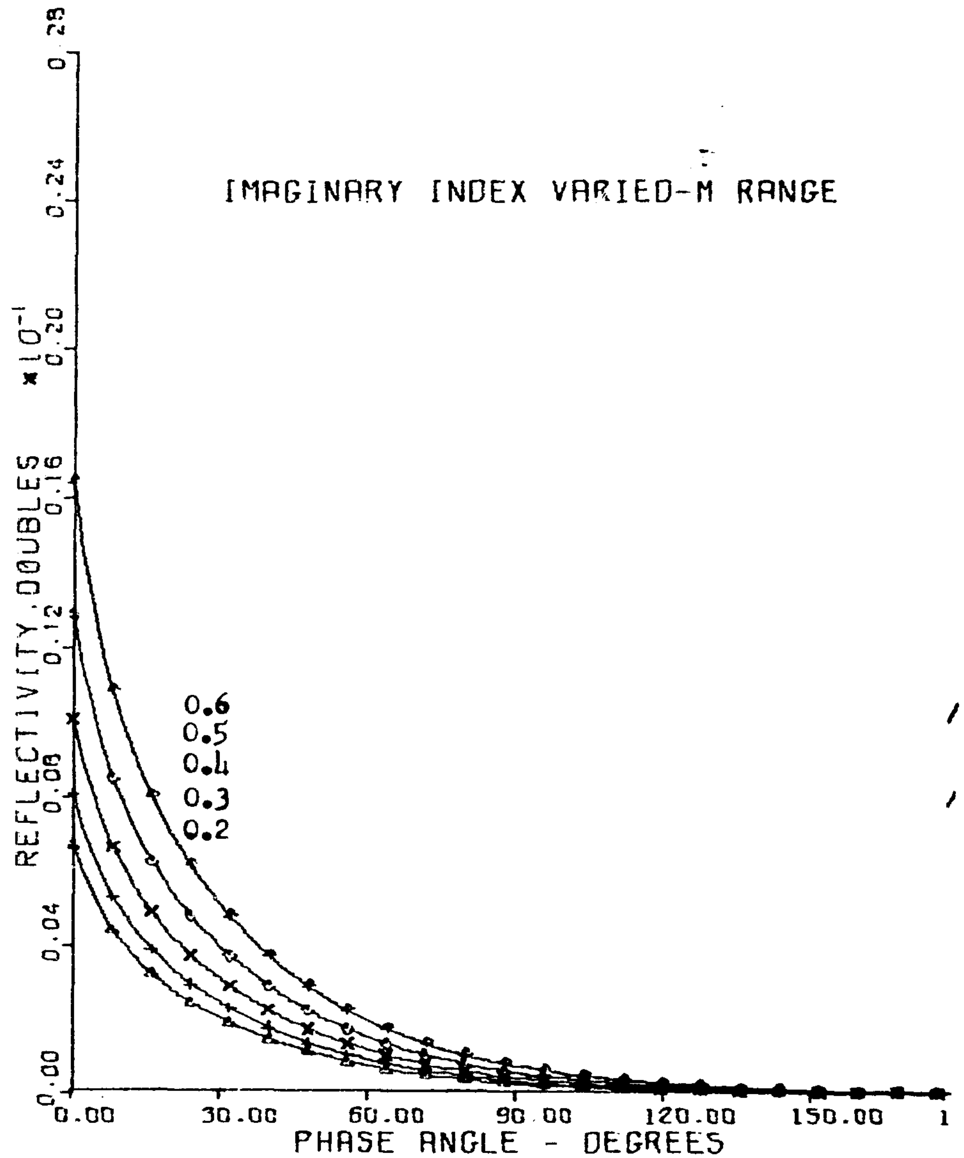

Figure 8 K. The intensity of the doubly-reflected component of light.

In the M-range of index, the total reflectivity is dominated by the large increase of Fresnel reflectivity due to the imaginary component of the index. Single and double reflections become the largest components.

IMAGINARY INDEX VARIED - VERY LARGE M-RANGE

Figure 9A to Figure 9K

These curves illustrate the extremely large values of the imaginary index which correspond to metals or pure crystals such as sulfur observed at wavelengths longer than yellow.
It is not clear that there exist any objects with these properties, or if they do exist, that their sufaces posses the pitted, particulate properties assumed in this computer surface model.

If this range of imaginary indices does exist in solar-system bodies, it is possible that the surface is smooth and only lightly pitted, for example like iron-nickel meteors. If this is true, then the polarization calculated for the positive branch would not be much changed, but the negative branch would be several times smaller.

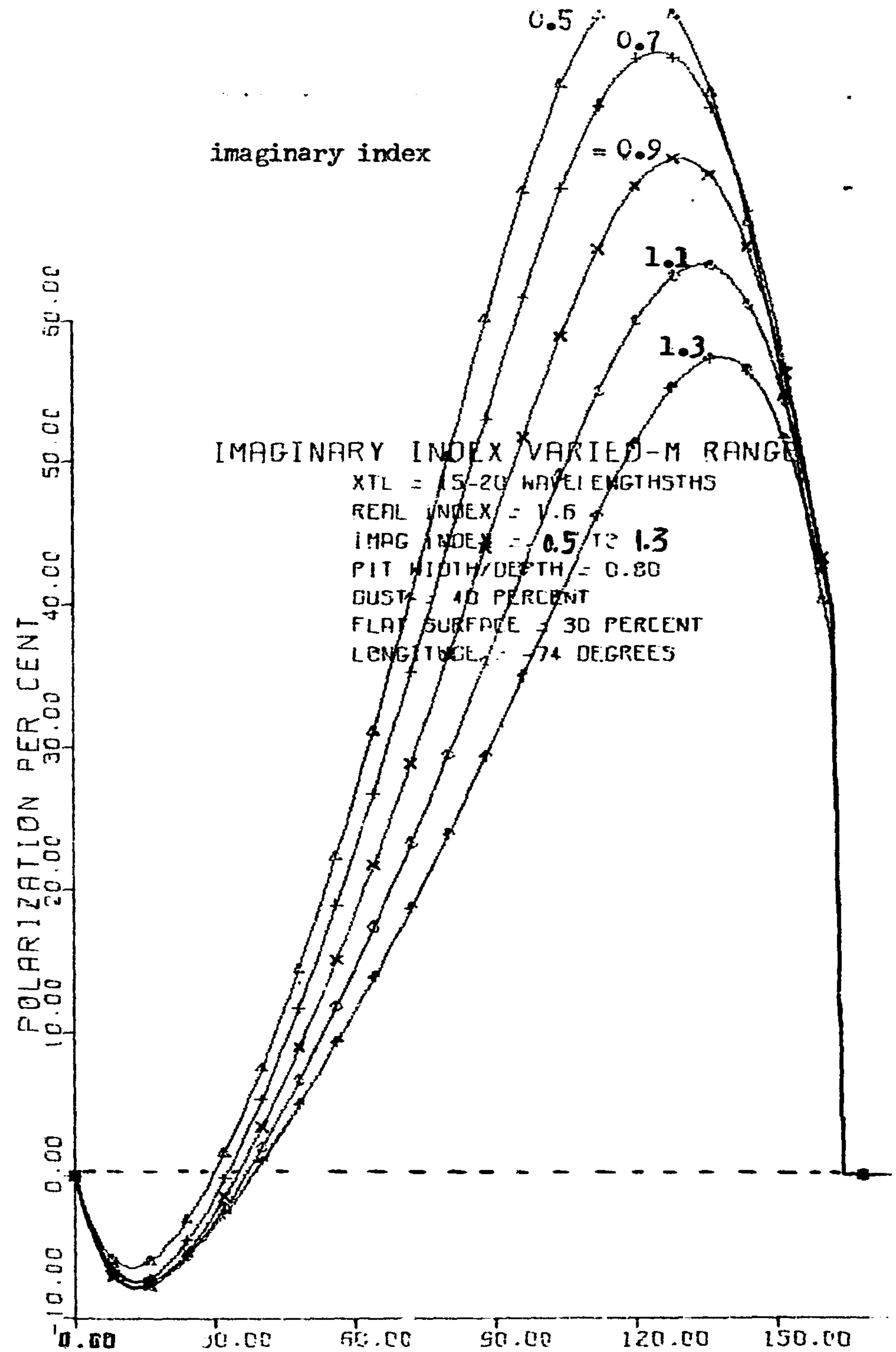

Figure 9 A. Polarization at a point on a planet.

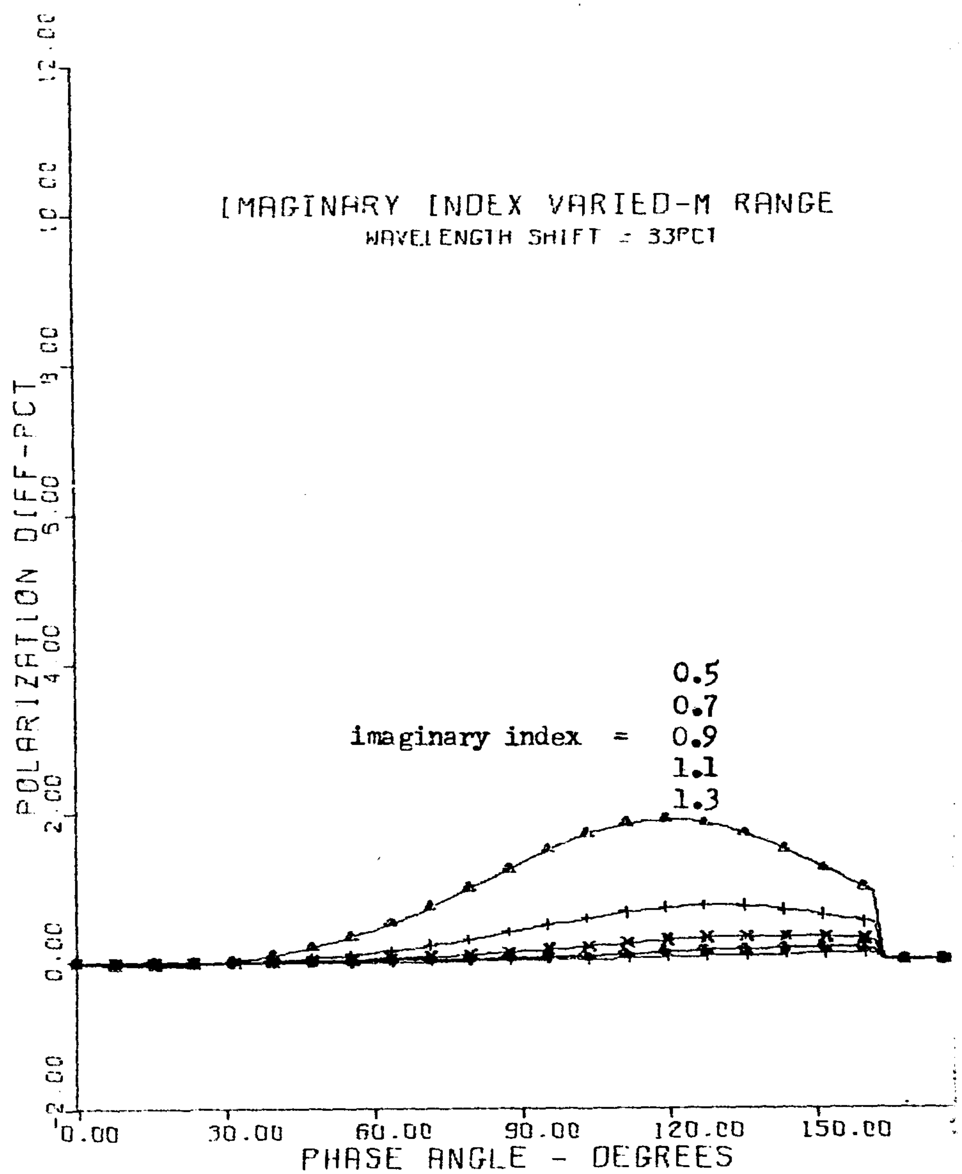

Figure __B. Polarization shift for a wavelength shift of 33 percent.

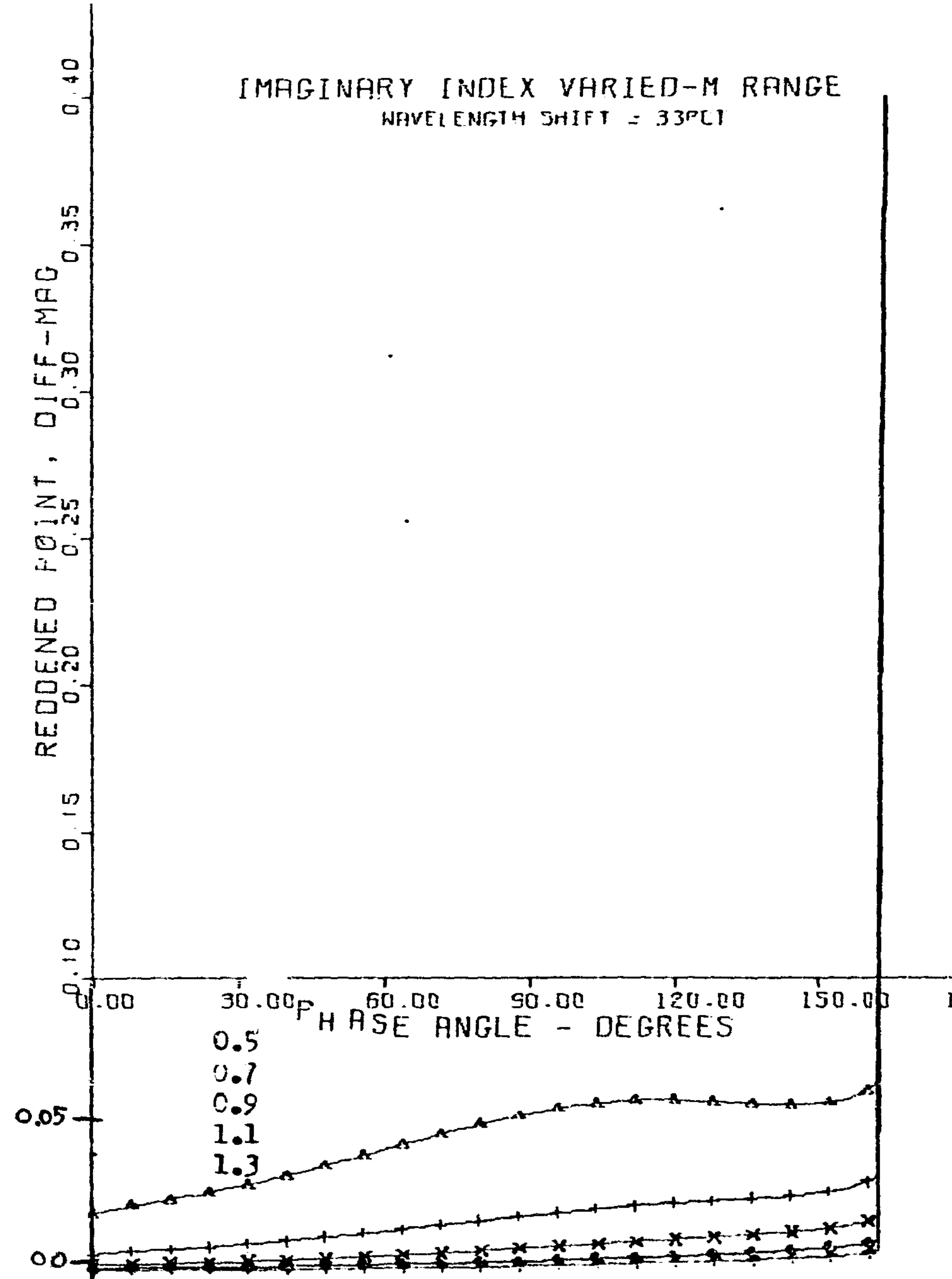

Figure __C. The reflectivity shift in magnitudes, of a point on the planet, for a wavelength shift of 33 percent.

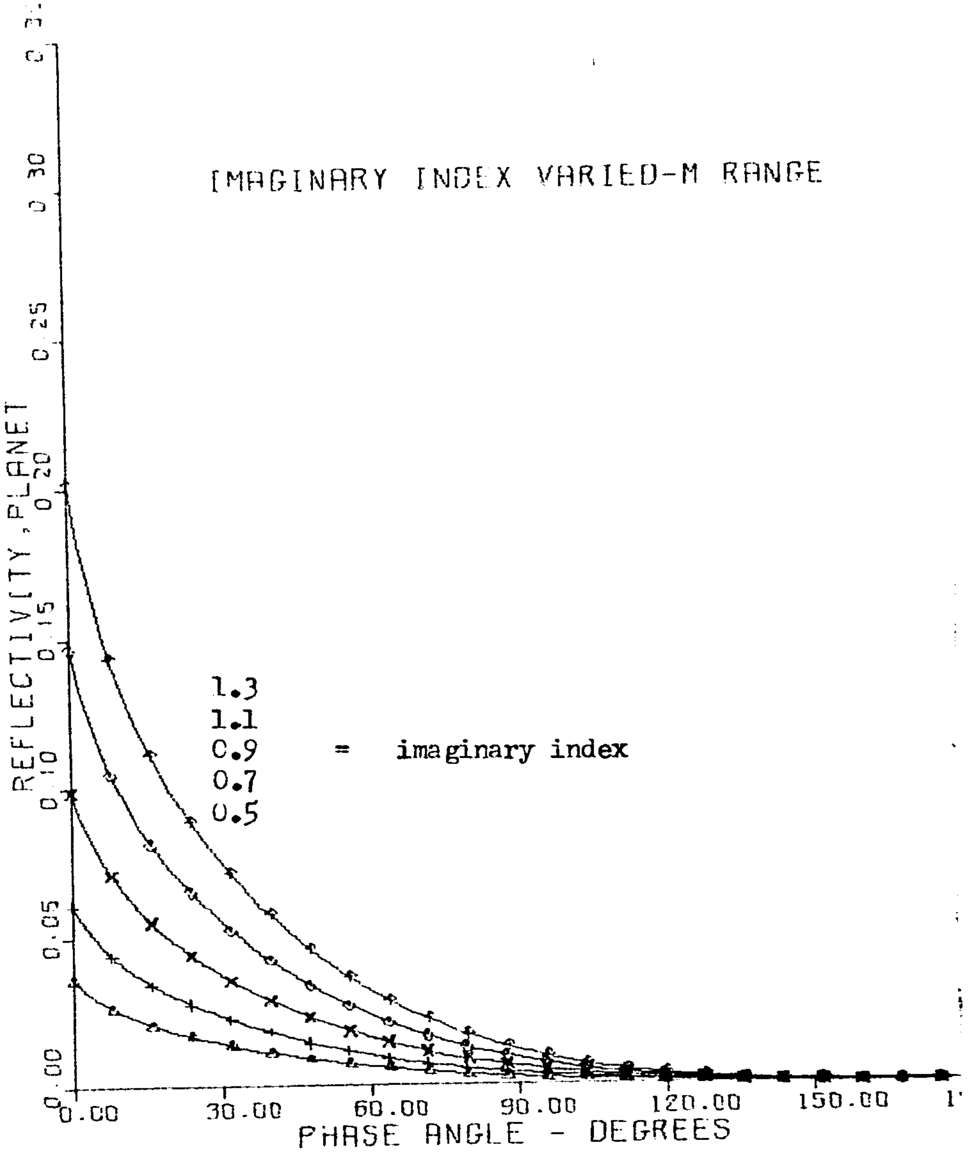

Figure 9 E. The integrated reflectivity of the entire planet.

Because of the large values of the imaginary index, well into the metallic range, the specular reflectivity makes almost the entire contribution to the planet's reflectivity.

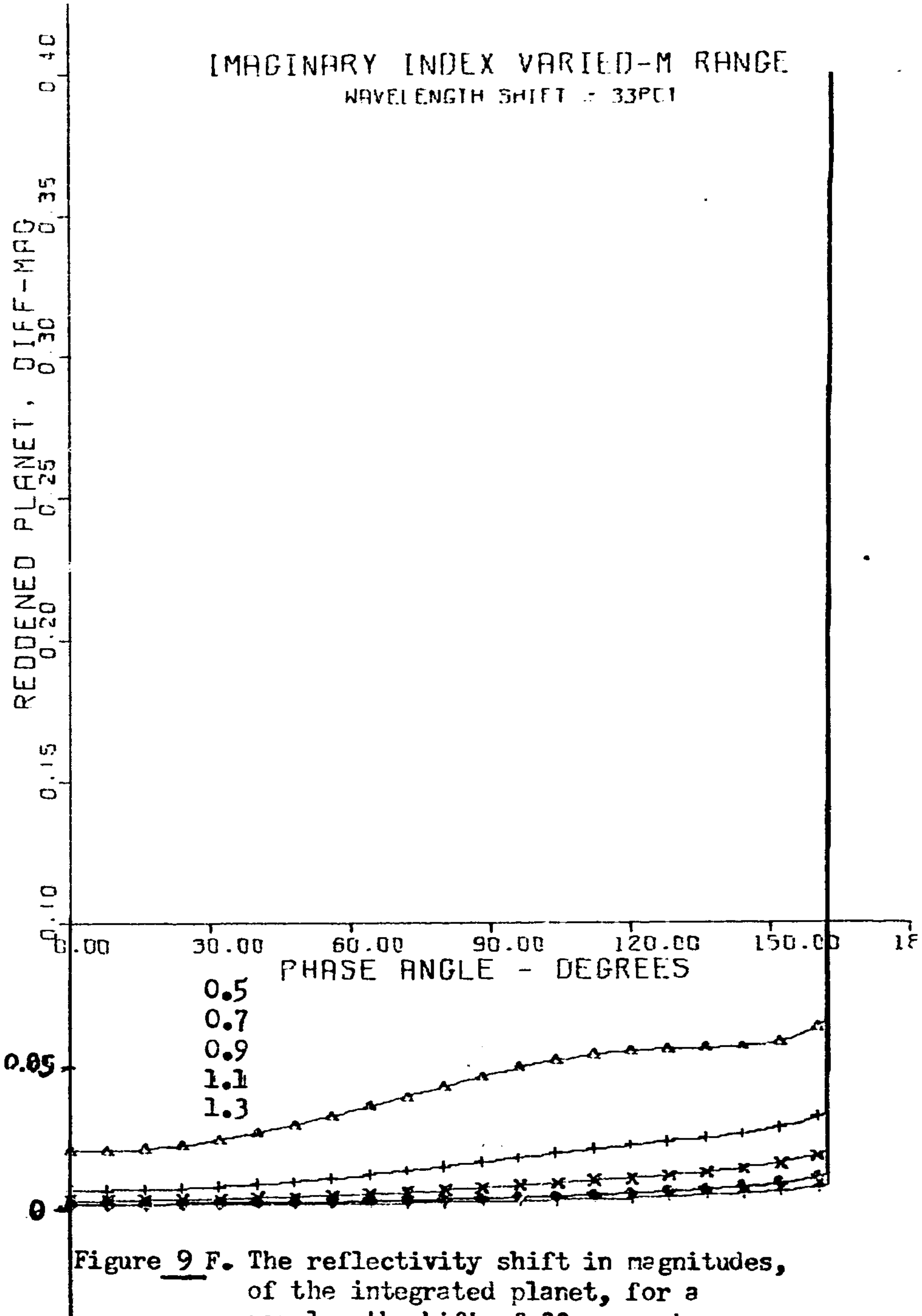

Figure 9 F. The reflectivity shift in magnitudes, of the integrated planet, for a wavelength shift of 33 percent.

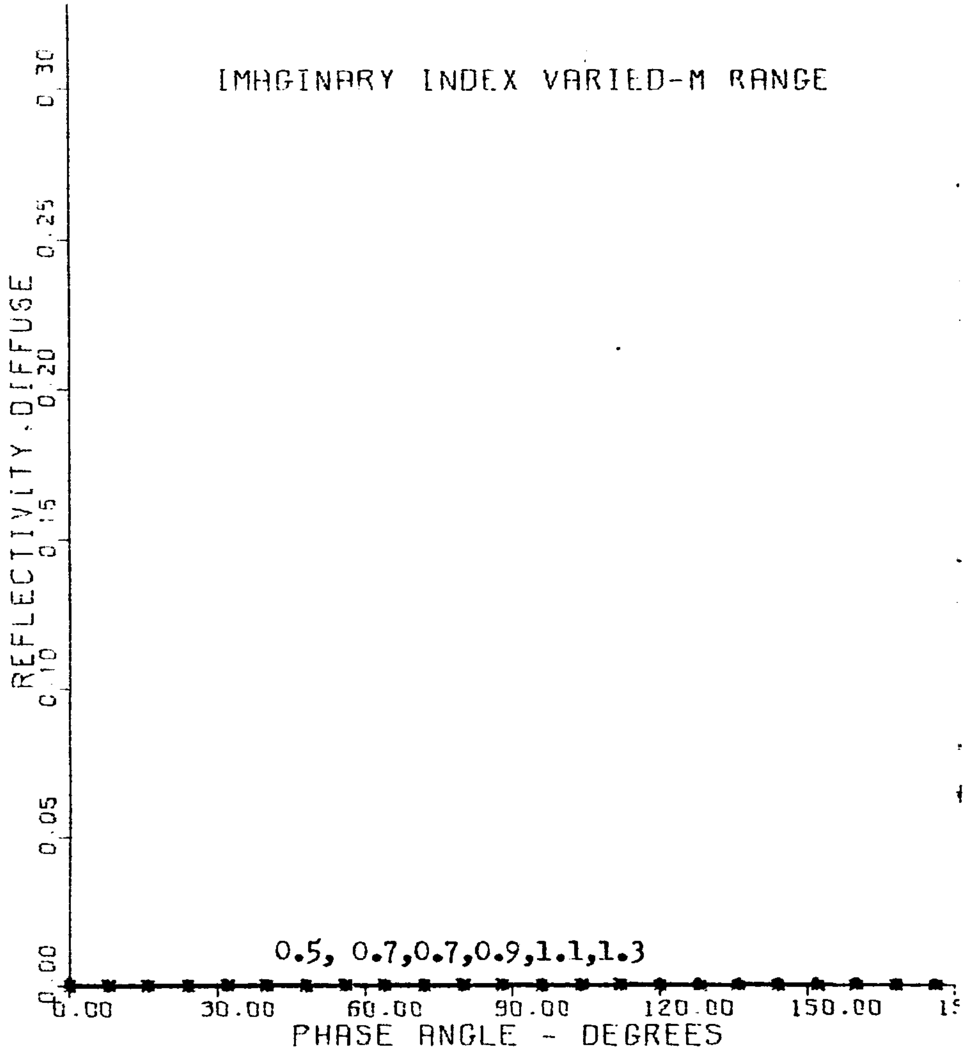

Figure 9 F. The diffuse reflectivity of light at a point on the planet.

The diffuse light is almost zero, because the large values of the imaginary index result in almost total absorbtion of all ight entering particles.

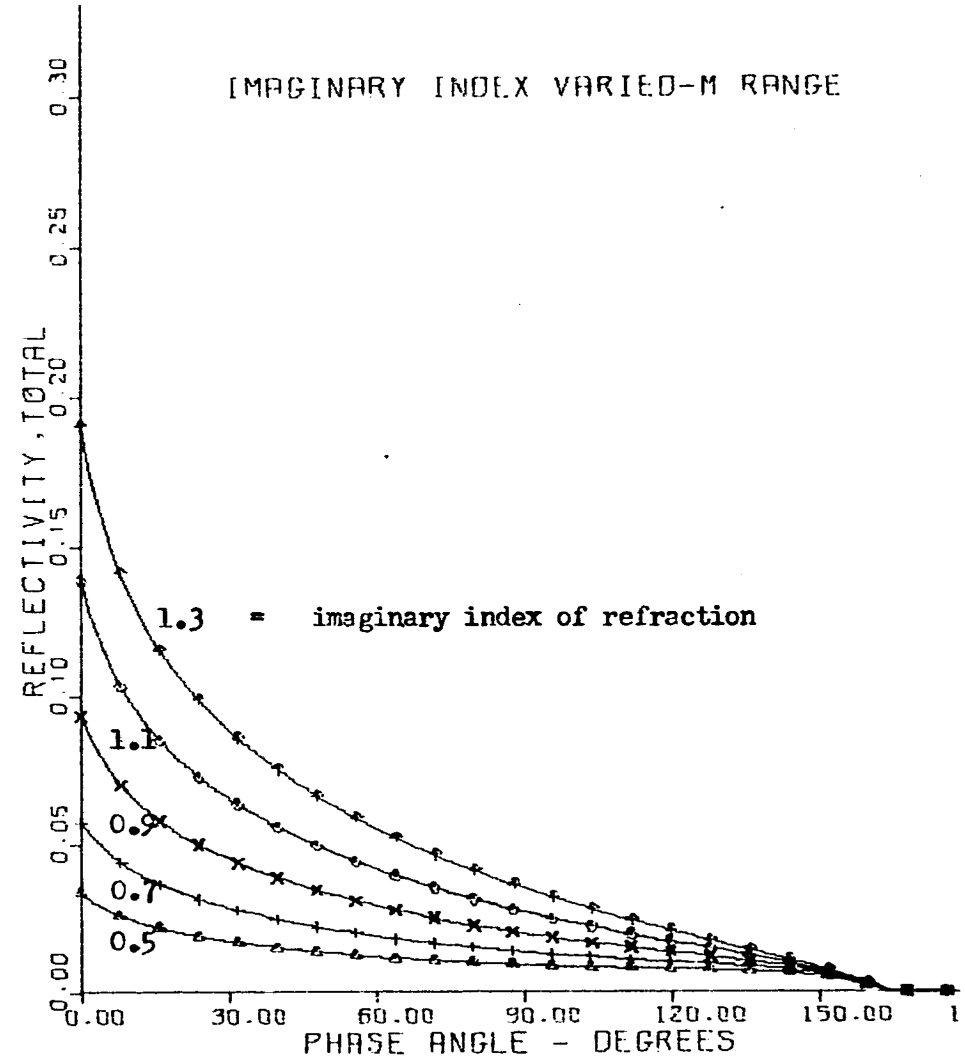

Figure 9 G. The total of all light components (singles + doubles + diffuse) at a point on the planet.

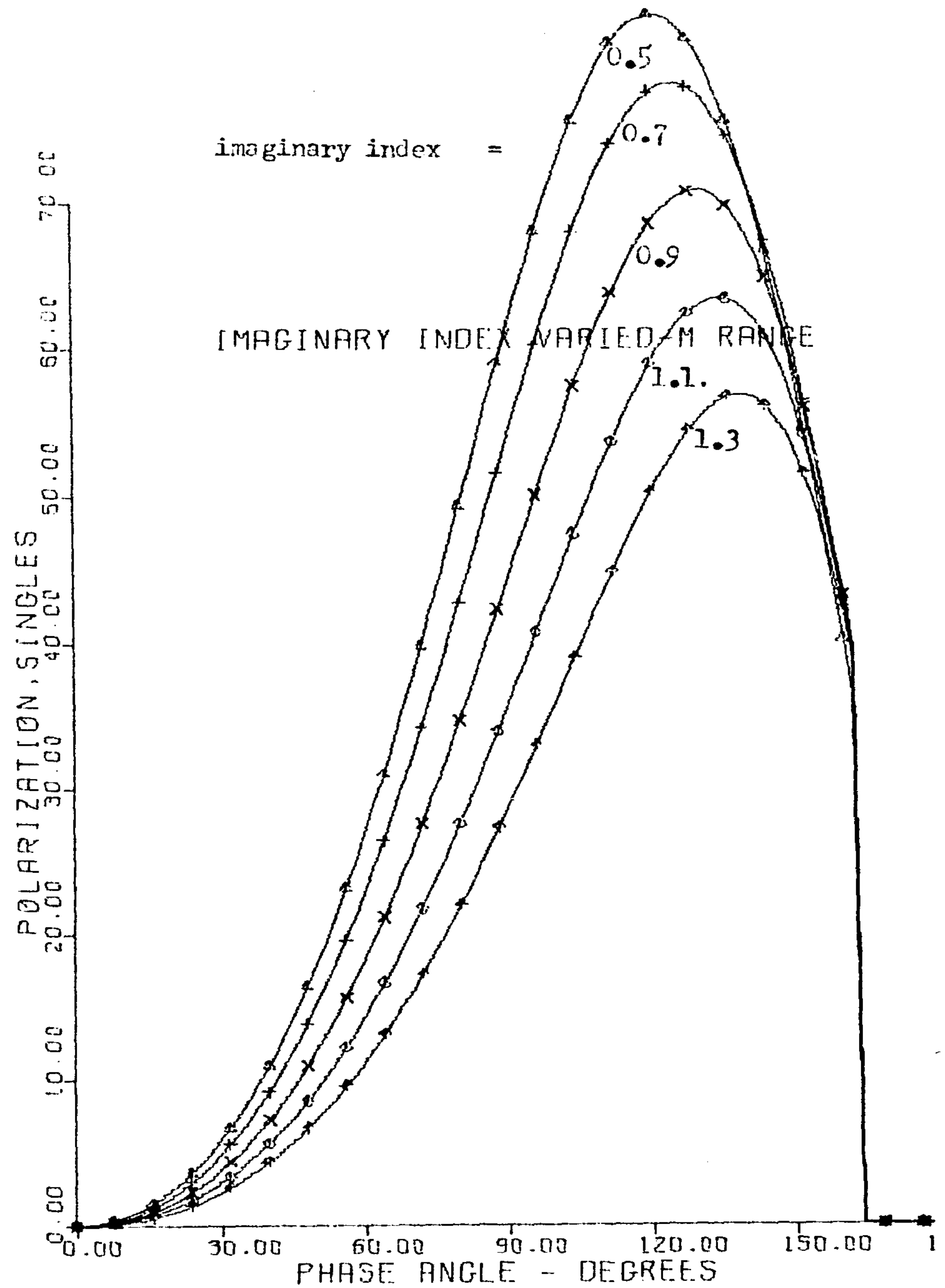

Figure 9 H. Polarization due to the singly-reflected component of light, alone.

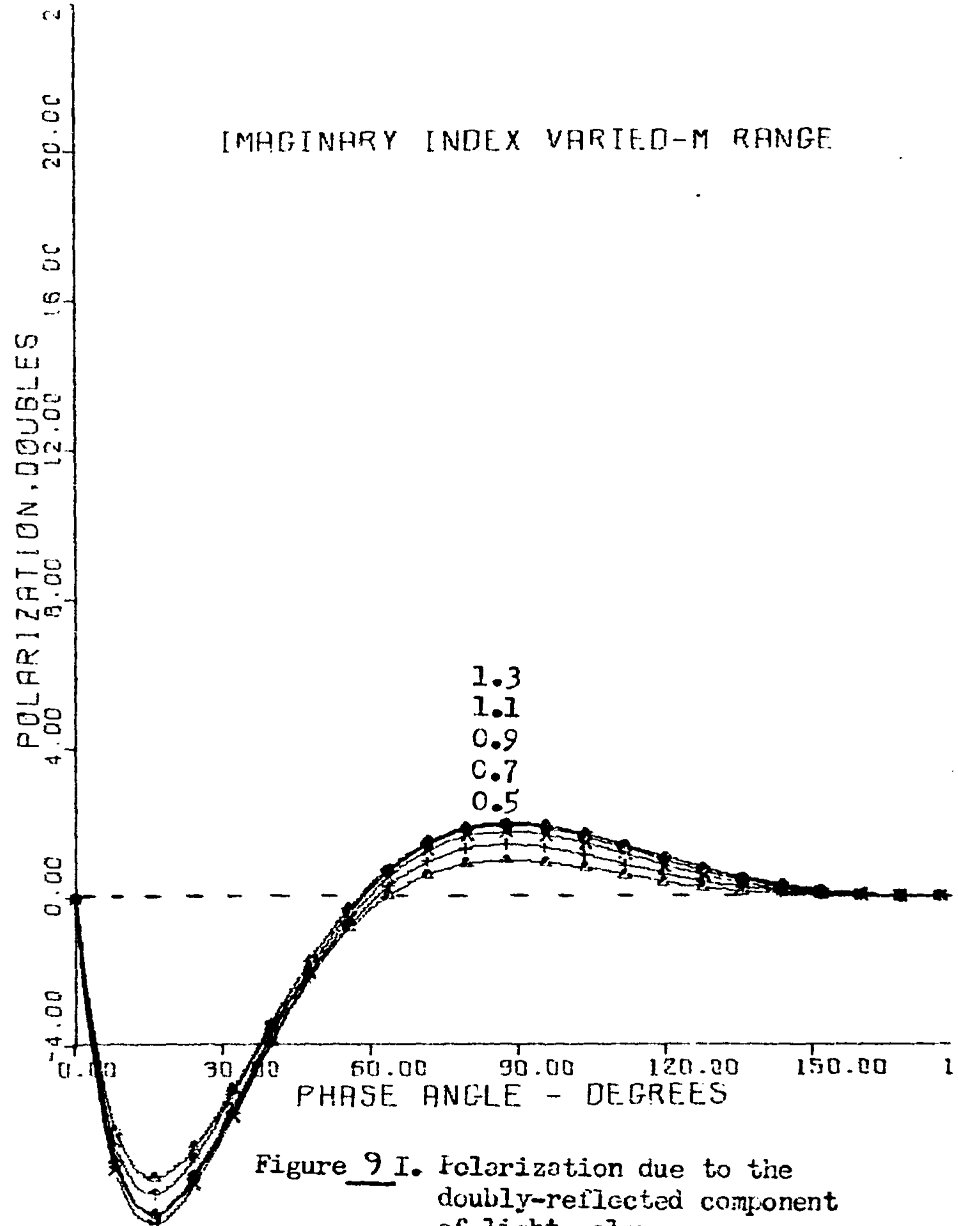

Figure 9 I. Polarization due to the doubly-reflected component of light, alone.

Such large values of doubles polarization have not yet been observed, and possibly indicate that the pitted,particulate model should be modified to a smoother surface in the metallic range of the imaginary index.

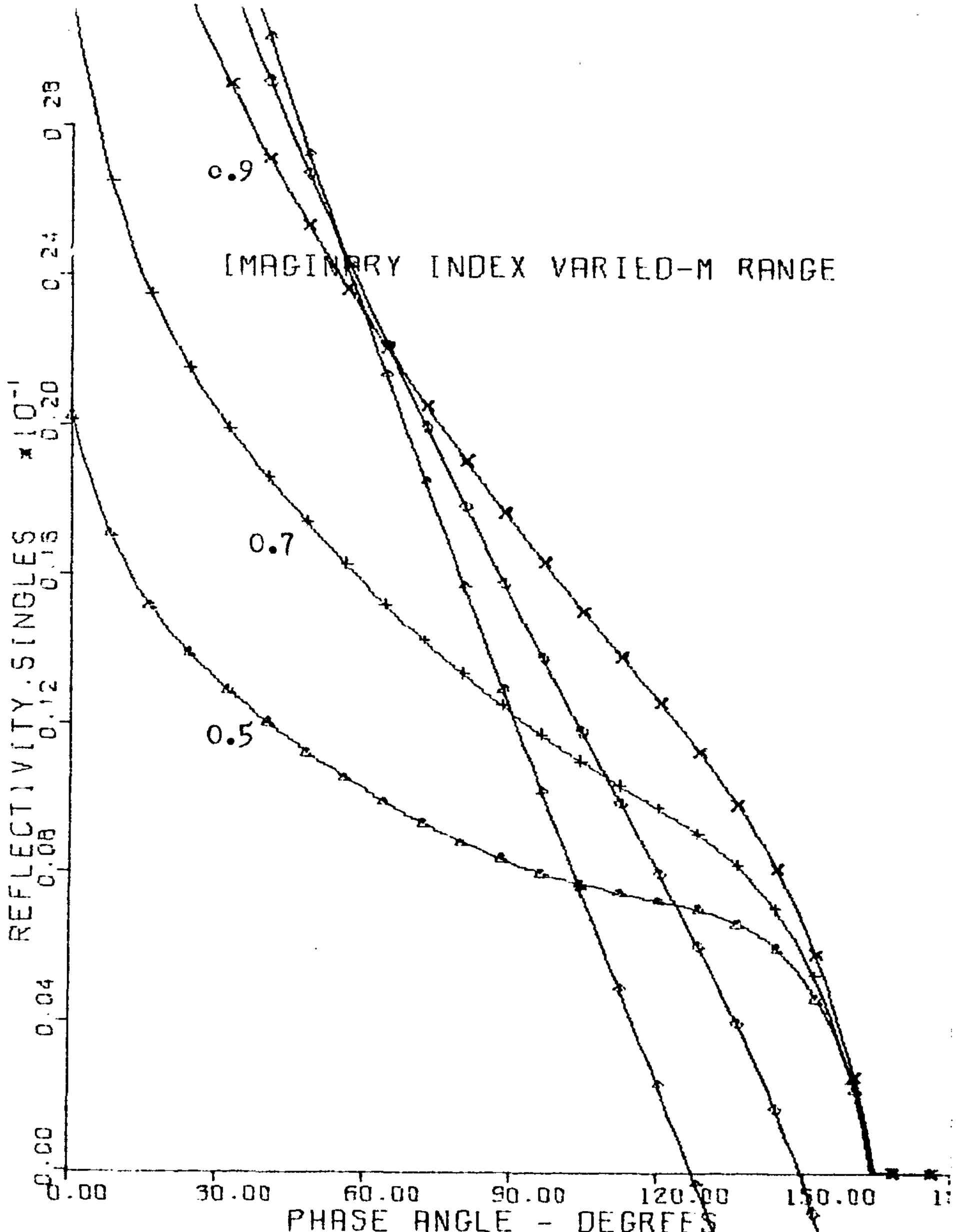

Figure 9 J. The intensity of the singly-reflected component of light.

THE PLOTTER HAS RUN UP AGAINST THE STOPS FOR THE TWO LARGEST VALUES.

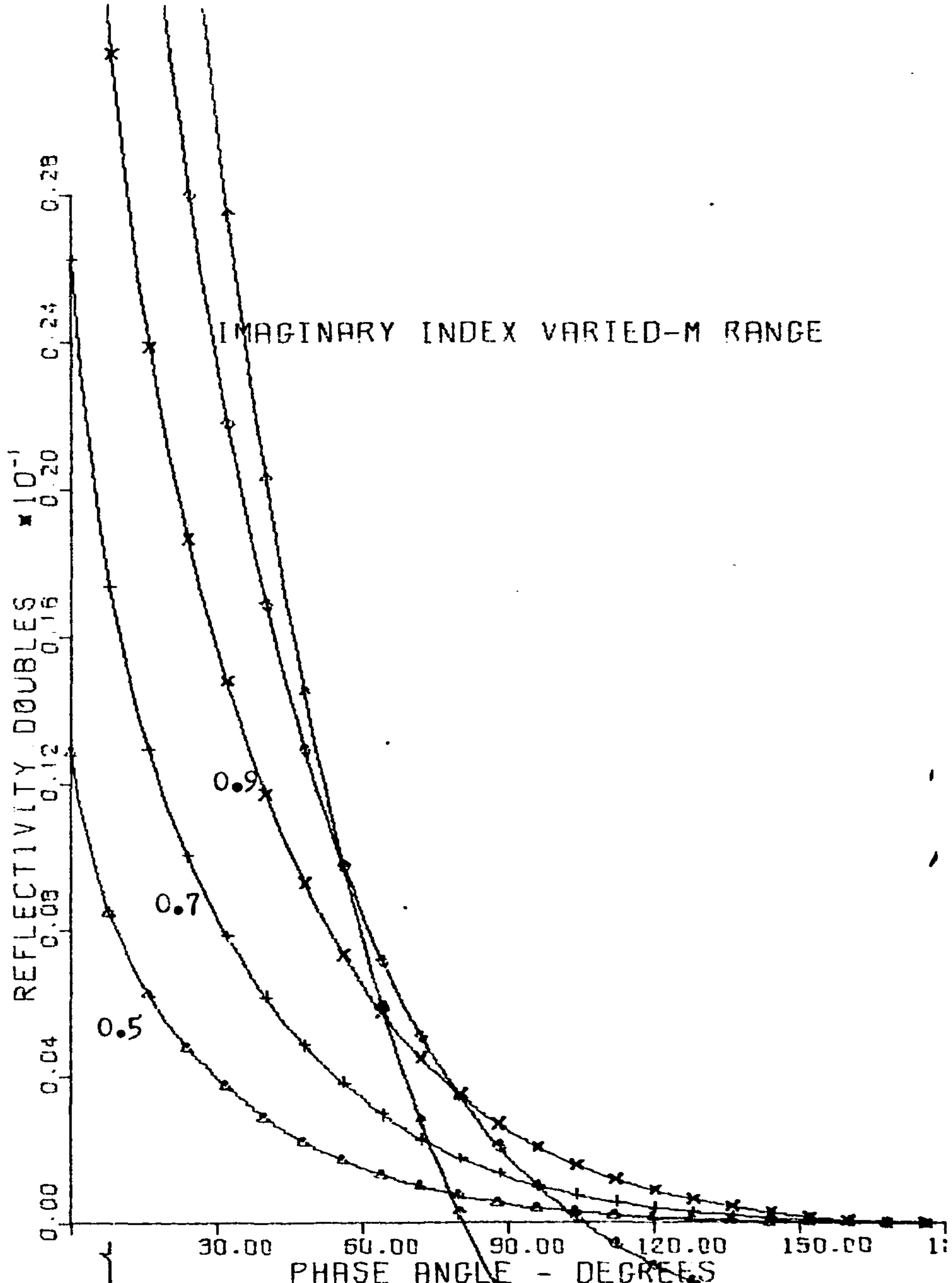

Figure 9 K. The intensity of the doubly-reflected component of light.

THE PLOTTER HAS RUN UP AGAINST THE STOPS FOR THE TWO LARGEST VALUES.

FLAT SURFACE (EXT) VARIED

Figure 10A to Figure 10K

These figures illustrate the effects of changing the amount of surface facing outwards that results in specular reflection. This "flat" surface is varied between zero and 40 percent.

In the model, external flat area is also changed by covering part of it with dust. Then the dust-covered part becomes a double-reflections source.

The equations for single-reflections use EXT in two ways. One equation computes singles reflecting from outside of pits,

outside singles = EXT x (1 - Dust) x . . .

and the other equation computes singles reflecting from inside of pits,

pit singles = (1 - EXT) x (1 - DUST) x . . .

In a complimentary fashion, doubles are also computed,

outside doubles = EXT x DUST x . . . .

pit doubles = (1 - EXT) x . . .

When trying to unravel meaning of polarization measurements, there is a simple geometric fact which becomes a powerful tool of analysis, "The sum of the pitted area plus the non-pitted area is a constant" . The sum of the two is, of course, the total area. This becomes immediately useful if pitted area is associated with the formation of the negative polarization branch, and , the non-pitted area is associated with the positive polarization branch.

For example, in the figure at right, as EXT is increased the positive branch grows, and the negative branch diminishes. This is immediately understood by applying the above principle ; if singles polarization is increased by geometric change, then the doubles polarization must decrease. Note, also, that the inversion point moves to the left.

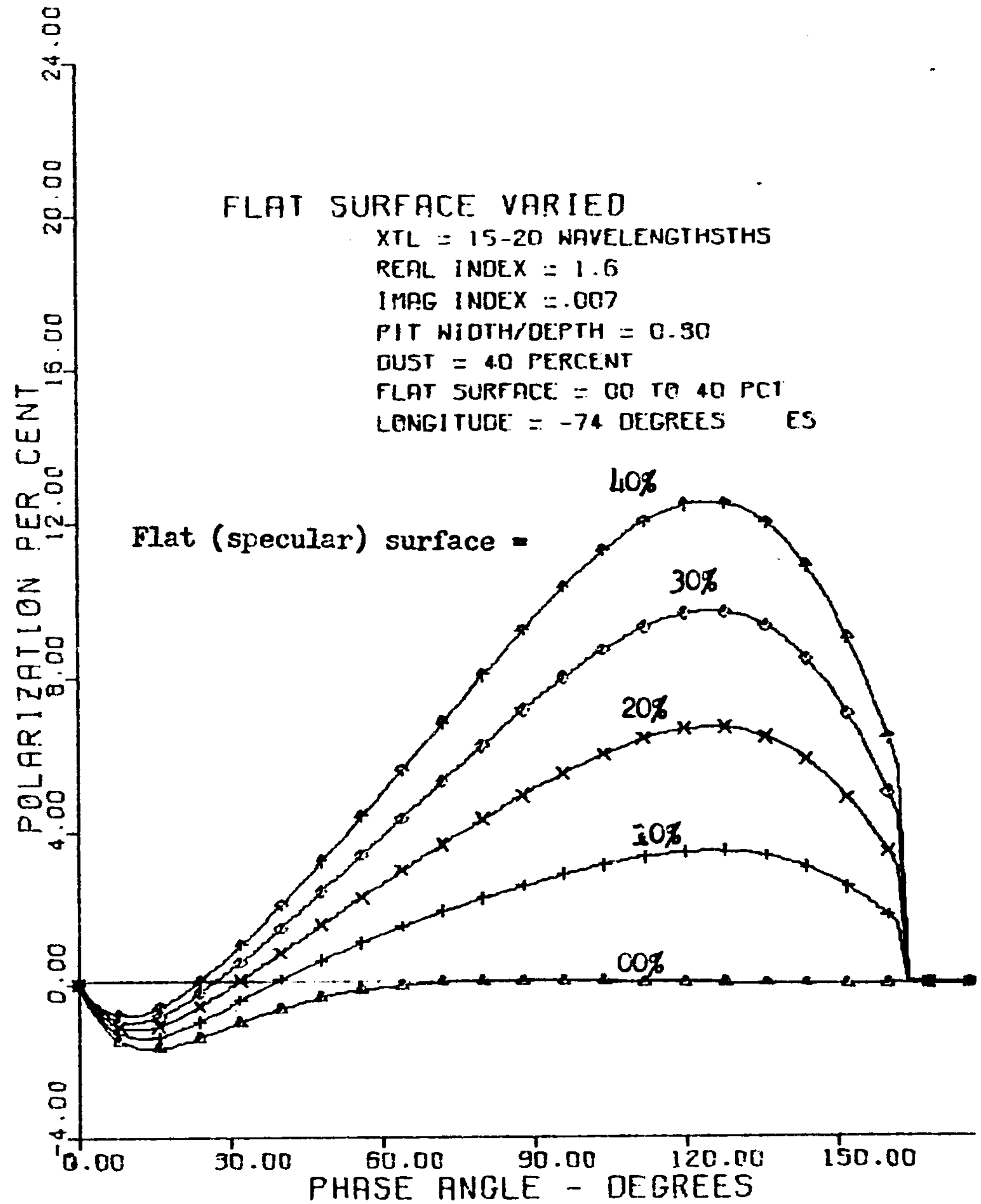

Figure 10 A. Polarization at a point on a planet.

Increasing the flat surface increases single reflection which produces + polarization. This competes with the - polarization due to double reflections, raising P(min) and pushing the inversion point to the left.

The low values of flat surface have not been observed for solar system bodies.

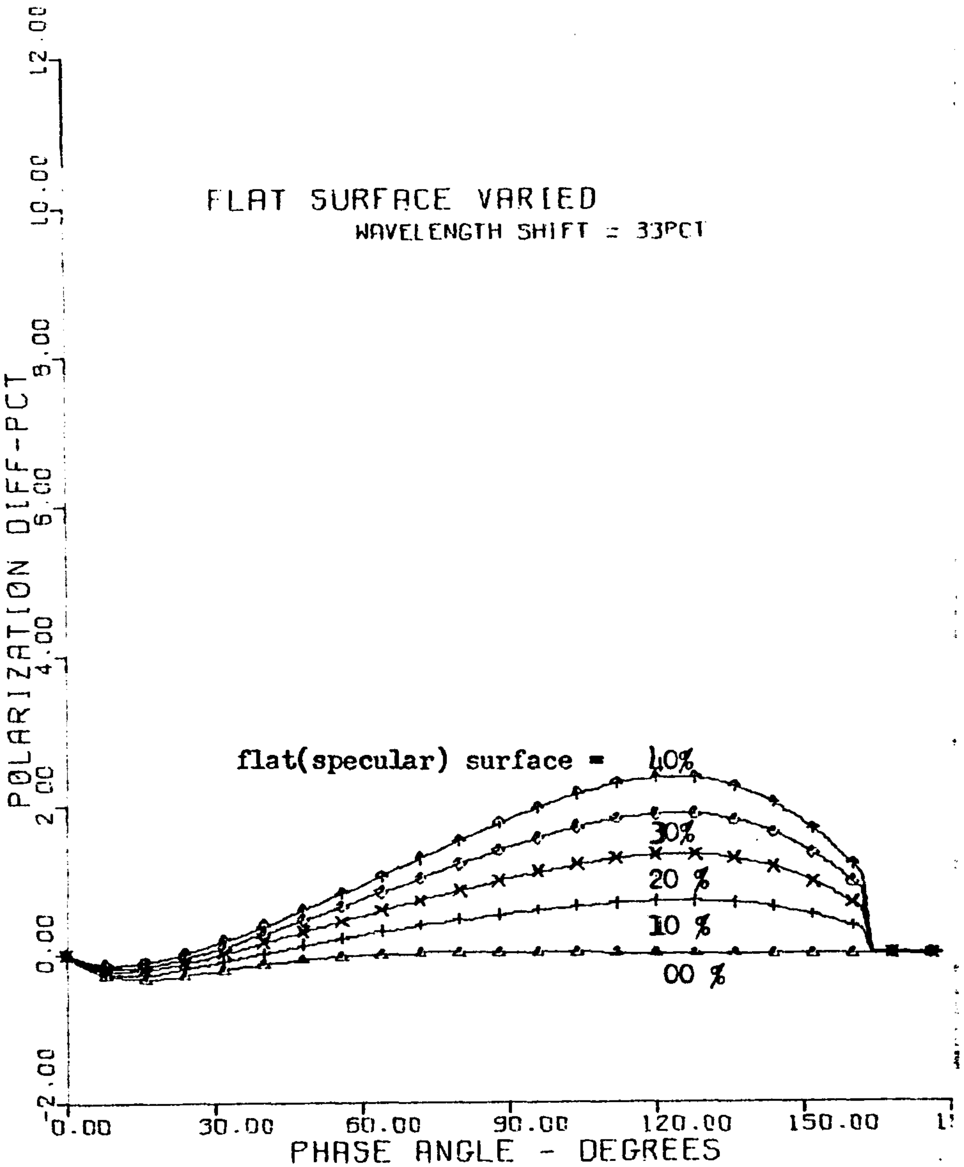

Figure 10B. Polarization shift for a wavelength shift of 33 percent.

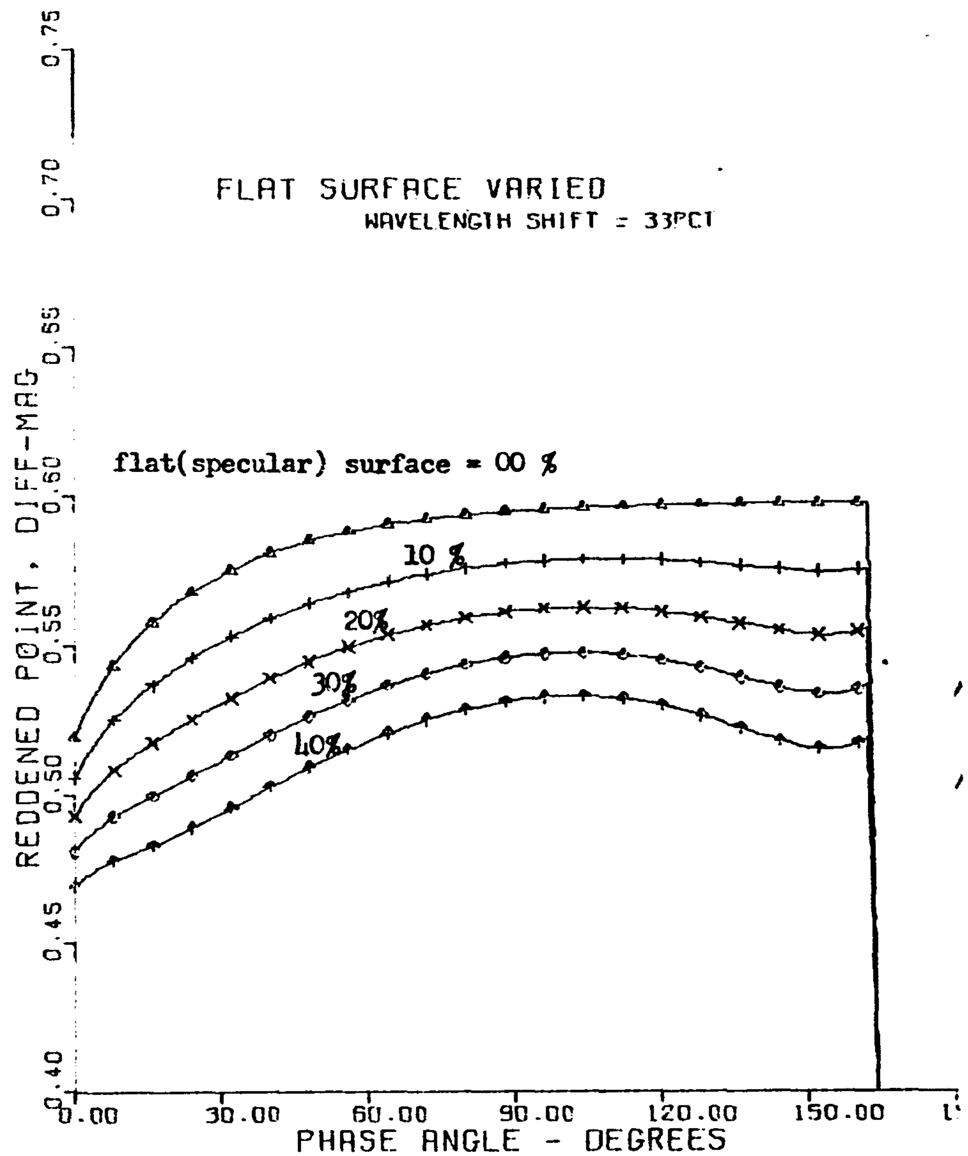

Figure 10C. The reflectivity shift, in magnitudes, of a point on the planet, for a wavelength shift of 33 percent.

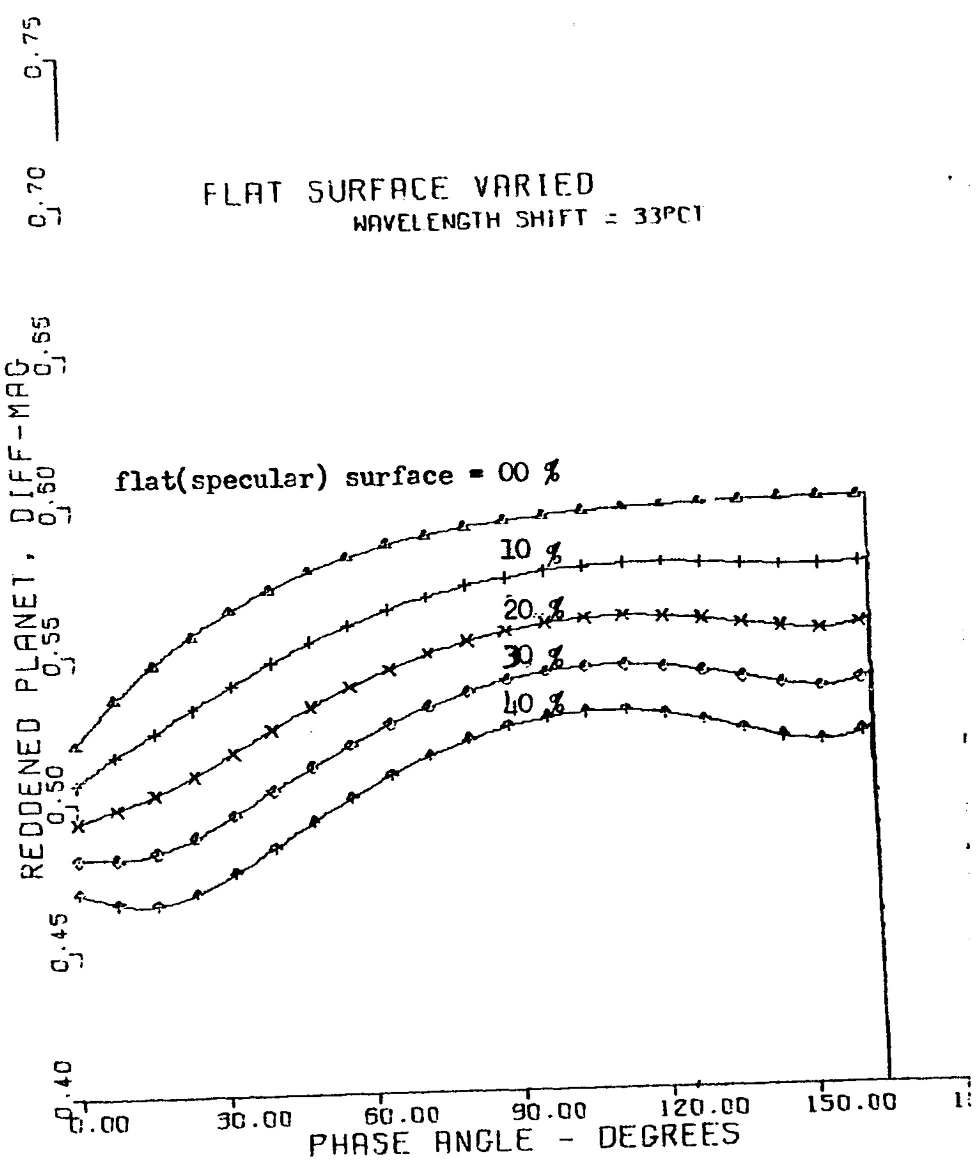

Figure 10D. The reflectivity shift, in magnitudes, of the integrated planet, for a wavelength shift of 33 percent.

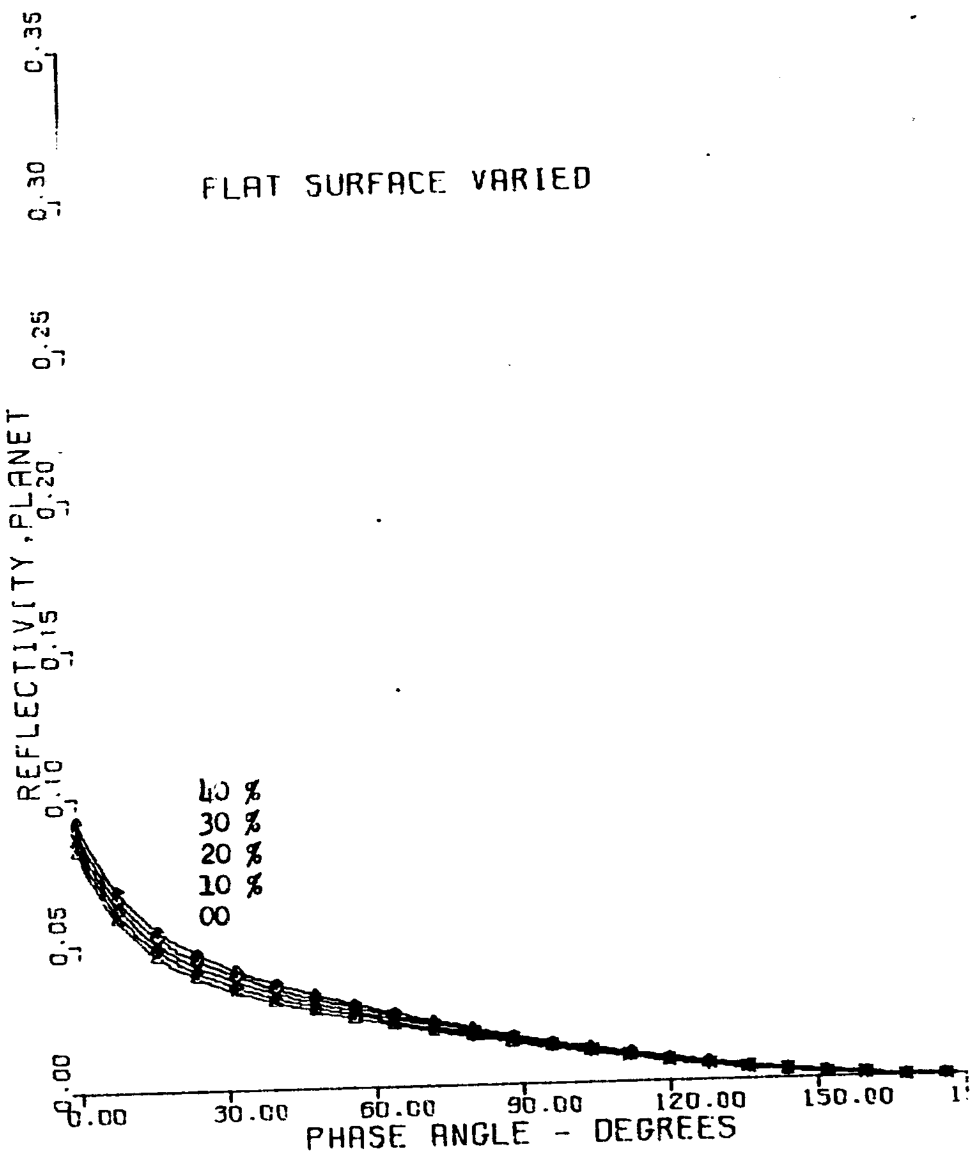

Figure 10 E. The integrated reflectivity of the entire planet.

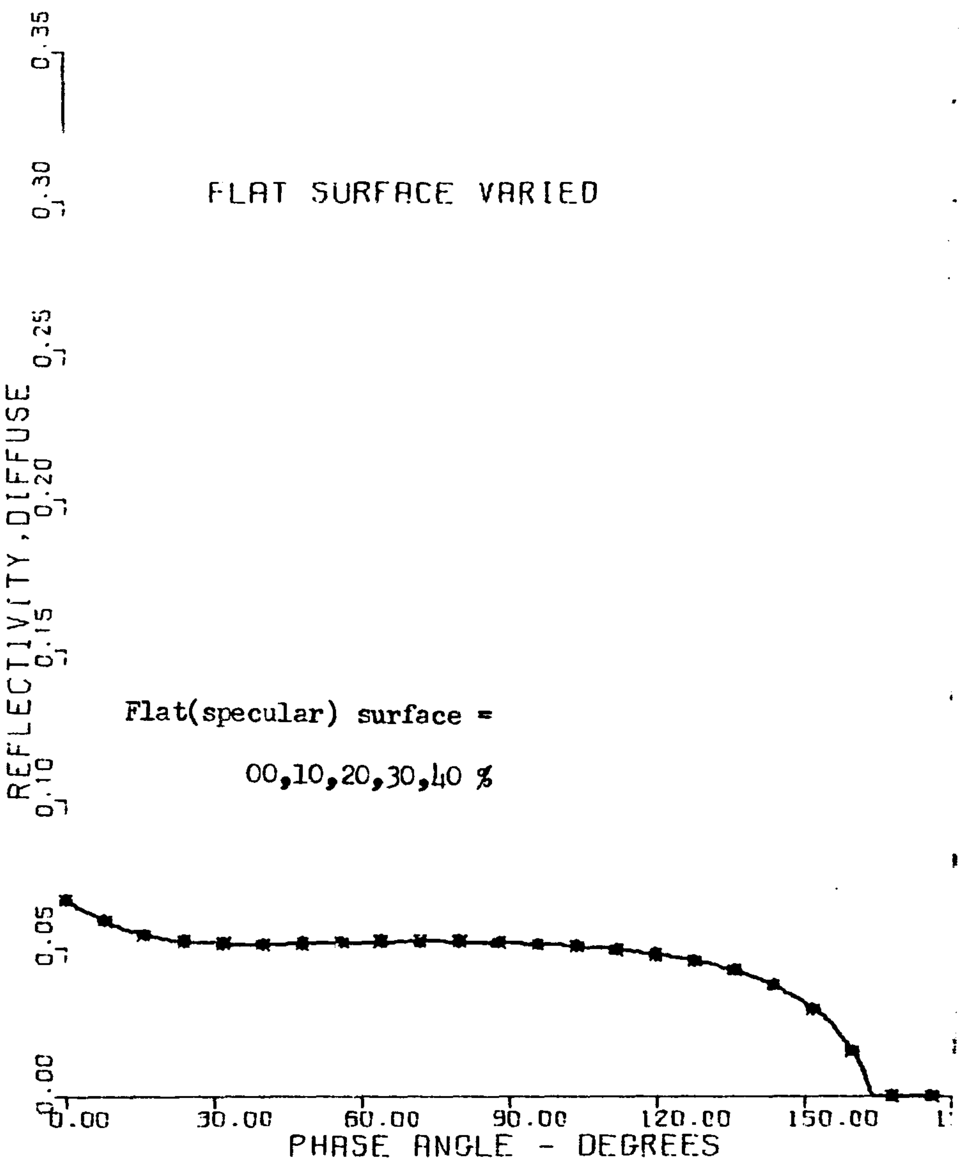

Figure 10 F. The diffuse component of light at a point on the planet. Diffuse light emerges from particles after inward refraction and multiple internal reflections.

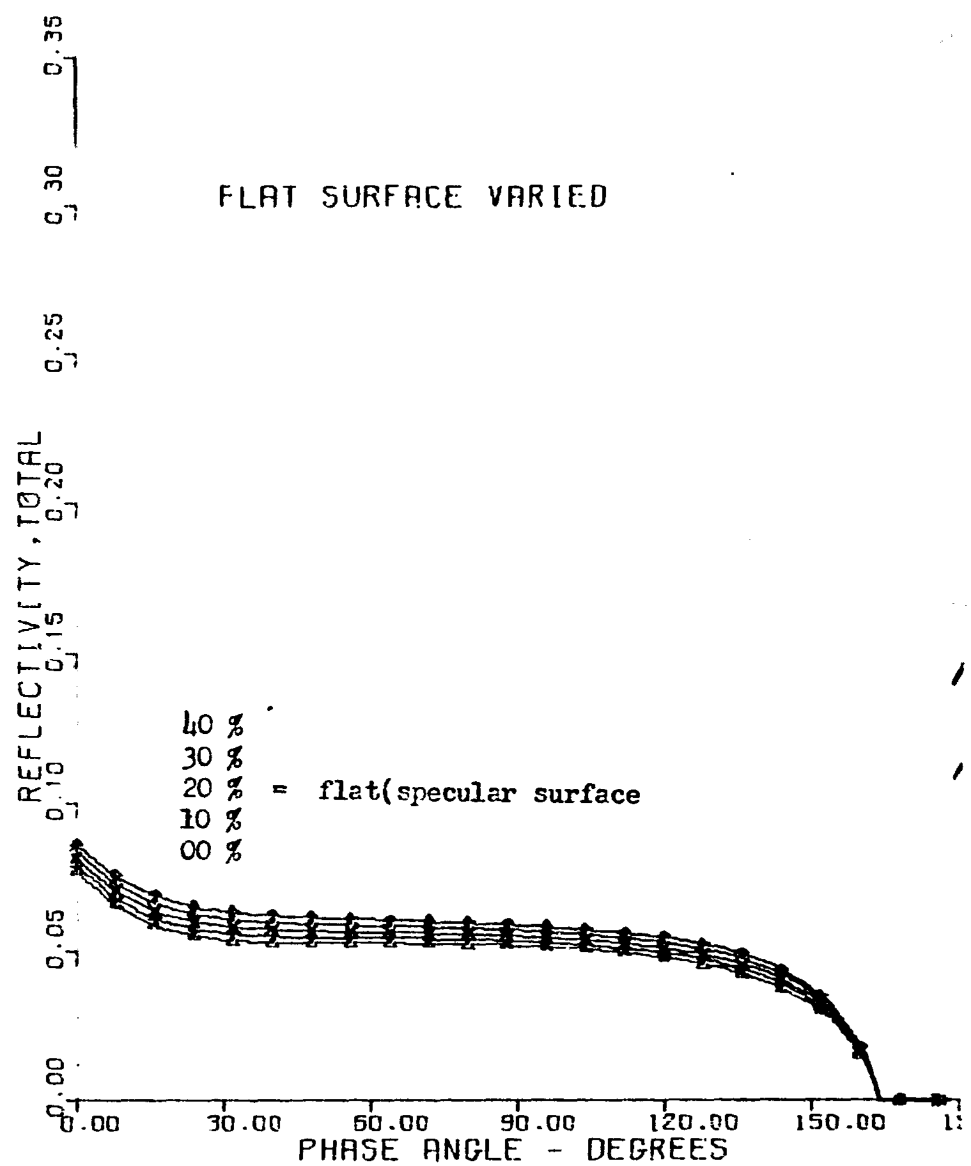

Figure 10 G. The total of all light components (singles + doubles + diffuse) at a point on the planet.

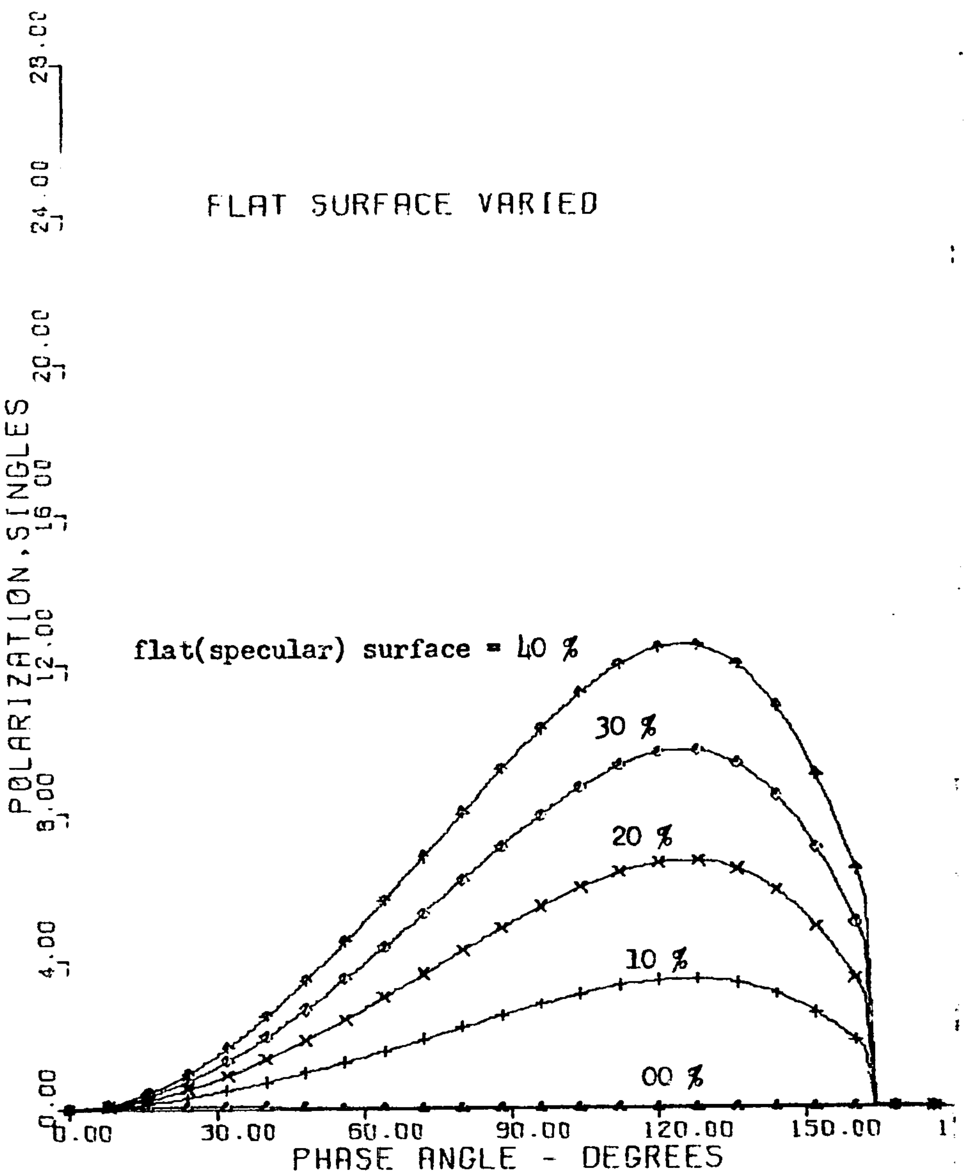

Figure 10 H. The polarization due to the singly-reflected component of light, alone.

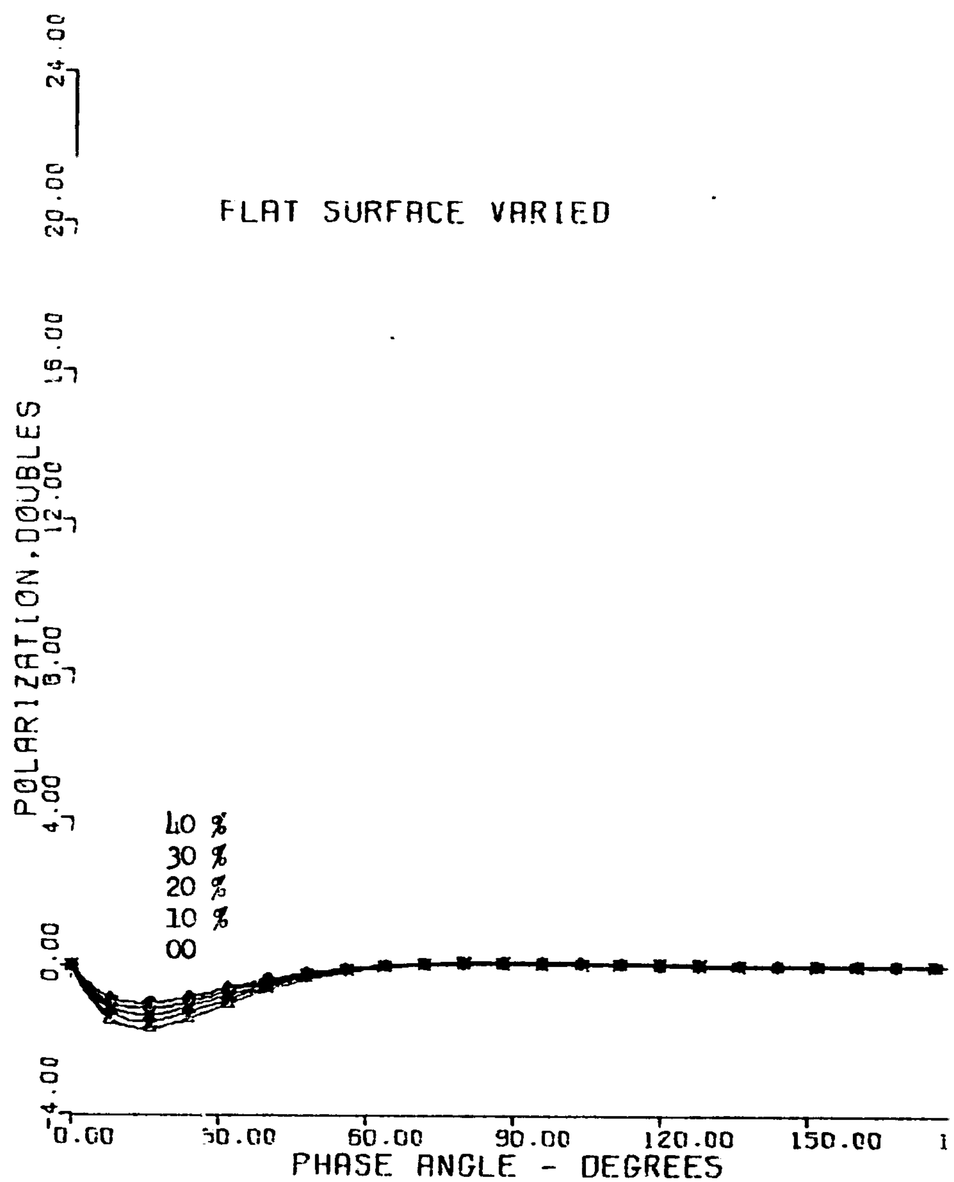

Figure 10 I. The polarization due to the doubly-reflected component of light, alone.

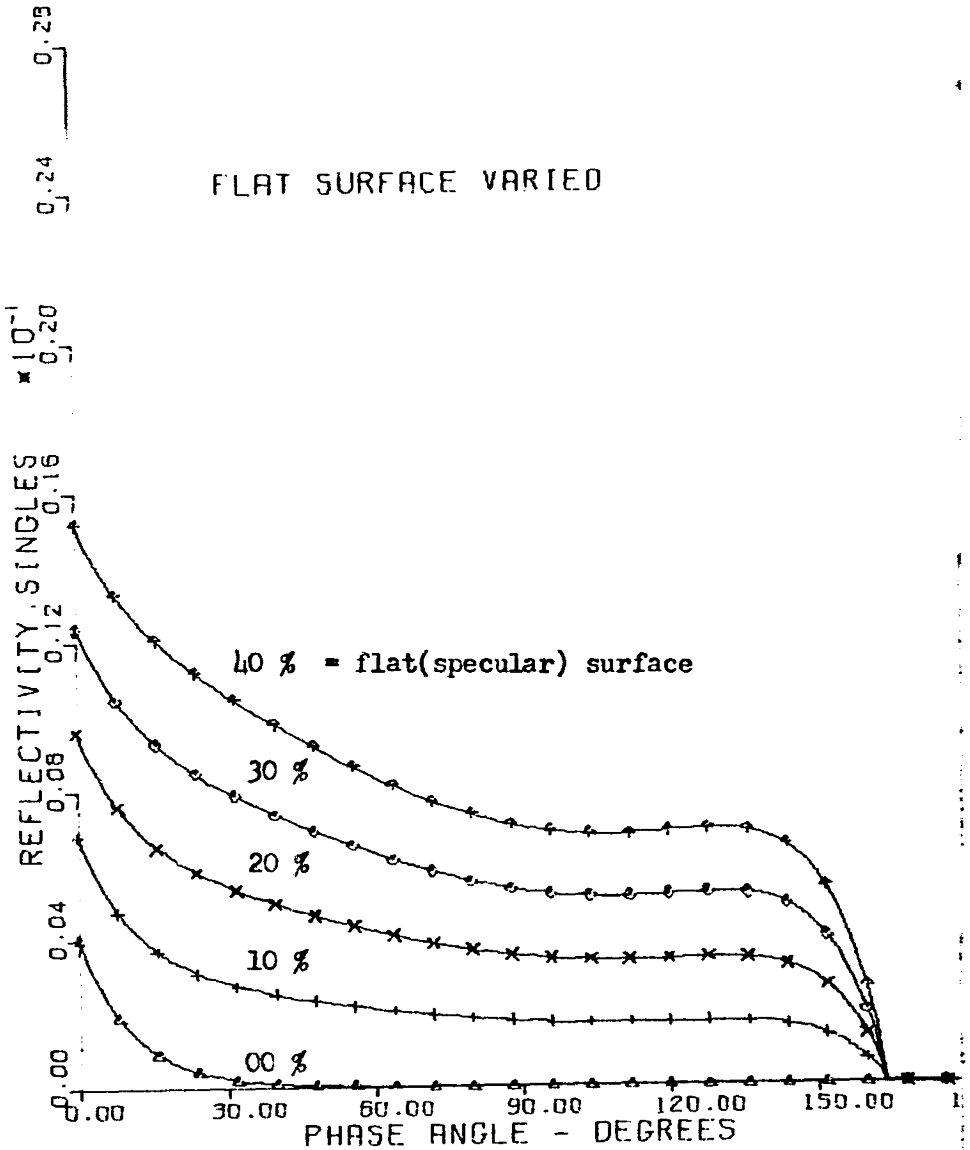

Figure 10 J. The intensity of the Singly-reflected component of light.

Note that the model still yields single reflections from inside pits, even though external flat surface = zero. Pit reflections are seen near opposition.

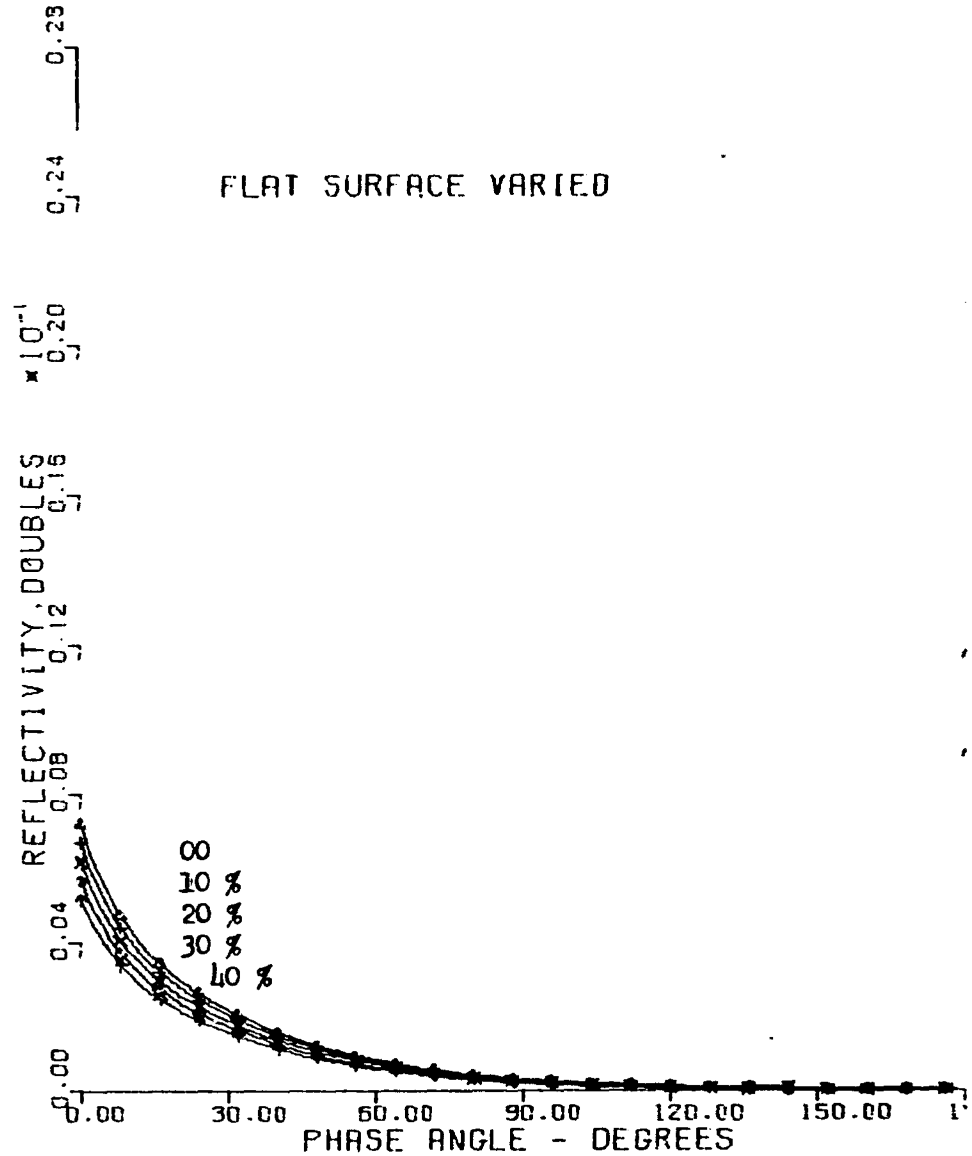

Figure 10 K. The intensity of the doubly-reflected component of light.

These two figures illustrate clearly that increasing the specular surface increases the singles reflections, but robs the doubles of opportunity for reflection because there is less area (non-specular) remaining.

WAVELENGTH (PARTICLE SIZE, XTL) VARIED
Figure 11A to Figure 11K

This set illustrates the effects of varying the wavelength of observed light. This is done by varying the size XTL of particles which are measured in wavelengths in the model. Wavelength is the fundamental measure of size in a problem of this sort.

The well-known dependency of refractive index on wavelength is not modeled in these figures. However, the effects of changing indices are shown in other figure sets. The reader must choose his own combinations.

The computer program changes particle size only in the diffuse light calculation. When size is increased, the light entering particles has farther to travel before getting out after multiple reflections. The longer path results in more absorbtion so that the diffuse light component is decreased.

Particle-size effects are not in the model for single and double reflected light components. However, if were included because of an appreciable presence of fine dust, one would expect single reflections to decrease, and double reflections to increase. This would accentuate most of the results of this figure set.

NOTE THAT FIGURES B,C,D OF ALL THESE SETS ALSO SHOW A DIFFERENTIAL EFFECT OF A WAVELENGTH SHIFT.

Figures C and D of all sets whichare applicable show that the wavelength-dependent size of surface particles is sufficient to explain color changes and reddening of the Moon and many other bodies at visible wavelengths. For Mars and some others, it is not sufficient and a change of refractive index must be invoked to explain observed color changes.

Similarly, the albedo changes of the Moon and the accompanying change of P-max are explained and quantitativly predicted by the figures of this set.

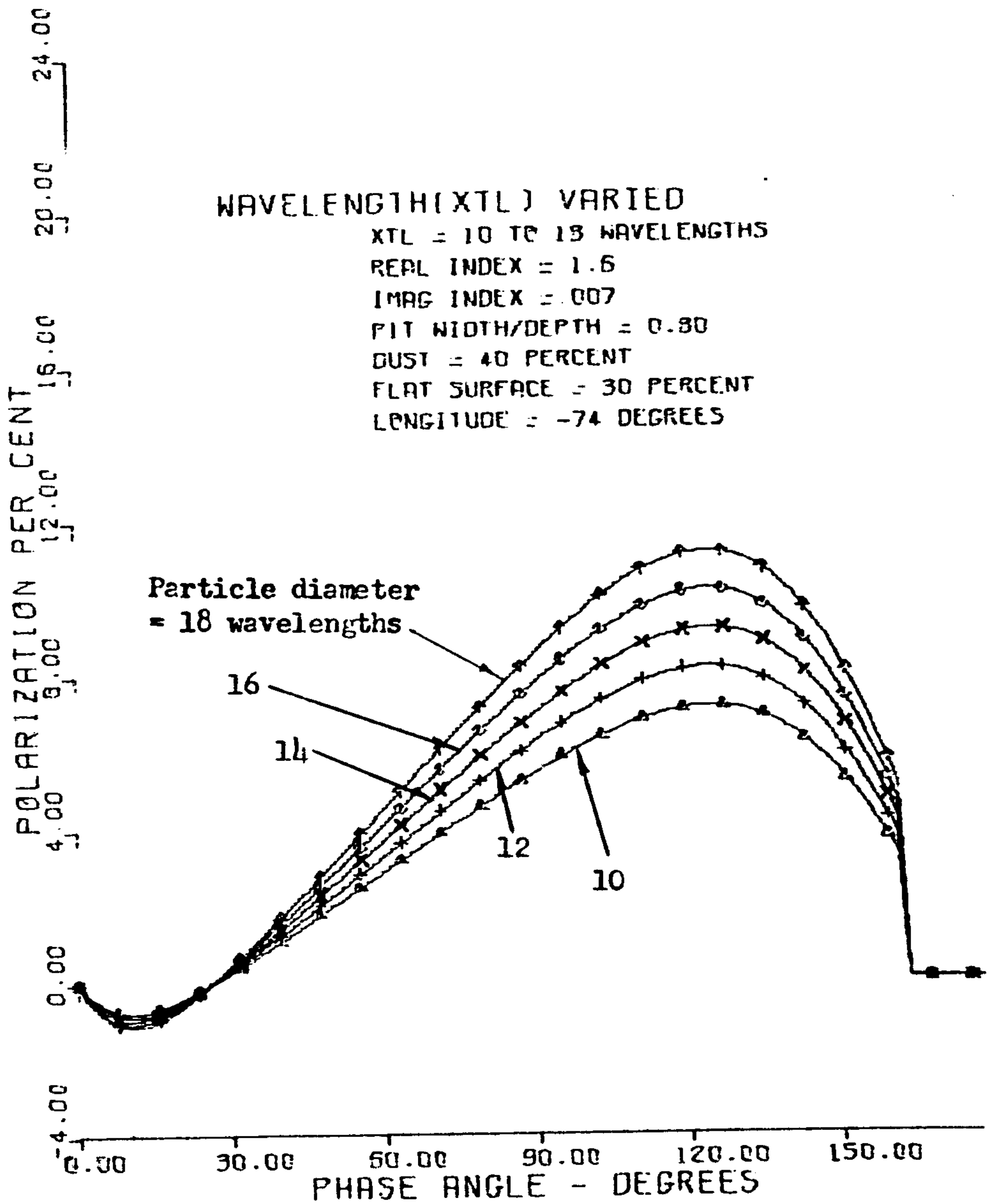

Figure 11 A. Polarization at a point on a planet.
Changing particle size is equivalent to changing wavelength, because the unit of size is wavelength. Smaller particles means longer wavelengths.
As wavelength is increased, the travel distance for diffuse light inside the particles becomes smaller resulting in less attenuation. This produces more diffuse light to dilute and decrease polarization.

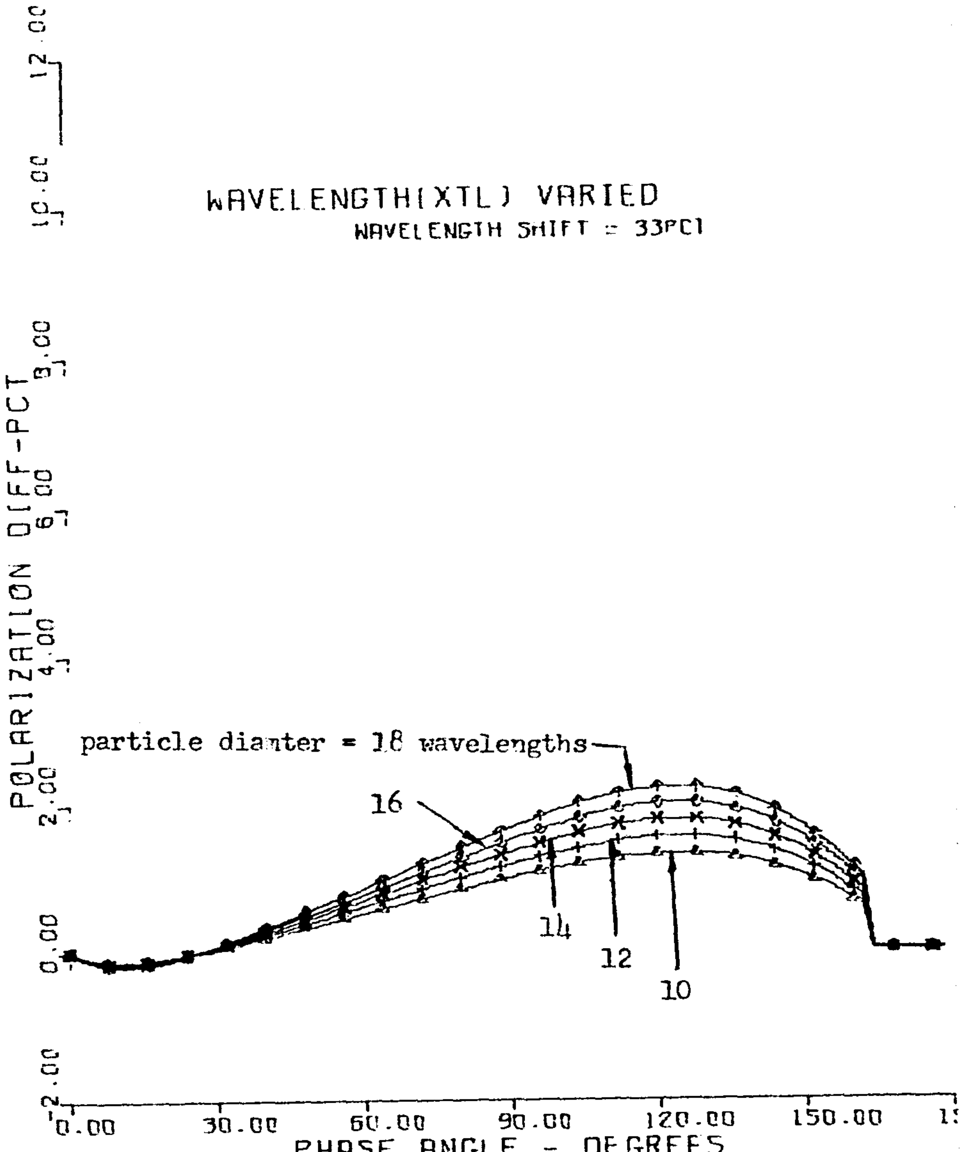

Figure 11 B. Polarization shift for a wavelength shift of 33 percent.

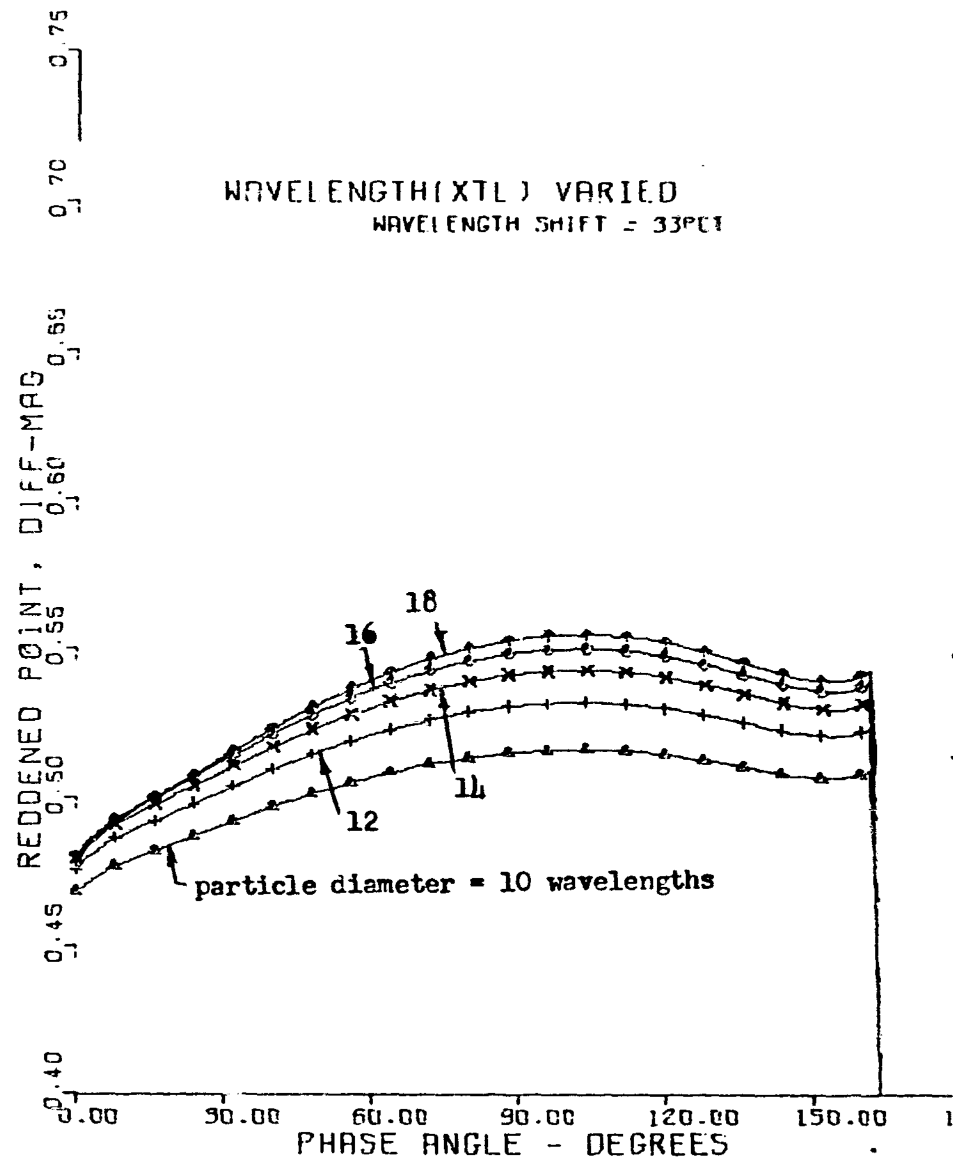

Figure 11 C. The reflectivity shift, in magnitudes, of a point on the planet for a wavelength shift of 33 percent.

Note that the "reddening" (slope of reflectivity) increases if the wavelength is smaller. This agrees with the observed rule that the darkest bodies show the greatest reddening.

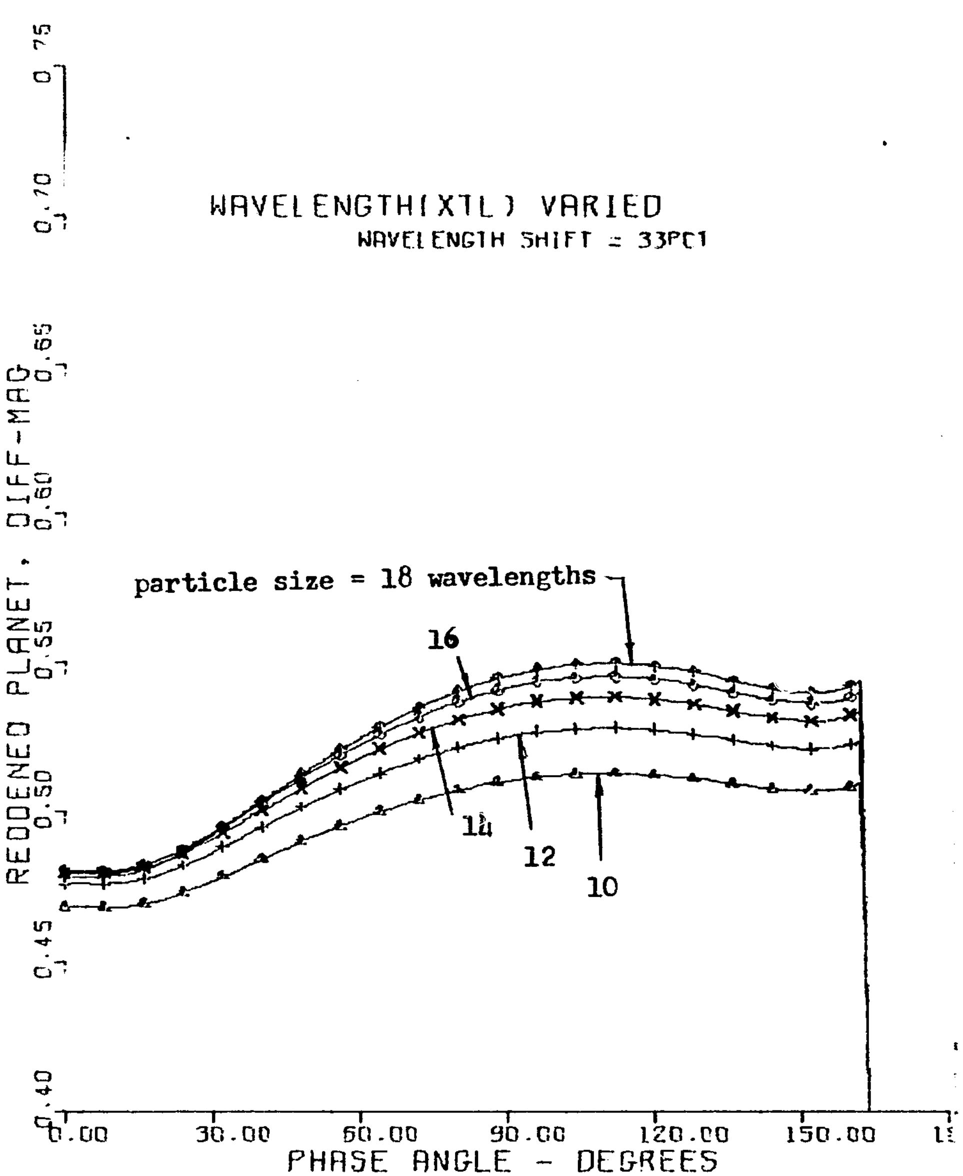

Figure 11 D. The reflectivity shift, in magnitudes, for a wavelength shift of 33 percent, of the integrated planet.

Note that "reddening" (slope) increases as observed, but the slope is not a constant as often approximated in the literature.

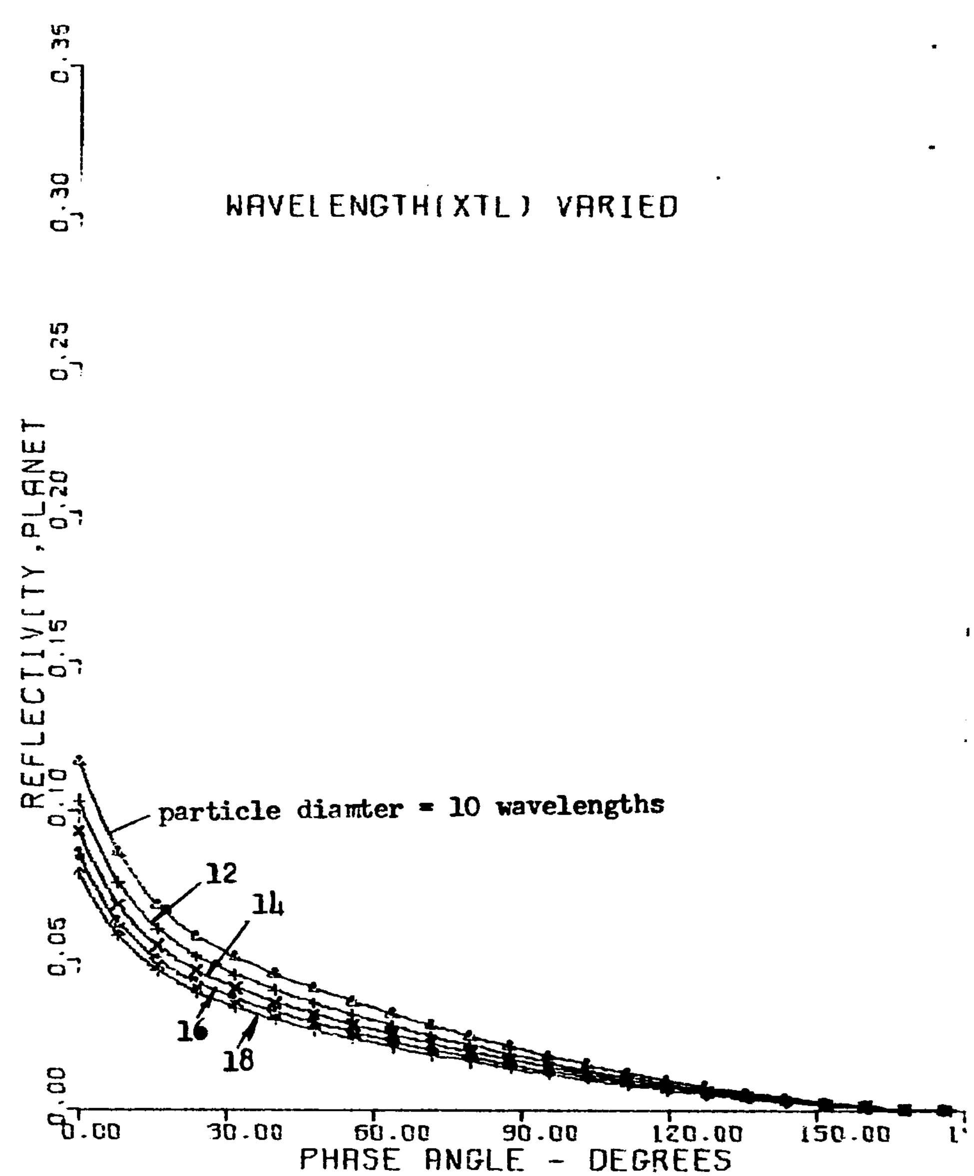

Figure 11 E. The integrated reflectivity of the entire planet.

Reflectivty decreases with decreasing wavelength, as observed for most bodies.

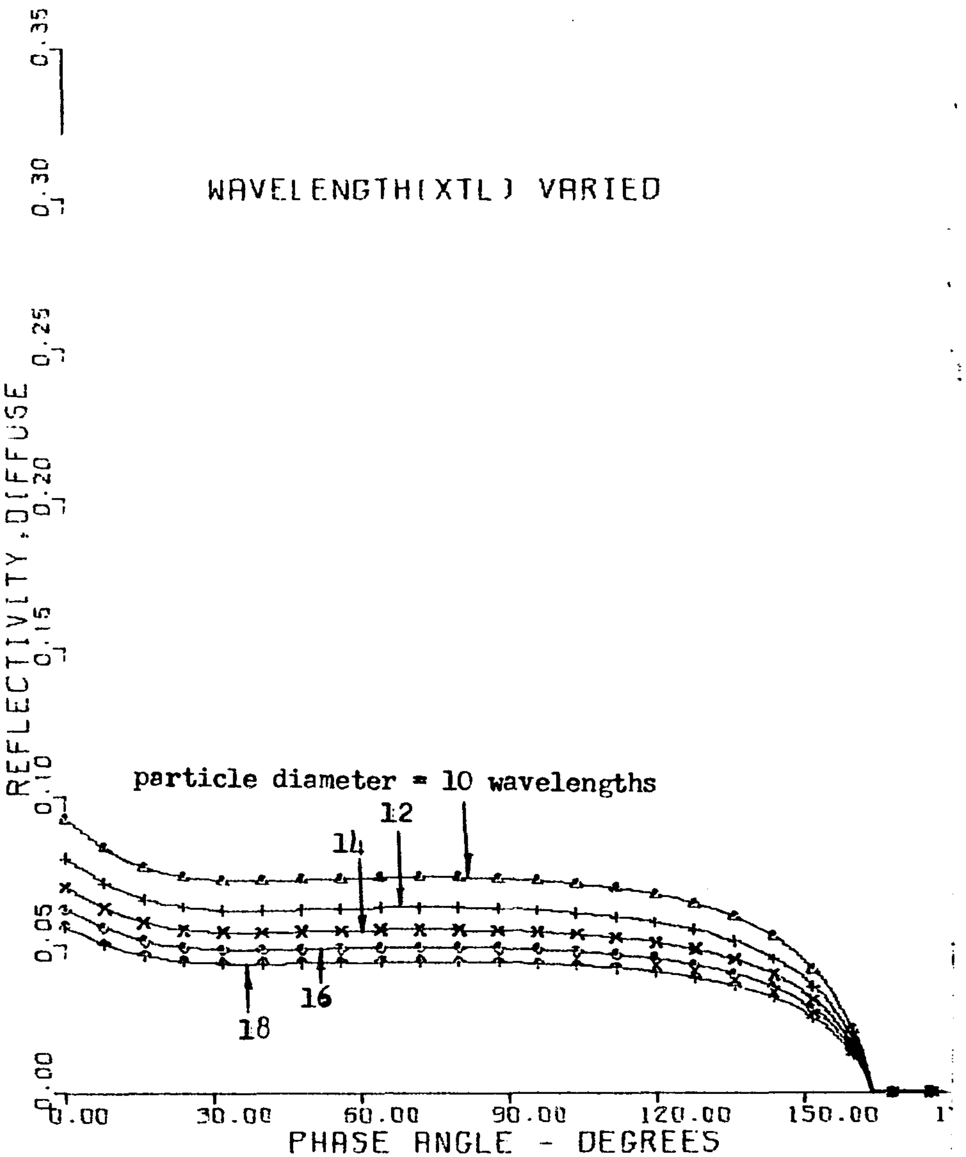

Figure 11 F. The diffuse component of light at a point on the planet. Diffuse light emerges from particles after inward refraction and internal reflections.

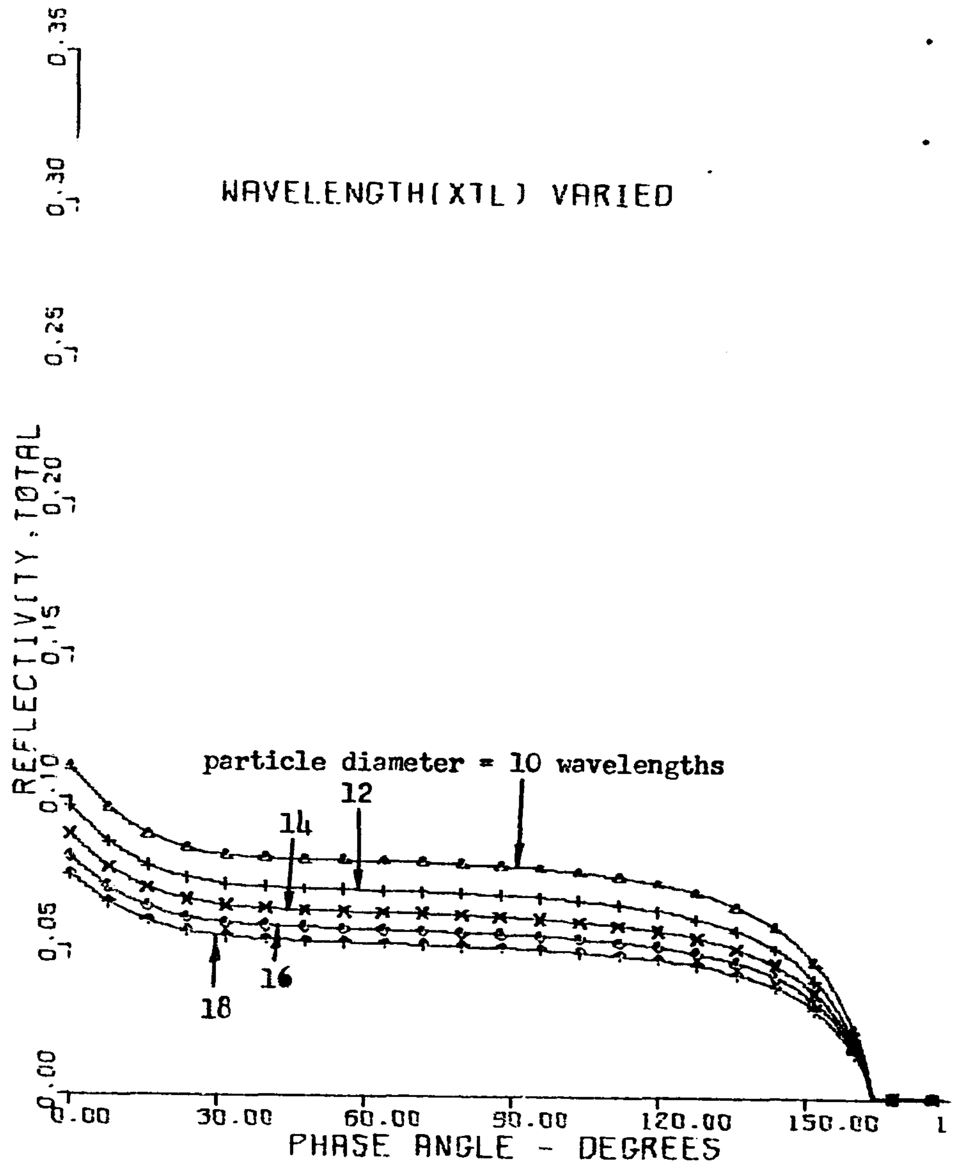

Figure 11 G. The total of all light components (singles + doubles + diffuse), at a point on the planet.

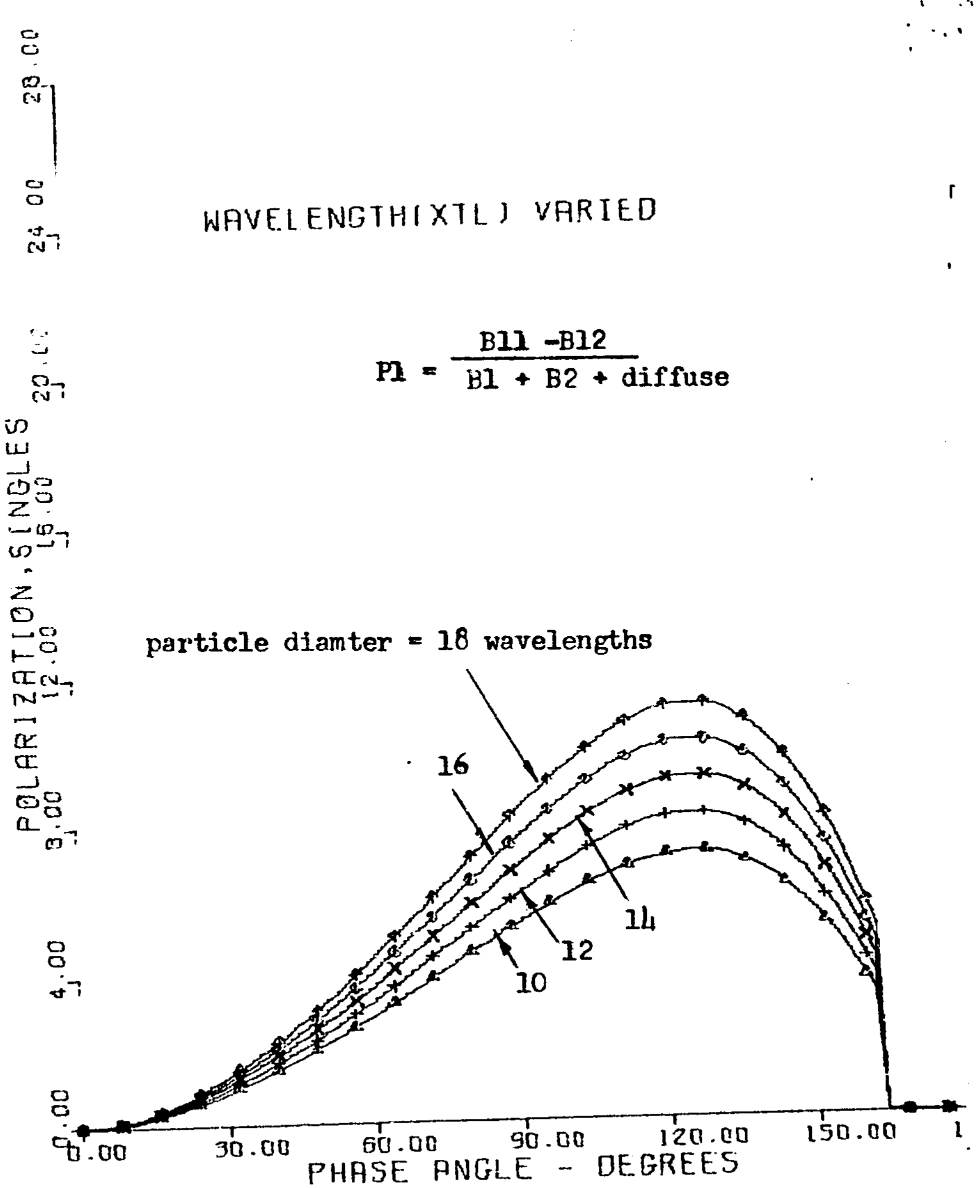

Figure 11 H. The polarization due to the singly-reflected component of light, alone.

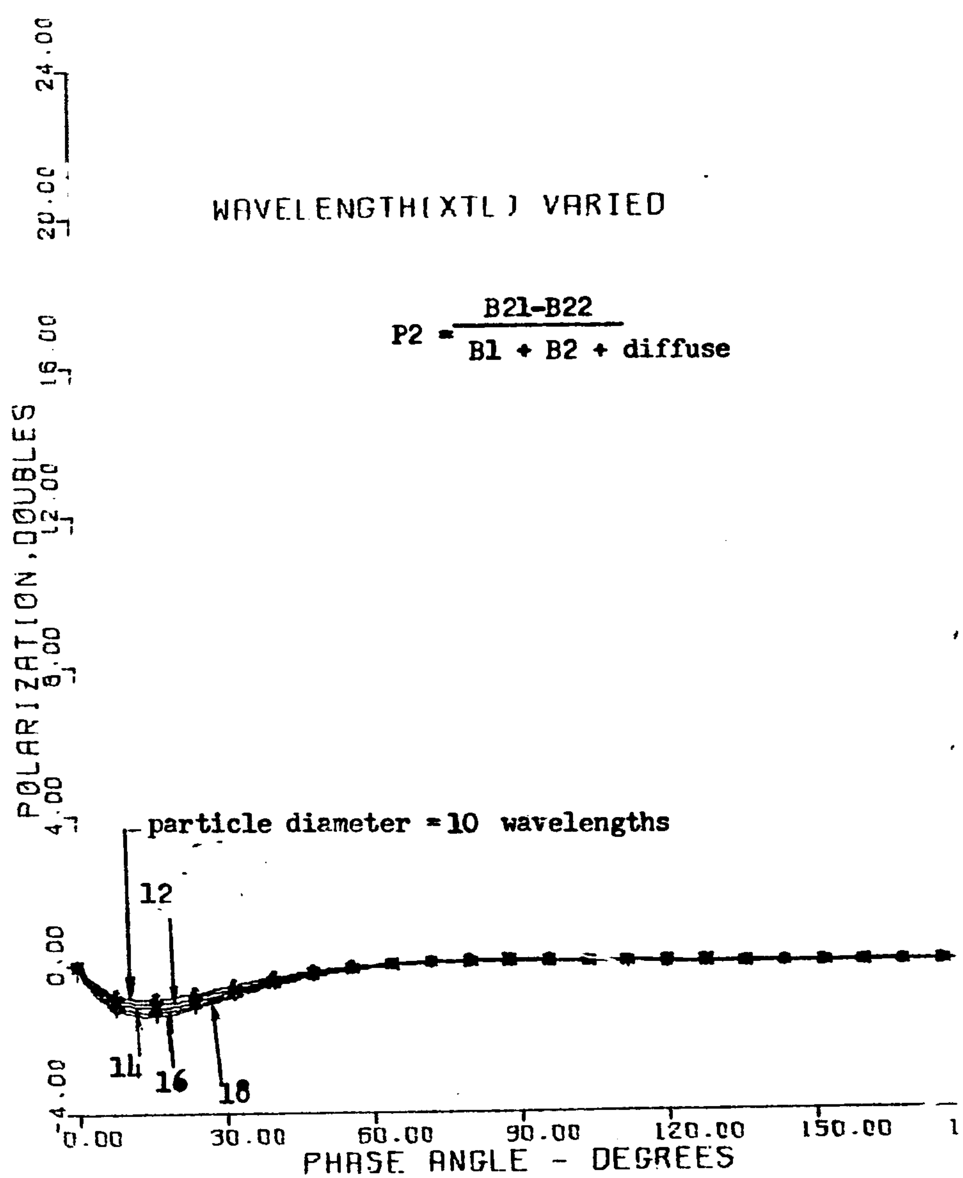

Figure 11 I. The polarization due to the doubly-reflected component of light, alone.

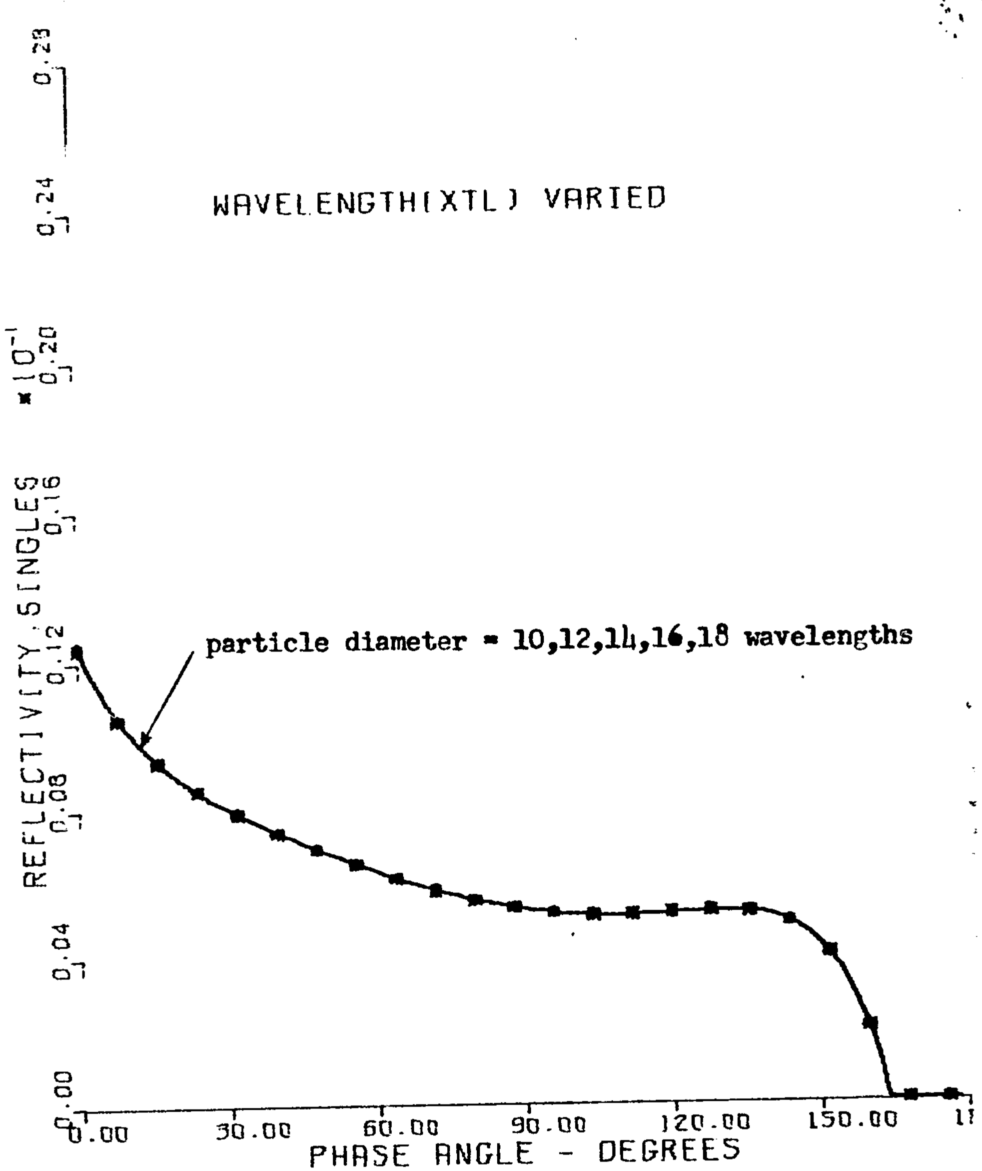

Figure 11 J. The reflected intensity of the singly-reflected component of light.

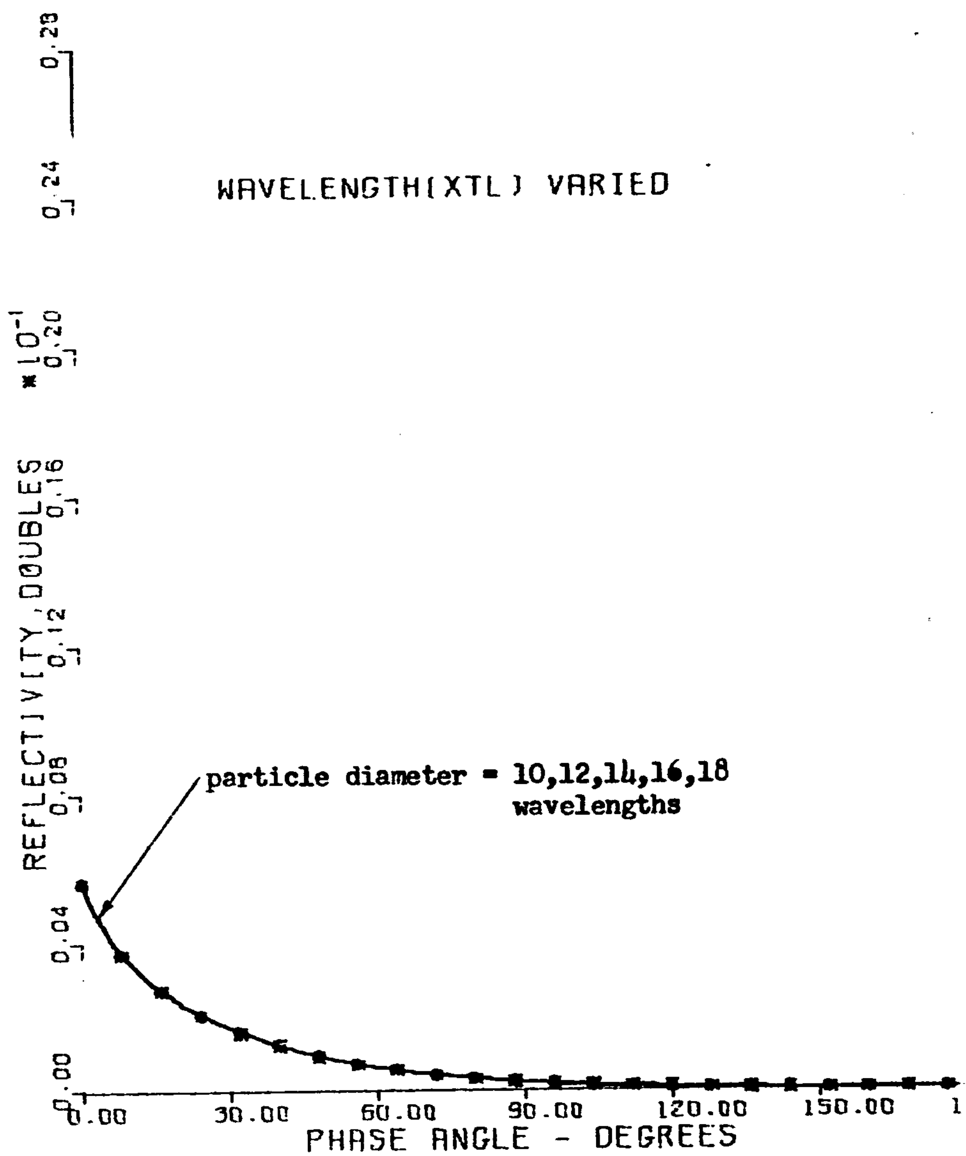

Figure 11 K. The intensity of the doubly-reflected component of light.

PIT WIDTH/DEPTH RATIO (WID) VARIED
Figure 12A to Figure 12K

This set shows the variation of the computer parameter WID which is closly related to the average ratio of width to depth of the pits and interstices of the reflecting surface. WID is used exclusively as an exponential constant to compute light components which decrease with phase angle such as the opposition effect and double reflections which come out of pits. For example,

$$\text{sideways doubles} = 2\exp(-G/4\mathrm{WID})\ x \ldots$$

The various uses of WID in the computer model imply geometric properties of the pitted, particulate surface, some of which are evident from the following list of constants which have been chosen :

light component	exponential constant
sideways doubles	4 WID
backwards doubles	8 WID
singles	WID
forward doubles	$\frac{1}{2}$ WID

The actual width/depth of the average pits on the surface is approximately 4 x WID.

In a later section of this report, some relations are derived between WID, the inversion angle, and the angular position of P-min.

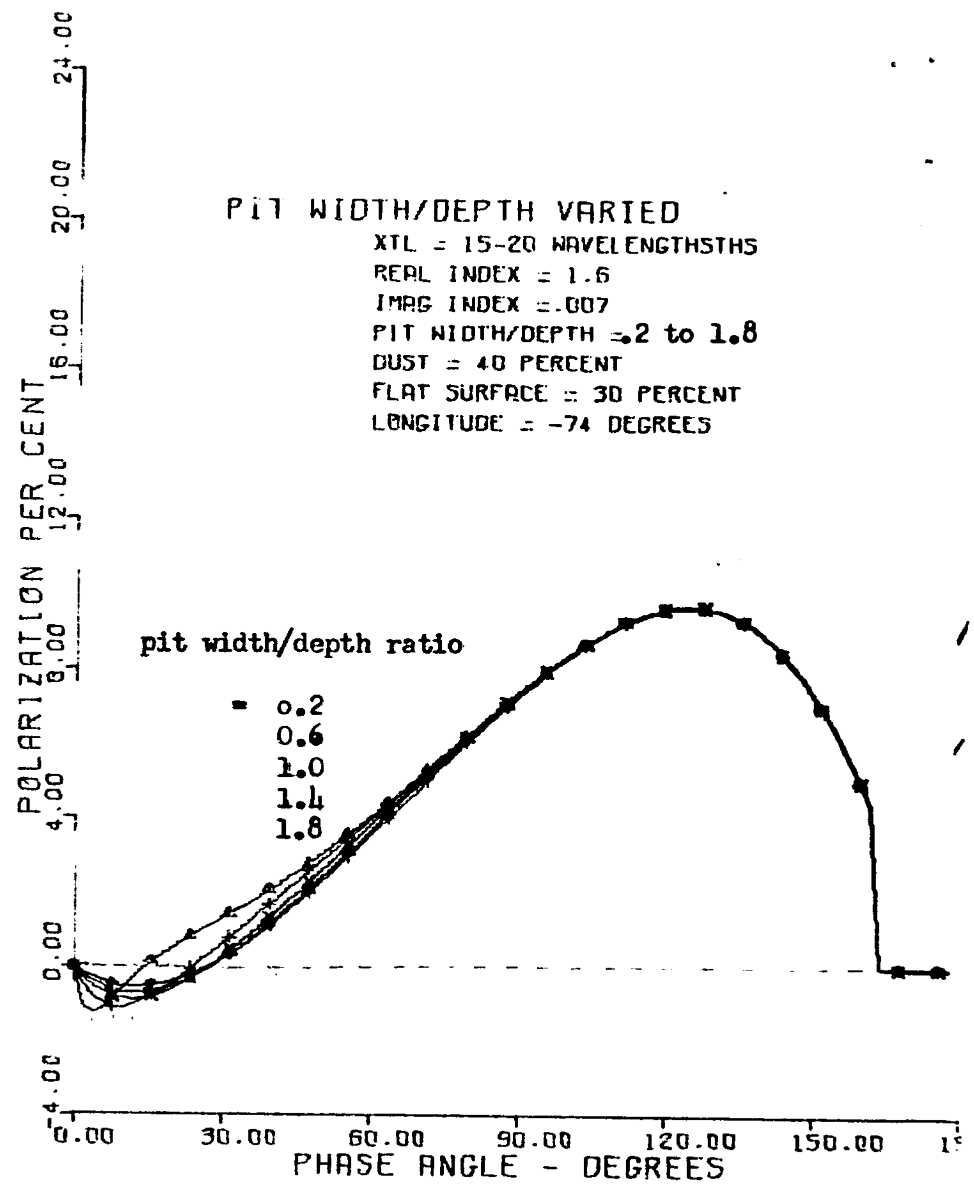

Figure 12A. Polarization at a point on a planet.

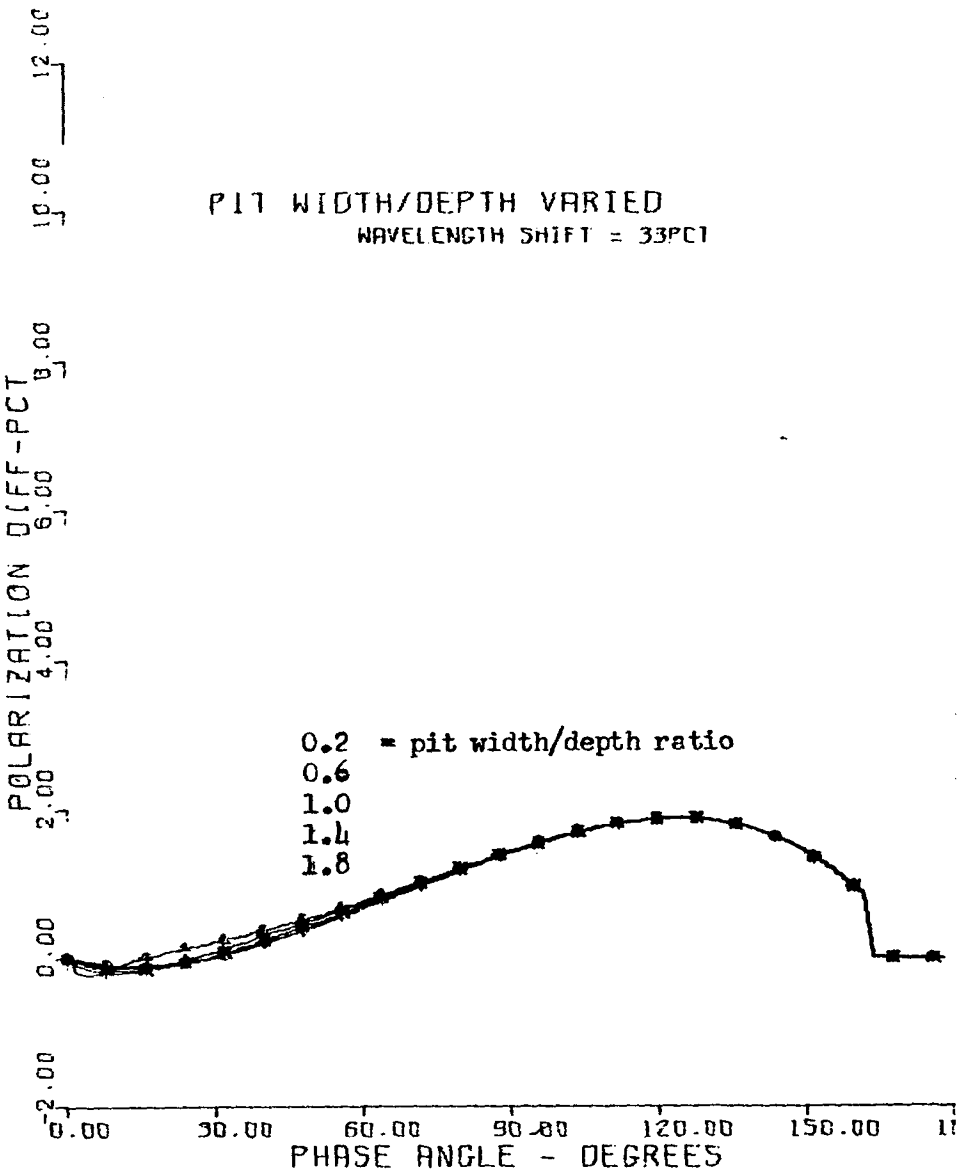

Figure 12B. Polarization shift for a wavelength shift of 33 percent.

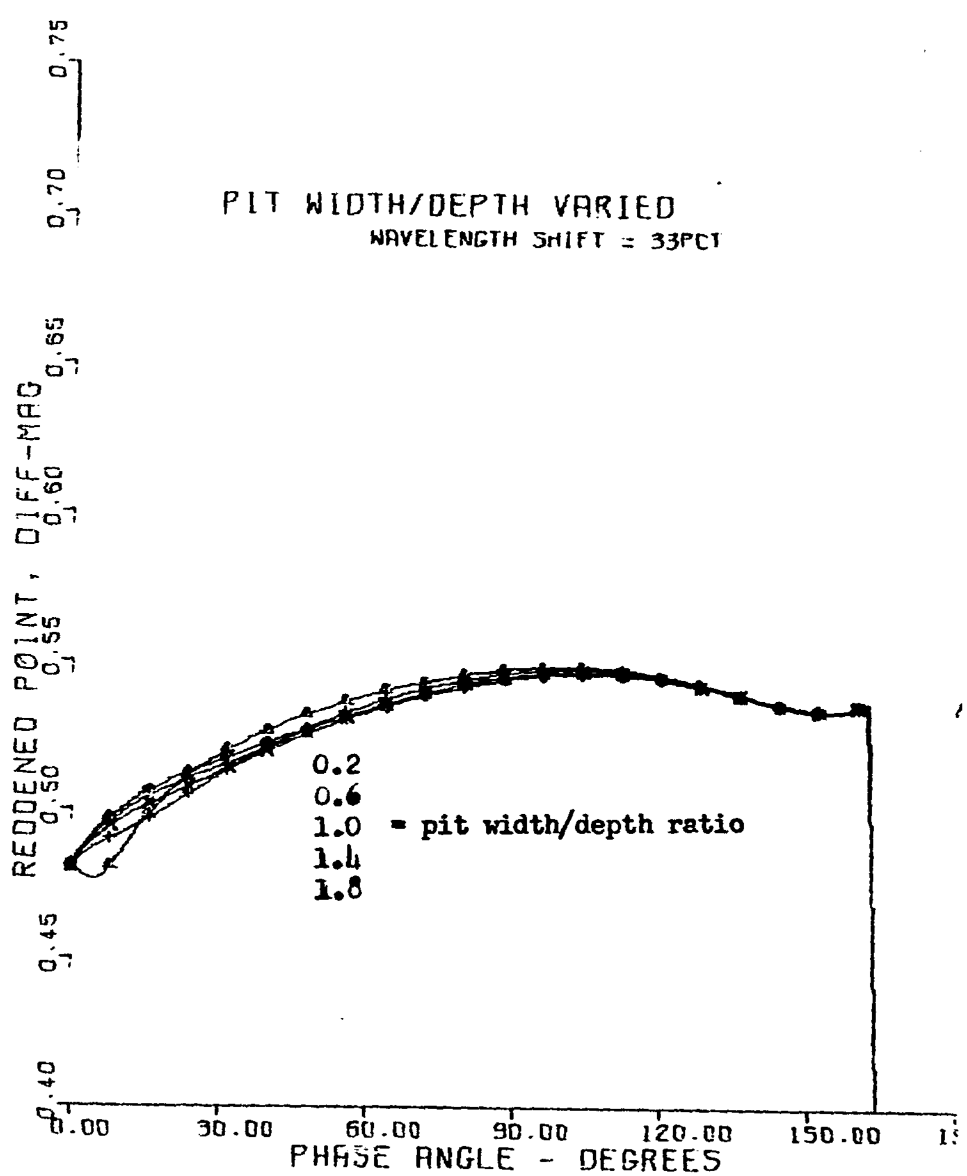

Figure 12C. The reflectivity shift, in magnitudes, of a point on a planet, for a wavelength shift of 33 percent.

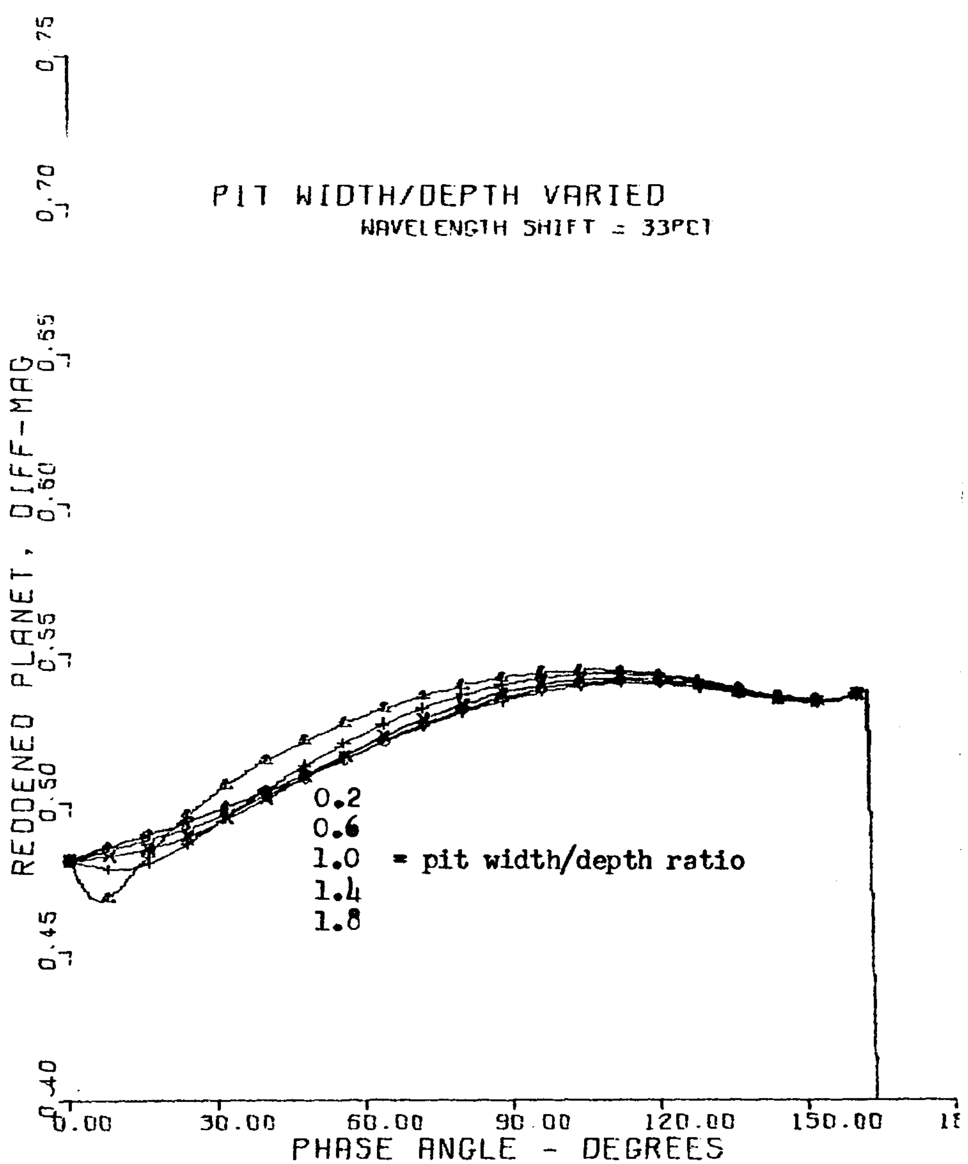

Figure 12D. The reflectivity shift, in magnitudes, of the integrated planet, for a wavelength shift of 33 percent.

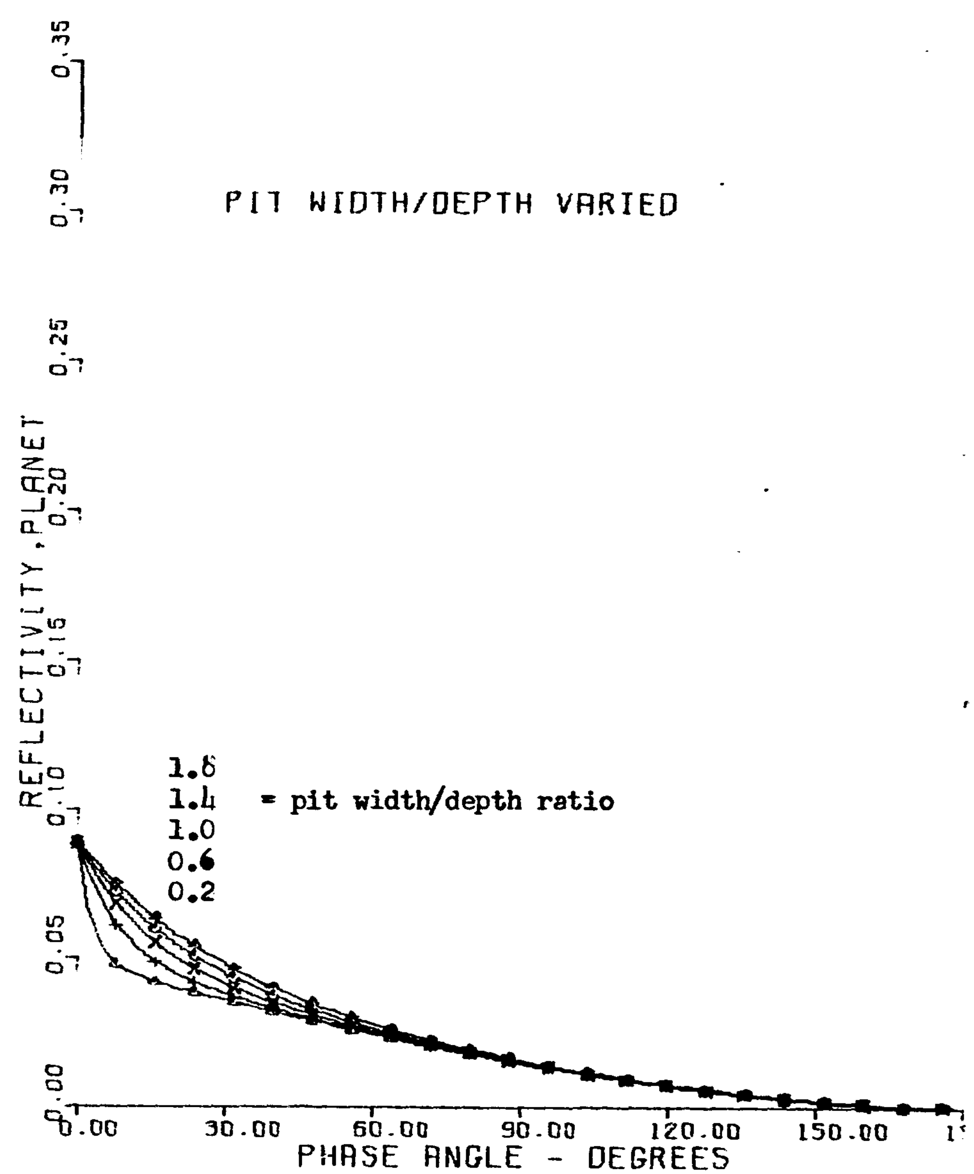

Figure 12E. The integrated reflectivity of the entire planet.

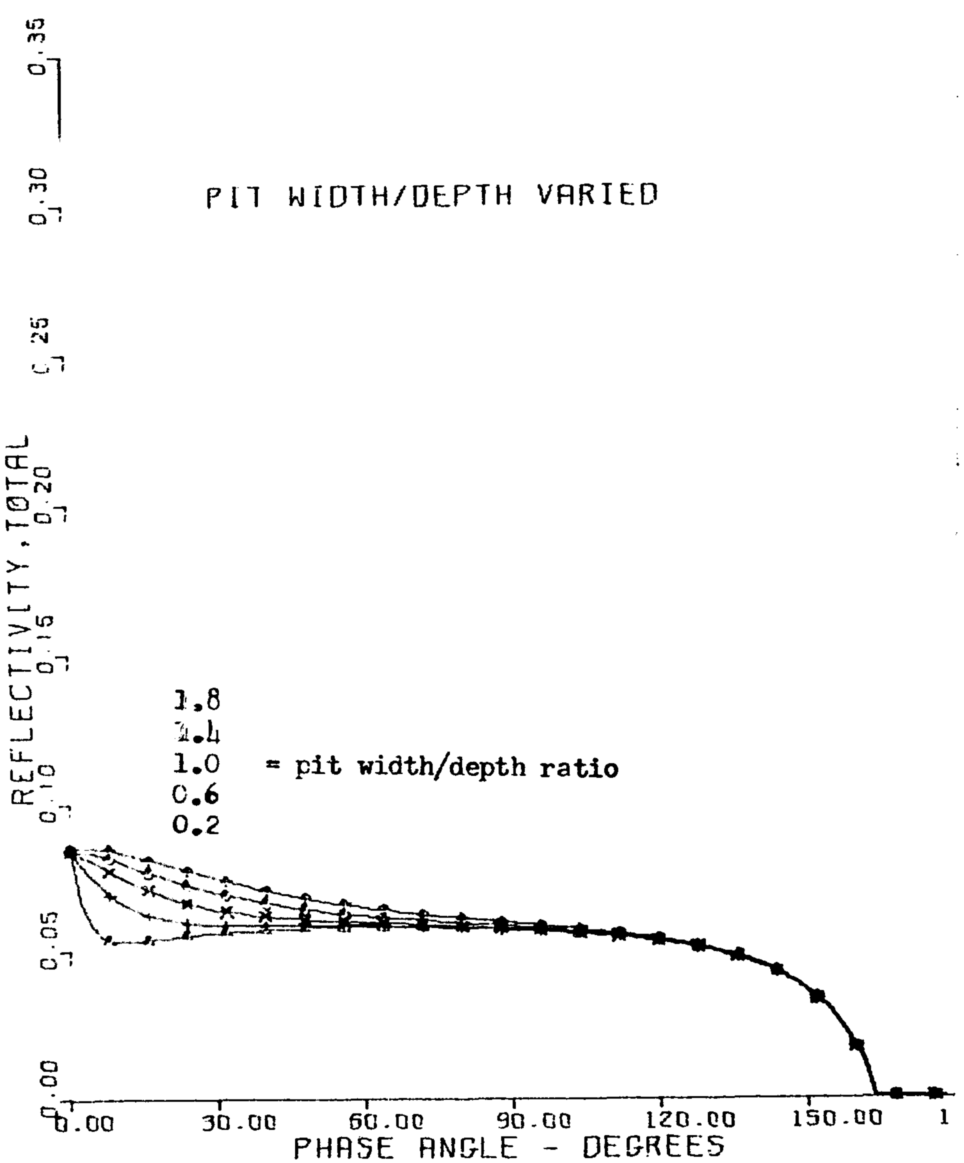

Figure 12G. The total of all light components (singles + doubles + diffuse) at a point on the planet.

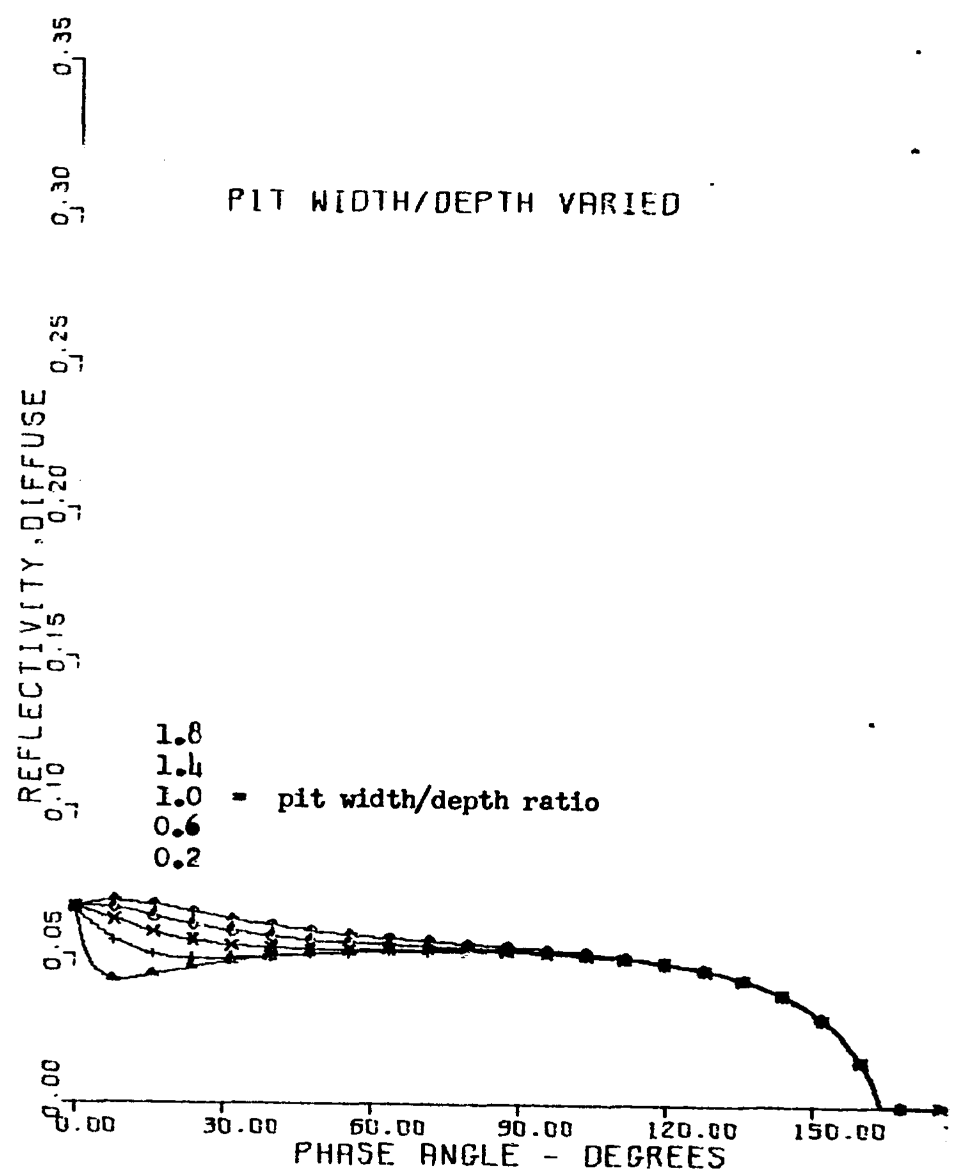

Figure 12F. The diffuse component of light at a point on the planet. Diffuse light emerges from particles after inward refraction and multiple internal reflections.

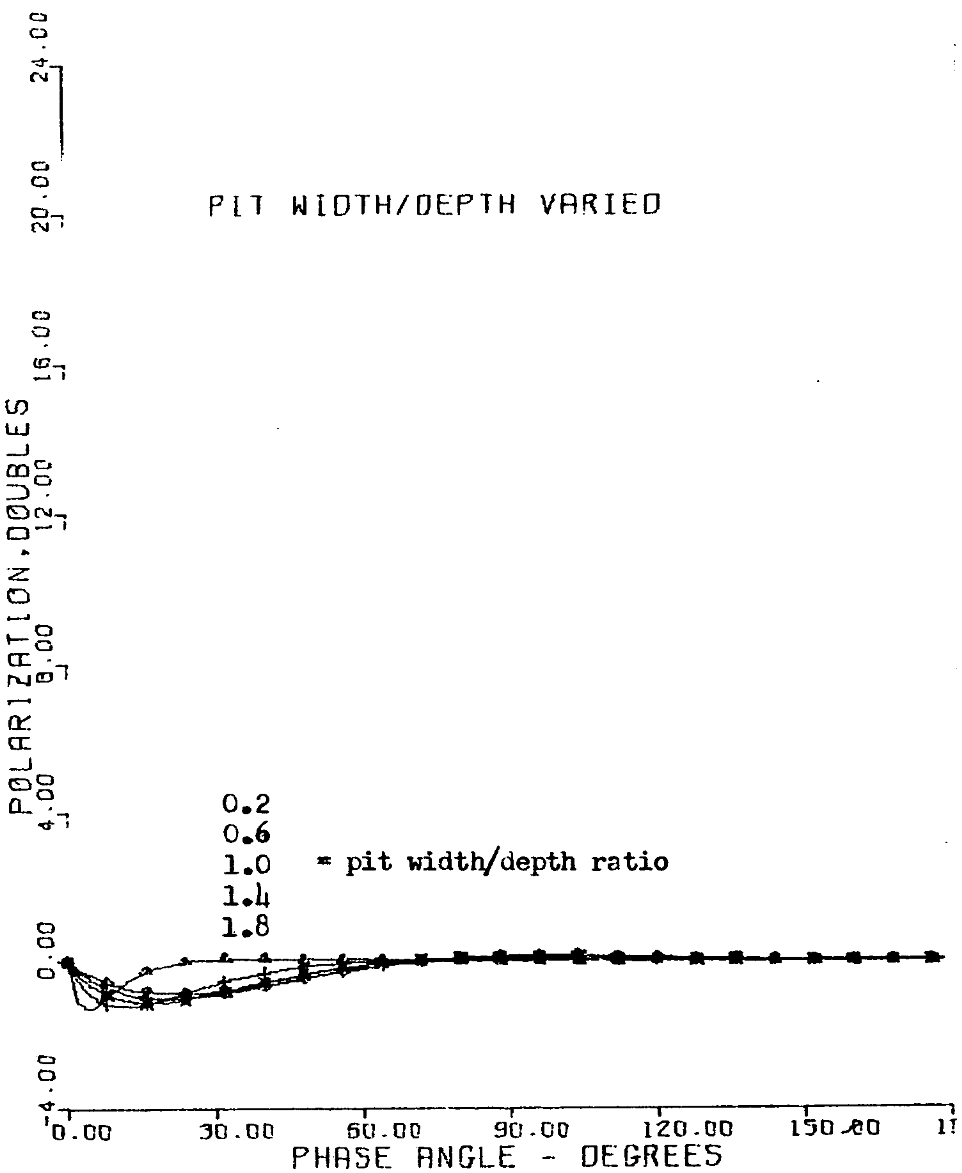

Figure 12I. The polarization due to the doubly-reflected component of light, alone.

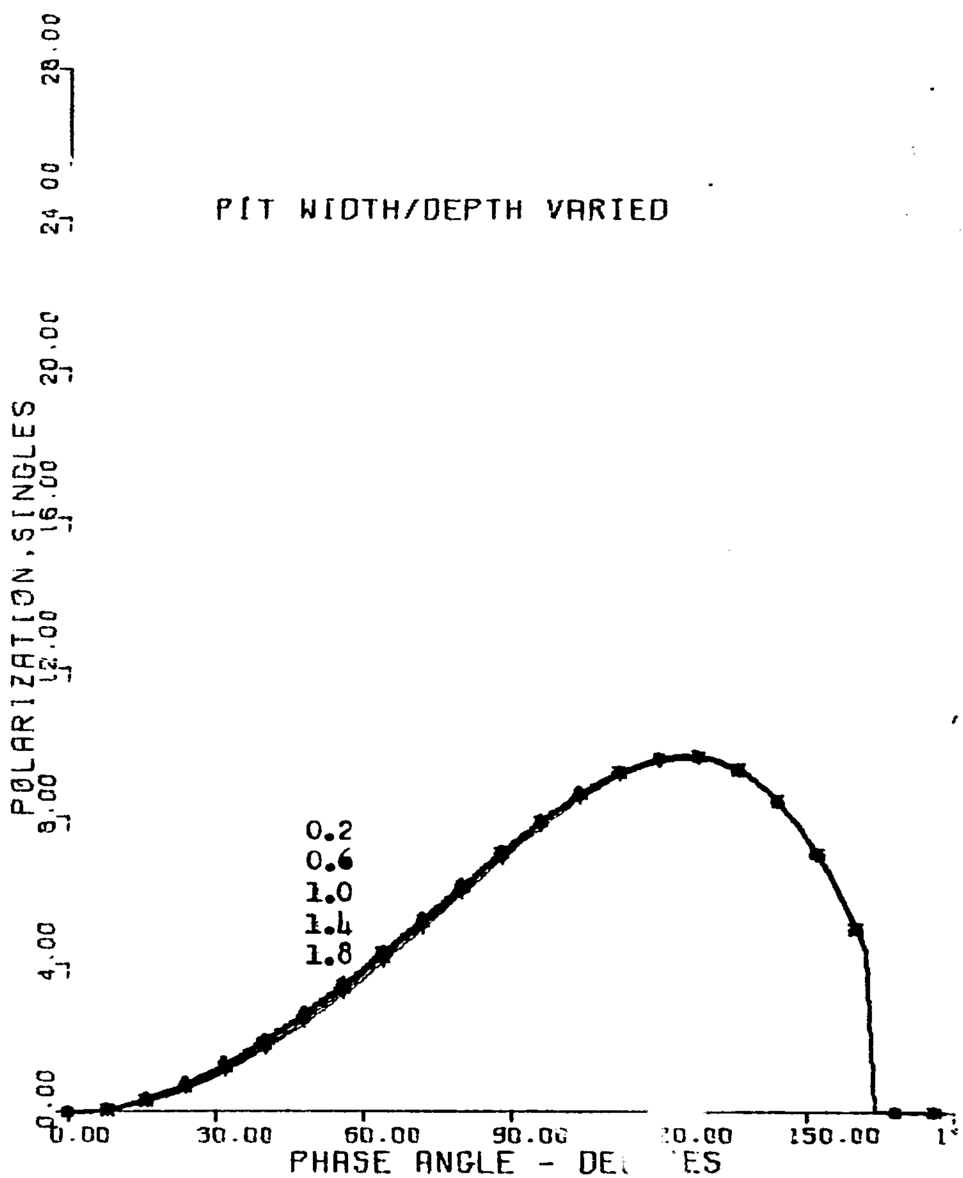

Figure 12H. The polarization due to the singly-reflected component of light, alone.

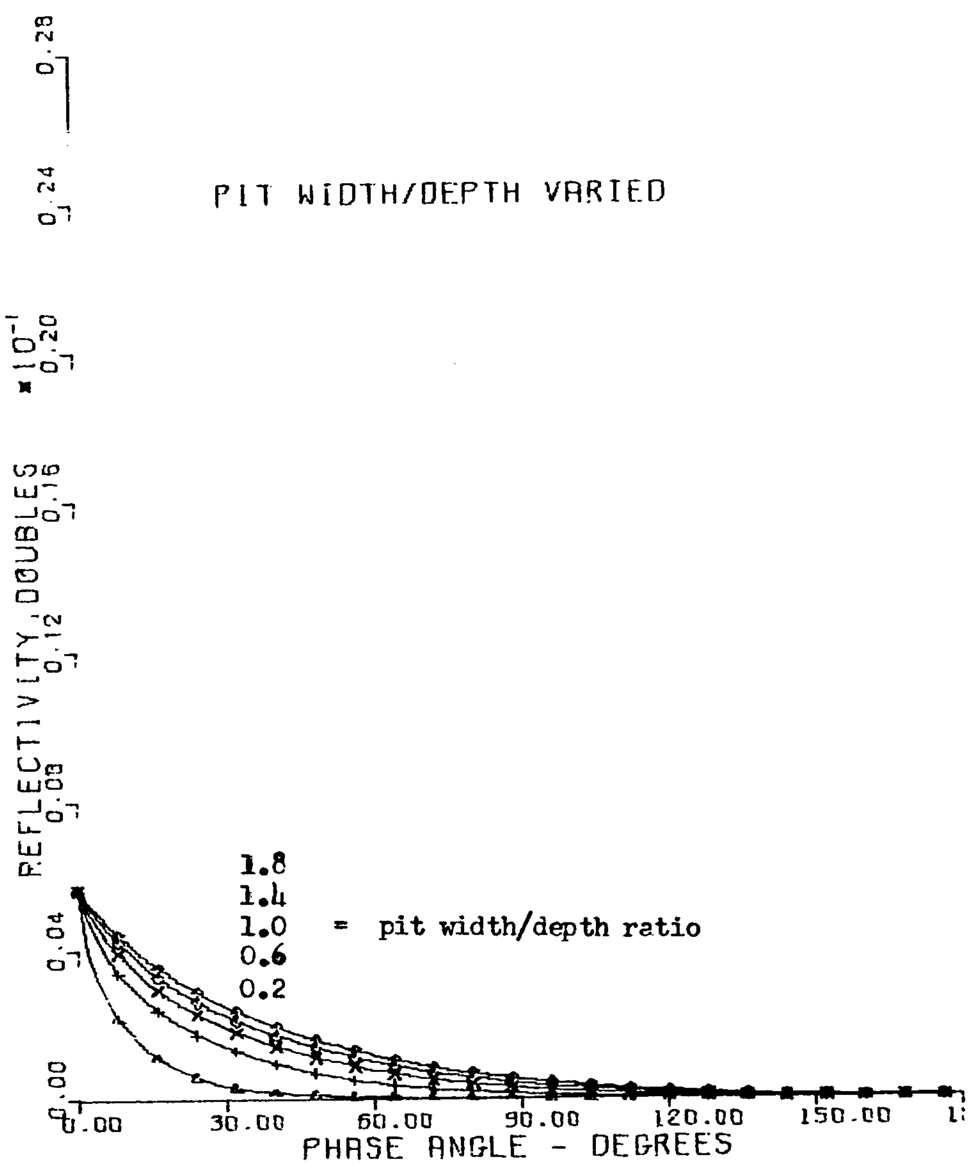

Figure 12K. The intensity of the doubly-reflected component of light.

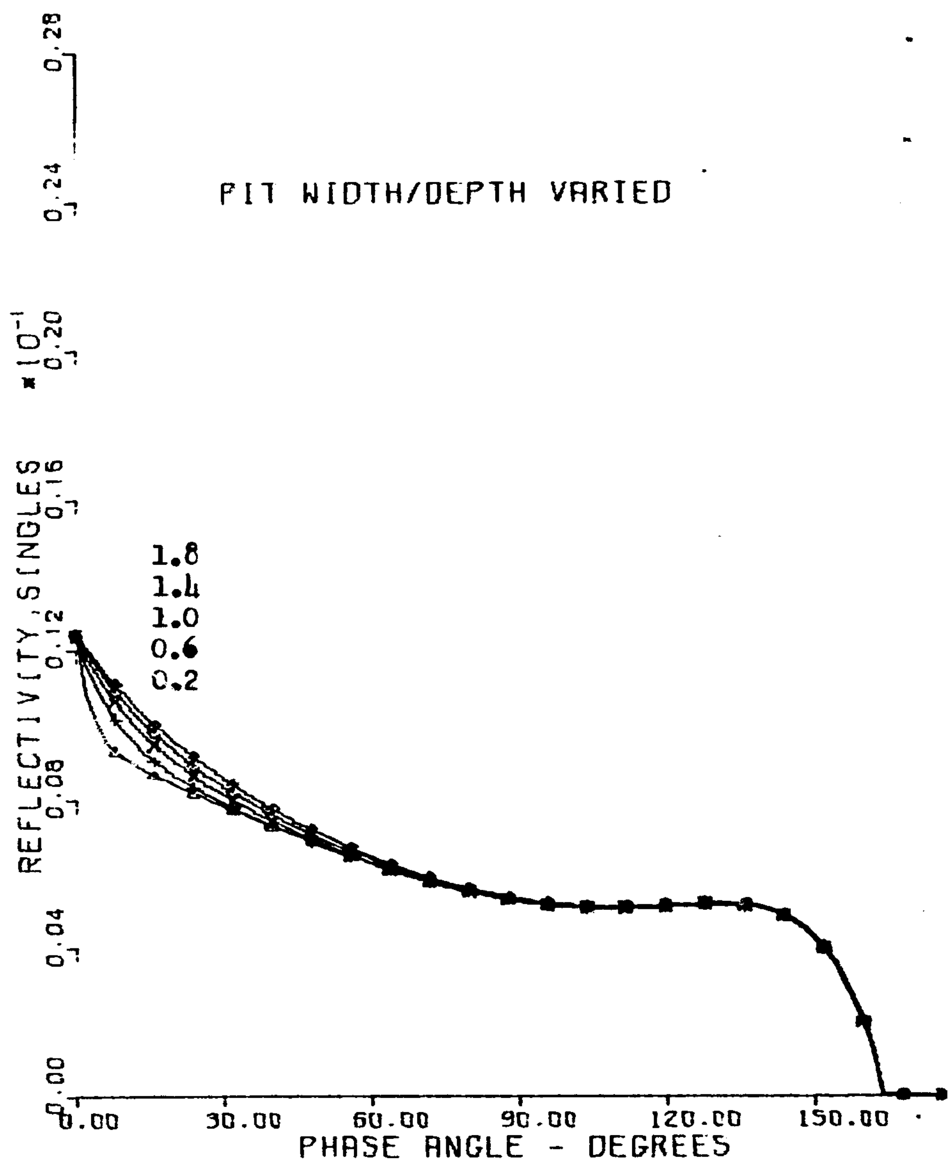

Figure 12J. The intensity of the singly-reflected component of light.

FINE DUST VARIED

Figure 13 A to Figure 13 K

These figures illustrate the effects of changing the amount of fine dust (size~1 wavelength) coating the larger particles (size~15-20 wavelengths).
The model makes three computations as the amount of dust is increased :
1) the average size of particles in the diffuse-light equation is decreased resulting in more diffuse light,
2) the amount of external surface available for specular reflection is decreased resulting in less singles and less positive polarization,
3) the amount of area available for doubles-reflection is increased resulting in more doubles and more negative polarization.

Keep in mind that the basic measure of particle size in this type of problem is wavelengths. As wavelength increases, effective particle size decreases. Thus on the Moon, increasing wavelength results in more diffuse light, less singles, and more doubles. The first and third changes can be equal and opposite resulting in a constant negative branch. Thus, fine dust seems to provide a partial explanation for the constant negative polarization which has had no explanation.

Fine dust also gives rise to the Hopfield (1966) effect which would produce the same qualitative changes as above, to the extent that the dust is comprised of conductive (metallic ?) material, and is wavelength-sized. This complex quantum-mechanical effect is not included in the model.

The principle of complimentarity between reflection of singles vs. doubles applies here because dust is a geometric change of the surface. Thus when positive polarization decreases, negative polarization increases.

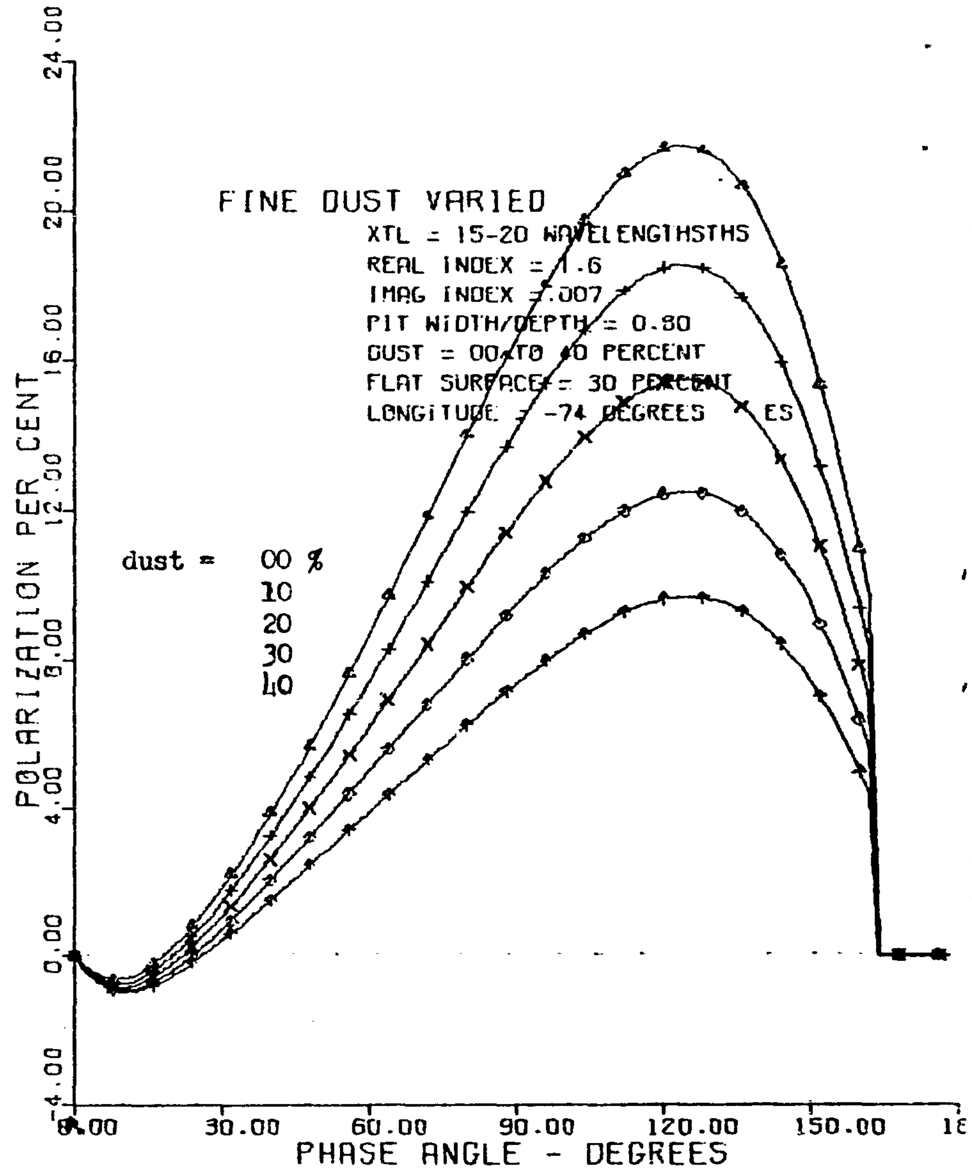

Figure 13A. Polarization at a point on a planet.

Increasing the amount of dust increases opportunity for double reflection and decreases single reflection.
Note that the inversion point moves to the left with increasing dust.

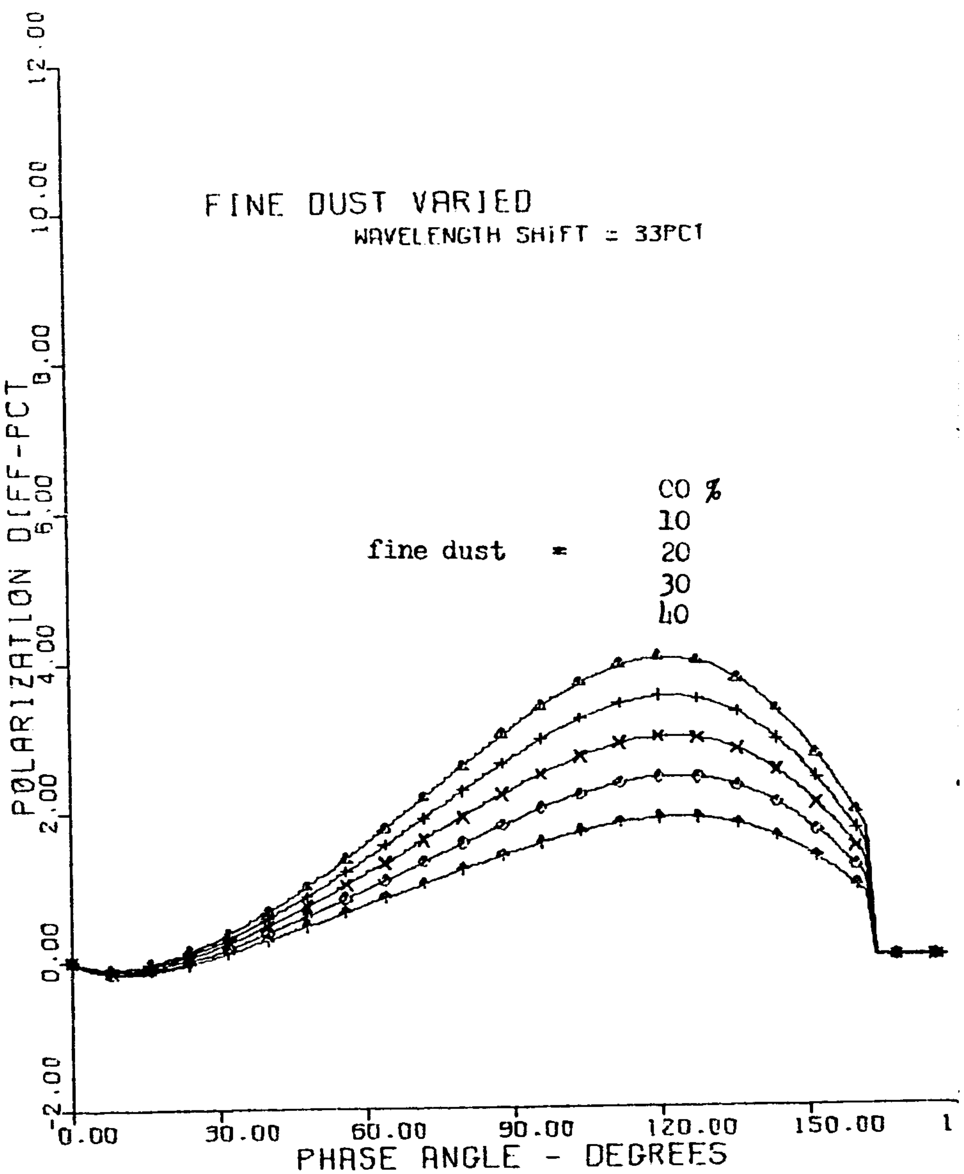

Figure 13B. Polarization shift for a wavelength shift of 33 percent.

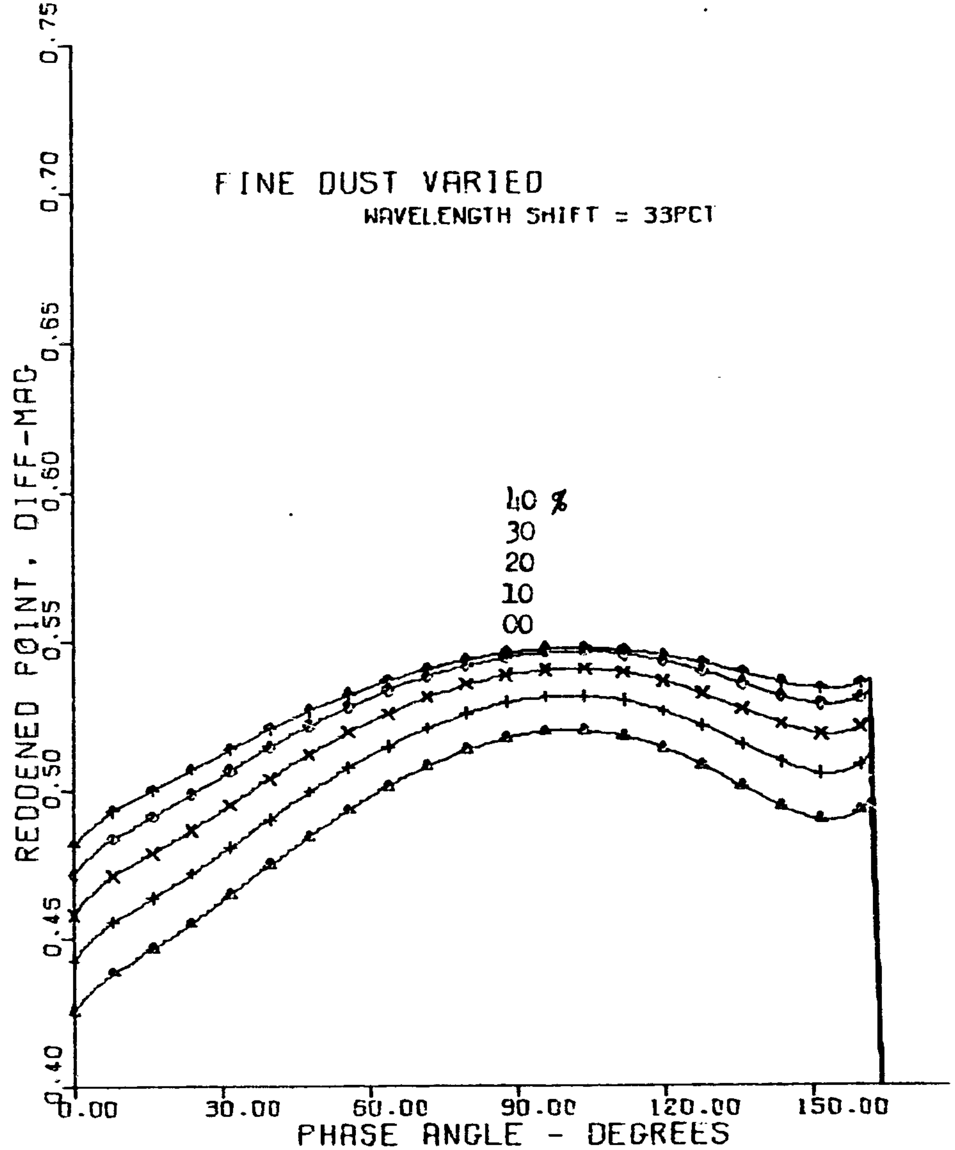

Figure 13C. The reflectivity shift, in magnitudes, of a point on the planet, for a wavelength shift of 33 percent.

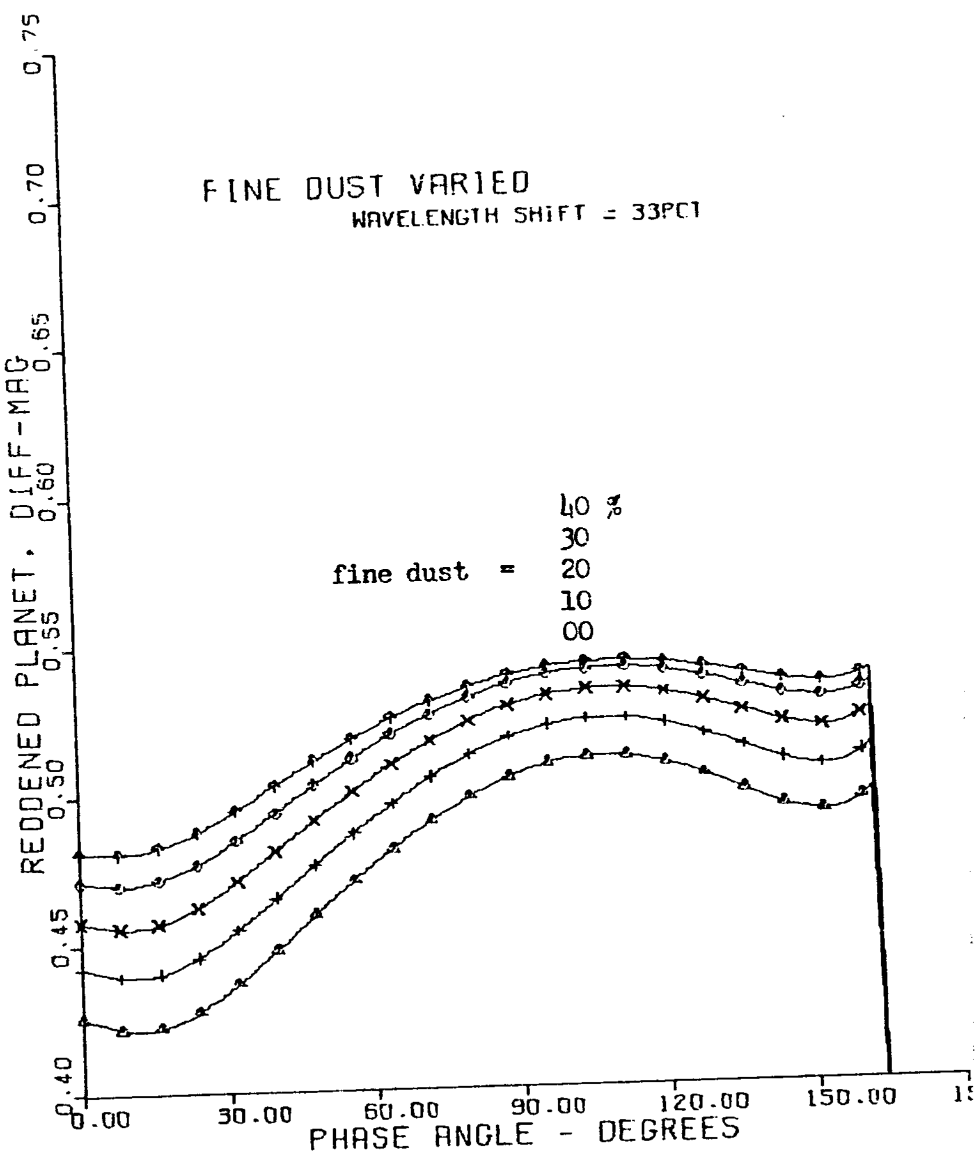

Figure 13D. The reflectivity shift, in magnitudes, of the integrated planet, for a wavelength shift of 33 percent.

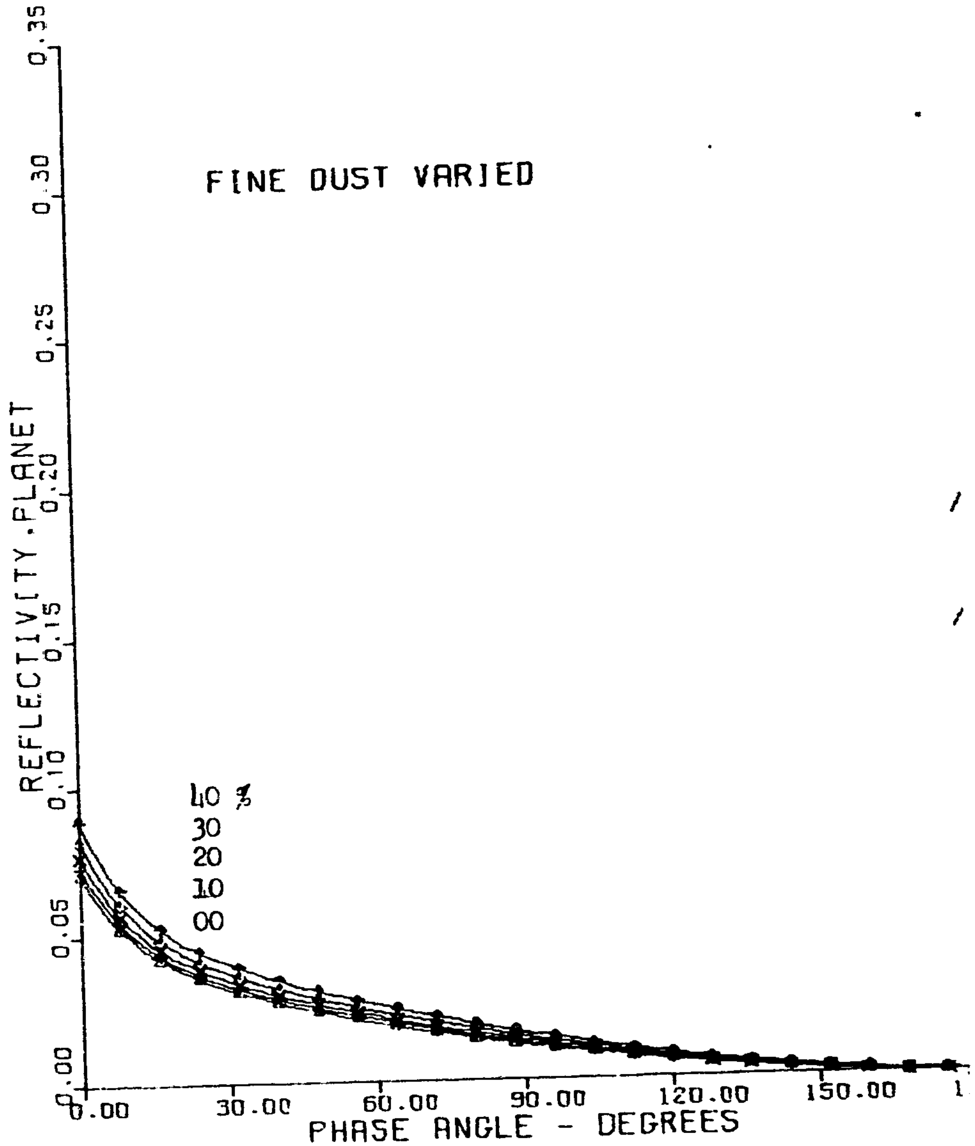

Figure 13E. The integrated reflectivity of the entire planet.

The whole planet behaves much like any mineral which is ground into finer and finer powders - it becomes more reflective.

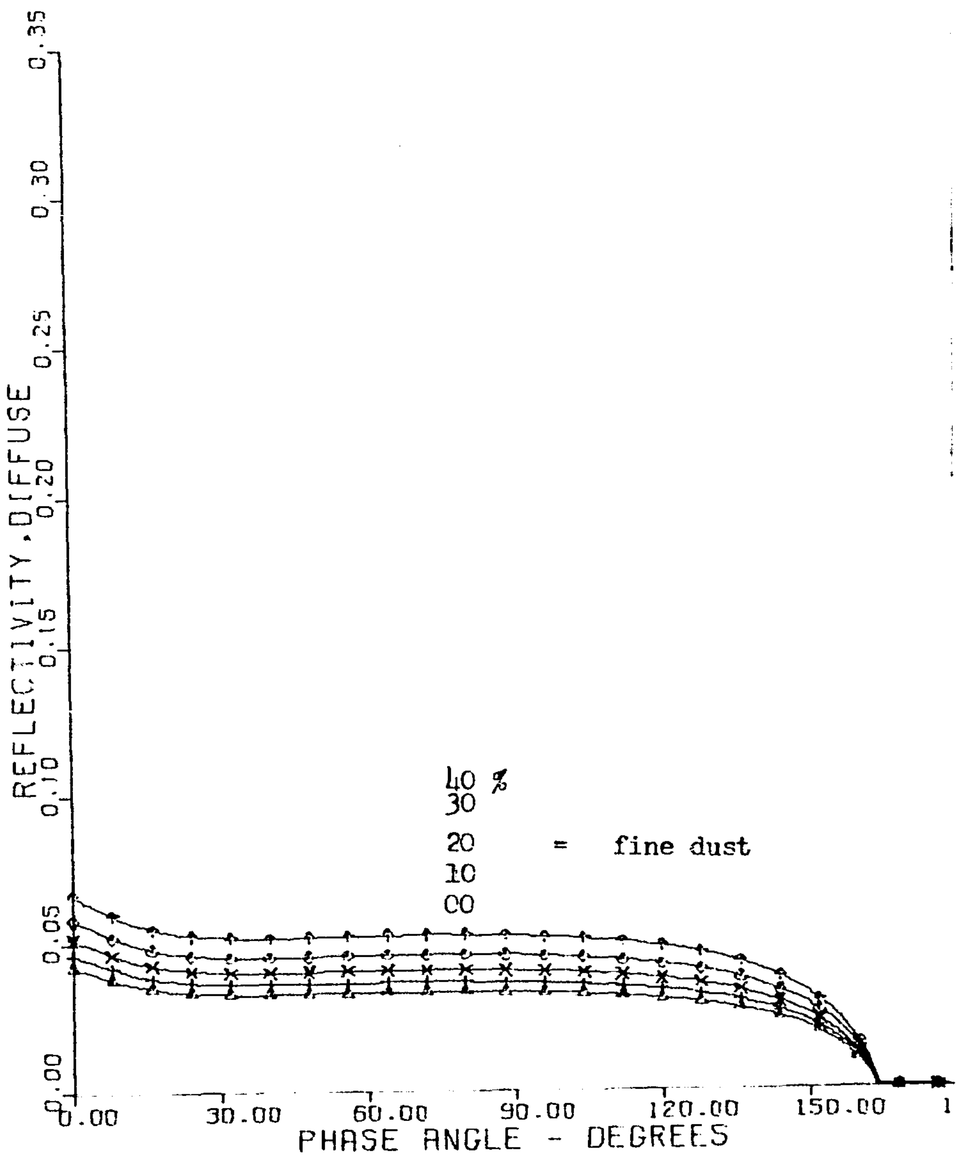

Figure 13F. The diffuse component of light at a point on the planet. Diffuse light emerges from particles after inward refraction and multiple internal reflections. Light entering dust particles travels only a short distance before emerging, thus under-going less absorbtion.

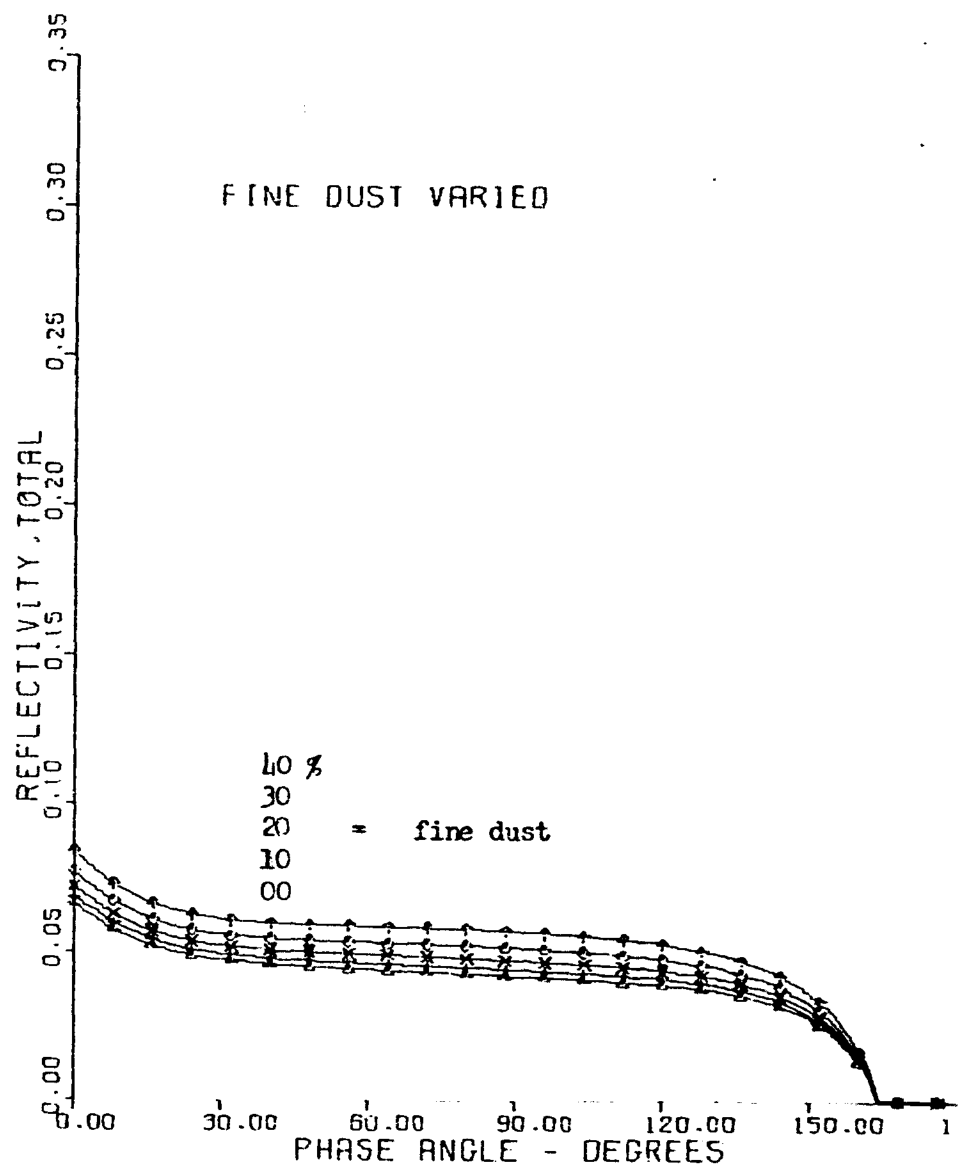

Figure 13G. The total of all light components (singles + doubles + diffuse), at a point on the planet.

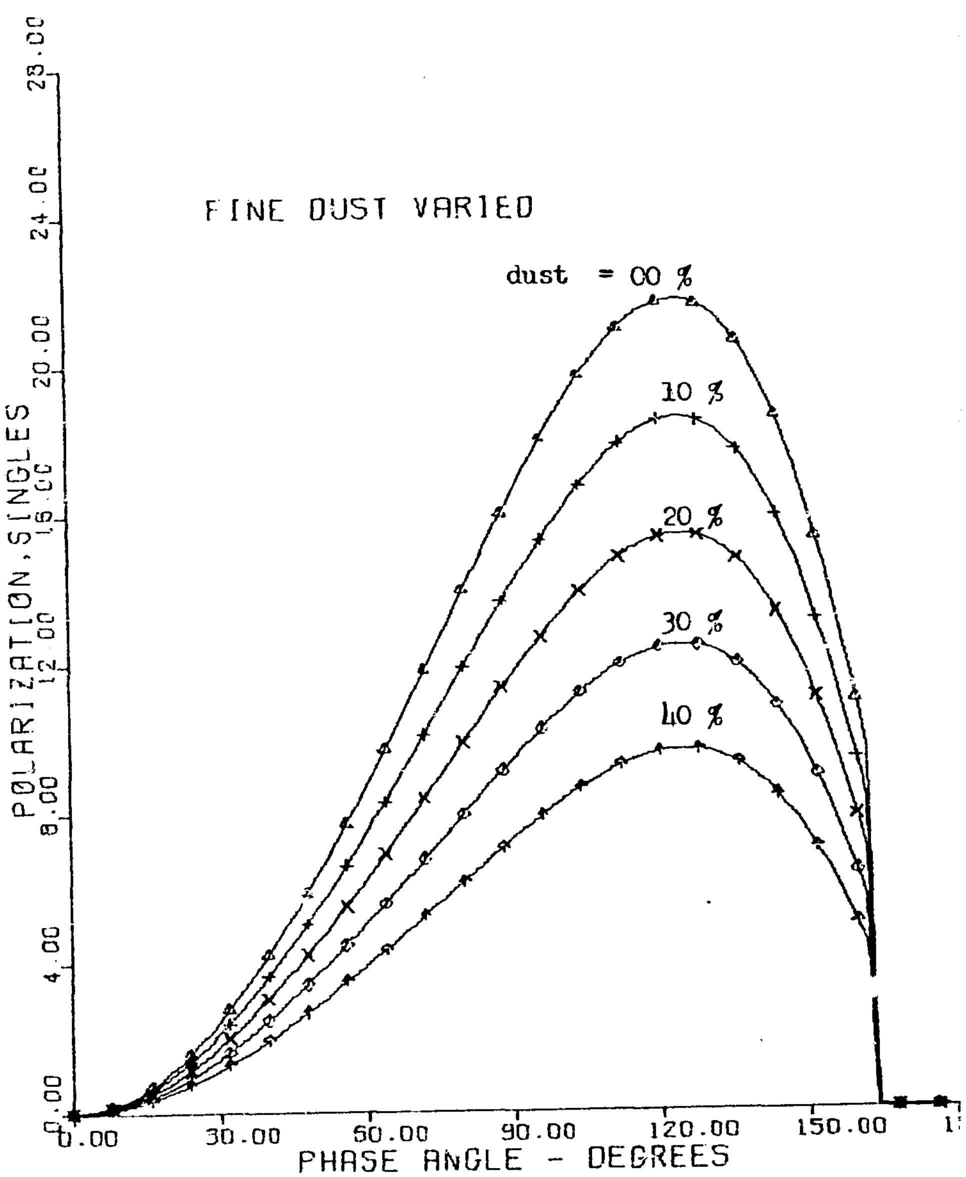

Figure 13H. The polarization due to the singly-reflected component of light, alone.

The decreased intensity of single reflection also results in less singles polarization. Accordingly, the positive polarization branch will decrease.

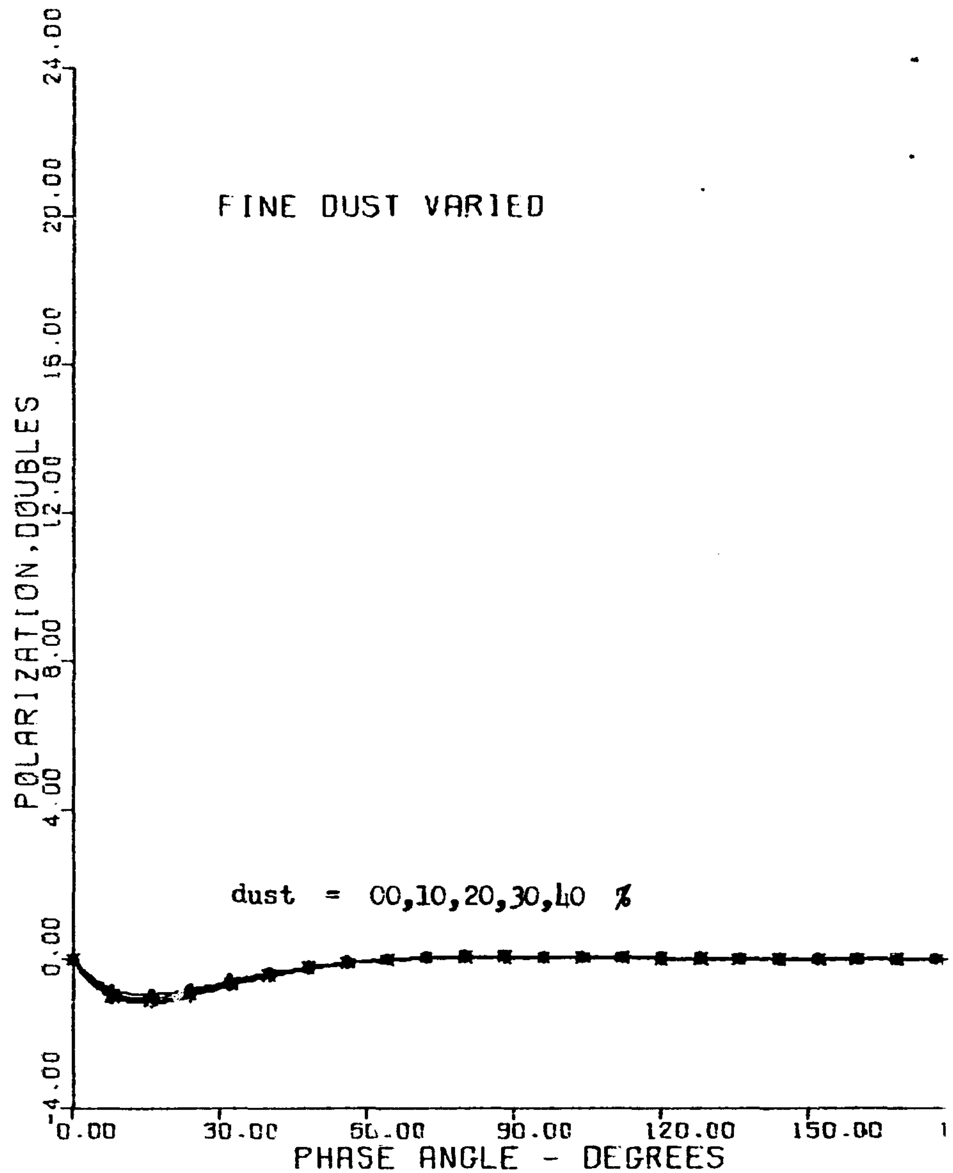

Figure 13I. The polarization due to the doubly-reflected component of light, alone.

Doubles polarization are relatively constant because the increase of doubles intensity is offset by the increase of diffuse light.

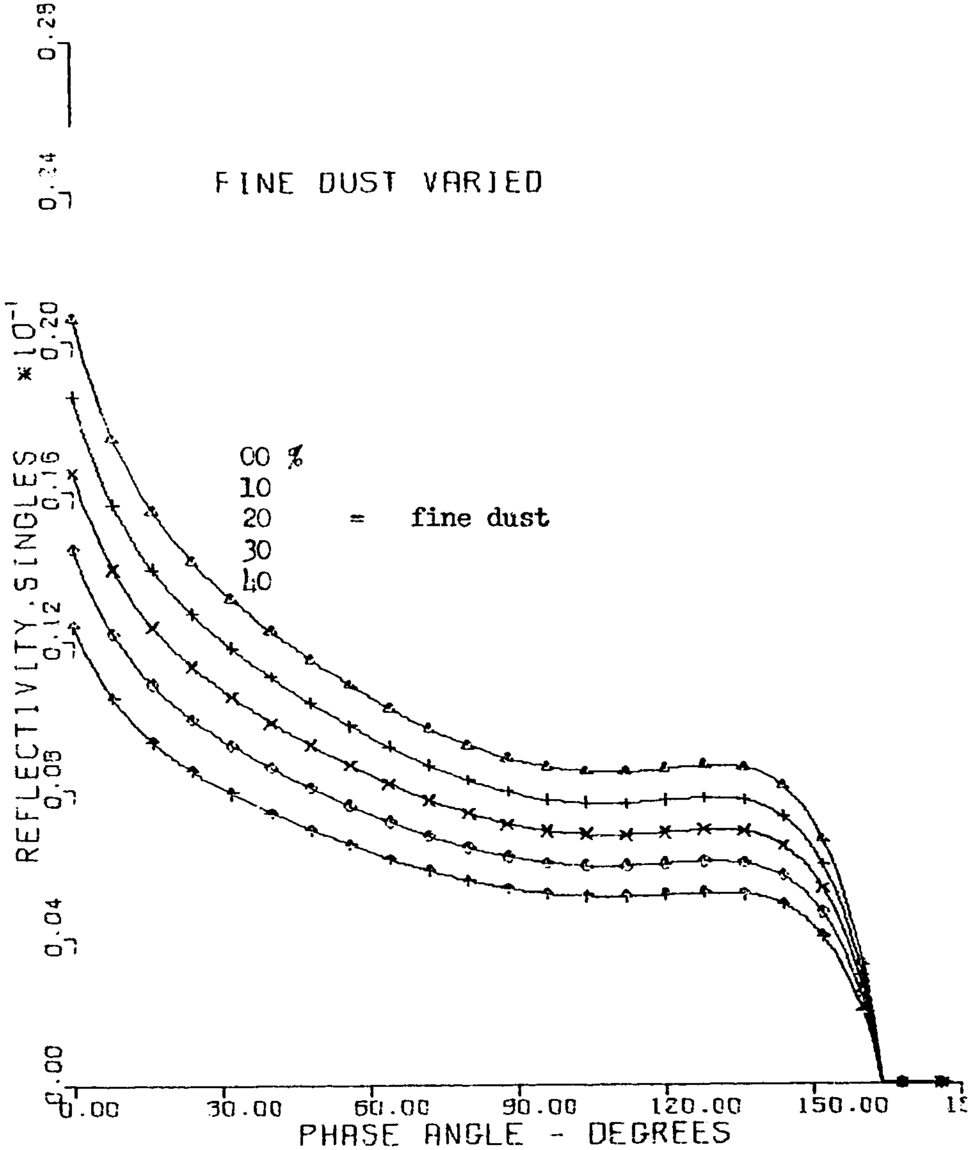

Figure 13J. The intensity of the singly-reflected component of light.

The presence of dust destroys specular area and thus reduces single reflections.

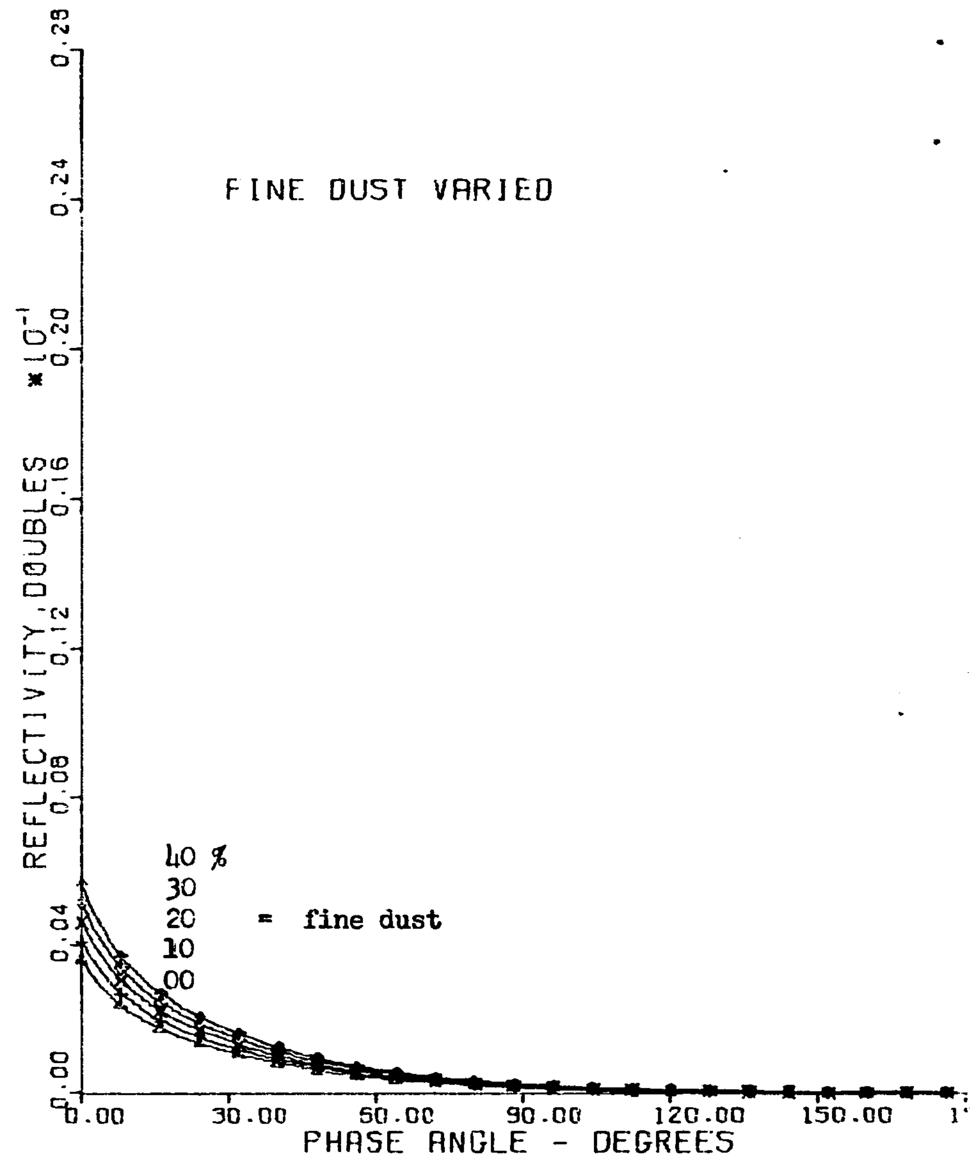

Figure 13K. The intensity of the doubly-reflected component of light.

Dust shape irregularities convert specular area on which it falls, into opportunities for double reflection.

LONGITUDE OF POINT VARIED

Figure 14A to Figure 14K

Lyot(1929) and Dollfus(1955) have measured polarization at different locations on the Moon, Mars, and Mercury to investigate variation due to location. In general they report polarization is almost independent of location, but Lyot reports a noticeable polarization increase at the terminator.

These figures tell the same story. The observeables computed here show some small variations, but these are probably less than the errors of measurement. Errors are a vexing problem because the surface texture variations are generally larger than the expected variations due to latitude or longitude dependence.

In the computer model, longitude L, appears in two factors called SHAD and COLGF :

$$\text{SHAD} = 1 + G/(L - \pi/2)$$

$$\text{COLGF} = \frac{2}{1 + \cos L/\cos(G + L)}$$

SHAD approximates the fractional area of a particle which is visible and illuminated, and creates a terminator at the right longitude. In the model it is a coefficient of all the singly and doubly-reflected light components.

COLGF takes account of the attenuation of diffuse light which emerges from the surface through varying paths because of the changing angles of observation, and, it creates a terminator at the right longitude. It is a coefficient of the diffuse light component.

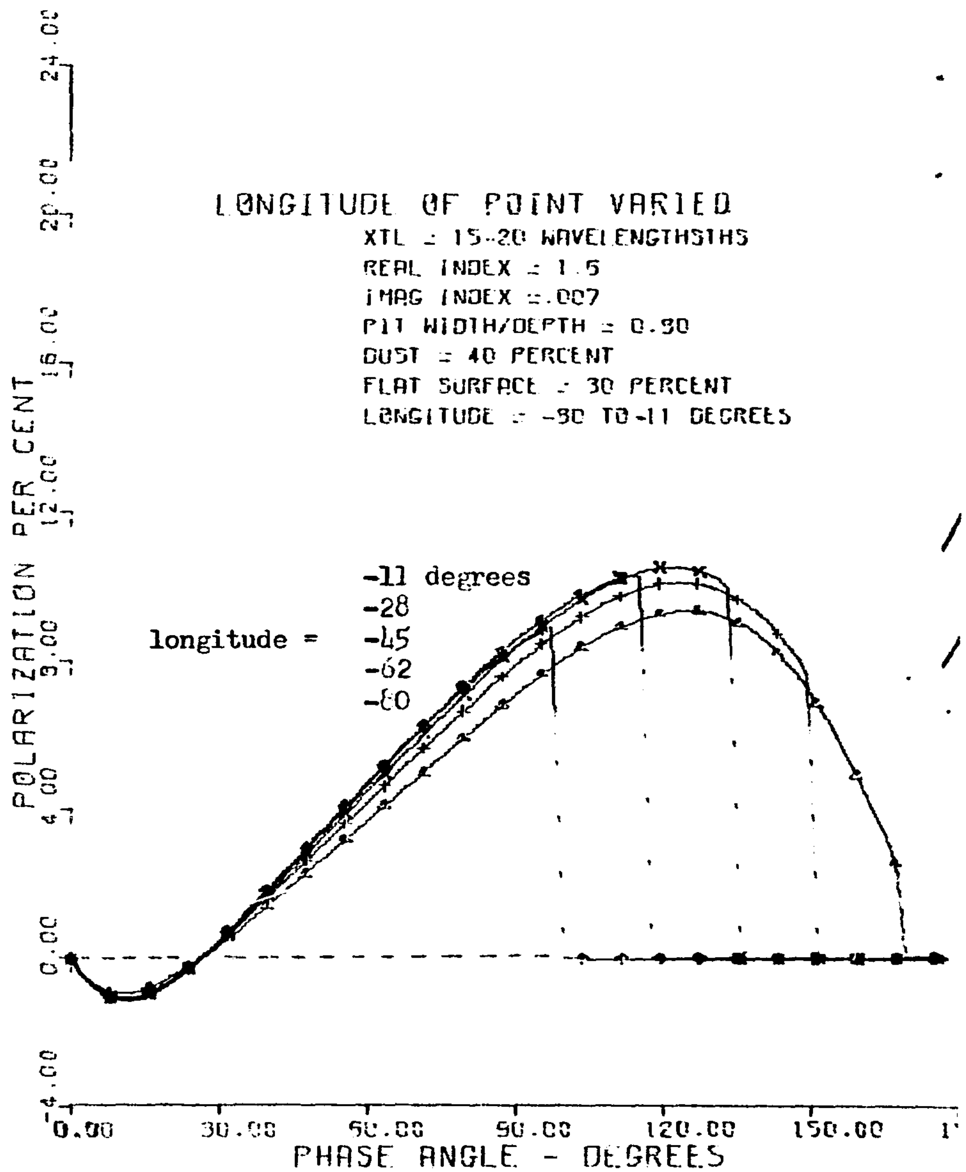

Figure 14A. Polarization at a point on a planet.

This figure agrees with the observation of Lyot that the polarization increases when near the terminator. The effect is small as generally reported.

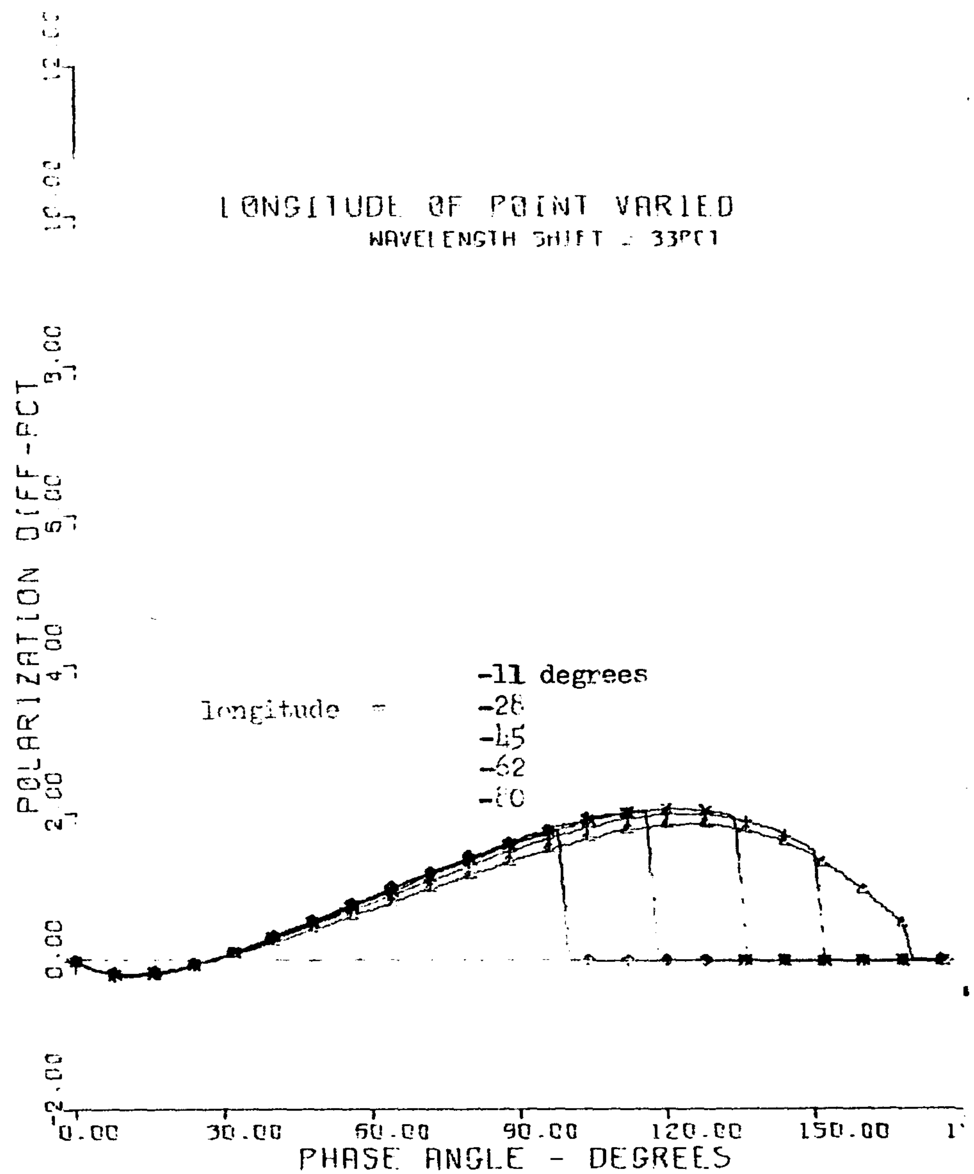

Figure 14B. Polarization shift for a wavelength shift of 33 percent

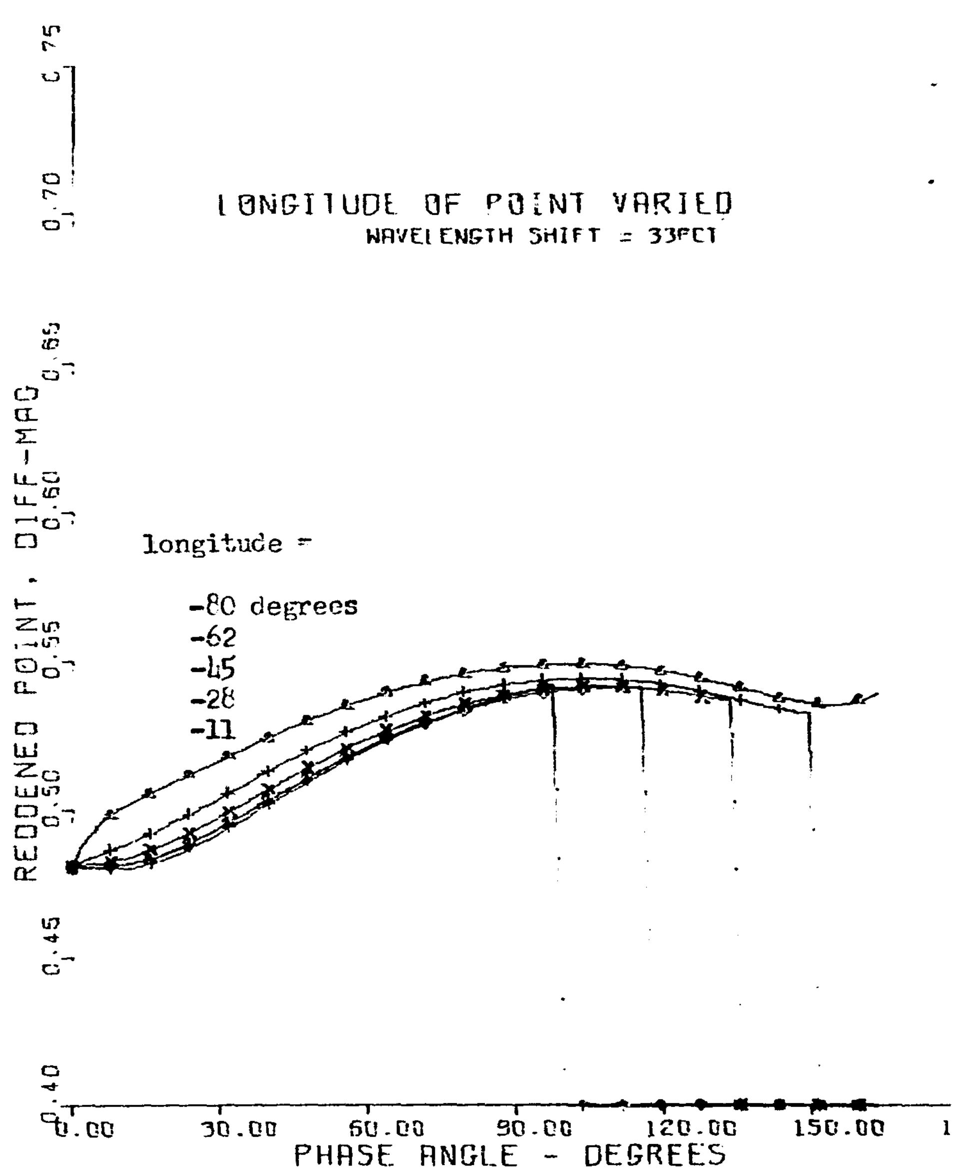

Figure 14C. The reflectivity shift, in magnitudes, of a point on the planet, for a wavelength shift of 33 percent.

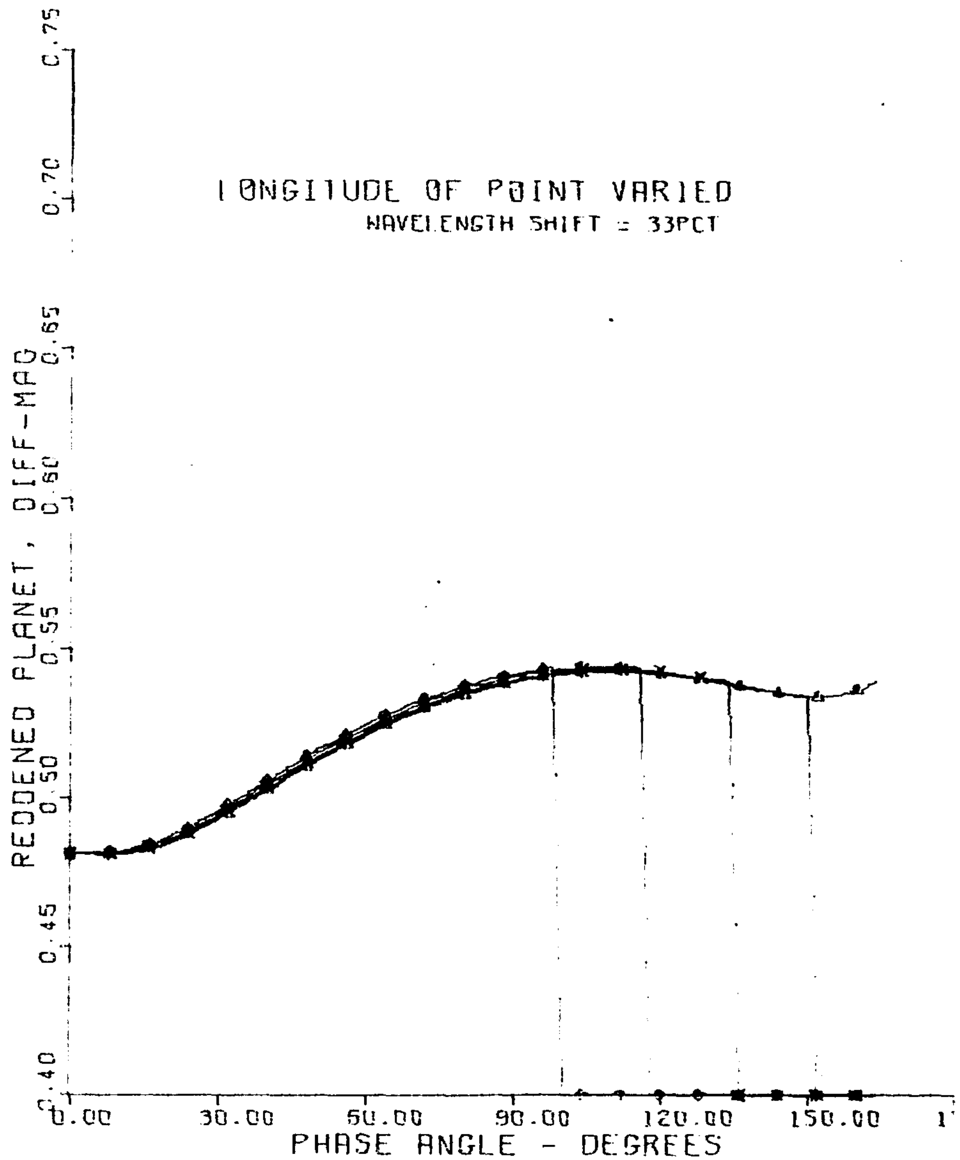

Figure 14-D. The reflectivity shift, in magnitudes, of the integrated planet, for a wavelength shift of 33 percent.

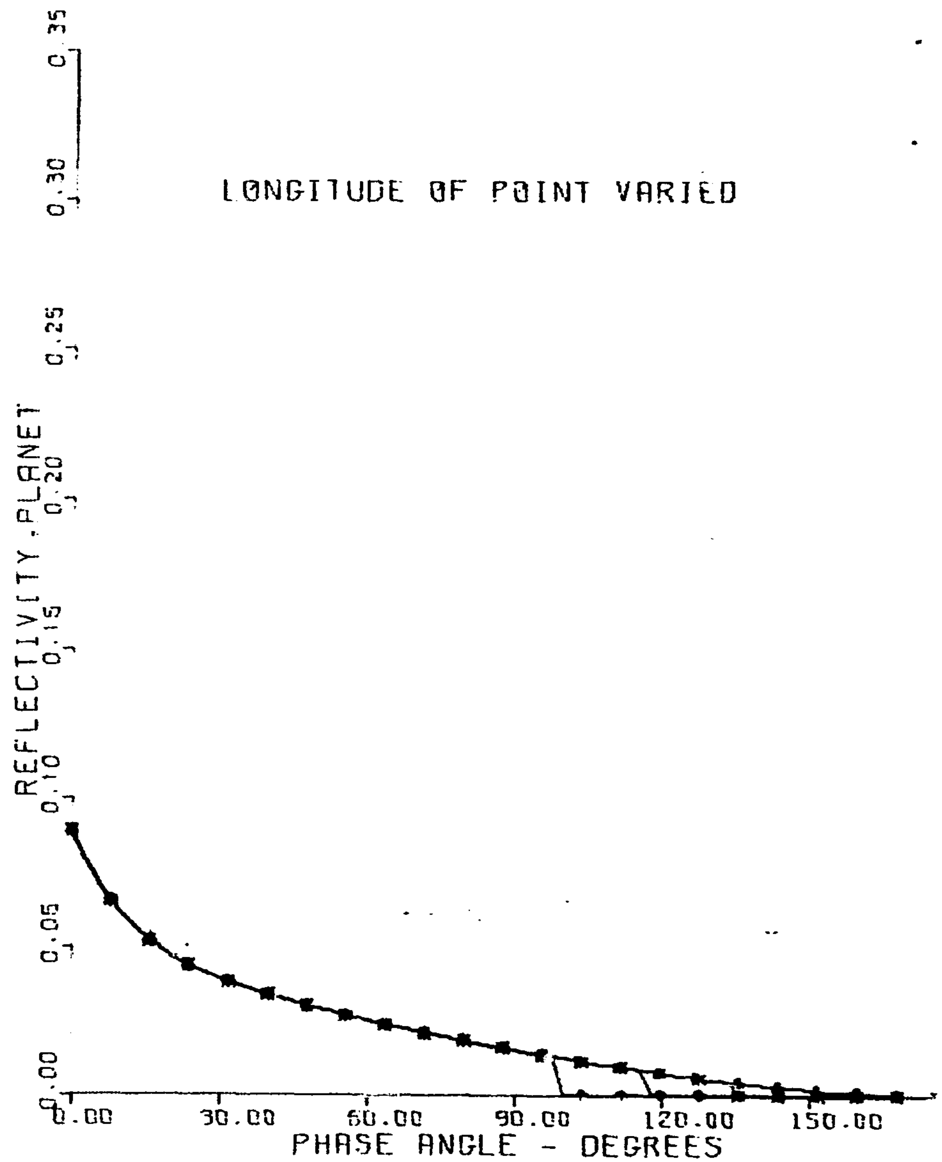

Figure 14-E. The integrated reflectivity of the entire planet.

Obviously, these two figures are not longitude dependent.

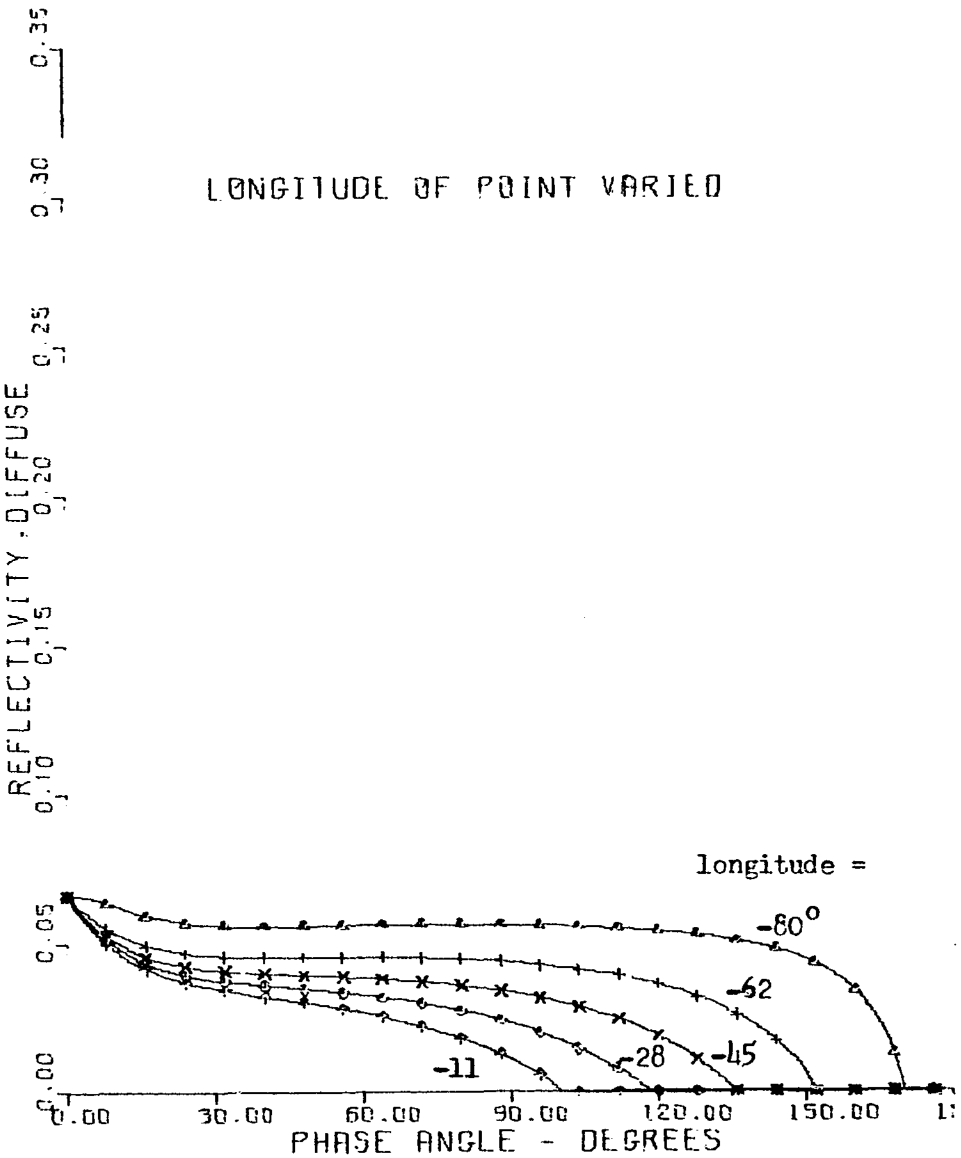

Figure 14F. The diffuse component of light at a point on the planet. diffuse light emerges from particles after inward refraction and multiple internal reflections.

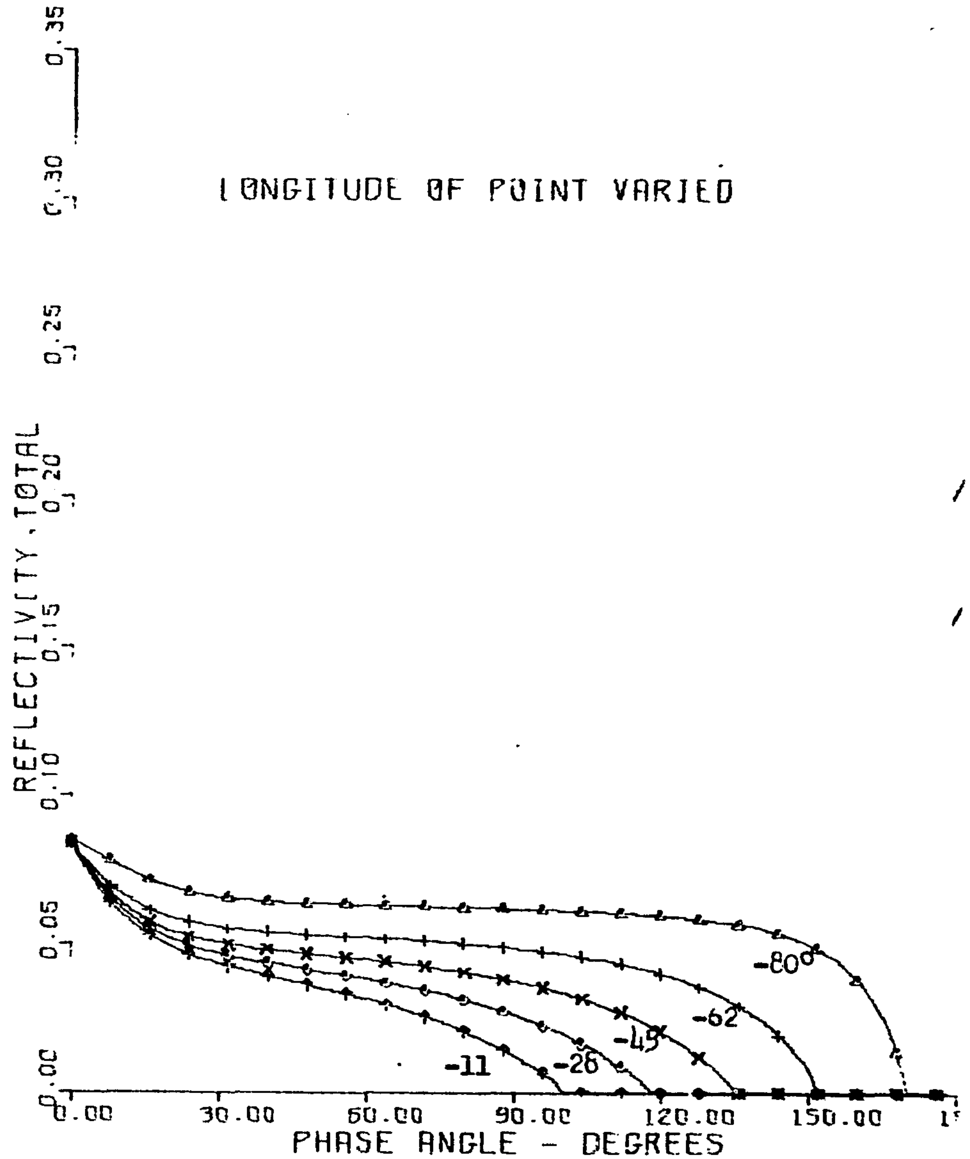

Figure 14G. The total of all light components (singles + doubles + diffuse) at a point on the planet.

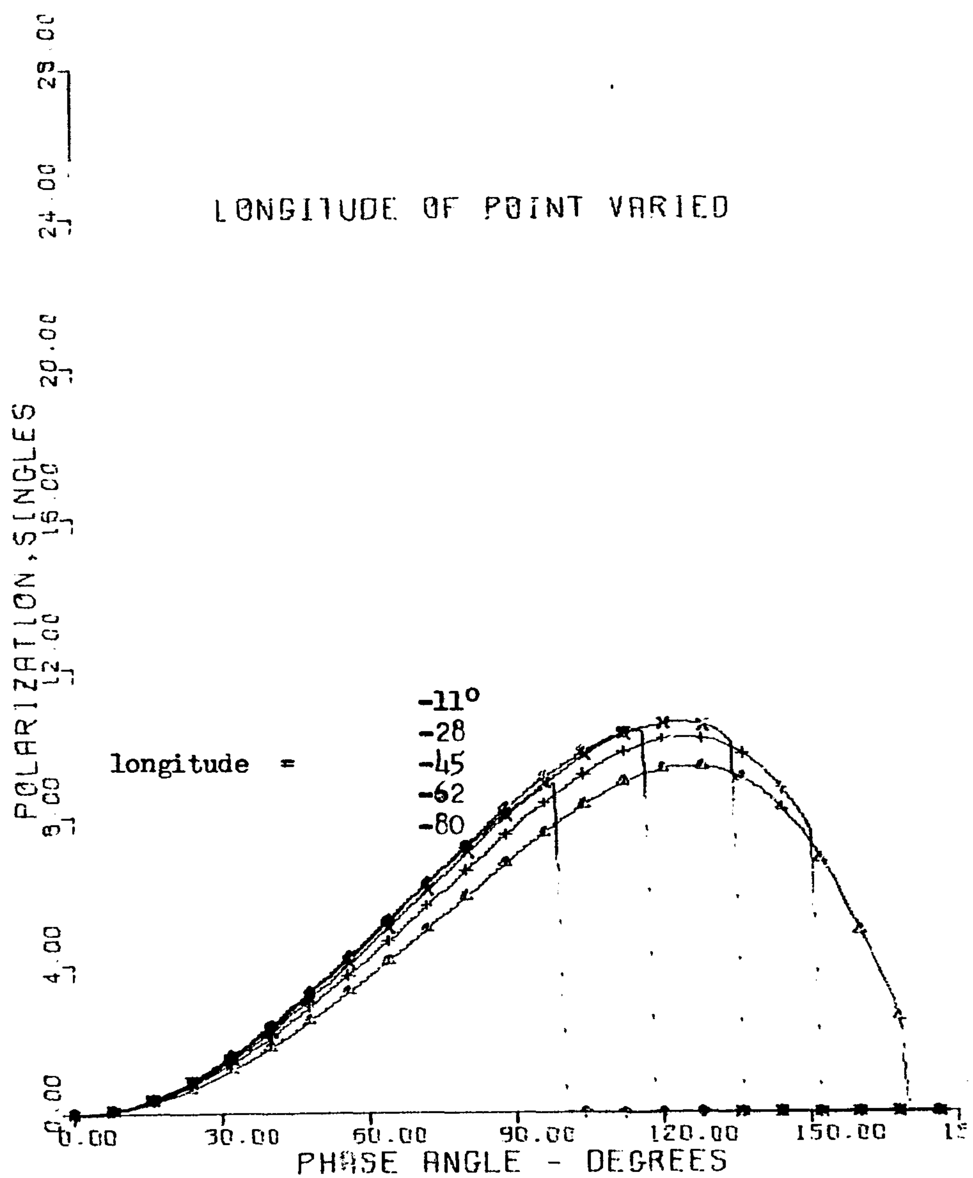

Figure 14H. The polarization due to the singly-reflected component of light, alone.

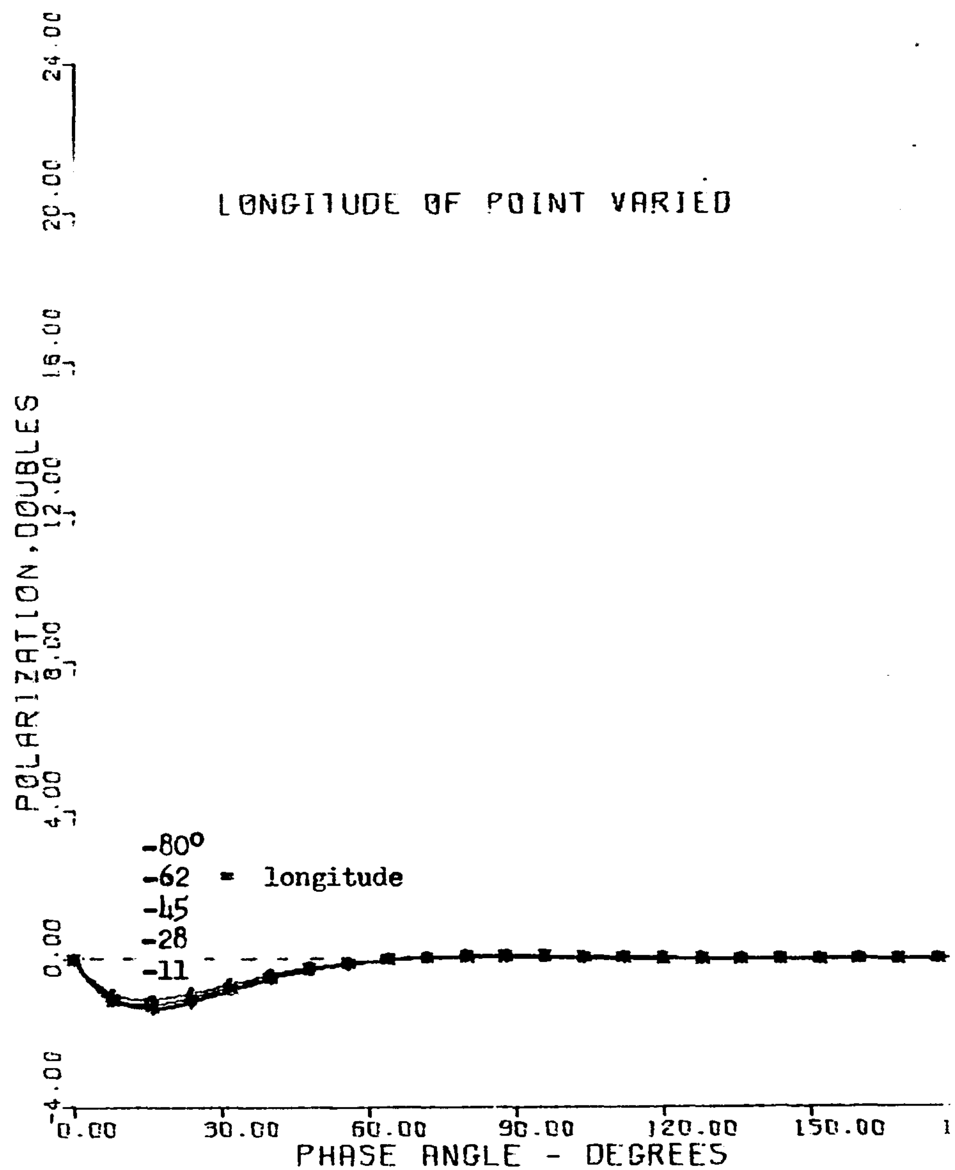

Figure 14I. The polarization due to the doubly-reflected component of light, alone.

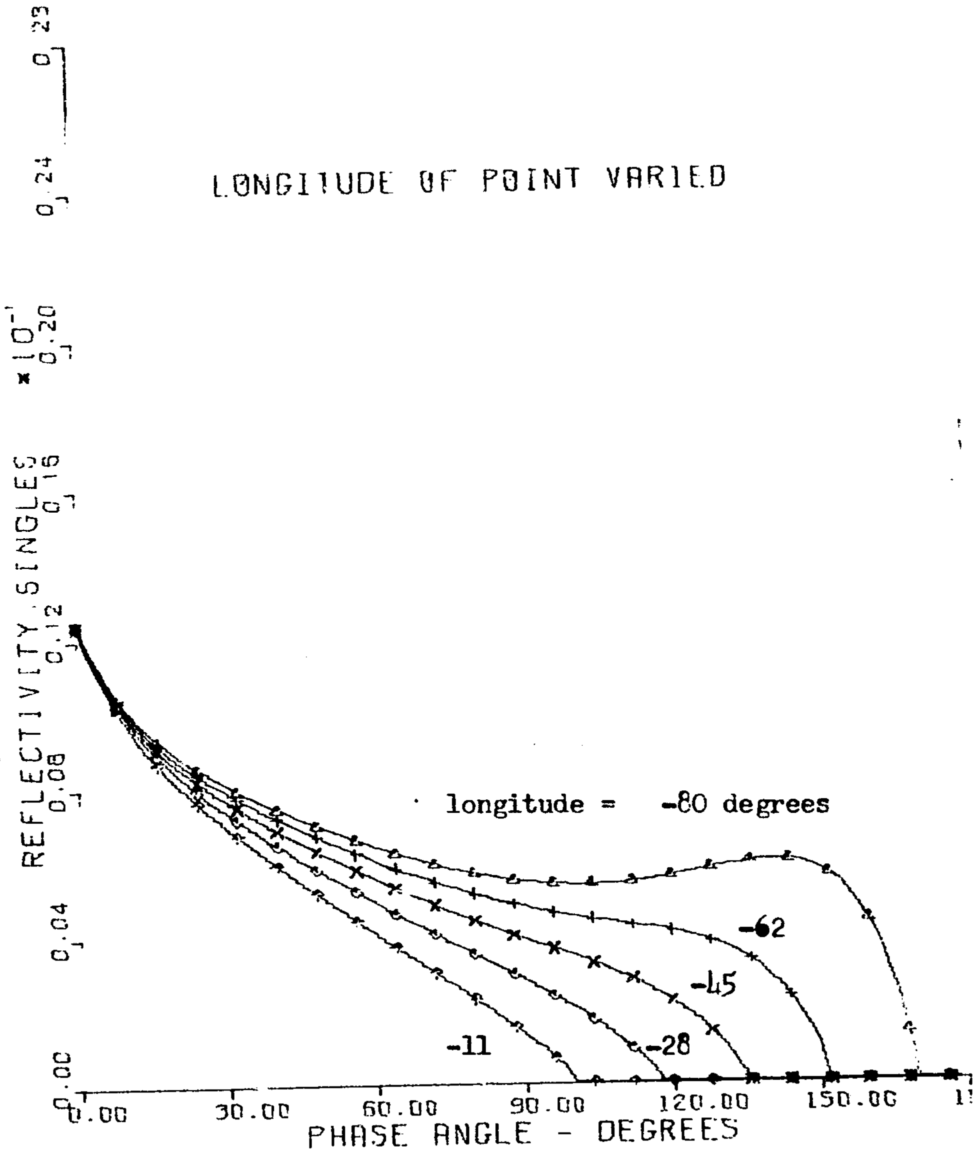

Figure 14J. The intensity of the singly-reflected component of light.

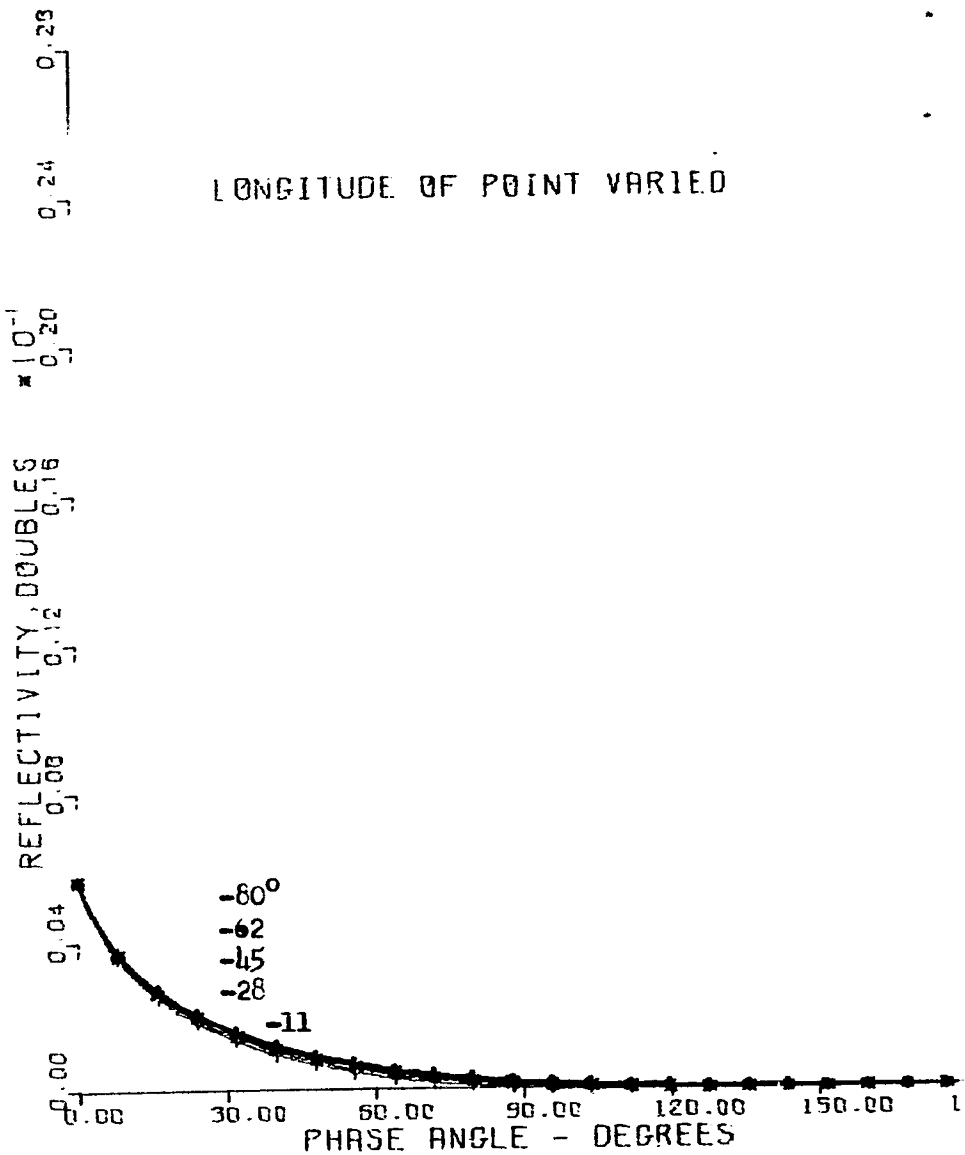

Figure 14K. The intensity of the doubly-reflected component of light.

IV. THEORY OF THE POLARAMETRIC NEGATIVE BRANCH

Besides indicating the presence of a pitted regolith, the negative branch has the potential of providing useful information, especially for the outer planets which are only visible at small phase angles. It follows that there is a need to understand the formation of the negative branch in quantitative detail so as to make use of the numerical information available. This section describes in detail the light components which contribute to the negative branch, and, formulae are derived for the approximate position of the inversion angle and the polarization minimum.

Figure 15 is a plot of the four components of light which contribute to the negative branch:

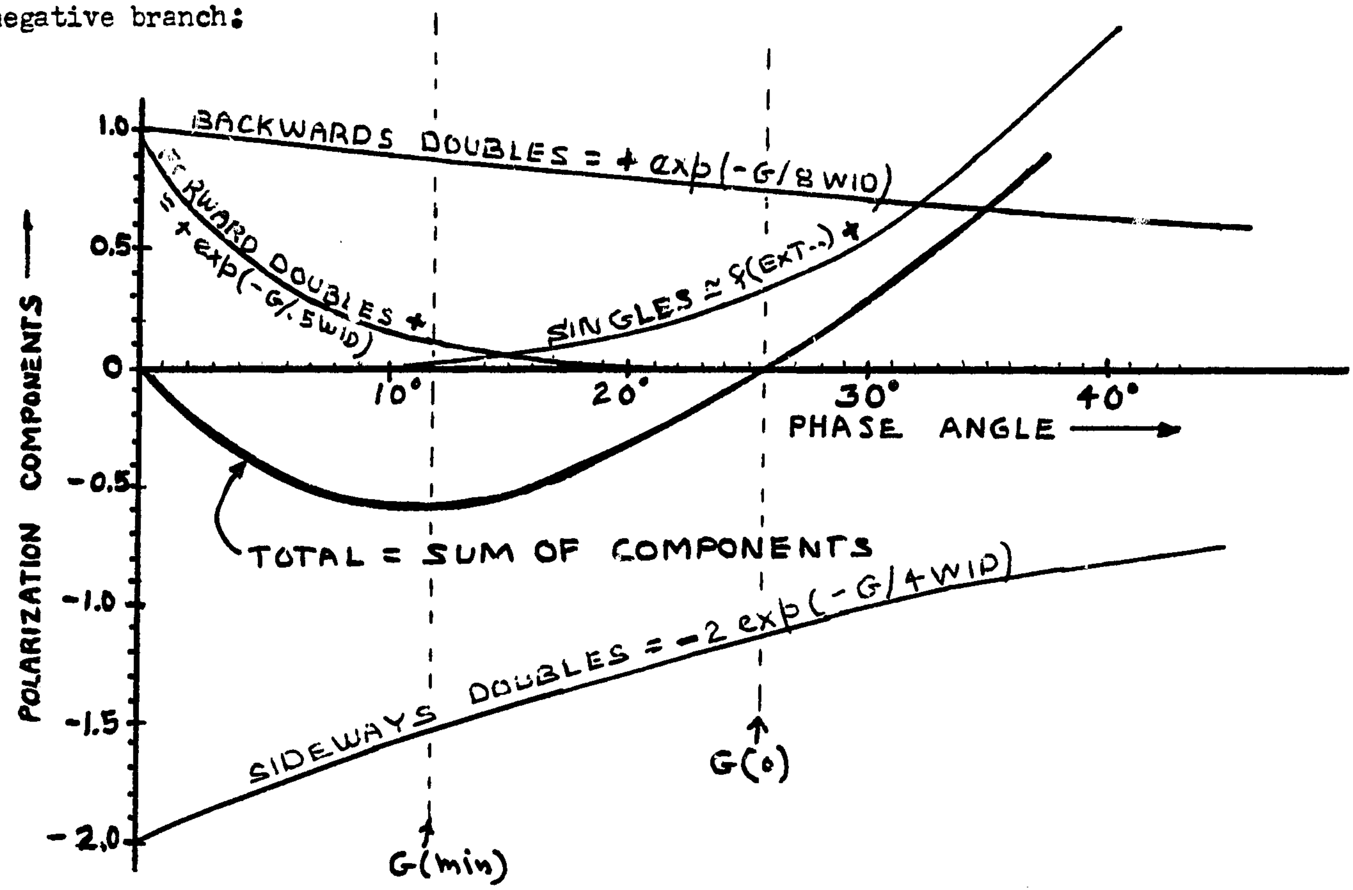

FIGURE 15. The light components which make up the negative branch.

The polarization minimum depends on functions of the pitwidths only. But the polarization inversion angle depends on the pit functions in competition with the specular polarization from external surfaces.

There is a common misconception that the angle of minimum is half of the inversion angle and therefore measure of either provides the same information. It is evident from the above figure that neither of these is true. The two angles are related to separate factors.

The components in the figure are those which contribute to polarization, and are defined with respect to the plane of vision (Sun-object-Earth) which is the plane of symmetry. Double-reflecting rays which go either side of the plane and then forward are termed sideways doubles. They are the source of negative polarization. Rays which reflect twice and stay in the forward quadrant are termed forward-doubles. They contribute little to the positive polarization because of rapid attenuation in getting out of the pits. Backward doubles are big contributors to positive polarization because their path makes it easy to get in and out of pits.

The Location of P-min .

In the figure near the location of P-min, the two most rapidly changing components are the sideways doubles (-) and the forward doubles (+) . When the rate of change of their sum is zero, a minimum occurs. The other two smaller components can be ignored, because they are both + , but since one is decreasing and the other increasing, even their small contribution is nullified.

accordingly, the minimum occurs when

$$\frac{d}{dG}\left[2\exp(-G/S)\right] \cong \frac{d}{dG}\left[\exp(-G/F)\right]$$

where G is the phase angle, S and F are constants derived from pit width/depth. After carrying out the differentiation, taking logs of both sides, and solving for G, the result is

$$G(\min) \simeq \frac{\ln(2\,F/S)}{(1/S - 1/F)} \times \mathrm{WID}$$

Thus the phase angle of P-min depends mainly on the geometry of the pits through the angular attenuation constants F for forward doubles, and S for sideways doubles. For example, if we use the values used in the computer program, S = 4, $F=\frac{1}{2}$, and WID = .20, then G(min) ≈ .8 x WID = 9° .

This approximation is gord if G(min) is small, say less than about 14^{o} . At larger angles, the approximation breaks down because of the presence of single (+) polarization which will make the observed angle small than the calculated approximation. This can be deduced from the figure.

With this understanding of P-min, one is immediately led to ask, Why do the asteroids have smaller pit width/depth ratios than the Moon, Mars or Mercury ? and What is the character of asteroid Ceres 1 which has an unusually low G(min) = 7^{o} ?

<u>The Inversion Point</u>

The point of inversion occurs when the sum of all components is zero. From the figure this condition is

$$\text{singles polarization (EXT,DUST..)} + e^{-G/B} = 2\, e^{-G/S}$$

It is not convienient to go further with this relation because of the complex dependence of the singles polarization on dust, external surface, Mi, MR, as well as the pit geometry. However it is possible to establish a useful qualitative principle. First, establish that backwards doubles and sideways doubles have a fairly fixed ratio regardless of the type of surface. This is true,exactly,at opposition because both kinds of rays follow the same kinds of paths with average reflection angles at 45^{o} for both. As phase angles become larger, the sideways-doubles average angles still remain near 45^{o},while the average angles for backwards doubles is $45^{o} - G/2$. If G is not too big, both types of double rays are affected almost the same.

It follows from the above thatthe most significant effects on polarization near the inversion point are due to the intensity of <u>singles relative to doubles</u>. Now, combine this idea with the geometric principle (discussed elsewhere) that the sum of pitted area (produces doubles) plus non-pitted area (produces singles) is a constant, and we arrive at the general qualitative principle that : <u>The Inversion Point is An Indicator of the Relative Amounts of Pitted and Non-pitted Area</u> . If pits are relatively larger, the inversion point moves to the right. If pits are smaller - to the left. This principle is good enough to merit quantitative calibration using laboratory objects.

Proof from Observation and Analysis

Ample evidence is available to substantiate these conclusions. Moon measurements always show an unchanging G(min) if wavelength is varied, but G(C) changes. This is because G(min) depends on pit ratios which don't change. In the figures of this report where EXT or DUST are varied, G(O) always moves right if these two factors are increased. This is because they increase the pitted area. Laboratory samples show the same effect. When looking at wavelength dependent data, recall that the measure of size should be the wavelength itself, so that increasing wavelength tends to decrease non-pitted area.

V. THE COMPUTER MODEL COMPARED TO CSM TAXONOMY

This surface model has provided results which may be closely compared to the CSM Taxonomy of Bowell et al (1978). Examination of the mathematics involved show that this has occured because the new model provides quantitative expressions for both diffuse light and specular light. The older model had no computation for diffuse light; it merely lumped in the required amount to obtain the desired reflectivity.

Especially, the diffuse light equation, which is a new result, is dependent on particle size, wavelength and both the real and imaginery indices of refraction. This results in a proper relation between those factors when computing diffuse light and when computing specular light. This important addition to the model and the resulting quantitative agreements with observation provide confidence that the model describes a pitted, particulate surface characteristic of airless planets, in an accurate fashion.

Two kinds of Reflected Light

The behavior of the new model becomes clear if one keeps in mind how the two kinds of light, specular and diffuse, change as the imaginary index changes.

Diffuse light is mainly due to light which enters particles, travels through them while undergoing several internal reflections, and eventually emerges after some absorbtion. As the absorbtion constant (imaginary index) is increased, this diffuse light steadily decreases in amplitude eventually reaching almost zero. When the imaginary index is small, diffuse light dominates over the specular (singles and doubles) light. However, there arrives a transition value when diffuse and specular light are about equal. Then, further increase of the index allows specular light to dominate.

The specular light basically depends on computations of Fresnel's equations the results of which are modulated to account for the effects of the pitted

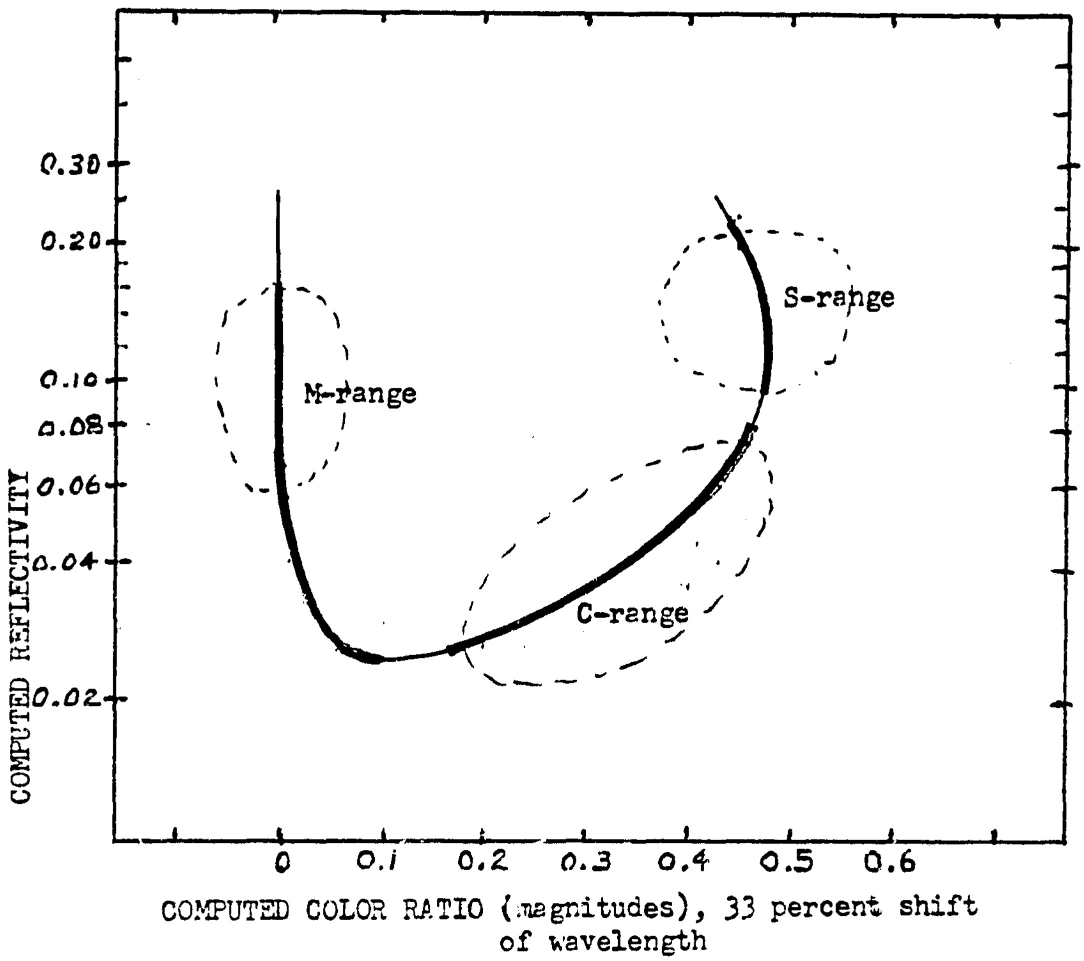

Figure 16. This figure was prepared for comparision with figures 1 and 2 of Bowell et al (1978) which show color indices against albedo in a scatter-diagram of a few hundred asteroids. Those figures form the basis for the CSM taxonomy of asteroids.

The agreement of this computer model with the S,C, and M groups of asteroids is excellent. In the figure, as you move along the heavy line beginning at the S-range, the imaginary index of refraction (absorbtion constant) steadily increases.

The quantitative agreement with asteroid measurement is all the more remarkable in view of the fact that no adjustable parameters have been used for fitting. The entire computer model was created, and then matched at only one point: the Moon, at the point P-min = 1 % and reflectivity = 9 %.

From that time onward, all calculations have been made with the same model. In view of the non-linear, complex functions for the two variables plotted above, agreement by coincidence seems impossible.

When making numerical comparisons, keep in mind that the computer model contains no variation of color due to molecular phenomena. If visible, the model material would appear as neutral shades of gray.

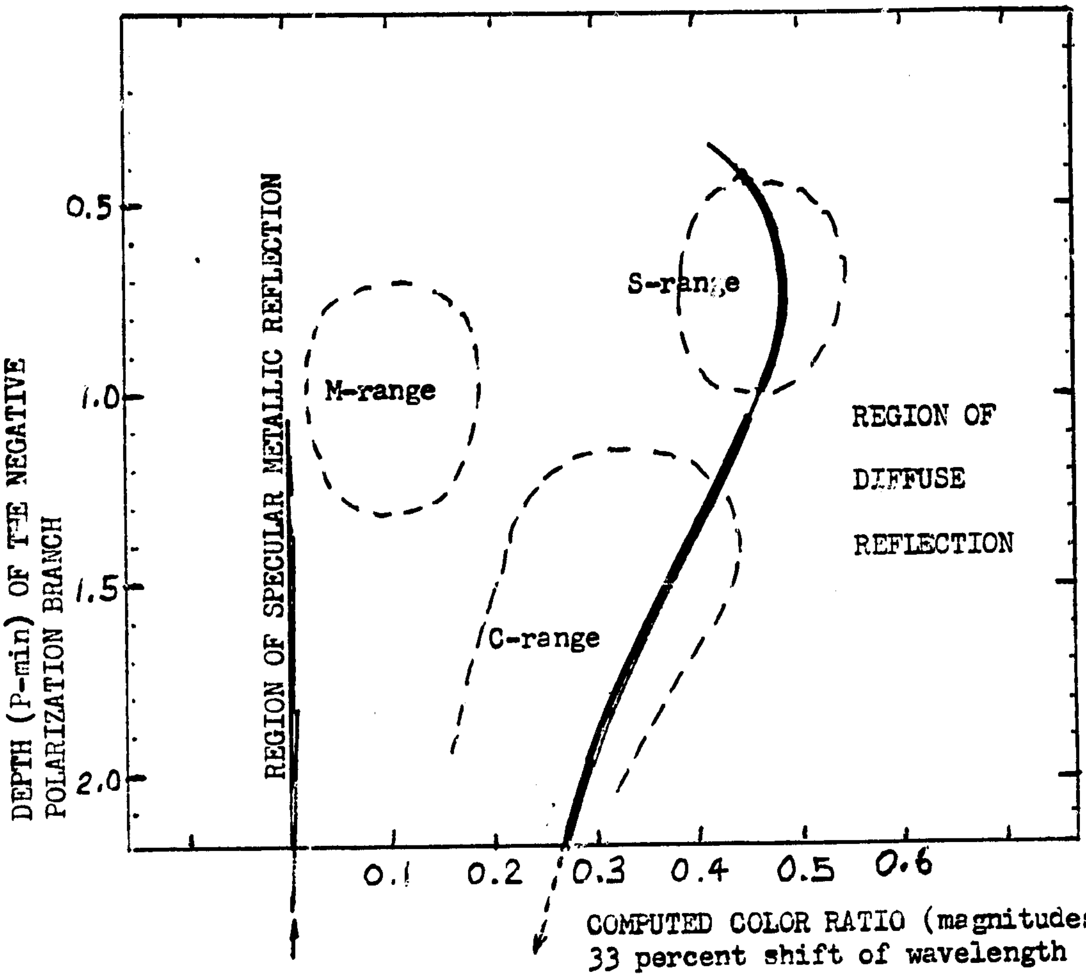

Figure 17. This figure was prepared for comparison with figure 3 of Bowell et al (1978), which is a scatter-diagram of asteroids using similar coordinates. Their diagram displays the grouping of the CSM taxonomy.

The agreement on the location of the S and C asteroids when comparing the computer model with measurements is very good, however the model's values of P-min are far too large in the M-range, or what ought to be the M-range. They run off scale above.

The puzzle is complicated by the lack of knowledge of the real observed M asteroids. It is not known whether, in fact, they possess surfaces, materials, or any characteristics compareable with the assumed computer model.

However, the computer model itself may be unrealistic for values of the imaginary index in the metallic specular range. The large computed values of P-min, 3 to 8 percent, are a result of the assumed presence of pits and particles made of glittering metallic material. Is this a correct description ? It might also be that the metallic material of the M asteroids is a malleable sort and does not form the pits and particles assumed.

surface. When the imaginary index is small, Fresnel's equations are practically unaffected by changes in the index. As it is increased, reflectivity slowly increases, and there arrives a value, about MI = 0.1, when the specular light is about equal to the decreasing diffuse light. At larger values of the index, the specular light increases rapidly. However, it should be noted that both the parallel and perpendicular components of the Fresnel calculation increase, but unequally, so that the weaker asymptotically approaches the other's value. Thus, polarization gradually comes close to zero for very large values of the imaginary index.

These calculations are strongly based upon the physical laws of optics. Even though one might quarrel with the details of diffuse reflection or the formation of the negative branch, the general trend of reflectivity and polarization are inevitably in accordance with the model. Accordingly, the evidence for the model's interpretation of the CSM taxonomy is equally strong. Figures 16 and 17 have been prepared using the same kind of coordinates and showing the same ranges of C, S and M asteroids as displayed by the authors of the CSM taxonomy (Bowell, etal, 1978). The coincidence of these diagrams, and other numerical agreements, can hardly be accidental especially in view of the complex variation of the diffuse and specular light, and the fact that there are no adjustable parameters to create "fits".

The Albedo Rules

Rules have been variously proposed and used to obtain the albedo of unresolveable planets using the slope of polarization, maximum polarization, and minimum polarization as a function of the phase angle. Figures 18 and 19 have been prepared to show how these rules appear from the calculations of the computer model. In all three cases, the computer model produces a quantitative agreement with the empirical rules in a linear range which corresponds to the S asteroids and part of the C asteroids.

These diagrams can be used to deduce reflectivity in the usual way, or

REPRODUCIBILITY OF THE
ORIGINAL PAGE IS POOR

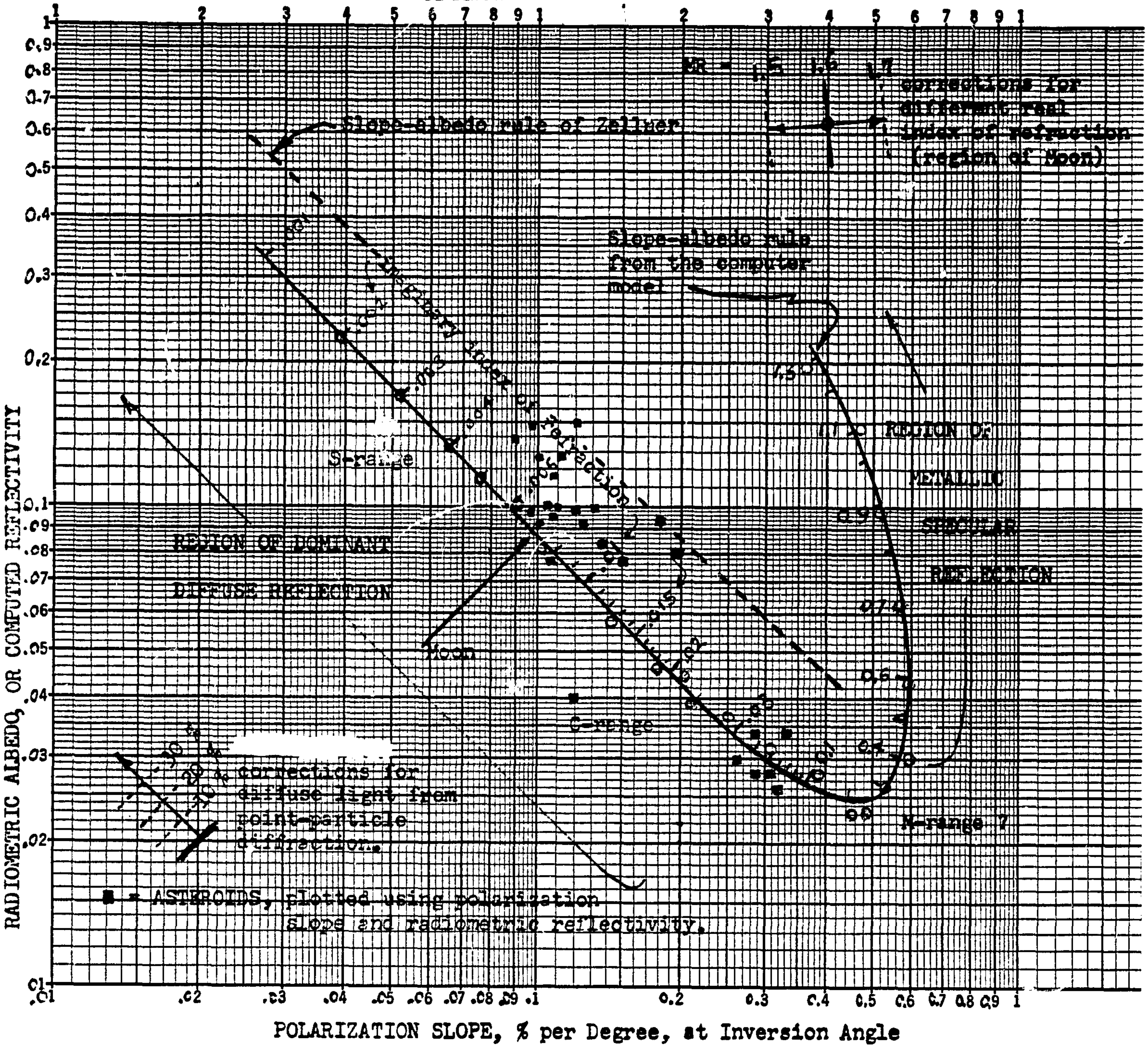

Figure 18. The Computed Polarametric Slope versus the Computed Albedo, and some Comparisons with Asteroid measurements.

The computer model agrees well with the measurements of asteroids, and supports the contention of Zellner that the Slope-albedo rule is linear ; in the S-range and part of the C-range. There is a saturation of the polarimetric slope in the M-range, due to the transition of reflectivity dominance from the diffuse mechanism to specular reflection.

The small diagrams in the lower left and the upper right show the magnitude and direction of corrections for conditions of diffuse light and real index other than that assumed for this figure.

The fact that the correction vector for point-particle diffuse light is parallel to the linear portion of the Slope-albedo Rule means that calibration error due to this cause will not occur, but subsequent use-error will be concealed; i.e. C-objects with extremely fine ($d < \lambda$) dust will be misinterpreted too far towards the S-range.

There is a theoretical minimum albedo of 2.5% for pitted, particulate bodies.

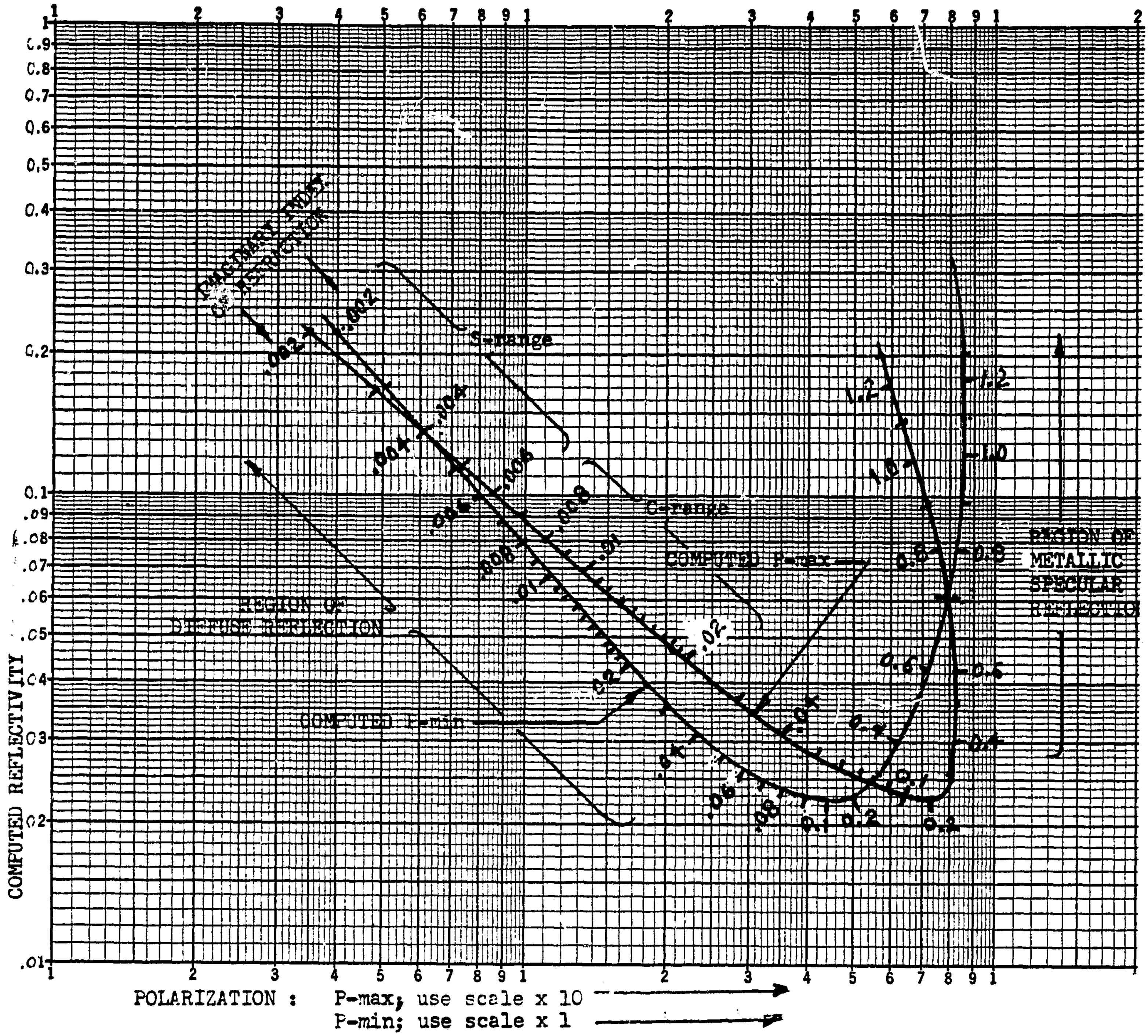

Figure 19. Maximum and Minimum Polarization From the Computer Model.

These two curves show a theoretical version of the corresponding rules to obtain albedo from P-max and P-min. These rules are not as reliable, it is thought, as the Slope-albedo rule. The reason, discussed elsewhere, is that errors in the P-min and P-max rules are opposite and tend to cancel in the Slope Rule.

The computed P-max Rule computed here agrees well with observations, however the P-min Rule here is drastically violated in the metallic M-range by asteroids presumed to be of this type.

Reasons for the M-range failure could be : the pitted, particulate model does not describe objects in the M-range; or, there do not exist any M-type objects, i.e. metallics with large absorption and pitted surfaces.

conversely, if the reflectivity canbe measured by an independent means such as radiometry, then the variation from the computed curve can be used to deduce variations from the assumptions of the computer model. Potentially computable variations include the real index of refraction and the existence of very fine dust which causes diffuse light by point-particle diffraction.

The Maximum and Minimum Polarization Rules

Figure 19 shows the computed rules. These rules have been found empiracally to be less accurate than a Slope-albedo Rule and the model offers a logical reason for this. Maximum polarization of the the positive branch depends on the amount of singly-reflected light compared to the diffuse light. The singly-reflected light, in turn, depends on the amount of specular area visible on the planet. Any variations of that area fraction must produce errors in the rule.

Similarly, the minimum polarization rule depends on the amount of doubly-reflected light compared to the diffuse light.The doubly-reflected light, in turn, depends on the amount of pitted, particulate area visible on the planet. Any variations of that area fraction produces errors in the minimum rule.

The Polarization Complementarity Principle

A very useful principle for interpreting polarimetry can be derived from a simple geometric concept concerning airless planets. It can be stated, "A geometry-dependent Increase of Positive Polarization is Always Accompanied by a Decrease of Negative Polarization" . It follows from these three assumptions :

1) On a planet, the area of pits plus the area of non-pits is a constant (equal to the total area).
2) Pits produce double reflections and negatively-polarized light.
3) Non-pits produce single reflections and positively-polarized light.

Thus, if the surface structure of a planet should vary from some norm which, say,characterizes an albedo rule, then the singly and doubly reflected light will vary inversely. An albedo rule dependent on the positive branch will have an error, but the albedo rule which depends on the negative branch will have the opposite error. Another example : If a geometry-dependent variation should occur in the study of polarization inversion angles, then a change which increases the positive branch will decrease the negative branch and the inversion point will move to the left. Oppositely, a variation decreasing positive polarization will cause the inversion angle to move to the right.

The Slope-albedo Rule

In a review of albedo rules, Bowell and Zellner (1974) clearly show that the empirical scatter of data is least for the Polarization-slope Albedo Rule. The computer model provides a logical reason why this should be true. It results from the Polarization Complimentarity Principle and the fortuitous choice of the inversion point to measure the slope. This point lies midway between the domains of the positive and negative polarization branches. If geometry-dependent variations from the Rule norm should occur, then by the Principle, opposite changes occur in the negative and positive polarization branches which tend to cancel each other in the slope. If the reader is not convinced, a little pencil and paper work drawing the slopes is quickly convincing. You will also notice, in pencil diagrams, that although the slope remains constant, the inversion angle moves to the left or right, depending on the type of variation chosen, as required by the Principle.

Despite these advantages of the Slope-albedo Rule, examination of Figure 18 shows that the linear rule may fail completely for some dark C objects and metallic objects. The double branch of the computed rule suggests that some M or C objects could be confused with each other, if independent means is not used to determine on which portion of the curve an object lies.

A New Reddening-Albedo Rule

Figure 20 shows a plot of reddening vs reflectivity as computed using the surface model. Like other rules, it has a linear portion and a second branch.

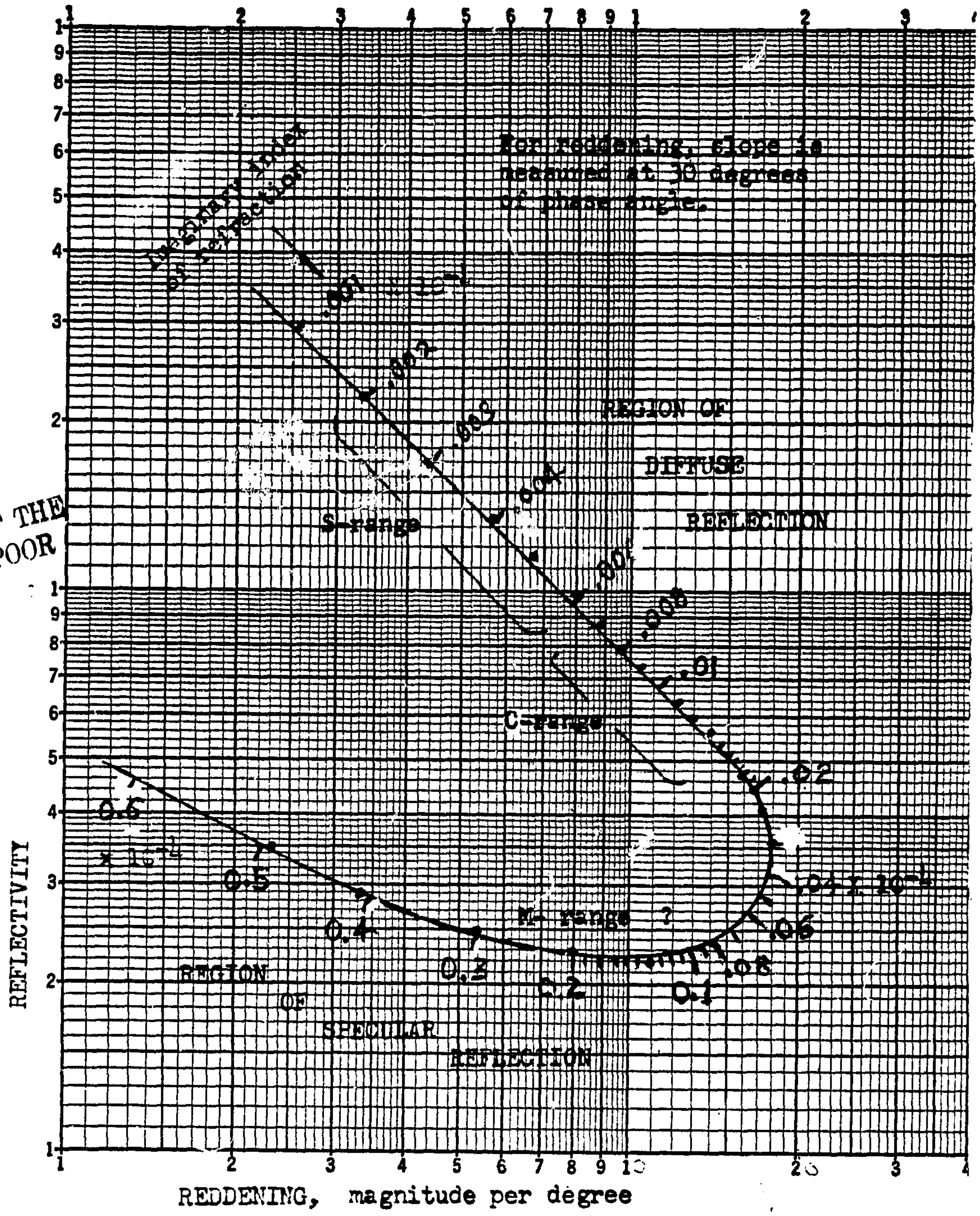

Figure 20. Reddening is defined as the increase of color ratio with increasing phase angle. The data for this figure was obtained by measuring the slope of the computed color ratio curves. Reflectivity is taken at zero phase angle. All data refers to curves for the integrated whole planet.

It is interesting that in both the diffuse reflection region and the specular region, the rule of thumb, "The Darkest Planets Show The Greatest Reddening" , is observed. However, there has never been any recognition of two branches to the rule, nor a failure of the rule in the M-range of asteroids. Reddening measurements have very large errors which is why it has been only a qualitative rule. Recent improvments in the sensitivity of photometry might change this situation.

It also probably is relatively free from geometry-caused error, like the Slope Rule, because reddening depends on the relative slopes of the diffuse light compared to the slope of the <u>sum</u> of singly and doubly-reflected light. If the reddening measurements are made at angles where the amplitudes of singly and doubly reflected light are about equal, then geometric variations in the surface will not produce errors. Such equality only occurs for the very-large values of the imaginary index and at phase angles near zero, thus it might be useful for outer solar-system objects which are metallic. However, this is some error cancellation for all values.

Unfortunately, the reddening rules requires great sensitivity and accuracy im the photometry, so that it would be useful only for bright objects.

<u>An Improved Polarization-minimum Rule</u>

The P-min Rule for finding albedo is very useful for objects in the outer solar-system where phase angles are always small, but it lacks the error-cancelling feature of the Slope-albedo Rule. However, an improved P-min Rule can have the error canelling feature by using the inversion angle as a negating parameter. For example, an adjusted P-min is calculated using

$$\text{ADJUSTED P-MIN} = \left[1 + \frac{G(C) - G_a}{kG_a}\right] \times \left[\text{P-min}\right]$$

where G_a is an average (calibrated) inversion angle and k is a calibration constant. This makes a correction for the geometry-induced errors in the same way as occurs naturally in the slope-albedo rule. The shift of the inversion angle G(C) detects the change of geometry and is used for correction.

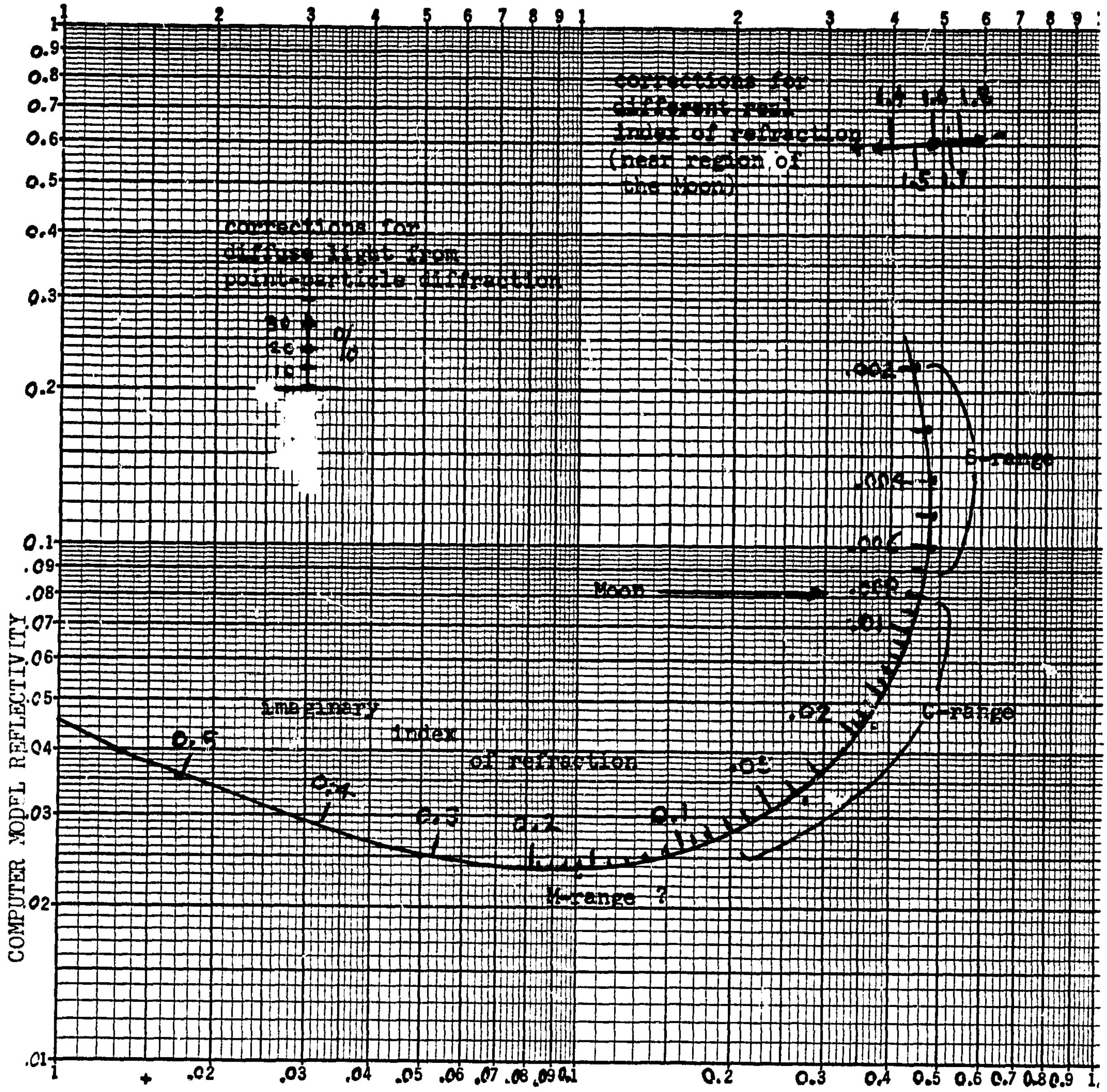

COLOR RATIO (difference in magnitudes) , computer model,
For a wavelength shift of 33 percent.

Figure 21. This figure shows the color ratios taken from the computer plots displayed in figures elsewhere. This color ratio is similar to color indices such as the U-V or the R/B index of Bowell et al (1978).

The color ratios and reflectivity numbers are taken from the computer-generated figures at zero phase angle.

The small diagrams at the top of the page provide corrections to the curves for values of parameters different than those assumed in the computer model. Note that the corrections are vectors.

Obtaining Added Information From Albedo Rule Variations

If independent means is available for measuring albedo, then the variations from the the values expected from polarization or reddening measurements, can be used to calculate other parameters of the surface. Two important such parameters are the real index of refraction and the amount of very-fine dust which causes diffuse light by diffraction.

Each of these two parameters causes variation of the computed reflectivity with a unique vector on the appropriate diagram. All portions of the diagrams can be calibrated with these vectors. Two examples are shown on the figures.

The R and E Type Asteroids

The R and E asteroids do not appear to fit immediately into the series of objects corresponding to an ordered variation of the imaginary index. However, this conclusion is very tentative because there are only 2or 3 of these objects identified. Nevertheless, such objects probably fit into the computer surface model because the only deviations of the objects are with respect to color, and color due to molecular/atomic absorbtions is not modelled. Furthermore, the position of these objects in the high albedo range means that there is considerable diffuse light and therefore color variations are strongly present.

Another Model Correspondence

The computer model agrees with the CSM taxonomy in yet another way. In the model there are various logical means to add color for S,M,E and R objects, but no way for the dark C types. And, indeed, there is only one observed C object, among the hundreds which shows color. Asteroid 85 Io has a small pyroxene band absorbtion. This observation seems mysterious.

VI. THE WAVELENGTH DEPENDENCE OF LIGHT FROM DARK, ROUGH PLANETARY SURFACE

Introduction

An obvious means of deducing some properties of the surface of airless planets is measurement of reflectance variation with varying wavelength. Such a measurement at one viewing angle will provide color information but cannot distinguish a flat sheet from a rocky landscape. To obtain information about the surface geometric structure, it is intuitively clear that the surface must be viewed at different angles seeking some variation as a consequence of the surface geometry. In practice, this means obtaining color data at different phase angles.

For this discussion, two sources of color variation are considered : One, where the absorbtion of light inside the surface material is due to wavelength-dependent interactions of light with the atomic and molecular energy levels. Two, where the observed color variations are to size and geometric factors of a pitted, particulate surface such as that of the airless solar-system bodies.

The former variations are often seen as absorbtion bands in the reflectance spectra. Such measurements and their analysis have been extensively carried out by Mike Gaffy and Tom McCord (1978), and Clark Chapman, to name a few investigators in an active field. The results can lead to identification of some of the mineral types making up the surface. This computer model does not model this effect; instead it is "neutral gray".

The second source is not so obvious because the color variations are mainly due to the relative sizes of particles compared to wavelengths. Observeable color changes are only significant when particle sizes are of the same order as the wavelength, say, $\lambda < d < 10\lambda$. Several phenomena can occur. In particles which 'trap' light temporarily by internal reflection, short wavelengths are absorbed more than long wavelengths, because the short wavelength path is a greater number of wavelengths and that is the factor upon which absorbtion depends. The result is increasing diffuse light reflectance with increasing wavelength.

Another phenomenon of the second type is the change of the ratio. of diffusely-reflected light to specular light as the viewing angle changes. This happens because diffuse light tends to emerge evenly at almost all angles, whereas single and double reflected light lends to emerge at angles close to the incident rays, if the surface is a pitted one. Since the diffuse reflectivity is wavelength dependent and the specular light is much less so, the result is a wavelength dependence on the phase angle.

These latter two geometric effects are implicitly included in this computer model of a pitted particulate surface.

Explanation of The Reddening Effect

An unexplained phenomenon of the airless planets is the reddening of their reflected light with increasing phase angle. This has been observed by Gehrels, Coffeen and Owings (1964) and Gehrels and Owings (1962) on the Moon; on Mars by Irvine et al (1968) and on the asteroids by Wooley et al (1955). These observers measured reflected light using photometers and band-pass filters in the IR, visible, and UV wavelengths. Reddening was reported as an increase of the ratio of long wavelength intensity compared to the shorter wavelength intensity, as a difference of magnitudes.

Various explanations of reddening have been suggested including a) Mie scattering from transparent particles of a dominating critical size, b) surface roughness concentrated in wavelength-sized dimensions that produce suitable diffraction, and c) electrostatically suspended dust. No quantitative analysis has resulted.

This computer surface model has been used to calculate reddening as a result of geometric effects (but not due to molecular colors). Each of the figure sets elsewhere in this report has a computer plot of color ratio as a function of phase angle. These plots agree perfectly with the observations to the extend that observational errors permit (errors are large). It can be concluded that the geometric reddening computed is sufficient to explain the observations of the Moon and asteroids. There is a possibility that molecular reddening may also increase the effect on Mars.

Reddening to Investigate Surface Structure

As mentioned above, reddening measurements which take place at sucessive view angles contain information about the three-dimensional surface structure. In principle, the same is true for polarization, and polarization difference measurements. For that reason, all of these plots have been provided in this report. Admittedly, I don't have any good scheme yet to use the polarization differences.

There is a converse idea. If the surface structure can be assumed, and of course this assumption is implicit in all the albedo rules which rely on the existence of a pitted particulate surface, then it is possible to deduce the reflectivity of the surface. The polarization-albedo rules are all well known, but reddening has never been used in a quantitative way. However, there is a qualitative rule of thumb, "The Darkest Objects Always show The Greatest Reddening" . I believe that the improvements in sensitivity of photometry now make it possible to obtain sufficiently accurate data.

A Reddening-albedo Rule has been plotted in Figure 20 using the slope of the color ratio, versus reflectivity. Slope is taken at 30 degrees phase angle and reflectivity is taken at zero phase. There are not enough accurate measurements existing to make a comparison with this theory meaningful, but it may be hoped that certain geometric sources of error will be balanced out, just as occurs in the polarization slope albedo rule.

Computer Calculations

To obtain Figures (B),(C),(D) of each figure set, the following formulas were used to calculate the ordinates :

$$\text{REDDENED POINT} = 2.5 \times \ln(B_1/B_2)$$

$$\text{REDDENED PLANET} = 2.5 \times \ln(\text{integrated } B_1 \,/\, \text{integrated } B_2)$$

$$\text{POLARIZATION DIFFERENCE} = P_2 - P_1$$

where the subscript 1 refers to a calculation with particle size(XTL) = 15 wavelengths, and subscript 2 for particle size(XTL) = 20 wavelengths. B_1 and B_2 are the total reflectivities.

The corresponding wavelength shift is (20 - 15)/15 = 33% or (20 - 15)/20 = 25%, depending on your point of view.

VII. THE RINGS OF SATURN

This computer model combined with polarimetry by Lyot (1929), Dollfus(1979),and P.Johnson et al (1979) provides confirmation of some of the models of the rings which are reviewed by Morrison (chapter 12, Planetary Satellites, J. Burns Ed, 1977) and by Cook and Franklin (ibid, Chapter 19) and, yields a calculation of the diameter of the bodies composing the rings.

Optical , infra-red, and microwave measurements of radiation plus radar returns have led to the identification of water-ice as a constituent of the ring bodies together with methane or ammonia compounds in the form of dirty rough snow balls. Size estimates are between 3 and 30 centimeters (Morrison) or 6 to 100 centimeters (Cook and Franklin). Alternatively, the balls could be much larger with smaller, imbedded, dense nodules of those dimensions, in order to account for the radar results.

The polarimetry , measured at phase angles of 6 degrees or less, shows a negative branch amplitude of 0.5 to 0.8 % . The angle of minimum is p[illegible]ly defined at about $1 \pm \frac{1}{2}$ degrees (Lyot) and $1.2 \pm \frac{1}{4}$ degrees(Johnson). The polarization were caused by a pitted surface, then the pits appear impossibly deep. Nevertheless the opposition effect has been observed with the same narrow width. The conclusion seems inescapable that the shadowing of opposition is respon-sible for the negative branch. (The suppression of forward-going double reflections by the shadowing is the cause of the negative branch.)

However, it is not necessary to invoke shadowing by surface pits only. Inter-ball shadowing is possible and likely, and creates no paradoxical geometries, so that negative polarization from it follows logically. The equivalent of pit/depth ratio, but for inter-ball shadowing, is the dimaeter/separation ratio. Let us estimate, using the polarization data, that the computer variable WID $\simeq 1 \pm \frac{1}{4}$ degrees, or that separation/diameter $= 14 \pm 3$.

It now becomes poosible to calculate the size of the dirty snowballs. The reported optical depth of the rings is slightly less than 1 . The thickness of the rings has been measured at about 1 kilometer. Thus a little geometry yields the average diameter of the balls as a little less than

$$\text{average ball diam} = \frac{\pi}{4} \times \frac{\text{RING THICKNESS}}{(\text{SEPARATION/DIAM})^3} = 28 \pm 10 \text{ centimeters}$$

This value agrees with the limitation imposed by the reported radiation and radar measurements mentioned above. It does exclude the very large snowballs with imbedded dense nodules.

It is possible that there is some negative polarization due to the pitted surface of the balls themselves, but it is not likely. The dimensions of the particles and pit walls are tiny - obviously much smaller than the balls themselves. In view of the reported high albedo, it is unlikely that these pits and particles produce much shadowing; because they are translucent. Shadows are the sin qua non of the negative branch. If there is no shadowing, there is no negative polarization. On the other hand, large balls are quite opaque, even though composed of particles which are translucent on a micro-scale, and produce first-class shadows.

The following figure shows an estimated inter-ball polarization together with a small possible surface polarization which sum to the observed data.

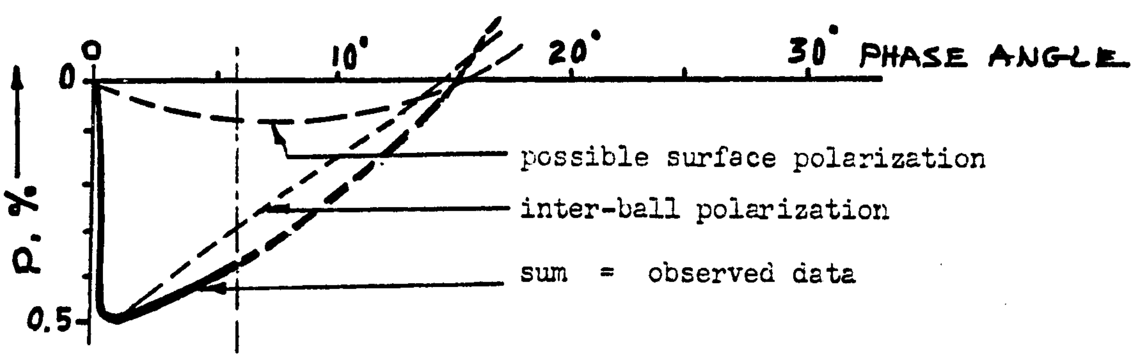

Figure . Estimates of the polarization components of Saturn's rings which match the observed data.

VIII. ACKNOWLEDGEMENTS

During the course of this work, it became increasingly apparent that extensive studies and meticulous observations of asteroids by the community of astronomers was a necessary base for the results which have been achieved here. Although it is not possible to mention every valuable research work, I have been especially grateful for the following admirable work :

1. Taxonomy of Asteroids by Edward Bowell, Clark Chapman, Johnathan Gradie, David Morrison and Ben Zellner.
2. Polarization measurements of asteroids by Ben Zellner and Colleagues at the University of Arizona.
3. Radiometric measurements of asteroids by David Morrison and Olav Hansen and Colleagues at the University of Hawaii.

IX REFERENCES

E. Bowell, C. Chapman, J. Gradie, D. Morrison, and B. Zellner, "Taxonomy of Asteroids", Icarus 35, 313-335, 1978

A. Cook and F. Franklin, Chapter 19, Planetary Satellites, J. Burns Ed. 1977

E. Bowell and B. Zellner, "Polarizations of Asteroids and Satellites", Planets, Stars and Nebulae Studied with Photopolarimetry, T. Gehrels, Ed. 1974

A. Dollfus and E. Bowell, "Polarimetric Properties of the Lunar Surface and Its Interpretation," Astron & Astrophys. 10, 29-53, 1971

A. Dollfus, Thesis, U of Paris, 1955, or NASA TTF-188 Translation, 1964

M. Gaffy and T. McCord, Space Science Rev. 21 555-628, "Asteroid Surface Materials: Mineralogical Characterizations from Reflection Spectra", 1978

T. Gehrels, T. Coffeen, and D. Owings, Astron. J. 69, 826, 1964

T. Gehrels and D. Owings, Astron. J. 135, 906, 1962

P. Johnson, J. Kemp, R. King, T. Parker, and M. Barbour, "Saturns Rings: New Results from Optical Polarimetry"... submitted Nature, 1979

O. Hansen, Astron. J. 81, 74-84, 1976

J. Hopfield, Science 151, 1380, 1966

W. Irvine, T. Simon, D. Menzel, C. Pikoos, and A. Young, Astron. J. 73, 807, 1962

B. Lyot, Ann. de Ob. de Paris, Meudon 8, No. 1, 1929 or NASA TTF-187 translation, 1964

D. Morrison, Astrophys. J. 194, 203-212, 1974

D. Morrison, Chapter 12, Planetary Satellites, J. Burns, Ed. 1977

M. Wolff, "Polarization of Light Reflected from Rough, Planetary Surface", Applied Optics 14, 1395-1505, 1975

R. Woolley, K. Gottlieb, W. Heintz, and A. DeVaucouleurs, Monthly Not. Roy, Astron. Soc. 115, 57, 1955

B. Zellner and J. Gradie, "Polarimetric Evidence of the Albedos and Compositions of 94 Asteroids," Astron. J. 81, 262-280, 1976

B. Zellner, M. Leake, T. Lebertre, and A. Dollfus, "Polarimetry of Meteorites and the Asteroid Albedo Scale," Lunar Science Conf. NASA VIII, 1977

X. THE FORTRAN PROGRAM
(Used for Figs. 8A to 8K)

```
@SYM PUNCH$,,ISDPCH
@FOR,IS  POLAR1
      REAL L,MR,MI
      COMPLEX CA,CB,CC,CM
      DIMENSION AB11(92,6),AB12(92,6),AB21(92,6),AB22(92,6),AB1(92,6),
     * AB2(92,6),AB3(92,6),AB(92,6),APOL(92,6),APB1(92,6),APB2(92,6),
     * APLNB(92,6),APLGF(92,6),ARED(92,6),AREDP(92,6),APOLWD(92,6)
3     FORMAT(1X,F6.3,15G7.2)
4     FORMAT(1X,I3,1X,16G7.2)
C INITIAL CONSTANTS  + START DO LOOPS
      WID=.20
      DUS=.4
      L=-1.3
      MR=1.6
      EXT=.3
      MI=.007
      DO 101 NDX=1,5
      MI=.2+(NDX-1)*.1
      M=NDX+1
      GP2=((1.-EXT)*(1.+DUS)+EXT*DUS)*0.5
      CM=CMPLX(MR,-MI)
      SUM=0.0
      DO 5 NR=1,90
      DG=(NR-0.5)/57.3
      CA=CMPLX(COS(DG),0.0)
      CB=CSQRT(CM**2-(SIN(DG))**2)
      CC=CA*(CM**2)
      FRESY=CABS(CC-CB)**2/CABS(CC+CB)**2
      FRESX=CABS(CA-CB)**2/CABS(CA+CB)**2
5     SUM=SUM+(FRESX+FRESY)*0.5
      REF=1.0-SUM/90.0
      CONE=3.14/CABS(CM)**2
      DO 100 NG=1,90
      GA=2.*(NG-1.0)
      G=GA/57.3
C PUT G VALUES INTO THE ARRAYS
      ARED(NG,M)=0.4
      AREDP(NG,M)=0.4
      AB11(NG,1)=GA
      AB12(NG,1)=GA
      AB21(NG,1)=GA
      AB22(NG,1)=GA
      AB1(NG,1)=GA
      AB2(NG,1)=GA
      AB3(NG,1)=GA
      AB(NG,1)=GA
      APB1(NG,1)=GA
      APB2(NG,1)=GA
      APOL(NG,1)=GA
      APLNB(NG,1)=GA
      AREDP(NG,1)=GA
      ARED(NG,1)=GA
      APOLWD(NG,1)=GA
      IF(G+L-1.54) 9
```

@SYM

```
              TO 100
      9     CONTINUE
            SHAD=1.+G/(L-1.57)
            COLGF=2/(1+COS(L)/COS(G+L))
            SIHG=SIN(0.5*G)
            COHG=COS(0.5*G)
      C FRESNEL FUNCTION ROUTINE
            GO TO 2
          1 CA=CMPLX(COS(DG),0.0)
            CB=CSQRT(CM**2-(SIN(DG))**2)
            CC=CA*(CM**2)
            FRESX=CABS(CA-CB)**2/CABS(CA+CB)**2
            FRESY=CABS(CC-CB)**2/CABS(CC+CB)**2
            GO TO(10,20,30,40),NF
        2   CONTINUE
            DG=.7854
            NF=1
            GO TO 1
       10   X45=FRESX
            Y45=FRESY
      C     CALCULATE SINGLE REFLECTION
            GP1=(EXT*(1.-DUS)+(1.-EXT)*(1.-DUS)*EXP(-(G/WID))/8.)*SHAD
            DG=0.5*G
            NF=2
            GO TO 1
       20   CONTINUE
            BX1=GP1*FRESX
            BY1=GP1*FRESY
            B1=0.5*(BX1+BY1)
      C SIDEWAYS DOUBLES AND MATRIX
            D1X=(COHG**2)*X45+(SIHG**2)*Y45
            D1Y=(SIHG**2)*X45+(COHG**2)*Y45
            D2X=D1X*Y45
            D2Y=D1Y*Y45
            X2L=(SIHG**2)*D2X+(COHG**2)*D2Y
            Y2L=(COHG**2)*D2X+(SIHG**2)*D2Y
      C CALCULATE FORWARD DOUBLES
            DG=.7854+G/4.
            NF=3
            GO TO 1
       30   X2F=FRESX**2
            Y2F=FRESY**2
      C BACKWARD DOUBLES
            DG=.7854-G/4.
            NF=4
            GO TO 1
       40   X2B=FRESX**2
            Y2B=FRESY**2
            SOB=EXP(-.13*G/WID)
            SOS=EXP(-.25*G/WID)
            BX2F=GP2*EXP(-(2.0*G/WID))*X2F*SHAD
            BY2F=GP2*EXP(-(2.0*G/WID))*Y2F*SHAD
            BX2L=2.*GP2*SOS*X2L*SHAD
            BY2L=2.*GP2*SOS*Y2L*SHAD
            BX2B=GP2*SOB*X2B*SHAD
            BY2B=GP2*SOB*Y2B*SHAD
            BX2=(BX2L+BX2F+BX2B)*0.38
```

```
      BY2=(BY2L +BY2F + BY2B)*0.38
      B2=(BX2+BY2)*.5
C RED CALCULATION
      B=.1
      PLANB=.1
      POL=.1
      DO 96 IRED=1,2
      XTL=(15.+5.*(IRED-1))*(1.-DUS)+1.
      B3=COLGF*REF*(.5+.5*EXP(-(G/WID)))/(1.+XTL*MI*158./CONE)
      RED=2.5*ALOG(B/(B1+B2+B3))
      B=B1+B2+B3
C PLANETARY INTEGRATION
      SUM=0.
      RLI=-1.57
 97   TB=B3*(2./(1.+COS(RLI)/COS(RLI+G)))/COLGF+B2+B1*(1.+G/(RLI-1.57))
     +/SHAD
      ORD=TB*((2./3.14)*COS(RLI)+(0.5-2./3.14)*COS(RLI)**2)
      SUM=SUM +ORD
      RLI=RLI+.04
      IF(RLI+G-1.57)97,97,98
 98   SUM=SUM*.04
      REDP=2.5*ALOG(PLANB/SUM)
      PLANB=SUM
      PB1=(BY1-BY1)/(2.*B)
      PB2=(BX2-BY2)/(2.*B)
      POLWD=PB1+PB2-POL
      POL=PB1+PB2
 96   CONTINUE
C COMPUTE FINAL RESULTS AND PUT INTO ARRAYS
      AB11(NG,M)=BX1
      AB12(NG,M)=BY1
      AB21(NG,M)=BX2
      AB22(NG,M)=BY2
      AB1(NG,M)=B1
      AB2(NG,M)=B2
      AB3(NG,M)=B3
      AB(NG,M)=B
      APB1(NG,M)=PB1*100.0
      APB2(NG,M)=PB2*100.0
      APOL(NG,M)=POL *100.0
      APLNB(NG,M)=PLANB
      AREDP(NG,M)=REDP
      ARED(NG,M)=RED
      APOLWD(NG,M)=POLWD*100.
      WRITE(6,4)NG,B1,RED,REDP,B3,B,PB1,PB2,POL,POLWD,PLANB,BX2L,
     *BY2L,BX2F,BY2F,BX2B,BY2B
 100  CONTINUE
 101  CONTINUE
C PLOT PROGRAMS
      CALL PLOTS(0.,0.,7)
      CALL FACTOR(0.4)
      CALL PLOT(2.0,2.0,-3)                                    17
      APOL(91,1)=0.
      APOL(92,1)=30.
      CALL AXIS(0.,0.,21HPHASE ANGLE - DEGREES,-21,6.0,0.,0.00,30.)
      CALL AXIS(0.0,0.0,21HPOLARIZATION PER CENT,21,7.0,90.,-10.,10.)
      CALL SYMBOL(1.,6.,.14,30HIMAGINARY INDEX VARIED-M RANGE ,0,30)
```

```
      CALL SYMBOL(2.0,5.8,.10,30HXTL = 15-20 WAVELENGTHSTHS      ,0,30)
      CALL SYMBOL(2.0,5.6,.10,30HREAL INDEX = 1.6               ,0,30)
      CALL SYMBOL(2.,5.4,.1,28HIMAG INDEX =0.2 TO 0.6      ,0.,28)
      CALL SYMBOL(2.0,5.2,.10,22HPIT WIDTH/DEPTH = 0.80,0,22)
      CALL SYMBOL(2.0,5.0,.10,24HDUST = 40 PERCENT       ,0,24)
      CALL SYMBOL(2.0,4.8,.10,30HFLAT SURFACE = 30 PERCENT       ,0,30)
      CALL SYMBOL(2.,4.6,.1,30HLONGITUDE = -74 DEGREES         ,0,30)
      DO 510 MLINE=2,6
      APOL(91,MLINE)=-10.
      APOL(92,MLINE)=10.
      CALL LINE(APOL(1,1),APOL(1,MLINE),90,1,4,MLINE)
  510 CONTINUE                                                          18
      CALL PLOT(12.0,0.0,-3)
      APOLWD(91,1)=0.
      APOLWD(92,1)=30.
      CALL AXIS(0.,0.,21HPHASE ANGLE - DEGREES,-21,6.0,0.,0.00,30.)
      CALL AXIS(0.0,0.0,21HPOLARIZATION DIFF-PCT,21,7.0,90.,-2.,2.)
      CALL SYMBOL(1.,6.,.14,30HIMAGINARY INDEX VARIED-M RANGE ,0,30)
      CALL SYMBOL(2.,5.8,.1,30HWAVELENGTH SHIFT = 33PCT        ,0,30)
      DO 519 MLINE=2,6
      APOLWD(91,MLINE)=-2.
      APOLWD(92,MLINE)=2.
      CALL LINE(APOLWD(1,1),APOLWD(1,MLINE),90,1,4,MLINE)
  519 CONTINUE
      CALL PLOT(12.0,0.0,-3)
      ARED(84,1)=0.
      ARED(85,1)=30.
      CALL AXIS(0.,0.,21HPHASE ANGLE - DEGREES,-21,6.0,0.,0.00,30.)
      CALL AXIS(0.,0.,28HREDDENED POINT, DIFF-MAG      ,28,7.,90.,.0,.05)
      CALL SYMBOL(1.,6.,.14,30HIMAGINARY INDEX VARIED-M RANGE ,0,30)
      CALL SYMBOL(2.,5.8,.1,30HWAVELENGTH SHIFT = 33PCT        ,0,30)
      DO 517 MLINE=2,6
      ARED(84,MLINE)=0.0
      ARED(85,MLINE)=.05
      CALL LINE(ARED(1,1),ARED(1,MLINE),83,1,4,MLINE)
  517 CONTINUE
      CALL PLOT(12.0,0.0,-3)
      AREDP(84,1)=0.
      AREDP(85,1)=30.
      CALL AXIS(0.,0.,21HPHASE ANGLE - DEGREES,-21,6.0,0.,0.00,30.)
      CALL AXIS(0.,0.,28HREDDENED PLANET, DIFF-MAG     ,28,7.,90.,.0,.05)
      CALL SYMBOL(1.,6.,.14,30HIMAGINARY INDEX VARIED-M RANGE ,0,30)
      CALL SYMBOL(2.,5.8,.1,30HWAVELENGTH SHIFT = 33PCT        ,0,30)
      DO 518 MLINE=2,6
      AREDP(84,MLINE)=.0
      AREDP(85,MLINE)=.05
      CALL LINE(AREDP(1,1),AREDP(1,MLINE),83,1,4,MLINE)
  518 CONTINUE
      CALL PLOT(12.0,0.0,-3)
      APLNB(91,1)=0.
      APLNB(92,1)=30.
      CALL AXIS(0.,0.,21HPHASE ANGLE - DEGREES,-21,6.0,0.,0.00,30.)
      CALL AXIS(0.0,0.0,21HREFLECTIVITY,PLANET   ,21,7.0,90.,0.0,.05)
      CALL SYMBOL(1.,6.,.14,30HIMAGINARY INDEX VARIED-M RANGE ,0,30)
      DO 509 MLINE=2,6
      APLNB(91,MLINE)=0.0
      APLNB(92,MLINE)=.05
```

```
      CALL LINE(APLNB(1,1),APLNB(1,MLINE),90,1,4,MLINE)
  509 CONTINUE
      CALL PLOT(12.0,0.0,-3)                                              194.
      AB3(91,1)=0.
      AB3(92,1)=30.
      CALL AXIS(0.,0.,21HPHASE ANGLE - DEGREES,-21,6.0,0.,0.00,30.)
      CALL AXIS(0.0,0.0,21HREFLECTIVITY,DIFFUSE ,21,7.0,90.,0.0,.05)
      CALL SYMBOL(1.,6.,.14,30HIMAGINARY INDEX VARIED-M RANGE ,0,30)
      DO 511 MLINE=2,6
      AB3(91,MLINE)=0.0
      AB3(92,MLINE)=.05
      CALL LINE(AB3(1,1),AB3(1,MLINE),90,1,4,MLINE)
  511 CONTINUE                                                            201.
      CALL PLOT(12.0,0.0,-3)                                              211.
      AB(91,1)=0.
      AB(92,1)=30.
      CALL AXIS(0.,0.,21HPHASE ANGLE - DEGREES,-21,6.0,0.,0.00,30.)
      CALL AXIS(0.0,0.0,21HREFLECTIVITY,TOTAL    ,21,7.0,90.,0.0,.05)
      CALL SYMBOL(1.,6.,.14,30HIMAGINARY INDEX VARIED-M RANGE ,0,30)
      DO 512 MLINE=2,6
      AB(91,MLINE)=0.0
      AB(92,MLINE)=.05
      CALL LINE(AB(1,1),AB(1,MLINE),90,1,4,MLINE)
  512 CONTINUE                                                            218
      CALL PLOT(12.0,0.0,-3)                                              228
      APB1(91,1)=0.
      APB1(92,1)=30.
      CALL AXIS(0.,0.,21HPHASE ANGLE - DEGREES,-21,6.0,0.,0.00,30.)
      CALL AXIS(0.0,0.0,21HPOLARIZATION,SINGLES ,21,7.0,90.,0.0,10.)
      CALL SYMBOL(1.,6.,.14,30HIMAGINARY INDEX VARIED-M RANGE ,0,30)
      DO 513 MLINE=2,6
      APB1(91,MLINE)=0.0
      APB1(92,MLINE)=10.
      CALL LINE(APB1(1,1),APB1(1,MLINE),90,1,4,MLINE)
  513 CONTINUE                                                            235
      CALL PLOT(12.0,0.0,-3)                                              245
      APB2(91,1)=0.
      APB2(92,1)=30.
      CALL AXIS(0.,0.,21HPHASE ANGLE - DEGREES,-21,6.0,0.,0.00,30.)
      CALL AXIS(0.0,0.0,21HPOLARIZATION,DOUBLES ,21,7.0,90.,-4.,4.0)
      CALL SYMBOL(1.,6.,.14,30HIMAGINARY INDEX VARIED-M RANGE ,0,30)
      DO 514 MLINE=2,6
      APB2(91,MLINE)=-4.0
      APB2(92,MLINE)=4.
      CALL LINE(APB2(1,1),APB2(1,MLINE),90,1,4,MLINE)
  514 CONTINUE                                                            252
      CALL PLOT(12.0,0.0,-3)
      AB1(91,1)=0.
      AB1(92,1)=30.
      CALL AXIS(0.,0.,21HPHASE ANGLE - DEGREES,-21,6.0,0.,0.00,30.)
      CALL AXIS(0.0,0.0,21HREFLECTIVITY,SINGLES ,21,7.0,90.,0.0,.004)
      CALL SYMBOL(1.,6.,.14,30HIMAGINARY INDEX VARIED-M RANGE ,0,30)
      DO 515 MLINE=2,6
      AB1(91,MLINE)=0.0
      AB1(92,MLINE)=.004
      CALL LINE(AB1(1,1),AB1(1,MLINE),90,1,4,MLINE)
  515 CONTINUE
```

```
      CALL PLOT(12.0,0.0,-3)
      AB2(91,1)=0.
      AB2(92,1)=30.
      CALL AXIS(0.,0.,21HPHASE ANGLE - DEGREES,-21,6.0,0.,0.00,30.)
      CALL AXIS(0.0,0.0,21HREFLECTIVITY,DOUBLES ,21,7.0,90.,0.0,.004)
      CALL SYMBOL(1.,6.,.14,30HIMAGINARY INDEX VARIED-M RANGE ,0,30)
      DO 516 MLINE=2,6
      AB2(91,MLINE)=0.0
      AB2(92,MLINE)=.004
      CALL LINE(AB2(1,1),AB2(I,MLINE),90,1,4,MLINE)
  516 CONTINUE
      CALL PLOT(12.0,0.0,999)
      END                                                              33:
      STOP                                                             34(
```